University of Vermont
ScholarWorks @ UVM

Graduate College Dissertations and Theses | Dissertations and Theses

2018

Arenavirus Transcription, Replication, and Interaction with Host-Cellular Components

Benjamin King
University of Vermont

Follow this and additional works at: https://scholarworks.uvm.edu/graddis

 Part of the Cell Biology Commons

Recommended Citation
King, Benjamin, "Arenavirus Transcription, Replication, and Interaction with Host-Cellular Components" (2018). *Graduate College Dissertations and Theses*. 830.
https://scholarworks.uvm.edu/graddis/830

This Dissertation is brought to you for free and open access by the Dissertations and Theses at ScholarWorks @ UVM. It has been accepted for inclusion in Graduate College Dissertations and Theses by an authorized administrator of ScholarWorks @ UVM. For more information, please contact donna.omalley@uvm.edu.

ARENAVIRUS TRANSCRIPTION, REPLICATION, AND INTERACTION WITH HOST-CELLULAR COMPONENTS

A Dissertation Presented

by

Benjamin Robert King

to

The Faculty of the Graduate College

of

The University of Vermont

In Partial Fulfillment of the Requirements
for the Degree of Doctor of Philosophy
Specializing in Cellular, Molecular and Biomedical Sciences

January, 2018

Defense Date: October 10th, 2017
Dissertation Examination Committee:

Jason W. Botten, Ph.D., Advisor
Jason Stumpff, Ph.D., Chairperson
Gary Ward, Ph.D.
Markus Thali, Ph.D.
Cynthia J. Forehand, Ph.D., Dean of the Graduate College

ABSTRACT

Arenaviruses are enveloped negative-strand RNA viruses that cause significant human disease. Despite decades of research, it is still unclear how these viruses establish a lifelong, asymptomatic infection in their rodent hosts while infection of humans often results in severe disease. Unable to enter a state of *bona fide* latency, the transcription and replication of the viral genomic RNA is likely highly regulated in time and subcellular space. Moreover, we hypothesize that the viral nucleoprotein (NP), responsible for the encapsidation of the viral RNA and the most highly expressed viral gene product, plays a key role in the regulation of the viral gene expression program. Further, exploring host-virus interactions may elucidate the basic aspects of arenavirus biology and how they cause such severe disease in humans. To explore these questions in greater detail, this dissertation has pursued three main avenues.

First, to better understand lymphocytic choriomeningitis mammarenavirus (LCMV) genome replication and transcription at the single-cell level, we established a high-throughput, single-molecule (sm)FISH image acquisition and analysis pipeline and followed viral RNA species from viral entry through the late stages of persistent infection *in vitro*. This work provided support for a cyclical model of persistence where individual cells are initially transiently infected, clear active infection, and become re-infected from neighboring reservoir cells within the population.

Second, we used FISH to visualize viral genomic RNA to describe the subcellular sites where LCMV RNAs localize during infection. We observed that, viral RNA concentrates in large subcellular structures located near the cellular microtubule organizing center and colocalizes with the early endosomal marker Rab5c and the viral glycoprotein in a proportion of infected cells. We propose that the virus is using the surface of a cellular membrane bound organelle as a site for the pre-assembly of viral components including genomic RNA and viral glycoprotein prior to their transport to the plasma membrane where new particles will bud.

Last, we used mass spectrometry to identify human proteins that interact with the NPs of LCMV and Junín mammareanavirus (JUNV) strain Candid #1. We provided a detailed map of the host machinery engaged by arenavirus NPs, and in particular, showed that NP associates with the double-stranded RNA (dsRNA)-activated protein kinase (PKR), a well-characterized antiviral protein that inhibits cap-dependent protein translation initiation via phosphorylation of eIF2α. We demonstrated that JUNV antagonizes the antiviral activity of PKR completely, effectively abrogating the antiviral activity of this surveillance pathway.

In sum, the work composing this dissertation has given us fresh insight into how arenaviruses establish and maintain persistence; the nature of the subcellular site where viral genomic RNA is transcribed, replicated, and assembled with other viral components; and a global view of the cellular machinery hijacked by the viral nucleoprotein. This work improves our basic understanding of the arenavirus life cycle and may suggest novel antiviral therapeutic targets that could be exploited in the future.

CITATIONS

Material from this dissertation has been published in the following form:

King, B. R., Hershkowitz, D., Eisenhauer, P. L., Weir, M. E., Ziegler, C. M., Russo, J., Bruce, E. A., Ballif, B. A., and Botten, J.. (2017). A Map of the Arenavirus Nucleoprotein-Host Protein Interactome Reveals that Junin Virus Selectively Impairs the Antiviral Activity of Double-Stranded RNA-Activated Protein Kinase (PKR). Journal of Virology 91.

King, B. R., Kellner, S., Eisenhauer, P. L., Bruce, E. A., Ziegler, C. M., Zenklusen, D., and Botten, J.. (2017). Visualization of the lymphocytic choriomeningitis mammarenavirus (LCMV) genome reveals the early endosome as a possible site for genome replication and viral particle pre-assembly. Journal of General Virology

Submitted for Publication

King, B. R., Samacoits, A., Eisenhauer, P. L., Ziegler, C. M., Bruce, E. A., Zenklusen, D., Zimmer, C., Mueller, F., and Botten, J.. Following arenavirus RNA species in individual cells by single-molecule fluorescence in situ hybridization (smFISH) reveals a model of cyclical infection and clearance during persistence. Journal of Virology

ACKNOWLEDGEMENTS

The last several years have been transformative in my life as a scientist and as an individual. Reflecting back, I am extraordinarily grateful for the numerous personal relationships with scientific mentors and friends that have shaped and nurtured the scientist that I am today. Most of all, I would like to thank my PhD advisor Jason Botten. Having worked side by side with Jason over the past years, I have learned much and am forever thankful for his patience and willingness to let me pursue unconventional paths. Moreover, I am indebted to the many members of the Botten team with whom I have had the good fortune to spend many hours in the lab.

I have had many scientific mentors who have helped me in their own ways and at different stages of my scientific journey. I thank Ralph Budd for having given me my first research experience as a recently graduated undergraduate and for his continuous role as a mentor in my life. I am grateful for the chance to have first experienced virology research when I worked with Cyrille Mathieu and Branka Horvat at the École Normale Supérieur de Lyon. I thank the members of my thesis committee for the invaluable scientific advice and insight that has made my dissertation work something of which I am truly proud. I am grateful to Matthew Poynter, Charles Irvin, and the Vermont Lung Center community who believed in the merit of my work and provided invaluable support, mentorship, and opened my eyes to the innumerable ways that basic and translational science intersect. I was lucky to have received the Chateaubriand Fellowship and am grateful for the chance it offered to

travel to France and work in the lab of Christophe Zimmer at the Institut Pasteur during the most memorable and scientifically fruitful eight months of my doctoral work.

For the hours that I was not in lab, I owe an enormous amount to my family and to so many close friends. They know who they are and do not need to be mentioned by name. I may have made it through graduate school without them, but it would not have been nearly as pleasant.

TABLE OF CONTENTS

Page

LIST OF TABLES

Table **Page**

LIST OF FIGURES

Figure **Page**

CHAPTER 1: COMPREHENSIVE LITERATURE REVIEW

1.1. Introduction

Arenaviruses are important human pathogens. There are no FDA approved vaccines to prevent human infections by arenaviruses. In addition, there are limited effective antiviral therapeutics available for the treatment of infected individuals. Gaps in our understanding of the fundamental stages of the arenavirus life cycle in the human host is a major contributing factor to the lack of effective preventive and treatment options. During my time in the Botten laboratory, my dissertation research has focused on elucidating critical, yet incompletely understood, aspects of the viral life cycle. My work has sought to improve our understanding of viral gene transcription and genomic replication. Taking advantage of new technologies permitting the visualization of RNA molecules with high sensitivity and specificity by fluorescence microscopy, it is possible for the first time to probe the dynamics of these events within individual infected cells and to explore previously intractable questions such as the nature of the viral gene expression program during persistence. Further, this approach makes it possible to examine the subcellular locations where these events occur to gain an appreciation for how the virus may be utilizing particular cellular structures to promote its replication. Last, we know that the viral nucleoprotein gene is the first viral gene expressed following infection and is the most highly expressed viral gene product in infected cells. Its canonical role during infection is the encapsidation of the viral genomic RNA. However, little is known regarding what additional accessory roles the viral NP may play and how these may be

mediated through protein-protein interactions with host cellular proteins. We have employed a proteomics approach to elucidate the protein-protein interaction network of the arenavirus nucleoprotein. This work has given us new insight into how NP plays an important role in manipulating the host cell environment to maintain conditions favorable for viral replication. What follows is a comprehensive literature review providing the necessary concepts to appreciate the intellectual contribution of the work constituting the three manuscripts produced during the course of this dissertation project.

1.2. Arenaviruses

1.2.1. History of the *Arenaviridae*

In 1929, Viets and Watts described a cluster of six patients presenting with an unusual form of meningitis. The cerebrospinal fluid of these patients contained abundant lymphocytes but no detectable bacteria. Further, the absence of other symptoms corresponding to other known causes of meningitis led the physicians to suggest a new disease of unknown etiology, which they initially referred to as aseptic (lymphocytic) meningitis (Viets and Watts, 1929a, b). Between 1934 and 1936 the viral etiology of this lymphocytic meningitis syndrome was independently established by Armstrong et al., Traub, McNair and Rivers, and Findlay et al. (Armstrong and Dickens, 1935; Armstrong and Lillie, 1934; Armstrong and Wooley, 1935; Findlay et al., 1936; Rivers and McNair Scott, 1935; Rivers and Scott, 1936; Traub, 1935). In 1934, Armstrong and Lillie described a viral agent that was able to provoke a disease closely resembling that described by Viets and Watts just five years previously by performing intracranial injections of infected brain

matter into naïve Rhesus macaques (Armstrong and Lillie, 1934). Other groups showed that cerebrospinal fluid or brain tissue from infected humans or animals was able to cause a similar aseptic meningitis following intracranial injection into mice and guinea pigs (Rivers and McNair Scott, 1935; Rivers and Scott, 1936; Scott and Rivers, 1936; Traub, 1935). Additional support for this being the causative agent for the aseptic lymphocytic meningitis seen in humans came with the observation that serum from aseptic lymphocytic meningitis survivors provided a high degree of protection to both Rhesus macaques, mice, and guinea pigs infected with isolated strains of virus (Armstrong and Dickens, 1935; Armstrong and Wooley, 1935; Rivers and Scott, 1936; Scott and Rivers, 1936). Additionally, animals surviving infection with one strain displayed immunity when subsequently reinoculated with additional strains isolated from other sources (Rivers and Scott, 1936). The viral nature of the causative agent of the disease was demonstrated through the ability of the infectious agent to pass through a filter with an average pore size of 150 μm and the inability to see bacteria, fungal, or protozoal cells via histology of infected tissue or failure to cultivate bacteria in rich growth media (Rivers and Scott, 1936). The virus determined to be the cause of this disease, and independently isolated by multiple researchers in both North America and Europe, came to be named lymphocytic choriomeningitis virus (LCMV), due to the large lymphocyte infiltration observed by histology in both the meninges and the choroid plexus in infected tissue, a pattern that was uniquely associated with infection with this viral agent (Armstrong and Dickens, 1935; Armstrong and Wooley, 1935; Findlay et al., 1936).

The study of LCMV continued during the following decades, but it was not until the mid-1960's that it became apparent that LCMV shared similar characteristics with other more recently described viruses including Lassa (LASV), Junín (JUNV), Machupo (MACV), and Tacaribe (TCRV) viruses. In 1970, an official classification for these viruses was proposed and the name for this virus family "arenovirus" was proposed (Lehmann-Grube, 1971; Rowe et al., 1970). The latin root *arenosus* (meaning sandy) was chosen to describe this newly classified family due to the hallmark grainy appearance of these viral particles in negative stained electron micrographs. These electron dense granules in viral particles were subsequently demonstrated to be host ribosomes (Farber and Rawls, 1975; Lehmann-Grube, 1971; Leung and Rawls, 1977; Rowe et al., 1970). Additional unifying features of this viral family consisted of their lipid envelope, serological relatedness, pleomorphic virion form, release of viral particles from infected cells by budding, and contained RNA (Lehmann-Grube, 1971; Rowe et al., 1970). In 1970, the International Committee for the Taxonomy of Viruses (ICTV) approved the official classification of this group of viruses, and the initially chosen name "arenovirus" was changed slightly to "arenavirus" to avoid confusion with the already recognized taxon "adenovirus" (Murphy, 1975; Wildy, 1971).

Recently, several new arenavirus-like viruses were discovered in snakes (Bodewes et al., 2014; Stenglein et al., 2012). This discovery prompted the ICTV to change the previously recognized genus "*Arenavirus*" to "*Mammarenavirus*". Further, within the family *Arenaviridae* a new genus called *"Reptarenavirus*" was created containing the

newly described snake viruses (ICTV, 2014a). In the newly revised official nomenclature, previously recognized names were altered such that lymphocytic choriomeningitis virus was renamed lymphocytic choriomeningitis mammarenavirus (ICTV, 2014b).

1.2.2. Arenavirus infections in humans

During the decades following their initial discovery, we have come to understand much about the disease pathology caused by these viruses and the molecular events underlying each stage of their life cycles. The arenavirus family is broadly divided into the Old World and New World groups. The classification of viruses into one group or the other is determined by genetic relatedness of viral genomes, geographic distribution, and serology (Buchmeier et al., 2013; Burri et al., 2012; Charrel et al., 2003; Emonet et al., 2006) (Table 1.1 and Figure 1.1 and 1.2).

The arenaviruses are zoonotic viruses, meaning that, in nature, they are maintained in animal reservoirs and human spillover is incidental (Buchmeier et al., 2013; Charrel and de Lamballerie, 2010; Vela, 2012). For most members of the genus *Mammarenavirus*, the viruses exploit rodent reservoirs. Only TCRV has been isolated from bats (Buchmeier et al., 2013). The endemic geographical range where arenavirus infections have been observed overlap with the geographical distribution of the known species of rodent reservoir utilized by each specific arenavirus (Charrel et al., 2008).

Transmission of arenavirus from infected rodents to humans is thought to occur primarily through inhalation, ingestion, or contact of skin wounds or abrasions with infected rodent excreta (Buchmeier et al., 2013; Charrel et al., 2008; Grant et al., 2012).

Several well documented cases of nosocomial acquired infections by health care providers have also been reported (Russier et al., 2012). LCMV can be transmitted vertically from mother to the developing fetus and is a significant teratogenic threat (Bonthius, 2009). Moreover, several cases of LCMV acquired through the transplantation of infected organs have recently been reported with nearly uniform rates of lethality (Fischer et al., 2006; Macneil et al., 2012). In immunocompetent individuals, LCMV infection is often subclinical and inapparent but can manifest as severe aseptic meningitis (Bonthius, 2012). Further evidence of the danger of LCMV is the high rates at which people are exposed to its reservoir, the house mouse *Mus musculus*. A serological study performed in Birmingham, Alabama, USA showed that greater than 4% of individuals were seropositive for LCMV antigen indicating prior exposure to this human pathogen (Stephensen et al., 1992).

Lassa virus is the greatest public health threat of any member of the arenavirus family. It is endemic in Western Africa where it infects up to 300,000 people annually (Yun and Walker, 2012). The ease of international airline travel has increased the risk that cases could spread worldwide. Lassa virus is maintained in *Mastomys* sp. rats, which are peridomestic and routinely come into close contact with people living in rural areas in its endemic region (Russier et al., 2012). Lassa virus infection can cause severe disease in humans, and can cause a hemorrhagic fever syndrome in serious cases (Russier et al., 2012; Yun and Walker, 2012). There are currently no vaccines to prevent Lassa virus infections despite a significant need (Charrel et al., 2011). The only antiviral therapeutic option is

ribavirin. However, the need for early administration and the risk of significant side effects limit its efficacy (Bausch et al., 2010; Vela, 2012).

One of several South American arenaviruses known to cause hemorrhagic fever, Junín virus is the etiologic agent of Argentine hemorrhagic fever (Grant et al., 2012). Maintained in *Calomys* sp. rodents, which prefer to live in close proximity to agriculture, farmers are the primary group at risk for infection with JUNV (Charrel and de Lamballerie, 2003). An attenuated strain of JUNV (strain Candid #1) was developed as a joint effort between the US Army Medical Research Institute of Infectious Diseases and the Argentine Ministry of Health and Social Action. This strain has been delivered as a live-attenuated vaccine to at risk populations in Argentina, and has shown efficacy in preventing new infections of vaccinated individuals. Despite efficacy, there is concern that the mutant virus could revert to wild type and thus does not have US Food and Drug Agency approval (Ambrosio et al., 2011).

1.2.3. The arenavirus life cycle

Members of the genus *Mammarenavirus* are enveloped with a host-derived lipid bilayer (Figure 1.3) (Buchmeier et al., 2013). The viral envelope glycoprotein is embedded in the virion membrane. The viral glycoprotein precursor (GPC) is proteolytically processed in the secretory pathway into three subunits: GP1, GP2, and a stable signal peptide, which is unusually long and remains associated with the viral glyocoprotein post-processing (Figure 1.3) (Buchmeier et al., 2013; Burri et al., 2012; Rojek and Kunz, 2008; Rojek et al., 2008). Three GP1, GP2, and SSP units associate to form homotrimers (Burri

et al., 2012). The viral Z protein is the *bona fide* viral matrix protein needed for viral budding (Figure 1.3) (Urata and Yasuda, 2012; Wolff et al., 2013b). Within the viral particle, the viral ribonucleoprotein (RNP) consists of the viral single-stranded RNA genome (which is encoded on two distinct segments), the viral nucleoprotein (NP), which encapsidates the genomic RNA, and the viral encoded RNA-dependent RNA polymerase (L) (Figure 1.3) (Buchmeier et al., 2013). The last component of arenavirus particles are packaged host ribosomes, whose presence in viral particles confers the family's characteristic grainy appearance in electron micrographs though their functional importance, if any, is still unknown (Buchmeier et al., 2013; Leung and Rawls, 1977).

Though differences do exist between members of the Old and the New World arenaviruses, the basic steps of the viral life cycle are shared among all members of the family (Figure 1.4). The first phase of an arenavirus infection is entry of the arenavirus particle into a naïve host cell (Burri et al., 2012; Rojek and Kunz, 2008; Rojek et al., 2008). The attachment to the host cell is mediated by the GP1 subunit of the envelope glycoprotein, which binds to the cell surface receptor. The Old World arenaviruses and Clade C of the New World arenaviruses use alpha-dystroglycan and Clade B of the New World arenaviruses use transferrin receptor (TfR1) as the cell surface receptor (Burri et al., 2012). The binding of the viral glycoprotein to the cellular receptor triggers endocytosis of the attached virion (Burri et al., 2012). Entry of New World arenaviruses is clathrin-dependent (Rojek et al., 2008). On the other hand, entry of the Old World arenaviruses is

clathrin, caveolin, and dynamin- independent and does not rely on Rab5 or Rab7 (Rojek and Kunz, 2008).

Upon cellular uptake by endocytosis, progressive acidification of endosomes leads to a conformational change in the GP2 subunit of the envelope glycoprotein triggering a fusion event between the viral envelope and the endosomal membrane (Figure 1.4) (Burri et al., 2012). Viral envelope fusion releases the viral RNP into the cytoplasm of the newly infected cell. There, the viral L polymerase begins transcribing the viral genomic RNA, and viral mRNAs are translated into polypeptides by host ribosomes (Figure 1.4) (Buchmeier et al., 2013; Meyer et al., 2002). Then, full length viral genome is replicated by the L polymerase (Figure 1.4) (Buchmeier et al., 2013; Meyer et al., 2002). Lastly, the viral genomic RNA and the viral proteins traffic to the plasma membrane where they assemble and bud as new infectious viral particles (Figure 1.4) (Urata and Yasuda, 2012; Wolff et al., 2013b).

1.3. Transcription and Replication of Viral RNA during Acute and Persistent Phases of Infection

Arenaviruses are enveloped viruses that have a single-stranded, bisegmented, negative-sense RNA genome. Each genomic RNA segment (named S and L) contains 2 viral open reading frames encoded in ambisense orientation (Figure 1.5) (Buchmeier et al., 2013). The canonical sequence of genetic events following release of arenavirus genomic RNA into the cytoplasm of a newly infected cell is primary transcription of the NP and L mRNAs from the viral S and L genomic segments, full length replication of the

antigenomic RNA, transcription of the GPC and Z mRNAs from the S and L antigenomic RNA, and finally replication of more genomic RNA (Figure 1.6) (Buchmeier et al., 2013; Ferron et al., 2017).

Early work aimed at elucidating the genetic composition of these viruses determined that they had a bisegmented single-stranded RNA genome (Carter et al., 1973). The presence of cellular ribosomes in arenavirus particles initially was suggestive that these viruses could possess a positive-sense RNA genome, however the presence of a viral RNA polymerase along with RNase protection assays suggested that the viral genomic RNAs from purified virions was indeed of negative-sense polarity (Carter et al., 1974; Leung et al., 1977). Determination of the full-length sequence of the viral S segment genomic RNA showed the first evidence of the arenaviral ambisense coding strategy where the NP gene is encoded in a negative-sense polarity on the 3' half of the viral genomic RNA and the GPC gene is encoded in a pseudo-positive-sense polarity on the 5' half (Auperin et al., 1984a; Southern et al., 1987). At the same time it was determined that the two viral genes are separated by an intergenic region (IGR) that was predicted to adopt a hairpin secondary structure, a potential means of transcription termination (Auperin et al., 1984a; Auperin et al., 1984b). The L segment was subsequently shown to encode the L protein in the same negative-sense polarity and position as the NP gene on the S segment (Singh et al., 1987). Z was shown to be encoded in pseudo-positive-sense polarity, analogous to GPC on the S segment, and is separated from the L gene by an intergenic region (Salvato and Shimomaye, 1989).

The discovery of the ambisense coding strategy employed by the arenaviruses suggested a mechanism by which these viruses could temporally regulate the expression of their various gene products (Auperin et al., 1984b; Southern et al., 1987). The use of sequence specific Northern blot probes made it possible to track the expression levels of different viral RNA species over time. Using Northern blot, it was confirmed that the appearance of the NP mRNA could be detected just 2 hours post infection, and this viral subgenomic RNA accumulated even in the absence of protein synthesis – which the authors inhibited with pactamycin treatment (Franze-Fernandez et al., 1987). On the other hand, the GPC mRNA was not detected until 4 hours post infection, and its expression was wholly dependent on the presence of active translation (Franze-Fernandez et al., 1987). These data suggested that translation of the NP and L protein were necessary for the production of the full length antigenomic RNA, which would serve as the template for GPC transcription. Significantly, this was the first demonstration of the hypothesized ability of the arenaviruses to temporally separate the different viral gene expression events. Further work suggested that S genome was expressed to a higher degree than the L genomic RNA (Fuller-Pace and Southern, 1988) and that viral RNAs increased in abundance over the first few days of infection and began to decrease after achieving those peak levels (Fuller-Pace and Southern, 1988; Iapalucci et al., 1994; Raju et al., 1990; Shivaprakash et al., 1988; Southern et al., 1987). qRT-PCR data has confirmed the trend of initial increase in RNA levels over the first 48 hours of infection followed by their subsequent decline (Haist et al., 2015).

Arenavirus mRNAs bear 5' 7-methylguanylate caps, which the virus presumably procures through a cap-snatching mechanism (Meyer and Southern, 1993; Polyak et al., 1995a; Raju et al., 1990) potentially conferred by an endonuclease activity present in the viral L polymerase (Morin et al., 2010). Further, viral mRNAs are not polyadenylated (Auperin et al., 1984b; Leung et al., 1977). The secondary structure created by the viral intergenic region serves as the viral transcription termination signal, and 3' termini of viral mRNAs are heterogeneous in length representing variablility in the position in which the viral polymerase terminates mRNA synthesis in response to secondary structural cues (Iapalucci et al., 1991; Lopez and Franze-Fernandez, 2007; Meyer et al., 2002; Pinschewer et al., 2005). It seems that sequence specificity of the IGR is not of paramount importance as chimeric genomic sequences containing heterologous IGR regions from distantly related arenaviruses are still able to serve as transcription termination signals, and recombinant viruses with these heterologous IGRs are viable (Iwasaki et al., 2016).

In contrast to the viral mRNAs, the viral genomic and antigenomic RNAs are uncapped. At the 3' and 5' termini of the viral genomic segments, there are important untranslated regions (UTR) that play roles in the initiation of transcription and replication. The terminal 19 nucleotides of the 3' UTR are highly conserved between the S and L segments, and the reverse complement of the 3' UTR is present in the 5' UTR (Auperin et al., 1982a; Auperin et al., 1982b; Meyer et al., 2002). It is proposed that the 3' and 5' UTRs will base pair, leading the genomic RNA to form a closed panhandle structure (Meyer et al., 2002). It appears that both the exact sequence and the double-stranded character of the

3’ and 5’ UTRs are critical for effective viral transcription and replication (Hass et al., 2006; Perez and de la Torre, 2003). In Lassa virus it appears that the requirement for sequence specificity from bases 13-19 of the conserved UTR is relaxed, and mutation in this region is permitted so long as double-stranded character is maintained (Hass et al., 2006).

Another striking feature of the arenavirus genomic RNAs is the presence of one non-templated base, most often a G, present at the 5’ terminus (Polyak et al., 1995a). The viral L polymerase uses a “prime-realign” mechanism to initiate replication of the viral genomic RNAs leaving a one base pair overhang at the 5’ terminus (Garcin and Kolakofsky, 1990, 1992; Raju et al., 1990). An important functional consequence of the presence of this 5’ nontemplated base pair is that RIG-I, an important innate immune sensor of cytoplasmic 5’ triphosphate bearing RNAs with dsRNA character, was unable to recognize RNA duplexes with a single nucleotide overhang and, thus, not induce the expression of type I interferon (IFN) (Marq et al., 2010).

A hallmark characteristic of arenavirus infections is their ability to establish lifelong persistent infection in rodents infected in utero or at birth (Francis et al., 1987). An understanding of the mechanism by which arenaviruses are able to establish persistence without adversely affecting their rodent hosts is important not just as a means to understand basic steps of the virus’ life cycle but also as a way to appreciate how and why severe disease often occurs in their incidental human hosts. Arenaviruses are unable to enter a *bona fide* latent state such as retroviruses like HIV-1 or herpes viruses like Epstein Barr

virus (Buchmeier et al., 2013; Meyer et al., 2002). Thus, persistently infected cells must maintain arenavirus genomic RNA over long periods of time, though how this occurs is still unclear, despite much study. A few principle models to explain the mechanism of arenavirus persistence have been proposed, and a detailed understanding of the genetics of persistence promises to yield a fresh outlook on this question that has long interested the field.

It is possible to recapitulate key elements of persistenct infection in cell culture models of infection, a fact that has greatly facilitated our ability to study arenaviral persistence in simplified *in vitro* systems (Lehmann-Grube, 1967; Lehmann-Grube et al., 1969; Meyer et al., 2002). One characteristic of cell culture models of persistent LCMV infection is the cyclical rise and fall of infectious virus released into cell culture supernatants over time, and these cycles have a periodicity of a few days (Hotchin, 1974a; Hotchin et al., 1975; Lehmann-Grube, 1967; Lehmann-Grube et al., 1969; Staneck et al., 1972). Additional features of arenavirus persistence is the continuous expression of NP and the downregulation of GPC surface expression (Oldstone and Buchmeier, 1982) and the resistance of cells to super infection with homologous virus (Ellenberg et al., 2004).

One hypothesis seeking to explain how persistent infection is established and maintained suggests that within a population of arenavirus infected cells, infection of a single cell is transient and self-limited. Further, upon clearance of an arenaviral infection, that cell becomes susceptible to being re-infected by neighboring reservoir cells within the population (Hotchin, 1973, 1974a, b; Hotchin et al., 1975). The primary evidence

supporting this model comes from the observation that when large numbers of single cell clones are established from a population where almost all cells were infected, virus was only detected in the supernatant of a small percentage of established clones (~5%) (Hotchin, 1973, 1974a, b; Hotchin et al., 1975). Additional evidence of the importance of viral clearance followed by re-infection in the maintenance of persistent arenavirus infections comes from the observation that treatment of persistently infected cultures with blocking arenavirus antisera leads to a progressive decline in the percentage of cells expressing viral antigen as visualized by immunofluorescence microscopy (Lehmann-Grube et al., 1969). Potential mechanisms that could be employed by arenaviruses to establish transient self-limiting infections in cells likely include the inhibition of the viral RNA dependent RNA polymerase by the viral Z protein (Cornu and de la Torre, 2001, 2002; Jacamo et al., 2003; Kranzusch and Whelan, 2011; Lopez et al., 2001) and the production of defective interfering particles (Burns and Buchmeier, 1993; Huang, 1973; Huang and Baltimore, 1970; Oldstone, 1998; Welsh et al., 1972; Ziegler et al., 2016a; Ziegler et al., 2016b).

A second hypothesis explaining arenaviral persistence suggests that the appearance of defective genomes during the persistent phase of arenavirus persistence leads to greatly reduced levels of infectious virus production (Rawls et al., 1981). The basis for this hypothesis is the observation that viral genomic RNAs are expressed at high levels *in vivo* in persistently infected animals (Francis and Southern, 1988b). Further it was shown that during persistence, truncated subgenomic RNAs appear *in vitro* (Francis and Southern,

1988a), and many of the genomic and antigenomic RNAs that appear to be full length actually have short (< 50 nucleotide) deletions at the 3' and 5' termini (Meyer and Southern, 1994). It was suggested that these terminally deleted genomes are replication competent as a specific 3' genomic deletion and the identical corresponding 5' antigenomic deletion were readily detected (Francis and Southern, 1988a; Meyer and Southern, 1994). However, these deletions were never observed in the 5' termini of viral mRNA sequences, suggesting that these truncated genomes are not transcriptionally competent (Meyer and Southern, 1993, 1994). There is a small amount of evidence that in some instances viral RNAs appeared to have additional nontemplated bases at their termini, suggesting a potential path by which terminally truncated genomes could be repaired (Meyer and Southern, 1997). By balancing the loss and replacement of genomic and antigenomic termini, the virus could potentially autoregulate viral transcription and production of infectious virions during persistence (Francis and Southern, 1988a; Meyer and Southern, 1993, 1994, 1997) – explaining the oscillatory behavior of viral release observed during persistent infection in cell culture.

Much of the work undertaken to probe the genetic events of viral transcription and replication has relied on Northern blot (Auperin et al., 1984b; Fuller-Pace and Southern, 1988; Polyak et al., 1995a, b; Raju et al., 1990; Shivaprakash et al., 1988; Southern et al., 1987) and qRT-PCR (Haist et al., 2015) to examine the levels of viral RNAs during infection. Studies using Northern blot to track viral RNAs during the course of infection have the advantage of being able to distinguish each of the viral RNAs (Auperin

et al., 1984b; Fuller-Pace and Southern, 1988; Polyak et al., 1995a, b; Raju et al., 1990; Shivaprakash et al., 1988). However, the extreme variability in detection sensitivity between independent studies and the inability to quantitatively compare the levels of viral RNAs labeled by different probe sets is a significant disadvantage of Northern blot (Auperin et al., 1984b; Fuller-Pace and Southern, 1988; Polyak et al., 1995a, b; Raju et al., 1990; Shivaprakash et al., 1988; Southern et al., 1987). qRT-PCR has also been implemented to track the dynamics of transcription and replication of viral RNAs by Haist *et al.* and has the advantage of exquisite sensitivity. However, qRT-PCR has the disadvantage of being unable to distinguish viral mRNAs from respective genomic or antigenomic RNA (Haist et al., 2015). A limitation to both approaches is that they measure gene expression of cell populations and are thus unsuitable to analyze the heterogeneity of individual cells (Auperin et al., 1984b; Fuller-Pace and Southern, 1988; Haist et al., 2015; Polyak et al., 1995a, b; Raju et al., 1990; Shivaprakash et al., 1988; Southern et al., 1987). While these methods have provided invaluable insight into the genetics of the viral life cycle, discerning between the two major hypotheses presented above will depend on a more nuanced view of the genetic events of infection in individual cells over time.

1.4. Viral Replication Complexes

The nucleoprotein is the major viral protein component of the viral RNPs (Ferron et al., 2017). LCMV NP in an infected cell localizes predominantly to punctate cytoplasmic structures during acute infection (Knopp et al., 2015; Ortiz-Riano et al., 2011; Young et al., 1987). In transfection experiments, ectopically expressed LCMV NP can adopt a

distribution similar to that observed during infection (Knopp et al., 2015; Ortiz-Riano et al., 2011). NP in cells infected with JUNV and TCRV, can exhibit a pattern of staining ranging from diffusely cytoplasmic to concentration of NP in punctate cytoplasmic structures (Baird et al., 2012; Ellenberg et al., 2002). The observation that NP can concentrate in specific subcellular locations during both infection and when NP is ectopically expressed suggests that the virus may benefit from compartmentalizing viral machinery in specific subcellular sites. The identification and description of these sites as well as the elucidation of how the virus may be benefitting by a particular localization pattern are of great interest.

It is known that many viruses take advantage of specific subcellular sites to facilitate their life cycles. A particularly rich literature exists describing the way viruses with single-stranded positive sense genomes hijack host membrane bound compartments to shield the transcription and replication of their genomes from cytoplasmic RIG-I like receptor (RLR) surveillance (Chan and Gack, 2016; den Boon and Ahlquist, 2010; den Boon et al., 2010; Novoa et al., 2005a). While less is known regarding how negative-strand viruses, like the arenaviruses, may rely on membrane bound cellular compartments, there are notable examples of other negative-strand viruses that rely on cellular organelles to promote genome replication, assembly, and/or trafficking phases of their life cycle including Influenza A virus and Bunyamwera virus (Amorim et al., 2011; Bruce et al., 2010; Novoa et al., 2005a; Novoa et al., 2005b).

To explore the question of whether arenaviruses take advantage of particular subcellular sites to promote their life cycle, Baird *et al*. performed the first comprehensive study to examine the subcellular localization of sites of active transcription and replication of TCRV and JUNV viral genomic RNA (Baird et al., 2012). The authors found that active sites of genome transcription and replication (or viral replication and transcription complexes; RTC) were localized to punctate structures in infected cells. Moreover, viral RNPs co-sedimented with membrane components by density-gradient centrifugation, providing the first hint that the virus may be co-opting some existing organelle membrane during the cytoplasmic phases of its life cycle (Baird et al., 2012). Nevertheless, Baird *et al*. were unable to identify the cytoplasmic organelle hijacked by the virus, and the identity of these subcellular sites of TCRV replication remain obscure (Baird et al., 2012).

1.5. The Viral Nucleoprotein

The arenavirus nucleoprotein, sometimes referred to as the nucleocapsid protein (abbreviated NP or N), is the viral protein expressed at the highest levels during infection. NP, consisting of between 558 and 570 amino acids, has a molecular weight ranging from 60-68 kDa depending upon the virus (Buchmeier, 2002). The viral gene encoding the NP protein is located on the S gene segment and is encoded in a negative-sense polarity – such that transcription of the genome yields a coding mRNA (Meyer et al., 2002). During the persistent phase of infection, while the expression of the other viral proteins becomes undetectable, NP levels remain high (Ellenberg et al., 2002). While NP plays multiple roles in the virus life cycle, classically, encapsidation of the viral genomic RNA and replicative

intermediate RNA (antigenomic RNA) has been considered to be NP's fundamental role (Buchmeier et al., 2013). Structural biology and mutagenesis approaches have made it possible to map the regions important for NP's various functions and in mediating its interactions with both viral and host proteins.

The primary amino acid sequence of the NP is highly conserved across the arenavirus family – including a high degree of similarity between the Old World and the New World arenaviruses (Buchmeier, 2002; Lan et al., 2008; Qi et al., 2010). Crystal structures of Lassa virus NP have been solved and have shown that NP folds into two discrete domains – an N terminal domain roughly encompassing residues 1-338 and a C terminal domain encompassing residues 364-561 with a flexible linking region connecting the two (Qi et al., 2010). In the N terminal domain, there is a deep cavity lined with basic residues at the bottom of which is located a patch of hydrophobic amino acids. It was initially suggested that this N terminal cavity coordinated the binding to the 7-methylguanylate cap (m^7G cap) which members of the arenavirus family have been demonstrated to use to cap their mRNAs. The authors hypothesized that the hydrophobic residues deep in the cavity coordinated the m^7G cap, and the basic channel coordinated the triphosphate bridge (Qi et al., 2010). When the authors mutated several key residues identified in this region, severe defects in viral transcription were observed – supporting their hypothesis that NP is involved in m^7G cap-snatching (Qi et al., 2010). Other groups have questioned this proposed model (Brunotte et al., 2011; Hastie et al., 2011b). The co-crystallization of LASV NP in complex with RNA has suggested that the N terminal cleft

does not bind m^7G caps. Rather, the cleft is responsible for binding single stranded viral RNA (Brunotte et al., 2011; Hastie et al., 2011b). It was shown that the basic amino acid residues lining the cavity were important in mediating the electrostatic interactions between the NP and the phosphate backbone of the ssRNA molecule (Brunotte et al., 2011; Hastie et al., 2011b).

LASV NP crystal structures have also given insight into the role of the C terminal domain. Two papers independently showed extensive 3d structure similarity between the C terminal domain of LASV NP and the DEDD superfamily of exonucleases despite little primary sequence identity (Hastie et al., 2011a; Qi et al., 2010). Structures reveal a deep cleft at the top of the C terminal domain of LASV NP. Moreover, these catalytic residues were shown to occupy the same positions as in the active site of the human DEDD family 3'-5' exonuclease TREX1 (Hastie et al., 2011a; Qi et al., 2010). Characterization of the enzymatic activity of the C terminal domain showed that NP degraded RNA but not DNA in a 3' to 5' direction, and that, moreover, this exoribonuclease activity was dependent upon a divalent Mn^{2+} cation coordinated by the C terminal domain (Hastie et al., 2011b; Qi et al., 2010). While Qi et al. (Qi et al., 2010) showed that NP degraded both ssRNA and dsRNA, Hastie et al. (Hastie et al., 2011a) demonstrated a clear preference of NP for dsRNA.

In addition to this initial crystallography examining the structure of LASV NP, the structure of TCRV, JUNV, and LCMV NP have all recently been solved and have been shown to possess a C terminal 3'-5' exoribonuclease domain (Jiang et al., 2013; West et

al., 2014; Zhang et al., 2013). TCRV NP was further shown to possess exonuclease activity with specificity for dsRNA ligands, like LASV NP (Jiang et al., 2013). However, JUNV NP was shown to lack exonuclease activity in an *in vitro* dsRNA degradation assay (Zhang et al., 2013). It is possible that the crystallization scheme utilized by these researchers led to the protein adopting an inactive conformation, lacking a key Zn^{2+} cation shown to be conserved in all other crystallized arenavirus NP's (West et al., 2014; Zhang et al., 2013). It is also possible JUNV does not possess the ability to degrade dsRNA substrates. Nevertheless, the potential diversity in NP functionality across members of the Old World and New World viruses is intriguing, and further work should be performed to better understand the divergent strategies employed by these related viruses to subvert effective host innate immune responses.

Other motifs present in the NP protein include a zinc finger motif in NP's C terminus (Parisi et al., 1996; Qi et al., 2010; Tortorici et al., 2001b). The zinc finger motif identified in the C terminus of LASV and JUNV was between amino acids 500 and 530. The position of the zinc finger motif in the crystal structure of the LASV NP suggests that it may play a role in coordinating the exoribonuclease domain (Qi et al., 2010; Tortorici et al., 2001b).

Important for encapsidation of the viral RNA genome, arenavirus NP has been shown to form homo-oligomers. The interaction between individual NP monomers has been suggested to be mediated by NP's N terminal domain (Levingston Macleod et al., 2011; Ortiz-Riano et al., 2011, 2012). However, C terminal to N terminal interactions also

appear to be of importance (Brunotte et al., 2011; Hastie et al., 2011b). X-Ray crystallography of LASV NP reveals homotrimers formed of monomers associated in a ring-like structure (Brunotte et al., 2011; Hastie et al., 2011b; Qi et al., 2010). NP subunits are arranged in either a symmetric head-tail fashion or an asymmetric fashion in the trimeric ring (Brunotte et al., 2011). However, complementary EM analysis of NP trimers in solution shows that NP trimers exist predominantly in a symmetric state (Brunotte et al., 2011). Crystallization has also suggested that NP monomers undergo a conformational change in their N terminal domain upon trimerization making the N terminal cleft unavailable for RNA binding (Hastie et al., 2011b). Thus, an open and a closed conformation of the N terminal domain of NP corresponds to monomeric and trimeric NP respectively. While unable to bind RNA, it is possible that homotrimeric NP has distinct biological roles in the viral life cycle. For example, it has been demonstrated that NP that is unable to trimerize is defective in its ability to promote transcription and replication in minigenome reporter assays but has no effect on interaction with other viral proteins or its ability to antagonize a type I IFN response (D'Antuono et al., 2014; Lennartz et al., 2013). It is possible that head to tail interactions between NP subunits bound upon the length of viral genomic (or antigenomic) RNA provide the structural basis for viral RNA encapsidation (Hastie et al., 2011b).

LCMV NP can be phosphorylated during infection on serine and threonine residues (Howard and Buchmeier, 1983). It is unclear what the significance of NP phosphorylation may be, though it seems that phosphorylation of the LCMV NP protein

increases over the course of an infection (Young and Howard, 1983). It was hypothesized that the phosphorylation of NP may play a role in regulation of the conformational changes in NP promoting or inhibiting its multimerization (Brunotte et al., 2011). More recently, mass spectrometry of the LCMV NP demonstrated phosphorylation at three serines, one threonine, and one tyrosine. Further, additional serine and threonine residues that could be phosphorylated were identified with predictive algorithms (Knopp et al., 2015). Mutation of a threonine residue predicted to be phosphorylated greatly changed the subcellular distribution of NP in transfected cells, negatively affected translation priming, and a recombinant virus bearing this mutation was not viable (Knopp et al., 2015). Mutation of the phosphorylated tyrosine was also shown to be critical as recombinant virus with a mutation at this site was not viable (Knopp et al., 2015).

While the majority of NP expressed in infected cells exhibits a molecular weight of 60-68 kDa, it is possible to visualize a 28 kDa and 36 kDa cleavage product of NP as well (Harnish et al., 1981). The functional importance of these two truncated NP's is unclear, but at late time points following infection (up to 20 days post infection), staining of NP in nuclear inclusions was observed in infected cells only when monoclonal antibodies capable of recognizing these short forms of NP were used (Young et al., 1987).

The first evidence to explain a potential role for these truncated NPs came with the observations that JUNV NP appeared to be cleaved by caspases and that expression of ectopic JUNV NP could prevent the activation of the effector caspase 3, a critical event in

the execution of apoptosis (Wolff et al., 2013a). Thus, the short forms of NP observed during infection may represent a strategy employed by the virus to prevent apoptosis.

Extensive work has been performed to characterize NP's role in mediating transcription and replication of the arenavirus' ssRNA genome. Expression of NP and the L protein are sufficient for the transcription and replication of a viral minigenome (Lee et al., 2000). A commonly accepted model for the switch from transcription to replication in arenaviruses was that an intergenic region (IGR), which separates the two genes in each viral gene segment, adopts a secondary structure hairpin loop whose formation in a transcribed mRNA leads to transcription termination. It was thought that as levels of NP increased over the course of infection, the IGR would be bound by NP upon exiting the polymerase thus becoming unable to adopt a hairpin, allowing the viral polymerase to proceed and transcribe the full length viral antigenome. This model was supported by the observation that when translation was blocked in cells infected with JUNV or TCRV, transcripts encoding the NP protein but not full length antigenome accumulated (Franze-Fernandez et al., 1987; Tortorici et al., 2001a).

Though appealing, this model for the regulation of viral transcription and replication has not been supported. Instead, it seems that as NP expression increased so did the levels of both viral minigenome replication and transcription (Pinschewer et al., 2003). Because viral mRNAs possess a 5' m^7G cap, and genomic and antigenomic RNAs do not (Meyer and Southern, 1993; Pinschewer et al., 2003; Tortorici et al., 2001a), it is possible that the "decision" to initiate either transcription or replication is made by the viral

polymerase at the moment of primer binding. That is, polymerase bound to a capped primer will prevent the encapsidation of the nascent RNA transcript and secondary structure of the transcribed IGR will terminate elongation. However, if the viral polymerase has bound an uncapped primer, encapsidation of the nascent RNA will occur, the secondary structure of the transcribed IGR will not be allowed to form, and the polymerase will continue until it reaches the end of the gene segment resulting in a full length antigenome (Pinschewer et al., 2003; Tortorici et al., 2001a). The authors hypothesized that increased levels of NP could increase the activity of the viral polymerase in a general manner, as has been observed for viruses in other families (Pinschewer et al., 2003).

The NP of all members of the arenavirus family have been shown to suppress the induction of type I interferon (IFN) expression – with the exception of MOPV whose NP seems to exhibit only weak anti-IFN activity (Martinez-Sobrido et al., 2007; Martinez-Sobrido et al., 2006; Ortiz-Riano et al., 2011; Pannetier et al., 2004). It was shown that expression of NP, in the absence of other viral proteins, was sufficient to prevent activation of the IRF3 responsive promoter (which controls expression of IFN-α/β) and nuclear translocation of IRF3 in response to infection with Sendai virus – a virus known to induce the expression of type I IFN (Martinez-Sobrido et al., 2007; Martinez-Sobrido et al., 2006). Mutational analysis has shown that the C terminal domain of the NP protein mediates the inhibition of the type I IFN response in LCMV (Martinez-Sobrido et al., 2009). Specifically, residues 382-386 were shown to be critical for the inhibition of the induction of IFN-β in LCMV and LASV (Carnec et al., 2011; Martinez-Sobrido et al., 2009). The

equivalent residues were shown to be present in the 3'-5' exoribonuclease domain of LASV NP (Hastie et al., 2011b; Qi et al., 2010).

The 3'-5' exoribonuclease domain of LASV NP is capable of degrading a wide range of dsRNA substrates, including arenaviral RNAs and Poly I:C (Hastie et al., 2011a; Qi et al., 2010). Moreover, mutation of residues in the exonuclease domain resulted in mutant NPs unable to suppress induction of IFN-β expression (Harmon et al., 2013; Hastie et al., 2011a; Huang et al., 2015; Jiang et al., 2013; Qi et al., 2010). Key residues in the exonuclease domain including G392 and R393 of LASV (corresponding to LCMV NP G385 and R386) are conserved in the primary sequence of every mammarenavirus (Harmon et al., 2013; Jiang et al., 2013; Qi et al., 2010). Mutation of these catalytic residues has been shown to inhibit the growth of mutant recombinant virus in cell lines known to have intact type I IFN signaling pathways as well as in *in vivo* models of infection (Huang et al., 2015; Pannetier et al., 2014; Russier et al., 2014).

RIG-I and MDA5 were both shown to be important in the detection of LCMV infection and the induction of IFN-β expression. It was shown that these two cytoplasmic sensors bound LCMV RNA. However, LCMV NP was able to suppress the induction of IFN- β by RIG-I and MDA5. NP, RIG-I and MDA5 were shown to physically associate which may be important for its inhibitory role in this signaling pathway (Zhou et al., 2010). Additionally, LCMV NP has been shown to interact with the kinase IKKε. This is significant because IKKε is a kinase important for type I IFN induction downstream of RIG-I. (Pythoud et al., 2012). In contrast to other arenaviruses, JUNV infection results in

robust induction of type I IFN expression, and this induction is dependent on RIG-I expression (Huang et al., 2012). Nevertheless, JUNV infection is unaffected by IFN treatment suggesting that it has additional mechanisms to evade a host antiviral response (Huang et al., 2012). Both New World and Old World NPs were shown to prevent the nuclear translocation of NF-κB and the activation of transcription of NF-κB responsive genes providing another way that arenaviruses may negatively modulate the amplitude of the host's innate immune response (Rodrigo et al., 2012).

Despite the putative role of truncated forms of NP in inhibition of apoptosis (Wolff et al., 2013a), in some cases, infected cells can undergo apoptosis. It appears that RIG-I signaling can lead to the initiation of the apoptotic pathway in JUNV infected cells (Kolokoltsova et al., 2014; Pythoud et al., 2015). While it was shown that LCMV effectively inhibits the induction of type I IFN through the activation of RIG-I, RIG-I induced apoptosis, a parallel, non-overlapping pathway, remained fully active in LCMV infected cells (Pythoud et al., 2015). In the case of JUNV infection, it is unclear to what extent the caspase decoy function of NP may play in modulating apoptosis, and the effect of viral strain, cell type, timing, and other variables remain to be explored.

The interaction of NP with other viral proteins is important at multiple steps in the arenavirus life cycle. While LCMV NP was shown to localize with GP in one study, this result has not been reproduced in other members of the arenavirus family (Burns and Buchmeier, 1991; Schlie et al., 2010). NP has been shown to interact with L polymerase from TCRV, LASV, MOPV, and LCMV (Jacamo et al., 2003; Kerber et al., 2011). While

the functional relevance of the NP-L interaction has yet to be defined, it was shown that within the Old World arenavirus clade, the activity of the MOPV and LASV L polymerase could be heterologously complemented by either MOPV, LASV, or LCMV NP. However, the activity of the LCMV L polymerase could not be complemented by MOPV or LASV NP (Kerber et al., 2011). Further, it appears that this interaction may be mediated via the viral genomic RNA and specifically the 3' and 5' UTRs (Iwasaki et al., 2015).

NP has been shown to interact with Z for all arenavirus species examined, with the exception of MOPV and TCRV (Casabona et al., 2009; Eichler et al., 2004; Jacamo et al., 2003; Ortiz-Riano et al., 2011; Salvato et al., 1992; Shtanko et al., 2010; Shtanko et al., 2011). The NP-Z interaction is purported to be important in the assembly of budding viral particles. While Z protein alone is sufficient to direct the budding of VLPs, the expression of NP along with Z can may be important for the recruitment of RNPs into budding particles (Casabona et al., 2009; Groseth et al., 2010; Ortiz-Riano et al., 2011; Schlie et al., 2010). The ability to interact with Z was mapped to the C terminal domain of NP, but mutation to key residues resulting in the loss of IFN inhibitory activity did not affect the ability of NP to bind Z suggesting that these two functions of the C terminal domain of NP are independent of each other (Ortiz-Riano et al., 2011).

In addition to NP's ability to interact with other viral proteins, NP has also been shown to interact with cellular proteins. JUNV NP was shown to interact with hnRNP A1/A2. hnRNP A1/A2 are RNA binding proteins which shuttle between the nucleus and the cytoplasm. While knockdown of these hnRNPs resulted in a defect in viral replication,

the mechanism of why this interaction could be important is, as yet, unknown (Maeto et al., 2011). Furthermore, LCMV NP was shown to interact with the intermediate filament protein Keratin 1. Cells infected with LCMV were shown to have a more extensive Keratin network than uninfected cells and an increased concentration of desmosomes at sites of cell to cell contact (Labudova et al., 2009). The increased stability of the intermediate filament network and increased cell contacts observed in LCMV infected cells facilitated the efficient transmission of virus between cells. Disruption of the keratin network resulted in decreased cell to cell transmission of virus (Labudova et al., 2009). MOPV NP and Z were both shown to interact with the ALIX/AIP1, part of the cellular ESCRT pathway – a protein complex involved in the budding of vesicles into multivesicular bodies (MVBs) (Shtanko et al., 2011). It appears that AIP1 interaction bridges NP and Z and may thus play a role in promoting RNP recruitment into budding MOPV particles (Shtanko et al., 2011).

Lastly, it was shown that NP may play an important role in regulating host cellular translation (Linero et al., 2011). Infection with JUNV as well ectopic expression of NP or GPC was able to prevent the formation of stress granules in response to cellular stress (Linero et al., 2011). Stress granules are transient non-membrane bound accumulations of stalled small ribosomal subunits along with their bound cap-dependent mRNA transcripts. Stress granules are temporary depots of non-essential transcripts and their accompanying translation machinery that are formed in response to a variety of cellular stresses that activate a member of the eIF2AK family of kinases, whose role it is to phosphorylate eIF2α and stall global cap-dependent translation. This permits the selective translation of stress

response mRNAs bearing alternate translation initiation signals such as internal ribosomal entry sites (IRES). Importantly, stress granules can dissolve following the resolution of the cellular stress and the resident mRNAs can re-enter the pool of actively translating cellular mRNAs (Anderson and Kedersha, 2008; Buchan and Parker, 2009; Thomas et al., 2011). As the stress of viral infection can initiate the formation of stress granules, many viruses have been shown to interfere with stress granule formation, function, and/or hijack stress granules to promote their own replication (Reineke and Lloyd, 2013; Valiente-Echeverria et al., 2012; White and Lloyd, 2012). How, then, JUNV NP (and/or GPC) may be affecting viral translation is a fascinating question. It is possible that JUNV NP's ability to interact with the eIF4 complex to promote cap-dependent translation (Linero et al., 2013) along with other, as yet, undescribed mechanisms may all play important roles in maintaining high rates of translation in infected cells.

The arenavirus nucleoprotein clearly performs many roles in the life cycle of the virus. While its classical role has been considered to be the encapsidation of the viral genomic and antigenomic RNA, NP's role in interacting with other viral proteins as well as inhibiting a cellular IFN response are also beginning to be appreciated. Crystal strutures of LASV NP have provided new insight into the molecular mechanism by which NP is able to perform such diverse functions as binding viral RNA, degrading immunogenic viral RNA, and self-associate in higher order trimeric structures. It appears that the ability of NP to associate with the viral Z protein may also be of great importance to direct the viral RNPs into budding virions. While still poorly understood, NP's ability to interact with host

proteins also seems to be important. There remains much work to be done in these veins to more fully understand the interplay between arenavirus and host in the pathogenesis of arenaviral infections.

1.6. Summary

Arenaviruses remain major public health threats in developed countries where populations are in constant exposure to LCMV and also worldwide where infection with Lassa virus and several South American viruses cause extremely dangerous hemorrhagic fever in infected individuals. Despite great effort, significant gaps remain in our understanding of the viral life cycle and in our appreciation of how the virus takes advantage of the host cell to its own benefit. These gaps in our understanding of arenavirus biology are highlighted by our limited arsenal of available preventive and antiviral therapeutic options. We believe that the development of new, more effective antiviral strategies will likely depend upon the elucidation of key aspects of basic arenavirus biology.

Toward this ambitious goal, a good starting point is to better understand the regulation of viral gene expression and genome replication, how the virus may be compartmentalizing these events within specific subcellular niches, and how the major viral protein component of the viral RNP, the viral nucleoprotein, may be playing heretofore unappreciated accessory roles to promote these and other steps of the viral life cycle. It was our hope that the work in this dissertation would help us better understand

how these viruses are able to establish persistent infections and how they are able to cause such severe disease in humans but asymptomatic infections in their rodent reservoir.

1.7. Tables

Table 1.1. Members of the genus *Mammarenavirus*
Viruses of the family *Arenaviridae*, their geographic distribution, reservoirs and associated human diseases. Adapted from Viruses, 5(2), S. Wolff, H. Ebihara, and A. Groseth, Arenavirus Budding: A Common Pathway with Mechanistic Differences, p. 528-549, 2013, under a Creative Commons Attribution license (CC-BY 4.0).

	Virus	Distribution	Reservoir	Human Disease
Old World	**Dandenong virus***	Yugoslavia, Australia (?)	Unknown	Febrile illness with encephalopathy (transplant-related)
	Gbagroube virus*	Argentina	*Mus (Nannomys) setulosus*	None known
	Ippy virus	Central African Republic	*Arvicanthus spp.*	None known
	Lassa virus	Western Africa	*Mastomys natalensis*	Febrile illness, hemorrhagic fever in severe cases
	Lymphocytic Choriomeningitis virus	Worldwide	*Mus musculus*	Febrile illness, aseptic meningitis in severe cases
	Lujo virus	Zambia	Unknown	Hemorrhagic fever
	Luna virus*	Zambia	*Mastomys natalensis*	None known
	Kodoko virus *	Guinea	*Mus (Nannomys) minutoides*	None known
	Menekre virus*	Côte d'Ivoire	Hylomyscus *spp.*	None known
	Merino Walk virus *	South Africa	*Myotomis unisulcatus*	None known
	Mobala virus	Central African Republic	*Praomys jacksoni*	None known
	Mopeia virus	Mozambique	*Mastomys natalensis*	None known
	Morogoro virus *	Tanzania	*Mastomys spp.*	None known
New World	**Allpahuayo virus**	Peru	*Oecomys spp.*	None known
	Amapari virus	Brazil	*Oryzomys gaeldi Neacomys guianae*	None known
	Bear Canyon virus	USA	Peromyscus californicus	None known
	Big Brushy Tank virus*	USA	*Neotoma albigula*	None known
	Catarina virus *	USA	*Neotoma micropus*	None known
	Chapare virus	Bolivia	Unknown	Hemorrhagic fever
	Cupixi virus	Brazil	*Oryzomys spp.*	None known
	Flexal virus	Brazil	*Oryzomys spp.*	Febrile illness(Lab-acquired)
	Guanarito virus	Venezuela	*Zygodontomys brevicauda*	Hemorrhagic fever
	Junín virus	Argentina	*Calomys musculinus*	Hemorrhagic fever
	Latino virus	Bolivia	*Calomys callosus*	None known
	Machupo virus	Bolivia	*Calomys callosus*	Hemorrhagic fever

	Oliveros virus	Argentina	*Bolomys spp.*	None known
	Paraná virus	Paraguay	*Oryzomys buccinatus*	None known
	Pichinde virus	Columbia	*Oryzomys albigularis*	None known
	Pinhal virus	Brazil	*Calomys tener*	None known
	Pirital virus	Venezuela	*Sigmodon alstoni*	None known
	Real de Catorce virus *	Mexico	*Neotoma leucodon*	None known
	Sabiá virus	Brazil	Unknown	Hemorrhagic fever
	Skinner Tank virus *	USA	*Neotoma mexicana*	None known
	Tacaribe virus	Trinidad	*Artibeus spp.* (bat)	Possible febrile illness (Lab-acquired)
	Tamiami virus	USA	*Sigmodon hispidus*	None known
	Tonto Creek virus	USA	*Neotoma albigula*	None known
	Whitewater Arroyo virus	USA	*Neotoma albigula*	Possible hemorrhagic fever

1.8. Figures

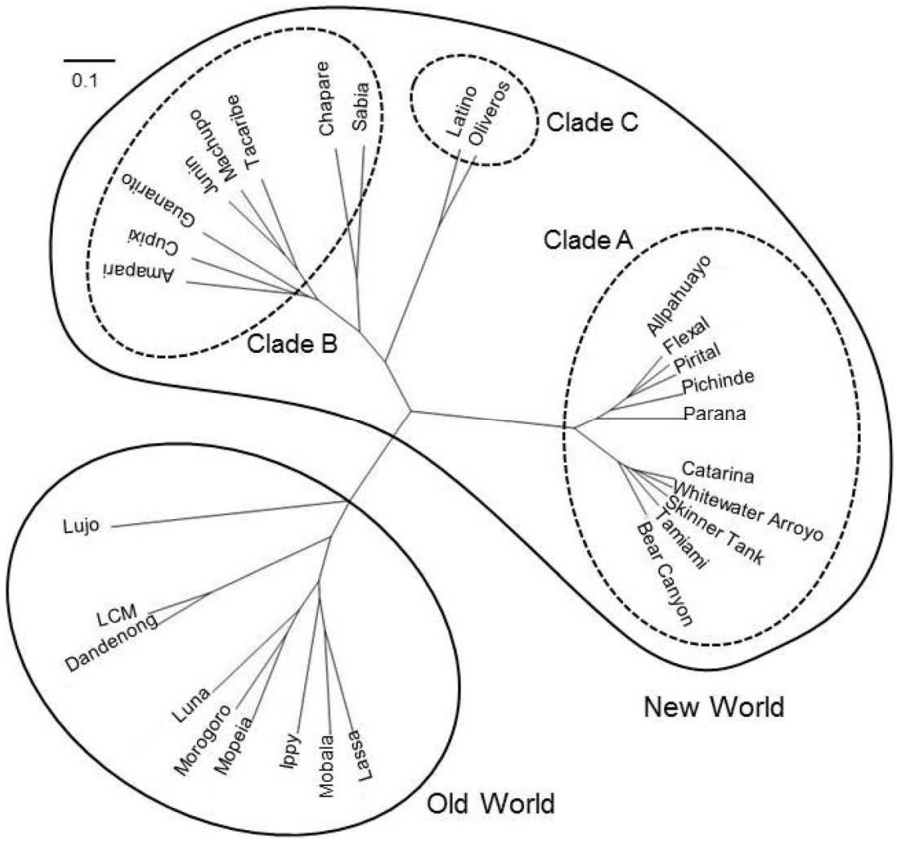

Figure 1.1. Phylogeny of the genus Mammarenavirus
Phylogenetic tree of arenavirus Z protein. Amino acid sequences of Z protein were used for analysis. The phylogenetic tree was drawn using GENETYX [1]. The scale bar indicates substitutions per site. Accession numbers for reference sequences are: ABY20731 (Dandenong), YP_516232 (Ippy), NP_694871.1 (LASV, Josiah), ABC96003 (LCMV, Armstrong), YP_002929492 (Lujo virus), YP_516228 (Mobala virus), ABC71136 (Mopeia virus), YP_003090216 (Morogoro virus), YP_004933732 (Luna virus), YP_001649213 (Allpahuayo virus), AEQ59327 (Bear Canyon virus), AEQ59329 (Catarina virus), YP_001936023 (Flexal virus), YP_001936027 (Parana virus), YP_138535 (Pichinde virus), YP_025092 (Pirital virus), AEQ59336 (Skinner Tank virus), YP_001911119 (Whitewater arroyo virus), YP_001649217 (Amapari virus), YP_001816784 (Chapare virus), YP_001649219 (Cupixi virus), NP_899220 (Guanarito virus), NP_899216 (Junin virus, XJ-13), NP_899215 (Machupo virus), YP_089659 (Sabia virus), Q88470 (Tacaribe virus), YP_001911117 (Tamiami virus), YP_001936025 (Latino virus), YP_001649215 (Oliveros virus). Reproduced from Viruses, 4(10), S. Urata and J. Yasuda, Molecular Mechanism of Arenavirus Assembly and Budding, p. 2049-2079, 2012, under a Creative Commons Attribution license (CC-BY 4.0).

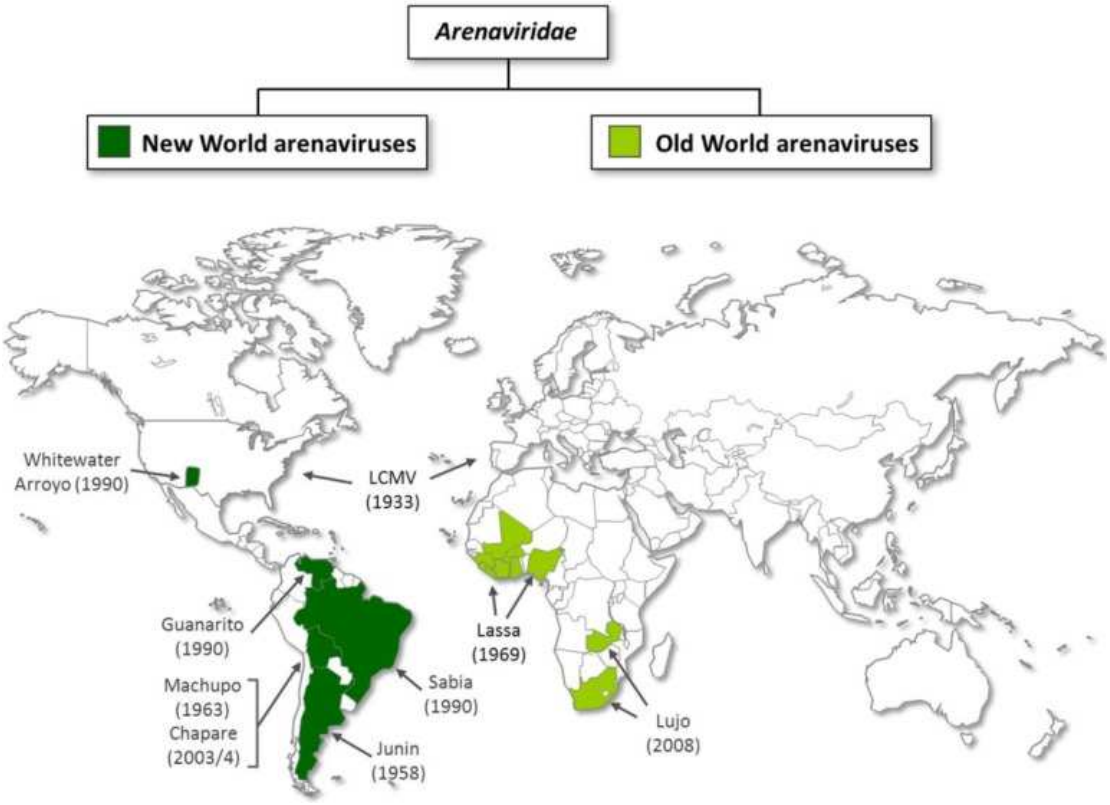

Figure 1.2. Geographic distribution of mammarenaviruses
Geographic distribution of human pathogenic arenaviruses. This map summarizes the distribution of human pathogenic New and Old World mammarenavirus species. The year of the first description is indicated in brackets. Reproduced from Viruses, 4(11), S. K. Fehling, F. Lennartz, and T. Strecker, Multifunctional Nature of the Arenavirus RING Finger Protein Z, p. 2973-3011, 2012, under a Creative Commons Attribution license (CC-BY 4.0).

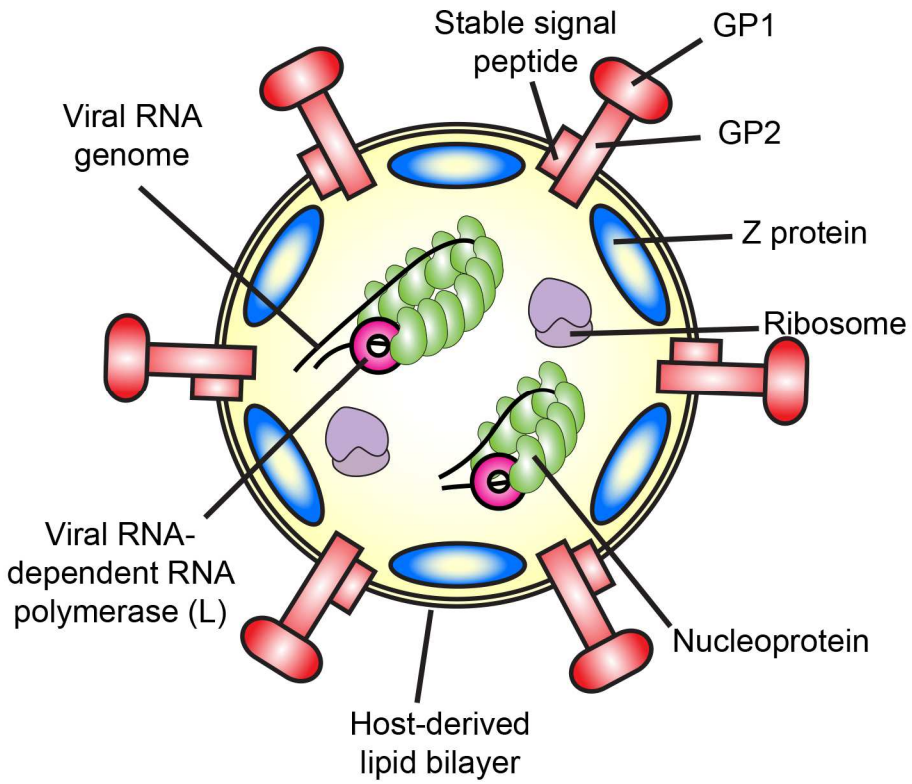

Figure 1.3. Arenavirus particle
Arenavirus particles are enveloped by a host-derived lipid bilayer. The viral envelope glycoprotein is a transmembrane protein made up of three subunits: GP1, GP2, and the SSP. Mature glycoprotein form homotrimers in the viral envelope (not shown). The viral Z protein is the *bona fide* viral matrix protein and is responsible for budding of nascent virions. The viral ribonucleoprotein complexes (vRNP) are made up of the viral genomic RNA, the viral L polymerase, and the viral nucleoprotein (NP). Though their functional relevance is unclear, arenaviruses also package cellular ribosomes in virions.

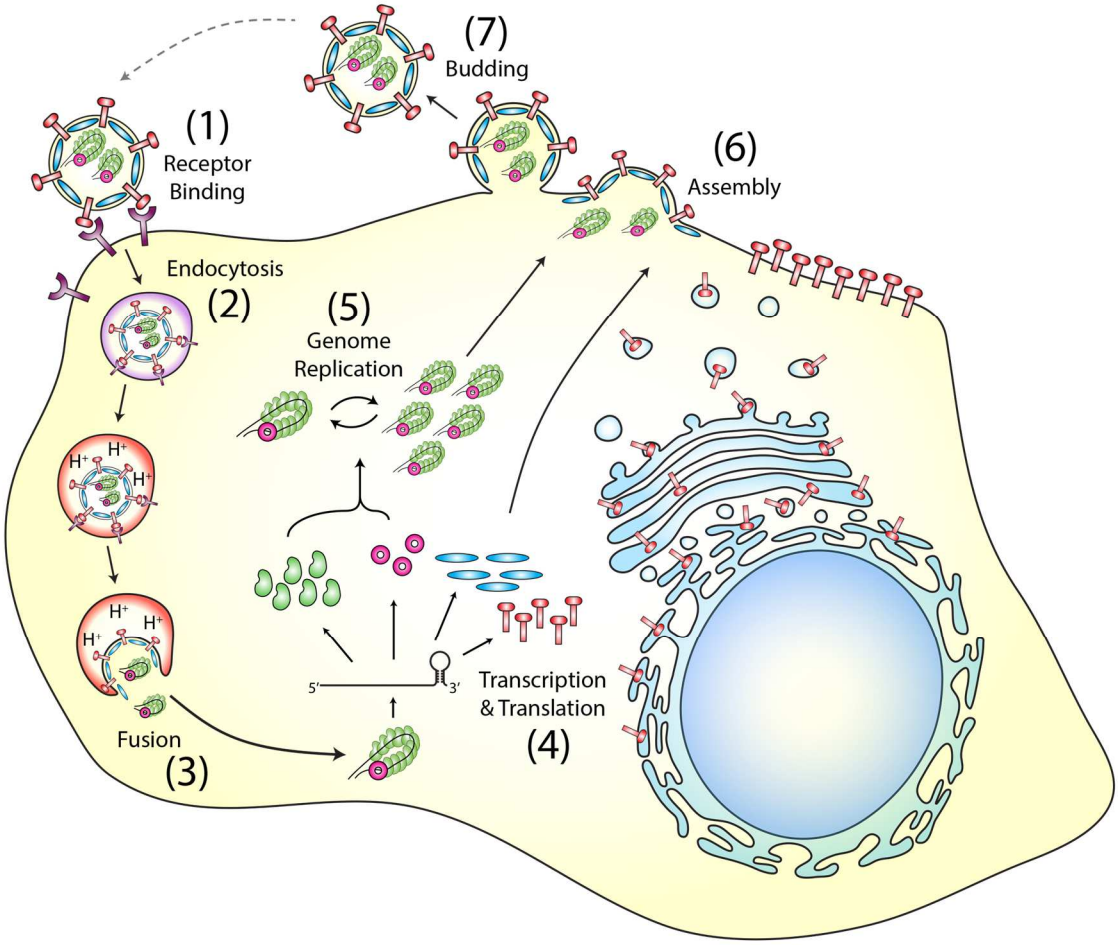

Figure 1.4. Arenavirus Life cycle
(1) The arenavirus life cycle begins with the envelope glycoprotein binding to its cell surface receptor. (2) Receptor binding triggers the uptake of the viral particle into an endocytic compartment. (3) Endosome acidification triggers a conformation change in GP2 and the fusion of the viral envelope with the endosomal membrane. (4) The released RNP is transcribed in the cytoplasm and viral mRNAs are translated into protein by host ribosomes. (5) Upon accumulation of viral protein, full length replication of the viral genomic RNA is permitted. (6) The individual viral protein and RNA components assemble and (7) bud as newly formed infectious virions from the cellular plasma membrane.

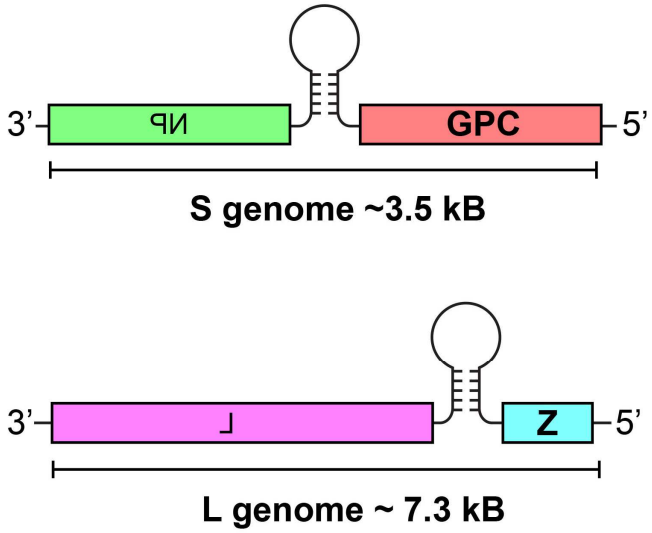

Figure 1.5. Arenavirus genomic organization
The single-stranded, negative-sense RNA genome is contained on two segments. The S segment encodes the NP gene in a negative orientation and the GPC gene in a pseudo-positive orientation. The L segment encodes the L gene in a negative orientation and the Z gene in a pseudo-positive orientation. For both the S and the L segment the two encoded gene products are separated by an intergenic region (IGR) that adopts a hairpin secondary structure and serves as the transcription termination signal. There are 3' and 5' untranslated regions (UTR) that provide critical sequence information needed for L polymerase recruitment and viral gene transcription and genome replication.

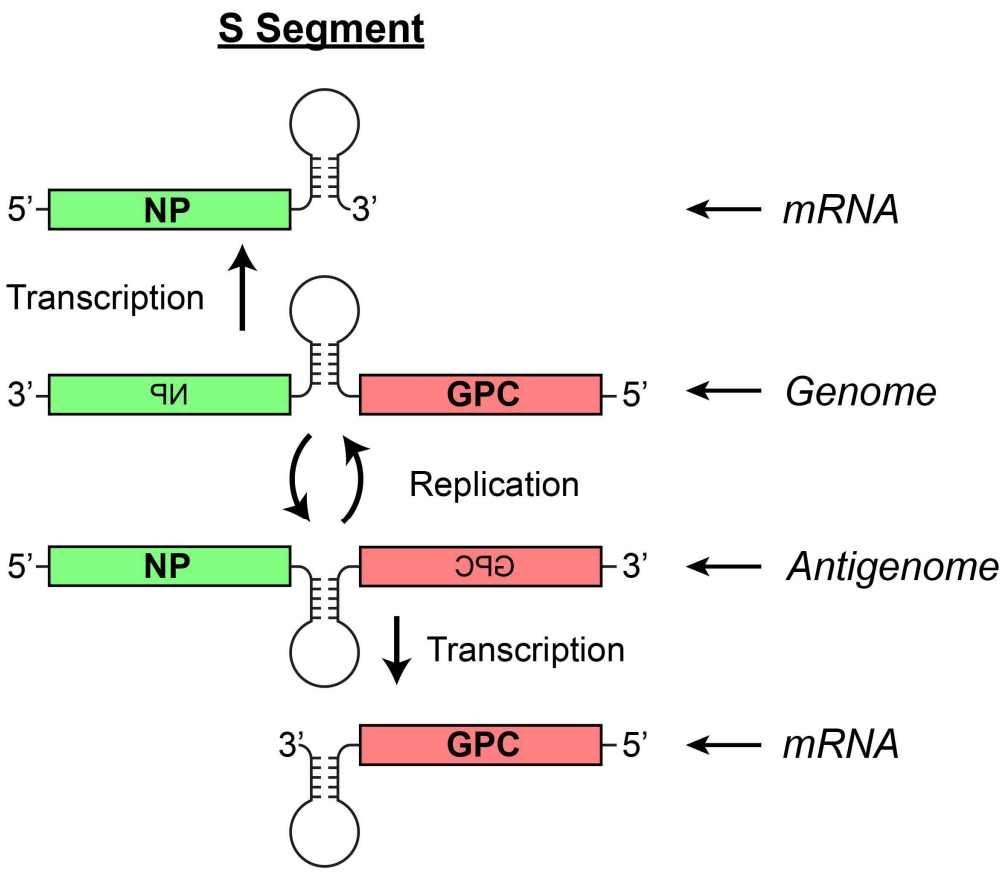

Figure 1.6. Arenavirus genomic RNA transcription and replication
The events of viral genome transcription are shown. The order of all events is identical for both the S and the L segment. For simplicity, only the S segment is shown. (1) First, the NP gene (the gene encoded a negative orientation) is transcribed by the viral L polymerase. The NP mRNA can be translated by cellular ribosomes. Upon accumulation of viral antigen, a switch to full length genome replication (2) occurs. The full-length RNA molecule complementary to the viral genome is called the antigenome. It serves as both the template for replication of more genomic RNA and (3) the transcription of the GPC gene (now in a negative orientation). The GPC mRNA can be translated into protein by cellular ribosomes.

1.9. References

Ambrosio, A., Saavedra, M., Mariani, M., Gamboa, G., and Maiza, A. (2011). Argentine hemorrhagic fever vaccines. Hum Vaccin *7*, 694-700.

Amorim, M.J., Bruce, E.A., Read, E.K., Foeglein, A., Mahen, R., Stuart, A.D., and Digard, P. (2011). A Rab11- and microtubule-dependent mechanism for cytoplasmic transport of influenza A virus viral RNA. Journal of virology *85*, 4143-4156.

Anderson, P., and Kedersha, N. (2008). Stress granules: the Tao of RNA triage. Trends Biochem Sci *33*, 141-150.

Armstrong, C., and Dickens, P.F. (1935). Benign Lymphocytic Choriomeningitis (Acute Aseptic Meningitis): A New Disease Entity. Public Health Reports *50*, 831-842.

Armstrong, C., and Lillie, R.D. (1934). Experimental Lymphocytic Choriomeningitis of Monkeys and Mice Produced by a Virus Encountered in Studies of the 1933 St. Louis Encephalitis Epidemic. Public Health Reports *49*, 1019-1027.

Armstrong, C., and Wooley, J.G. (1935). Studies on the Origin of a Newly Discovered Virus Which Causes Lymphocytic Choriomeningitis in Experimental Animals. Public Health Reports *50*, 537-541.

Auperin, D., Dimock, K., Cash, P., Rawls, W.E., Leung, W.C., and Bishop, D.H. (1982a). Analyses of the genomes of prototype pichinde arenavirus and a virulent derivative of Pichinde Munchique: evidence for sequence conservation at the 3' termini of their viral RNA species. Virology *116*, 363-367.

Auperin, D.D., Compans, R.W., and Bishop, D.H. (1982b). Nucleotide sequence conservation at the 3' termini of the virion RNA species of New World and Old World arenaviruses. Virology *121*, 200-203.

Auperin, D.D., Galinski, M., and Bishop, D.H. (1984a). The sequences of the N protein gene and intergenic region of the S RNA of pichinde arenavirus. Virology *134*, 208-219.

Auperin, D.D., Romanowski, V., Galinski, M., and Bishop, D.H. (1984b). Sequencing studies of pichinde arenavirus S RNA indicate a novel coding strategy, an ambisense viral S RNA. Journal of virology *52*, 897-904.

Baird, N.L., York, J., and Nunberg, J.H. (2012). Arenavirus infection induces discrete cytosolic structures for RNA replication. Journal of virology *86*, 11301-11310.

Bausch, D.G., Hadi, C.M., Khan, S.H., and Lertora, J.J. (2010). Review of the literature and proposed guidelines for the use of oral ribavirin as postexposure prophylaxis for Lassa fever. Clin Infect Dis *51*, 1435-1441.

Bodewes, R., Raj, V.S., Kik, M.J., Schapendonk, C.M., Haagmans, B.L., Smits, S.L., and Osterhaus, A.D. (2014). Updated phylogenetic analysis of arenaviruses detected in boid snakes. Journal of virology *88*, 1399-1400.

Bonthius, D.J. (2009). Lymphocytic choriomeningitis virus: a prenatal and postnatal threat. Adv Pediatr *56*, 75-86.

Bonthius, D.J. (2012). Lymphocytic choriomeningitis virus: an underrecognized cause of neurologic disease in the fetus, child, and adult. Semin Pediatr Neurol *19*, 89-95.

Bruce, E.A., Digard, P., and Stuart, A.D. (2010). The Rab11 pathway is required for influenza A virus budding and filament formation. Journal of virology *84*, 5848-5859.

Brunotte, L., Kerber, R., Shang, W., Hauer, F., Hass, M., Gabriel, M., Lelke, M., Busch, C., Stark, H., Svergun, D.I., Betzel, C., Perbandt, M., and Gunther, S. (2011). Structure of the Lassa virus nucleoprotein revealed by X-ray crystallography, small-angle X-ray scattering, and electron microscopy. The Journal of biological chemistry *286*, 38748-38756.

Buchan, J.R., and Parker, R. (2009). Eukaryotic stress granules: the ins and outs of translation. Molecular cell *36*, 932-941.

Buchmeier, M.J. (2002). Arenaviruses: protein structure and function. Current topics in microbiology and immunology *262*, 159-173.

Buchmeier, M.J., de la Torre, J.C., and Peters, C.J. (2013). Arenaviridae. In Fields Virology, D.M. Knipe, P.M. Howley, J.I. Cohen, D.E. Griffin, R.A. Lamb, M.A. Martin, V.R. Racaniello, and B. Roizman, eds. (Philadelphia, PA: Wolters Kluwer Heath/Lippincott Williams & Wilkins), pp. 1283-1303.

Burns, J.W., and Buchmeier, M.J. (1991). Protein-protein interactions in lymphocytic choriomeningitis virus. Virology *183*, 620-629.

Burns, J.W., and Buchmeier, M.J. (1993). Glycoproteins of the arenaviruses. In The Arenaviridae, M.S. Salvato, ed. (New York: Plenum Press), pp. 17-35.

Burri, D.J., da Palma, J.R., Kunz, S., and Pasquato, A. (2012). Envelope glycoprotein of arenaviruses. Viruses *4*, 2162-2181.

Carnec, X., Baize, S., Reynard, S., Diancourt, L., Caro, V., Tordo, N., and Bouloy, M. (2011). Lassa virus nucleoprotein mutants generated by reverse genetics induce a robust type I interferon response in human dendritic cells and macrophages. Journal of virology *85*, 12093-12097.

Carter, M.F., Biswal, N., and Rawls, W.E. (1973). Characterization of nucleic acid of pichinde virus. Journal of virology *11*, 61-68.

Carter, M.F., Biswal, N., and Rawls, W.E. (1974). Polymerase activity of Pichinde virus. Journal of virology *13*, 577-583.

Casabona, J.C., Levingston Macleod, J.M., Loureiro, M.E., Gomez, G.A., and Lopez, N. (2009). The RING domain and the L79 residue of Z protein are involved in both the rescue of nucleocapsids and the incorporation of glycoproteins into infectious chimeric arenavirus-like particles. Journal of virology *83*, 7029-7039.

Chan, Y.K., and Gack, M.U. (2016). Viral evasion of intracellular DNA and RNA sensing. Nature reviews. Microbiology *14*, 360-373.

Charrel, R.N., Coutard, B., Baronti, C., Canard, B., Nougairede, A., Frangeul, A., Morin, B., Jamal, S., Schmidt, C.L., Hilgenfeld, R., Klempa, B., and de Lamballerie, X. (2011). Arenaviruses and hantaviruses: from epidemiology and genomics to antivirals. Antiviral Res *90*, 102-114.

Charrel, R.N., and de Lamballerie, X. (2003). Arenaviruses other than Lassa virus. Antiviral Res *57*, 89-100.

Charrel, R.N., and de Lamballerie, X. (2010). Zoonotic aspects of arenavirus infections. Vet Microbiol *140*, 213-220.

Charrel, R.N., de Lamballerie, X., and Emonet, S. (2008). Phylogeny of the genus Arenavirus. Curr Opin Microbiol *11*, 362-368.

Charrel, R.N., Lemasson, J.J., Garbutt, M., Khelifa, R., De Micco, P., Feldmann, H., and de Lamballerie, X. (2003). New insights into the evolutionary relationships between arenaviruses provided by comparative analysis of small and large segment sequences. Virology *317*, 191-196.

Cornu, T.I., and de la Torre, J.C. (2001). RING finger Z protein of lymphocytic choriomeningitis virus (LCMV) inhibits transcription and RNA replication of an LCMV S-segment minigenome. Journal of virology *75*, 9415-9426.

Cornu, T.I., and de la Torre, J.C. (2002). Characterization of the arenavirus RING finger Z protein regions required for Z-mediated inhibition of viral RNA synthesis. Journal of virology *76*, 6678-6688.

D'Antuono, A., Loureiro, M.E., Foscaldi, S., Marino-Buslje, C., and Lopez, N. (2014). Differential contributions of tacaribe arenavirus nucleoprotein N-terminal and C-terminal residues to nucleocapsid functional activity. Journal of virology *88*, 6492-6505.

den Boon, J.A., and Ahlquist, P. (2010). Organelle-like membrane compartmentalization of positive-strand RNA virus replication factories. Annual review of microbiology *64*, 241-256.

den Boon, J.A., Diaz, A., and Ahlquist, P. (2010). Cytoplasmic viral replication complexes. Cell host & microbe *8*, 77-85.

Eichler, R., Strecker, T., Kolesnikova, L., ter Meulen, J., Weissenhorn, W., Becker, S., Klenk, H.D., Garten, W., and Lenz, O. (2004). Characterization of the Lassa virus matrix protein Z: electron microscopic study of virus-like particles and interaction with the nucleoprotein (NP). Virus research *100*, 249-255.

Ellenberg, P., Edreira, M., Lozano, M., and Scolaro, L. (2002). Synthesis and expression of viral antigens in Vero cells persistently infected with Junin virus. Archives of virology *147*, 1543-1557.

Ellenberg, P., Edreira, M., and Scolaro, L. (2004). Resistance to superinfection of Vero cells persistently infected with Junin virus. Archives of virology *149*, 507-522.

Emonet, S., Lemasson, J.J., Gonzalez, J.P., de Lamballerie, X., and Charrel, R.N. (2006). Phylogeny and evolution of old world arenaviruses. Virology *350*, 251-257.

Farber, F.E., and Rawls, W.E. (1975). Isolation of ribosome-like sturctures from Pichinde virus. The Journal of general virology *26*, 21-31.

Fehling, S.K., Lennartz, F., and Strecker, T. (2012). Multifunctional nature of the arenavirus RING finger protein Z. Viruses *4*, 2973-3011.

Ferron, F., Weber, F., de la Torre, J.C., and Reguera, J. (2017). Transcription and replication mechanisms of Bunyaviridae and Arenaviridae L proteins. Virus research *234*, 118-134.

Findlay, G.M., Alcock, N.S., and Stern, R.O. (1936). The Virus Ætiology Of One Form Of Lymphocytic Meningitis. Lancet *227*, 650-654.

Fischer, S.A., Graham, M.B., Kuehnert, M.J., Kotton, C.N., Srinivasan, A., Marty, F.M., Comer, J.A., Guarner, J., Paddock, C.D., DeMeo, D.L., Shieh, W.J., Erickson, B.R., Bandy, U., DeMaria, A., Jr., Davis, J.P., Delmonico, F.L., Pavlin, B., Likos, A., Vincent, M.J., Sealy, T.K., Goldsmith, C.S., Jernigan, D.B., Rollin, P.E., Packard, M.M., Patel, M., Rowland, C., Helfand, R.F., Nichol, S.T., Fishman, J.A., Ksiazek, T., Zaki, S.R., and Team, L.i.T.R.I. (2006). Transmission of lymphocytic choriomeningitis virus by organ transplantation. N Engl J Med *354*, 2235-2249.

Francis, S.J., and Southern, P.J. (1988a). Deleted viral RNAs and lymphocytic choriomeningitis virus persistence in vitro. The Journal of general virology *69 (Pt 8)*, 1893-1902.

Francis, S.J., and Southern, P.J. (1988b). Molecular analysis of viral RNAs in mice persistently infected with lymphocytic choriomeningitis virus. Journal of virology *62*, 1251-1257.

Francis, S.J., Southern, P.J., Valsamakis, A., and Oldstone, M.B. (1987). State of viral genome and proteins during persistent lymphocytic choriomeningitis virus infection. Current topics in microbiology and immunology *133*, 67-88.

Franze-Fernandez, M.T., Zetina, C., Iapalucci, S., Lucero, M.A., Bouissou, C., Lopez, R., Rey, O., Daheli, M., Cohen, G.N., and Zakin, M.M. (1987). Molecular structure and early events in the replication of Tacaribe arenavirus S RNA. Virus research *7*, 309-324.

Fuller-Pace, F.V., and Southern, P.J. (1988). Temporal analysis of transcription and replication during acute infection with lymphocytic choriomeningitis virus. Virology *162*, 260-263.

Garcin, D., and Kolakofsky, D. (1990). A novel mechanism for the initiation of Tacaribe arenavirus genome replication. Journal of virology *64*, 6196-6203.

Garcin, D., and Kolakofsky, D. (1992). Tacaribe arenavirus RNA synthesis in vitro is primer dependent and suggests an unusual model for the initiation of genome replication. Journal of virology *66*, 1370-1376.

Grant, A., Seregin, A., Huang, C., Kolokoltsova, O., Brasier, A., Peters, C., and Paessler, S. (2012). Junin virus pathogenesis and virus replication. Viruses *4*, 2317-2339.

Groseth, A., Wolff, S., Strecker, T., Hoenen, T., and Becker, S. (2010). Efficient budding of the tacaribe virus matrix protein z requires the nucleoprotein. Journal of virology *84*, 3603-3611.

Haist, K., Ziegler, C., and Botten, J. (2015). Strand-Specific Quantitative Reverse Transcription-Polymerase Chain Reaction Assay for Measurement of Arenavirus Genomic and Antigenomic RNAs. PloS one *10*, e0120043.

Harmon, B., Kozina, C., Maar, D., Carpenter, T.S., Branda, C.S., Negrete, O.A., and Carson, B.D. (2013). Identification of critical amino acids within the nucleoprotein of Tacaribe virus important for anti-interferon activity. The Journal of biological chemistry *288*, 8702-8711.

Harnish, D.G., Leung, W.C., and Rawls, W.E. (1981). Characterization of polypeptides immunoprecipitable from Pichinde virus-infected BHK-21 cells. Journal of virology *38*, 840-848.

Hass, M., Westerkofsky, M., Muller, S., Becker-Ziaja, B., Busch, C., and Gunther, S. (2006). Mutational analysis of the lassa virus promoter. Journal of virology *80*, 12414-12419.

Hastie, K.M., Kimberlin, C.R., Zandonatti, M.A., MacRae, I.J., and Saphire, E.O. (2011a). Structure of the Lassa virus nucleoprotein reveals a dsRNA-specific 3' to 5' exonuclease activity essential for immune suppression. Proceedings of the National Academy of Sciences of the United States of America *108*, 2396-2401.

Hastie, K.M., Liu, T., Li, S., King, L.B., Ngo, N., Zandonatti, M.A., Woods, V.L., Jr., de la Torre, J.C., and Saphire, E.O. (2011b). Crystal structure of the Lassa virus nucleoprotein-RNA complex reveals a gating mechanism for RNA binding. Proceedings of the National Academy of Sciences of the United States of America *108*, 19365-19370.

Hotchin, J. (1973). Transient virus infection: spontaneous recovery mechanism of lymphocytic choriomeningitis virrus-infected cells. Nat New Biol *241*, 270-272.

Hotchin, J. (1974a). Cyclical phenomena in persistent virus infection. J Reticuloendothel Soc *15*, 304-311.

Hotchin, J. (1974b). The role of transient infection in arenavirus persistence. Prog Med Virol *18*, 81-93.

Hotchin, J., Kinch, W., Benson, L., and Sikora, E. (1975). Role of substrains in persistent lymphocytic choriomeningitis virus infection. Bull World Health Organ *52*, 457-463.

Howard, C.R., and Buchmeier, M.J. (1983). A protein kinase activity in lymphocytic choriomeningitis virus and identification of the phosphorylated product using monoclonal antibody. Virology *126*, 538-547.

Huang, A.S. (1973). Defective interfering viruses. Annual review of microbiology *27*, 101-117.

Huang, A.S., and Baltimore, D. (1970). Defective viral particles and viral disease processes. Nature *226*, 325-327.

Huang, C., Kolokoltsova, O.A., Yun, N.E., Seregin, A.V., Poussard, A.L., Walker, A.G., Brasier, A.R., Zhao, Y., Tian, B., de la Torre, J.C., and Paessler, S. (2012). Junin virus infection activates the type I interferon pathway in a RIG-I-dependent manner. PLoS Negl Trop Dis *6*, e1659.

Huang, Q., Shao, J., Lan, S., Zhou, Y., Xing, J., Dong, C., Liang, Y., and Ly, H. (2015). In vitro and in vivo characterizations of pichinde viral nucleoprotein exoribonuclease functions. Journal of virology *89*, 6595-6607.

Iapalucci, S., Chernavsky, A., Rossi, C., Burgin, M.J., and Franze-Fernandez, M.T. (1994). Tacaribe virus gene expression in cytopathic and non-cytopathic infections. Virology *200*, 613-622.

Iapalucci, S., Lopez, N., and Franze-Fernandez, M.T. (1991). The 3' end termini of the Tacaribe arenavirus subgenomic RNAs. Virology *182*, 269-278.

ICTV, A.S.G. (2014a). Create a new genus, Reptarenavirus, comprising three new species in the family
Arenaviridae. (Internation Committee on the Taxonomy of Viruses).

ICTV, A.S.G. (2014b). Rename one (1) genus and twenty-five (25) species in the family Arenaviridae. (International Committee on Taxonomy of Viruses
).

Iwasaki, M., Cubitt, B., Sullivan, B.M., and de la Torre, J.C. (2016). The High Degree of Sequence Plasticity of the Arenavirus Noncoding Intergenic Region (IGR) Enables the Use of a Nonviral Universal Synthetic IGR To Attenuate Arenaviruses. Journal of virology *90*, 3187-3197.

Iwasaki, M., Ngo, N., Cubitt, B., and de la Torre, J.C. (2015). Efficient Interaction between Arenavirus Nucleoprotein (NP) and RNA-Dependent RNA Polymerase (L) Is Mediated by the Virus Nucleocapsid (NP-RNA) Template. Journal of virology *89*, 5734-5738.

Jacamo, R., Lopez, N., Wilda, M., and Franze-Fernandez, M.T. (2003). Tacaribe virus Z protein interacts with the L polymerase protein to inhibit viral RNA synthesis. Journal of virology *77*, 10383-10393.

Jiang, X., Huang, Q., Wang, W., Dong, H., Ly, H., Liang, Y., and Dong, C. (2013). Structures of arenaviral nucleoproteins with triphosphate dsRNA reveal a unique mechanism of immune suppression. The Journal of biological chemistry *288*, 16949-16959.

Kerber, R., Rieger, T., Busch, C., Flatz, L., Pinschewer, D.D., Kummerer, B.M., and Gunther, S. (2011). Cross-species analysis of the replication complex of old world arenaviruses reveals two nucleoprotein sites involved in L protein function. Journal of virology *85*, 12518-12528.

Knopp, K.A., Ngo, T., Gershon, P.D., and Buchmeier, M.J. (2015). Single nucleoprotein residue modulates arenavirus replication complex formation. mBio *6*, e00524-00515.

Kolokoltsova, O.A., Grant, A.M., Huang, C., Smith, J.K., Poussard, A.L., Tian, B., Brasier, A.R., Peters, C.J., Tseng, C.T., de la Torre, J.C., and Paessler, S. (2014). RIG-I enhanced interferon independent apoptosis upon Junin virus infection. PloS one *9*, e99610.

Kranzusch, P.J., and Whelan, S.P. (2011). Arenavirus Z protein controls viral RNA synthesis by locking a polymerase-promoter complex. Proceedings of the National Academy of Sciences of the United States of America *108*, 19743-19748.

Labudova, M., Tomaskova, J., Skultety, L., Pastorek, J., and Pastorekova, S. (2009). The nucleoprotein of lymphocytic choriomeningitis virus facilitates spread of persistent infection through stabilization of the keratin network. Journal of virology *83*, 7842-7849.

Lan, S., McLay, L., Aronson, J., Ly, H., and Liang, Y. (2008). Genome comparison of virulent and avirulent strains of the Pichinde arenavirus. Archives of virology *153*, 1241-1250.

Lee, K.J., Novella, I.S., Teng, M.N., Oldstone, M.B., and de La Torre, J.C. (2000). NP and L proteins of lymphocytic choriomeningitis virus (LCMV) are sufficient for efficient transcription and replication of LCMV genomic RNA analogs. Journal of virology *74*, 3470-3477.

Lehmann-Grube, F. (1967). A carrier state of lymphocytic choriomeningitis virus in L cell cultures. Nature *213*, 770-773.

Lehmann-Grube, F. (1971). Lymphocytic choriomeningitis virus, Vol 10 (Wien: Springer-Verlag).

Lehmann-Grube, F., Slenczka, W., and Tees, R. (1969). A persistent and inapparent infection of L cells with the virus of lymphocytic choriomeningitis. The Journal of general virology *5*, 63-81.

Lennartz, F., Hoenen, T., Lehmann, M., Groseth, A., and Garten, W. (2013). The role of oligomerization for the biological functions of the arenavirus nucleoprotein. Archives of virology *158*, 1895-1905.

Leung, W.C., Ghosh, H.P., and Rawls, W.E. (1977). Strandedness of Pichinde virus RNA. Journal of virology *22*, 235-237.

Leung, W.C., and Rawls, W.E. (1977). Virion-associated ribosomes are not required for the replication of Pichinde virus. Virology *81*, 174-176.

Levingston Macleod, J.M., D'Antuono, A., Loureiro, M.E., Casabona, J.C., Gomez, G.A., and Lopez, N. (2011). Identification of two functional domains within the arenavirus nucleoprotein. Journal of virology *85*, 2012-2023.

Linero, F., Welnowska, E., Carrasco, L., and Scolaro, L. (2013). Participation of eIF4F complex in Junin virus infection: blockage of eIF4E does not impair virus replication. Cellular microbiology *15*, 1766-1782.

Linero, F.N., Thomas, M.G., Boccaccio, G.L., and Scolaro, L.A. (2011). Junin virus infection impairs stress-granule formation in Vero cells treated with arsenite via inhibition of eIF2alpha phosphorylation. The Journal of general virology *92*, 2889-2899.

Lopez, N., and Franze-Fernandez, M.T. (2007). A single stem-loop structure in Tacaribe arenavirus intergenic region is essential for transcription termination but is not required for a correct initiation of transcription and replication. Virus research *124*, 237-244.

Lopez, N., Jacamo, R., and Franze-Fernandez, M.T. (2001). Transcription and RNA replication of tacaribe virus genome and antigenome analogs require N and L proteins: Z protein is an inhibitor of these processes. Journal of virology *75*, 12241-12251.

Macneil, A., Stroher, U., Farnon, E., Campbell, S., Cannon, D., Paddock, C.D., Drew, C.P., Kuehnert, M., Knust, B., Gruenenfelder, R., Zaki, S.R., Rollin, P.E., Nichol, S.T., and Team, L.T.I. (2012). Solid organ transplant-associated lymphocytic choriomeningitis, United States, 2011. Emerg Infect Dis *18*, 1256-1262.

Maeto, C.A., Knott, M.E., Linero, F.N., Ellenberg, P.C., Scolaro, L.A., and Castilla, V. (2011). Differential effect of acute and persistent Junin virus infections on the nucleo-cytoplasmic trafficking and expression of heterogeneous nuclear ribonucleoproteins type A and B. The Journal of general virology *92*, 2181-2190.

Marq, J.B., Kolakofsky, D., and Garcin, D. (2010). Unpaired 5' ppp-nucleotides, as found in arenavirus double-stranded RNA panhandles, are not recognized by RIG-I. The Journal of biological chemistry *285*, 18208-18216.

Martinez-Sobrido, L., Emonet, S., Giannakas, P., Cubitt, B., Garcia-Sastre, A., and de la Torre, J.C. (2009). Identification of amino acid residues critical for the anti-interferon activity of the nucleoprotein of the prototypic arenavirus lymphocytic choriomeningitis virus. Journal of virology *83*, 11330-11340.

Martinez-Sobrido, L., Giannakas, P., Cubitt, B., Garcia-Sastre, A., and de la Torre, J.C. (2007). Differential inhibition of type I interferon induction by arenavirus nucleoproteins. Journal of virology *81*, 12696-12703.

Martinez-Sobrido, L., Zuniga, E.I., Rosario, D., Garcia-Sastre, A., and de la Torre, J.C. (2006). Inhibition of the type I interferon response by the nucleoprotein of the prototypic arenavirus lymphocytic choriomeningitis virus. Journal of virology *80*, 9192-9199.

Meyer, B.J., de la Torre, J.C., and Southern, P.J. (2002). Arenaviruses: genomic RNAs, transcription, and replication. Current topics in microbiology and immunology *262*, 139-157.

Meyer, B.J., and Southern, P.J. (1993). Concurrent sequence analysis of 5' and 3' RNA termini by intramolecular circularization reveals 5' nontemplated bases and 3' terminal heterogeneity for lymphocytic choriomeningitis virus mRNAs. Journal of virology *67*, 2621-2627.

Meyer, B.J., and Southern, P.J. (1994). Sequence heterogeneity in the termini of lymphocytic choriomeningitis virus genomic and antigenomic RNAs. Journal of virology *68*, 7659-7664.

Meyer, B.J., and Southern, P.J. (1997). A novel type of defective viral genome suggests a unique strategy to establish and maintain persistent lymphocytic choriomeningitis virus infections. Journal of virology *71*, 6757-6764.

Morin, B., Coutard, B., Lelke, M., Ferron, F., Kerber, R., Jamal, S., Frangeul, A., Baronti, C., Charrel, R., de Lamballerie, X., Vonrhein, C., Lescar, J., Bricogne, G., Gunther, S., and Canard, B. (2010). The N-terminal domain of the arenavirus L protein is an RNA endonuclease essential in mRNA transcription. PLoS pathogens *6*, e1001038.

Murphy, F.A. (1975). Arenavirus taxonomy: a review. Bull World Health Organ *52*, 389-391.

Novoa, R.R., Calderita, G., Arranz, R., Fontana, J., Granzow, H., and Risco, C. (2005a). Virus factories: associations of cell organelles for viral replication and morphogenesis. Biology of the cell / under the auspices of the European Cell Biology Organization *97*, 147-172.

Novoa, R.R., Calderita, G., Cabezas, P., Elliott, R.M., and Risco, C. (2005b). Key Golgi factors for structural and functional maturation of bunyamwera virus. Journal of virology *79*, 10852-10863.

Oldstone, M.B. (1998). Viral persistence: mechanisms and consequences. Curr Opin Microbiol *1*, 436-441.

Oldstone, M.B., and Buchmeier, M.J. (1982). Restricted expression of viral glycoprotein in cells of persistently infected mice. Nature *300*, 360-362.

Ortiz-Riano, E., Cheng, B.Y., de la Torre, J.C., and Martinez-Sobrido, L. (2011). The C-Terminal Region of Lymphocytic Choriomeningitis Virus Nucleoprotein Contains Distinct and Segregable Functional Domains Involved in NP-Z Interaction and Counteraction of the Type I Interferon Response. Journal of virology *85*, 13038-13048.

Ortiz-Riano, E., Cheng, B.Y., de la Torre, J.C., and Martinez-Sobrido, L. (2012). Self-association of Lymphocytic Choriomeningitis Virus Nucleoprotein is mediated by its N-terminal region and is not required for its anti-interferon function. Journal of virology.

Pannetier, D., Faure, C., Georges-Courbot, M.C., Deubel, V., and Baize, S. (2004). Human macrophages, but not dendritic cells, are activated and produce alpha/beta interferons in response to Mopeia virus infection. Journal of virology *78*, 10516-10524.

Pannetier, D., Reynard, S., Russier, M., Carnec, X., and Baize, S. (2014). Production of CXC and CC chemokines by human antigen-presenting cells in response to Lassa virus or closely related immunogenic viruses, and in cynomolgus monkeys with lassa fever. PLoS Negl Trop Dis *8*, e2637.

Parisi, G., Echave, J., Ghiringhelli, D., and Romanowski, V. (1996). Computational characterisation of potential RNA-binding sites in arenavirus nucleocapsid proteins. Virus genes *13*, 247-254.

Perez, M., and de la Torre, J.C. (2003). Characterization of the genomic promoter of the prototypic arenavirus lymphocytic choriomeningitis virus. Journal of virology *77*, 1184-1194.

Pinschewer, D.D., Perez, M., and de la Torre, J.C. (2003). Role of the virus nucleoprotein in the regulation of lymphocytic choriomeningitis virus transcription and RNA replication. Journal of virology *77*, 3882-3887.

Pinschewer, D.D., Perez, M., and de la Torre, J.C. (2005). Dual role of the lymphocytic choriomeningitis virus intergenic region in transcription termination and virus propagation. Journal of virology *79*, 4519-4526.

Polyak, S.J., Zheng, S., and Harnish, D.G. (1995a). 5' termini of Pichinde arenavirus S RNAs and mRNAs contain nontemplated nucleotides. Journal of virology *69*, 3211-3215.

Polyak, S.J., Zheng, S., and Harnish, D.G. (1995b). Analysis of Pichinde arenavirus transcription and replication in human THP-1 monocytic cells. Virus research *36*, 37-48.

Pythoud, C., Rodrigo, W.W., Pasqual, G., Rothenberger, S., Martinez-Sobrido, L., de la Torre, J.C., and Kunz, S. (2012). Arenavirus nucleoprotein targets interferon regulatory factor-activating kinase IKKepsilon. Journal of virology *86*, 7728-7738.

Pythoud, C., Rothenberger, S., Martinez-Sobrido, L., de la Torre, J.C., and Kunz, S. (2015). Lymphocytic Choriomeningitis Virus Differentially Affects the Virus-Induced Type I Interferon Response and Mitochondrial Apoptosis Mediated by RIG-I/MAVS. Journal of virology *89*, 6240-6250.

Qi, X., Lan, S., Wang, W., Schelde, L.M., Dong, H., Wallat, G.D., Ly, H., Liang, Y., and Dong, C. (2010). Cap binding and immune evasion revealed by Lassa nucleoprotein structure. Nature *468*, 779-783.

Raju, R., Raju, L., Hacker, D., Garcin, D., Compans, R., and Kolakofsky, D. (1990). Nontemplated bases at the 5' ends of Tacaribe virus mRNAs. Virology *174*, 53-59.

Rawls, W.E., Chan, M.A., and Gee, S.R. (1981). Mechanisms of persistence in arenavirus infections: a brief review. Can J Microbiol *27*, 568-574.

Reineke, L.C., and Lloyd, R.E. (2013). Diversion of stress granules and P-bodies during viral infection. Virology *436*, 255-267.

Rivers, T.M., and McNair Scott, T.F. (1935). Meningitis in Man Caused by a Filterable Virus. Science *81*, 439-440.

Rivers, T.M., and Scott, T.F. (1936). Meningitis in Man Caused by a Filterable Virus : Ii. Identification of the Etiological Agent. J Exp Med *63*, 415-432.

Rodrigo, W.W., Ortiz-Riano, E., Pythoud, C., Kunz, S., de la Torre, J.C., and Martinez-Sobrido, L. (2012). Arenavirus nucleoproteins prevent activation of nuclear factor kappa B. Journal of virology *86*, 8185-8197.

Rojek, J.M., and Kunz, S. (2008). Cell entry by human pathogenic arenaviruses. Cellular microbiology *10*, 828-835.

Rojek, J.M., Sanchez, A.B., Nguyen, N.T., de la Torre, J.C., and Kunz, S. (2008). Different mechanisms of cell entry by human-pathogenic Old World and New World arenaviruses. Journal of virology *82*, 7677-7687.

Rowe, W.P., Murphy, F.A., Bergold, G.H., Casals, J., Hotchin, J., Johnson, K.M., Lehmann-Grube, F., Mims, C.A., Traub, E., and Webb, P.A. (1970). Arenoviruses: proposed name for a newly defined virus group. Journal of virology *5*, 651-652.

Russier, M., Pannetier, D., and Baize, S. (2012). Immune responses and Lassa virus infection. Viruses *4*, 2766-2785.

Russier, M., Reynard, S., Carnec, X., and Baize, S. (2014). The exonuclease domain of Lassa virus nucleoprotein is involved in antigen-presenting-cell-mediated NK cell responses. Journal of virology *88*, 13811-13820.

Salvato, M.S., Schweighofer, K.J., Burns, J., and Shimomaye, E.M. (1992). Biochemical and immunological evidence that the 11 kDa zinc-binding protein of lymphocytic choriomeningitis virus is a structural component of the virus. Virus research *22*, 185-198.

Salvato, M.S., and Shimomaye, E.M. (1989). The completed sequence of lymphocytic choriomeningitis virus reveals a unique RNA structure and a gene for a zinc finger protein. Virology *173*, 1-10.

Schlie, K., Maisa, A., Freiberg, F., Groseth, A., Strecker, T., and Garten, W. (2010). Viral protein determinants of Lassa virus entry and release from polarized epithelial cells. Journal of virology *84*, 3178-3188.

Scott, T.F., and Rivers, T.M. (1936). Meningitis in Man Caused by a Filterable Virus : I. Two Cases and the Method of Obtaining a Virus from Their Spinal Fluids. J Exp Med *63*, 397-414.

Shivaprakash, M., Harnish, D., and Rawls, W. (1988). Characterization of temperature-sensitive mutants of Pichinde virus. Journal of virology *62*, 4037-4043.

Shtanko, O., Imai, M., Goto, H., Lukashevich, I.S., Neumann, G., Watanabe, T., and Kawaoka, Y. (2010). A role for the C terminus of Mopeia virus nucleoprotein in its incorporation into Z protein-induced virus-like particles. Journal of virology *84*, 5415-5422.

Shtanko, O., Watanabe, S., Jasenosky, L.D., Watanabe, T., and Kawaoka, Y. (2011). ALIX/AIP1 is required for NP incorporation into Mopeia virus Z-induced virus-like particles. Journal of virology *85*, 3631-3641.

Singh, M.K., Fuller-Pace, F.V., Buchmeier, M.J., and Southern, P.J. (1987). Analysis of the genomic L RNA segment from lymphocytic choriomeningitis virus. Virology *161*, 448-456.

Southern, P.J., Singh, M.K., Riviere, Y., Jacoby, D.R., Buchmeier, M.J., and Oldstone, M.B. (1987). Molecular characterization of the genomic S RNA segment from lymphocytic choriomeningitis virus. Virology *157*, 145-155.

Staneck, L.D., Trowbridge, R.S., Welsh, R.M., Wright, E.A., and Pfau, C.J. (1972). Arenaviruses: cellular response to long-term in vitro infection with parana and lymphocytic choriomeningitis viruses. Infect Immun *6*, 444-450.

Stenglein, M.D., Sanders, C., Kistler, A.L., Ruby, J.G., Franco, J.Y., Reavill, D.R., Dunker, F., and Derisi, J.L. (2012). Identification, characterization, and in vitro culture of highly divergent arenaviruses from boa constrictors and annulated tree boas: candidate etiological agents for snake inclusion body disease. mBio *3*, e00180-00112.

Stephensen, C.B., Blount, S.R., Lanford, R.E., Holmes, K.V., Montali, R.J., Fleenor, M.E., and Shaw, J.F. (1992). Prevalence of serum antibodies against lymphocytic choriomeningitis virus in selected populations from two U.S. cities. J Med Virol *38*, 27-31.

Thomas, M.G., Loschi, M., Desbats, M.A., and Boccaccio, G.L. (2011). RNA granules: the good, the bad and the ugly. Cellular signalling *23*, 324-334.

Tortorici, M.A., Albarino, C.G., Posik, D.M., Ghiringhelli, P.D., Lozano, M.E., Rivera Pomar, R., and Romanowski, V. (2001a). Arenavirus nucleocapsid protein displays a transcriptional antitermination activity in vivo. Virus research *73*, 41-55.

Tortorici, M.A., Ghiringhelli, P.D., Lozano, M.E., Albarino, C.G., and Romanowski, V. (2001b). Zinc-binding properties of Junin virus nucleocapsid protein. The Journal of general virology *82*, 121-128.

Traub, E. (1935). A Filterable Virus Recovered from White Mice. Science *81*, 298-299.

Urata, S., and Yasuda, J. (2012). Molecular mechanism of arenavirus assembly and budding. Viruses *4*, 2049-2079.

Valiente-Echeverria, F., Melnychuk, L., and Mouland, A.J. (2012). Viral modulation of stress granules. Virus research *169*, 430-437.

Vela, E. (2012). Animal models, prophylaxis, and therapeutics for arenavirus infections. Viruses *4*, 1802-1829.

Viets, H.R., and Watts, J.W. (1929a). Aseptic (Lymphocytic) Meningitis. JAMA *93*, 1553-1555.

Viets, H.R., and Watts, J.W. (1929b). Three Cases of Aseptic (Lymphocytic) Meningitis. N Engl J Med *200*, 633-634.

Welsh, R.M., O'Connell, C.M., and Pfau, C.J. (1972). Properties of defective lymphocytic choriomeningitis virus. The Journal of general virology *17*, 355-359.

West, B.R., Hastie, K.M., and Saphire, E.O. (2014). Structure of the LCMV nucleoprotein provides a template for understanding arenavirus replication and immunosuppression. Acta Crystallogr D Biol Crystallogr *70*, 1764-1769.

White, J.P., and Lloyd, R.E. (2012). Regulation of stress granules in virus systems. Trends in microbiology *20*, 175-183.

Wildy, P. (1971). Classification and Nomenclature of Viruses. In Monographs in Virology, J.L. Melnick, ed. (Basel/New York: S. Karger).

Wolff, S., Becker, S., and Groseth, A. (2013a). Cleavage of the Junin virus nucleoprotein serves a decoy function to inhibit the induction of apoptosis during infection. Journal of virology *87*, 224-233.

Wolff, S., Ebihara, H., and Groseth, A. (2013b). Arenavirus budding: a common pathway with mechanistic differences. Viruses *5*, 528-549.

Young, P.R., Chanas, A.C., Lee, S.R., Gould, E.A., and Howard, C.R. (1987). Localization of an arenavirus protein in the nuclei of infected cells. The Journal of general virology *68 (Pt 9)*, 2465-2470.

Young, P.R., and Howard, C.R. (1983). Fine structure analysis of Pichinde virus nucleocapsids. The Journal of general virology *64 (Pt 4)*, 833-842.

Yun, N.E., and Walker, D.H. (2012). Pathogenesis of Lassa fever. Viruses *4*, 2031-2048.

Zhang, Y., Li, L., Liu, X., Dong, S., Wang, W., Huo, T., Guo, Y., Rao, Z., and Yang, C. (2013). Crystal structure of Junin virus nucleoprotein. The Journal of general virology *94*, 2175-2183.

Zhou, S., Cerny, A.M., Zacharia, A., Fitzgerald, K.A., Kurt-Jones, E.A., and Finberg, R.W. (2010). Induction and inhibition of type I interferon responses by distinct components of lymphocytic choriomeningitis virus. Journal of virology *84*, 9452-9462.

Ziegler, C.M., Eisenhauer, P., Bruce, E.A., Beganovic, V., King, B.R., Weir, M.E., Ballif, B.A., and Botten, J. (2016a). A novel phosphoserine motif in the LCMV matrix protein Z regulates the release of infectious virus and defective interfering particles. The Journal of general virology *97*, 2084-2089.

Ziegler, C.M., Eisenhauer, P., Bruce, E.A., Weir, M.E., King, B.R., Klaus, J.P., Krementsov, D.N., Shirley, D.J., Ballif, B.A., and Botten, J. (2016b). The Lymphocytic Choriomeningitis Virus Matrix Protein PPXY Late Domain Drives the Production of Defective Interfering Particles. PLoS pathogens *12*, e1005501.

CHAPTER 2:

FOLLOWING ARENAVIRUS RNA SPECIES IN INDIVIDUAL CELLS BY SINGLE-MOLECULE FLUORESCENCE IN SITU HYBRIDIZATION (smFISH) REVEALS A MODEL OF CYCLICAL INFECTION AND CLEARANCE DURING PERSISTENCE

Benjamin R. King[1,2], Aubin Samacoits[3,4], Philip L. Eisenhauer[1], Christopher M. Ziegler[1], Emily A. Bruce[1], Daniel Zenklusen[5], Christophe Zimmer[3,4], Florian Mueller[3,4], and Jason Botten[1,6#]

[1]Department of Medicine, Division of Immunobiology, University of Vermont, Burlington, VT 05405, USA, [2]Cellular, Molecular, and Biomedical Sciences Graduate Program, University of Vermont, Burlington, VT 05405, USA, [3]Unité Imagerie et Modélisation, Institut Pasteur, Paris, France, [4] C3BI, USR 3756 IP CNRS, Paris, France, [5]Departement de Biochimie et Médecine Moléculaire, Université de Montréal, Montréal, QC H3T 1J4, Canada, [6]Department of Microbiology and Molecular Genetics, University of Vermont, Burlington, VT 05405, USA, [#]Corresponding author

Running Title: Cyclical LCMV infection and clearance in persistence

2.1. Abstract

Lymphocytic choriomeningitis mammarenvirus (LCMV) is an enveloped, negative-strand RNA virus that causes serious disease in humans but establishes an asymptomatic, lifelong infection in reservoir rodents. Different models have been proposed to describe how arenaviruses regulate the replication and transcription of their bisegmented, single-stranded RNA genomes, particularly during persistent infection. However, these models were largely based on viral RNA profiling data derived from entire populations of cells. To better understand LCMV replication and transcription at the single-cell level, we established a high-throughput, single-molecule (sm)FISH image acquisition and analysis pipeline and followed viral RNA species from viral entry through the late stages of persistent infection *in vitro*. We observed transcription of viral nucleoprotein and polymerase mRNAs from the incoming S and L segment genomic RNAs, respectively, within 1 hr of infection, whereas transcription of glycoprotein mRNA from the S segment antigenome required ~4-6 hr. This confirms the temporal separation of viral gene expression expected due to the ambisense coding strategy of arenaviruses and also suggests that antigenomic RNA contained in virions is not transcriptionally active upon entry. Viral replication and transcription peaked at 36 hours post-infection, followed by a progressive loss of viral RNAs over the next several days. During persistence, the majority of cells in culture showed repeating cyclical waves of viral transcription and replication followed by clearance of viral RNA. Thus, our data support a model of LCMV persistence whereby infected cells spontaneously clear infection and become reinfected by viral reservoir cells that remain in the population.

2.2. Importance

Arenaviruses are human pathogens that can establish asymptomatic, life-long infections in their rodent reservoirs. Lymphocytic choriomeningitis mammarenavirus (LCMV) is carried in nature by the common house mouse and can be transmitted from mother to pup. Because pups recognize viral antigens as self, they are unable to mount an effective T cell response to clear infection. Yet LCMV, despite being able to infect most cells in the host, restricts its spread and several models have been proposed to explain this regulation. We developed a high throughput, single-molecule RNA FISH assay to profile the dynamics of LCMV genome replication and transcription in individual cells. Our findings provide novel insights in the timing of replication and transcription, the composition of virus particles and the functionality of their packaged viral RNA species, and suggest a revised model for how LCMV restricts its spread among susceptible host cells during persistent infection.

2.3. Introduction

Several members of the arenavirus family are significant threats to human health. Lassa virus and Junín virus cause hemorrhagic fever syndromes while lymphocytic choriomeningitis virus (LCMV), the prototypic member of the family, is a well-known cause of severe birth defects and is highly lethal in immunocompromised individuals (Buchmeier et al., 2007; Fischer et al., 2006). A critical imperative to better understand the key steps of the arenavirus life cycle is made evident by the fact that there are no FDA-approved vaccines to prevent arenavirus transmission and only a very limited repertoire of antivirals (Enria et al., 2008; McCormick et al., 1986). New strategies to prevent and treat arenavirus infections will likely hinge upon an improved understanding of key phases of the life cycle of these important human pathogens.

Arenaviruses are enveloped viruses that have a single-stranded, bisegmented, negative-sense RNA genome. The ~3.5 kb small (S) and ~7.2 kb large (L) genomic RNA segments each encode two viral open reading frames in ambisense orientation (Figure 2.1A) (Buchmeier et al., 2007). The nucleoprotein (NP) and polymerase (L) genes are encoded in typical negative-sense orientation on genomic RNA while the glycoprotein (GPC) and matrix protein (Z) genes are encoded in pseudo positive-sense orientation. The canonical sequence of genetic events following the release of arenavirus genomic RNA into the cytoplasm of a newly infected cell is (i) primary transcription of the NP and L mRNAs from the viral S and L genomic segments, respectively, followed by (ii) full length replication of the S and L segment antigenomic RNAs and subsequent transcription of the GPC and Z mRNAs from the S and L antigenomic RNAs, respectively, and (iii) replication

of additional full-length genomic RNAs from the antigenomic RNA templates (Figure 2.1A) (Buchmeier et al., 2007; Meyer et al., 2002).

While rodent-borne arenaviruses cause severe diseases in humans, they are thought to be asymptomatic in their sylvatic hosts, where they can establish a persistent, life-long infection (Buchmeier et al., 2007). LCMV is carried by the common house mouse and can be transmitted vertically from mother to pup (Buchmeier et al., 1980; Buchmeier and Zajac, 1999; Lehmann-Grube et al., 1983). The pups are born infected but never mount an effective immune response to clear the virus as viral proteins are seen as self-antigens by the pup's developing immune system (Buchmeier et al., 1980; Buchmeier and Zajac, 1999; Lehmann-Grube et al., 1983) . Paradoxically, while LCMV can infect most cells in the host rodent, it tightly regulates its spread and therefore does not overrun its host. Several hypotheses have been proposed for how LCMV restricts its spread, including through (i) the production of defective interfering (DI) particles (Burns and Buchmeier, 1993; Huang and Baltimore, 1970; Oldstone, 1998), which can enter susceptible host cells and make them refractory to productive infection (Huang, 1973; Welsh et al., 1972) and (ii) the accumulation of transcriptionally-defective genomic and antigenomic RNAs, which limit viral protein expression and infectious virus production (Meyer et al., 2002; Meyer and Southern, 1994, 1997). It has also been proposed that LCMV can establish a cyclical, transient pattern of infection such that susceptible cells are productively infected for a short time before clearing the virus and once again becoming susceptible to reinfection by

neighboring cells that remain productively infected (Hotchin, 1973, 1974a, b; Hotchin et al., 1975).

A current gap in our knowledge of how arenaviruses restrict their dissemination is that we lack a detailed understanding of how the events of viral genome replication and transcription are regulated during the acute and persistent phases of infection. Previous studies examining the genetic events of arenavirus replication and transcription, including those described above regarding the accumulation of transcriptionally defective RNAs (Meyer et al., 2002; Meyer and Southern, 1994, 1997), relied on techniques such as Northern blot or quantititative RT-PCR. Both are powerful techniques used to examine RNA. Quantitative RT-PCR is exquisitely sensitive (Haist et al., 2015), and Northern blot is able to specifically distinguish between each of the viral RNA species (Auperin et al., 1984b; Francis and Southern, 1988a, b; Franze-Fernandez et al., 1987; Fuller-Pace and Southern, 1988, 1989; Meyer and Southern, 1997; Polyak et al., 1995b; Shivaprakash et al., 1988; Southern et al., 1987). However, both techniques measure RNA at a population level and thus provide population average data. Variability in RNA expression between individual cells in a heterogeneous population cannot be evaluated using these approaches. Single-molecule RNA fluorescence in situ hybridization (smFISH) can bridge this technical gap to allow for detection of RNAs with single-copy sensitivity in individual cells by fluorescence microscopy (Raj et al., 2008). In the present study, we designed specific smFISH probe sets to fluorescently-label different LCMV RNA species (Figure 2.1A) and to quantitatively characterize their expression in single cells during the entire time course

of arenavirus infection. Our studies confirm the temporal separation of LCMV negative-sense and pseudo positive-sense gene expression and reveal a striking pattern of cyclical loss and reappearance of viral RNA in individual cells during persistence. Our studies provide fresh insight into the functional genetic composition of infectious virions, the kinetics of transcription and replication in the hours immediately following initial infection, and suggest a revised model of how viral replication and transcription are regulated during persistence to restrict virus spread. Further, the image acquisition and analysis pipeline developed here is easily adaptable to other viruses.

2.4. Results

2.4.1. Visualization of LCMV RNA species in infected cells.

To visualize LCMV RNAs in cells by fluorescence microscopy, we designed smFISH probe sets complementary to different viral RNA species (see overview in Figure 2.1A). An important feature of smRNA FISH is the ability to detect single RNA molecules using multiple, singly-labeled oligonucleotide probes (Raj et al., 2008). The high signal-to-noise ratio of the probe set binding to a specific target RNA yields single RNAs that appear as bright spots. To validate our ability to specifically label arenavirus RNAs, we used a cellular mRNA smFISH probe set specific for the housekeeping gene MDN1 as a control (Figure 2.1B) for comparison with a smFISH probe set designed to target both the viral S genome RNA and GPC mRNA (Figure 2.1C). MDN1 probes detect single cytoplasmic mRNAs as well as sites of active transcription in the nucleus, where multiple nascent RNAs are detected as more intense signals (Figure 2.1B). Next, we confirmed that the viral RNA smFISH probe set is highly specific as fluorescent signal was absent in uninfected cells, but bright spots were detected in LCMV-infected cells fixed at 24 hpi (Figure 2.1C). Moreover, similar to smFISH staining obtained with our control MDN1, individual smFISH spots were homogeneous in size, shape, and fluorescence intensity (Figure 2.1B and C) consistent with the detection of single RNAs, as shown previously (Raj et al., 2008; Zenklusen et al., 2008). Furthermore, in contrast to the nuclear transcribed MDN1 mRNAs, viral RNAs were largely excluded from the nucleus, consistent with the cytoplasmic viral life cycle (Figure 2.1B to C).

2.4.2. smFISH probes complementary to viral mRNA species provide high signal-to-noise staining.

We designed multiple smFISH probe sets to have specificity for different RNA species produced during the course of the LCMV life cycle (Figure 2.1A). Specifically, these probe sets target (i) S genome only, (ii) GPC mRNA and S genome, (iii) NP mRNA and S antigenome, or (iv) L mRNA and L antigenome. When infected cells were stained with probe sets complementary to "S genome only" or "S genome and GPC mRNA" (referred to has "GPC mRNA/S genome" from this point forward), we noted high quality staining with the GPC mRNA/S genome probes as evidenced by homogeneity in spot size, shape, and intensity (Figure 2.2A) and high signal-to-noise ratio (Figure 2.3). The NP mRNA/S antigenome and L mRNA/L antigenome probe sets yielded similar high quality staining as evidenced by high signal-to-noise ratios (Figure 2.3). However, we noted lower quality staining with the "S genome only" probes as evidenced by the dimmer staining (Figure 2.2) and low signal-to-noise ratio (Figure 2.3). Moreover, the "S genome only" probes yielded greater non-specific staining in uninfected cells, potentially leading to detection of false-positive spurious events (Figure 2.2C) – perhaps an artifact of the long exposure times and high light intensity needed to detect this less sensitive probe set binding to its target. Similarly low signal-to-noise ratios were observed with probe sets specific for "S antigenome only" or "L genome only" (data not shown). It is possible that the encapsidation of genome and antigenome by viral nucleoprotein partially occludes smFISH probe hybridization with these target RNA sequences and thus leads to the lower signal-

to-noise ratio observed with these probe sets. Therefore, use of these probe sets with cells containing small numbers of viral RNAs would be problematic due to the level of background staining observed (Figure 2.2C). However, these probe sets are effective when paired with cells containing abundant copies of viral genome or antigenome (Figure 2.2B and data not shown), which easily exceeds the quantity of background spots observed in mock-infected control cells (Figure 2.2C). Because the probe sets that targeted an mRNA plus either genome or antigenome provided the highest quality staining and sensitivity, we elected to use these probe sets to follow the kinetics of viral transcription and replication events in infected cells.

2.4.3. smFISH spot detection and quantification in individual LCMV-infected cells.

A primary goal of our study was to globally describe the kinetics of transcription and replication of the LCMV genome from the early hours following viral entry through the late stages of persistence. Ideally, we would be able to infect cells at a high multiplicity of infection (MOI) and take snapshots of a population of synchronously infected cells at time points throughout the entire course of arenavirus infection. However, we were obliged to infect cells at a low MOI due to the characteristic high prevalence of DI particles present in LCMV stocks (Ziegler et al., 2016b). Because only a small proportion of cells would be productively infected upon viral inoculation, we needed to image a large population of cells at each time point tested to provide an accurate portrait of the heterogeneity present in a population of asynchronously infected cells. Thus, it was important for this study to both image and quantitatively characterize the smFISH staining of viral RNAs in a high-

throughput fashion. To accomplish this goal, we automatically segmented the nuclei using DAPI and cell outlines using CellMask Green fluorescent staining with CellProfiler software (Kamentsky et al., 2011) (Figure 2.4A). Next, smFISH-labeled viral RNAs were detected using FISH-quant software (Mueller et al., 2013) (Figure 2.4B). We were able to image two distinct RNA smFISH probe sets labeled with spectrally-distinct fluorophores in individual cells. This allowed us to characterize relative viral RNA expression levels and compare localization of different viral RNAs (Figures 2.4B to C). We were able to robustly quantify viral RNAs using FISH-quant across a range of expression levels. We observed a linear relationship between the quantity of detected viral RNAs and the total fluorescence signal in the smFISH channel up to approximately 1,000 RNAs/cell, after which the number of detected viral RNAs reached a plateau (Figure 2.4D). This represents the point at which smFISH spots are so dense, that we were no longer able to accurately distinguish closely spaced RNAs. Examples of a cell displaying moderate levels of viral RNAs where identification of diffraction limited spots was robust (Figure 2.4B) and a cell with very high expression of viral RNAs where overcrowded spots are unable to be effectively spatially resolved (Figure 2.4C) are shown for reference. Thus, when viral RNA levels are relatively low (less than several hundred copies per cell) we have high confidence in the accuracy of the quantification provided by FISH-quant. However, when viral RNA levels are at their peak and RNAs are very dense, quantification should be considered an underestimate of RNA expression levels.

2.4.4. Viral RNA transcription and replication following viral entry.

We next aimed to monitor the early events of viral genomic transcription and replication immediately following viral entry. Cells were infected with LCMV at an MOI of 0.1, fixed at multiple time points, stained for NP mRNA/S antigenome, GPC mRNA/S genome, or L mRNA/L antigenome, and several hundred cells were imaged and analyzed at each time point (Table S2.1). As discussed above in relation to Figure 2.2, our probes sets specific for only genome or antigenome (but not an additional complementary viral mRNA) have low signal-to-noise ratios and sensitivity when compared to probe sets that also target a viral mRNA. Importantly, FISH-quant was unable to detect viral genome or antigenome spots in cells that had been infected with LCMV for less than 8 h (Figure 2.2 and data not shown). However, by 8 hpi and later, genome and antigenome spots become detectable with these probe sets (Figure 2.2, B.R. King, S. Kellner, P.L. Eisenhauer, E.A. Bruce, C.M. Ziegler, D. Zenklusen, and J. Botten, submitted for publication, and data not shown). Therefore, in this set of experiments, smFISH spots detected with the NP mRNA/S antigenome, GPC mRNA/S genome, or L mRNA/L antigenome probe sets prior to 8 hpi are presumed to represent only the designated mRNA target in each case, whereas at 8 hpi and later it is possible to detect a mixture of the targeted RNAs.

Representative images of cells infected from 0 to 6 hpi are shown (Figure 2.5A to B). Notably, transcription of the NP mRNA and L mRNA is detected as early as 1 hour following infection (Figure 2.5 and 2.6A to B) indicating primary transcription of the S and L genomic RNA occurs soon after entry and uncoating of arenavirus virions. The GPC

mRNA, on the other hand, is first detected at 6 hours following infection (Figure 2.5A and 2.6A and C). This delayed appearance of the GPC mRNA indicates that transcriptionally competent S antigenomic RNA is not delivered into cells by incoming virions. Further, it suggests that a 4-6 hour lag is required for the production of S antigenomic RNA, which serves as the template for transcription of GPC mRNA (Figure 2.1A). This result is in agreement with previous studies that examined arenavirus mRNA synthesis via Northern blot (Franze-Fernandez et al., 1987; Meyer et al., 2002).

When examining the subcellular localization of NP mRNA and GPC mRNA or NP mRNA and L mRNA pairs at 6 hpi or earlier, no overt colocalization between viral mRNAs was noted (Figure 2.5A to B).

2.4.5. Disproportionate transcription of S segment genes early after infection.

For each probe set used in the experiments shown in Figures 2.5 and 2.6, the number of false-positive viral RNAs detected in mock-infected cells was used to establish a threshold to classify cells as either "positive" or "negative" for each of the tested viral RNA species. At 6 hpi (a time point before virus in the initially infected cells could have completed its life cycle and spread to adjacent, initially uninfected cells (Buchmeier et al., 1978; Dutko and Pfau, 1978; Lehmann-Grube, 1971; Lehmann-Grube et al., 1975), we observed that 65-90% of cells were positive for NP mRNA and 40% were positive for GPC mRNA (Figure 2.6C to D). This high frequency of cells containing S segment-derived transcripts was surprising given the fact we initially infected cells at an MOI of 0.1, and thus would have expected approximately only 10% of cells to have been expressing viral

RNAs at this early time point. However, at this same early time point, only 8% of cells were positive for L segment-derived L mRNA (Figure 2.6D), which is consistent with the expected frequency of viral RNA-positive cells based on the initial MOI. This result may suggest that a high proportion of viral particles either fail to package the L genome or alternatively deliver a transcriptionally-defective L genome.

2.4.6. Viral RNA replication and transcription at peak of acute infection.

To profile LCMV RNAs at the peak of infectious virus release during acute infection, cells were infected with LCMV at an MOI of 0.01, fixed at various time points between 12 and 96 hpi, stained for NP mRNA/S antigenome, GPC mRNA/S genome, or L mRNA/L antigenome, and several hundred cells were imaged and analyzed at each time point (Table S2.1). Levels of viral RNAs detected by each probe set rapidly increased over the first 24 hours of infection (Figure 2.7A to B and 2.8A to B). The proportion of cells positive for these viral RNAs also rapidly increased over the first 24 hours of infection such that almost all cells had substantial levels of all viral RNAs (Figure 2.8C to D). Peak viral transcription and replication occurred at 36 hours post infection (Figure 2.7A to B and 2.8A to B). At this time point, viral smFISH signal was very dense and true levels of viral NP mRNA and GPC mRNA were likely underestimated due to inability of FISH-quant to accurately count tightly packed viral RNAs in the cytoplasm of infected cells (Figure 2.4B to C, 2.7A to B, and 2.8A to B). Furthermore, RNAs detected by the S segment-specific probe sets greatly exceeded those detected by the L segment-specific probe set (10-35 fold greater) between 12 and 96 hpi (Figure 2.8A to B, Table 2.1). Following peak viral

transcription and replication at 36 hours post-infection, levels of viral RNAs began to decrease (Figure 2.7A to B and 2.8A to B). The proportion of cells positive for L mRNA/L antigenome expression decreased steadily beginning at 48 hours post-infection (Figure 2.8D). In contrast, all cells maintained NP mRNA/S antigenome and GPC mRNA/S expression over this entire time period (Figure 2.8C to D).

2.4.7. Cyclical patterns of genome transcription and replication during persistent infection.

Lastly, we wanted to examine the transcription and replication dynamics of arenavirus genomic RNA during the persistent phase of infection. Cells were infected with LCMV at an MOI of 0.01, fixed at multiple time points between 1.5 and 41 days (d)pi, stained for NP mRNA/S antigenome, GPC mRNA/S genome, or L mRNA/L antigenome, and several hundred cells were imaged and analyzed at each time point (Table S2.1). Following peak RNA transcription and replication at 36 hpi, we observed the levels of NP mRNA/S antigenome, GPC mRNA/S genome, or L mRNA/L antigenome decrease over the next several days such that at 8 dpi, the majority of cells are negative for all of these viral RNAs (Figure 2.9A to F). However, by 13 dpi, the levels of viral RNAs detected by each probe set increase and the majority of cells are again positive for all viral RNAs (Figure 2.9C and F). Viral RNA levels again fall and many cells are no longer positive for viral RNA by 16 dpi. (Figure 2.9C and F). These cycles of increased levels of viral RNA expression and increased frequency of viral RNA expressing cells in the population repeat in a cyclical fashion multiple times over the first 41 days following infection (Figure 2.9).

In summary, the sequential loss and reappearance of viral gene expression observed here suggest a potential genetic signature of populations of cells persistently infected with LCMV.

Throughout the time course of persistence examined in this study, NP mRNA/S antigenome is generally expressed at higher levels than GPC mRNA/S genome (up to 5-fold higher levels) (Figure 2.9B and Table 2.1). The ratio between levels of NP mRNA/S antigenome and L mRNA/L antigenome over this time period is much more variable. At time points such as 13 and 20 dpi when most cells in the culture are positively expressing all viral RNA species, NP mRNA/S antigenome greatly outnumbers L mRNA/L antigenome (~25-fold higher levels) (Figure 2.9E and Table 2.1). However, at other times such as 8, 16, 27, and 34 dpi when substantial proportions of cells have lost expression of one or more viral RNAs, the ratio between NP mRNA/S antigenome and L mRNA/L antigenome in the double-positive cells is greatly reduced (~2-fold higher levels of NP than L mRNA) (Figure 2.9E and Table 2.1). Notably, the magnitude of viral RNA expression during persistence never returned the high levels observed at the peak of acute infection (Figure 2.9).

2.5. Discussion

In the current study, we developed a high throughput smFISH assay that allowed us to visualize, single copies of LCMV RNAs in individual cells. Taking advantage of the sensitivity and quantitative aspect of this assay, we tracked the dynamics of viral replication and transcription spanning the moments following initial virus entry to late times during persistent infection. We observed that transcription of the negative-sense encoded NP and L mRNAs precede that of the pseudo positive-sense encoded GPC mRNA, confirming the temporal separation of gene expression predicted by the ambisense coding strategy of the arenaviruses and suggesting that antigenomic RNA in virions is not transcriptionally active following release into a newly infected cell. Our studies demonstrated a hierarchal pattern of expression among viral RNAs and indicate that many infecting virus particles may lack L genomic RNA. Finally, over the course of persistent infection, we observed repeated cycles whereby cells transition from supporting active viral replication and transcription to clearing all viral RNAs. Collectively, these studies advance our understanding of the natural history of arenavirus replication and transcription and suggest a modified model for how arenaviruses may regulate these processes to limit their impact on the fitness of their rodent reservoirs.

The smFISH assay developed here provided us with an opportunity to build upon prior studies and examine arenavirus genome replication and transcription with greater sensitivity and detail. Previous studies aimed at elucidating the early events of arenavirus transcription and genome replication used Northern blot to visualize individual viral RNA species (Franze-Fernandez et al., 1987; Fuller-Pace and Southern, 1988; Shivaprakash et

al., 1988). Analysis of RNA from cells infected with LCMV or the New World arenavirus Pichinde failed to detect viral RNA from infected cells prior to 9 hpi (Fuller-Pace and Southern, 1988) or 12 hpi (Shivaprakash et al., 1988), respectively. In the setting of infection with the New World arenavirus Tacaribe, Franze-Fernandez *et al.* detected S genomic RNA and NP mRNA at 2 hpi and S antigenomic RNA at 4 hpi, while GPC mRNA appeared several hours following the synthesis of S antigenomic RNA (Franze-Fernandez et al., 1987). The earliest the viral L segment has been observed was at 12 hpi (Fuller-Pace and Southern, 1988). In the current study, we are able to detect viral NP and L mRNAs at 1 hpi. Our data supports previous observations that viral NP mRNA expression occurs immediately following infection, and that GPC mRNA expression occurs following a lag of several hours (Franze-Fernandez et al., 1987; Meyer et al., 2002). By probing single cells, we build upon this prior work by demonstrating that GPC mRNA expression is not detected, even at low levels, in the first hours following infection. In light of previous observations that antigenomic L and S segment RNAs are packaged in viral particles (Franze-Fernandez et al., 1987; Haist et al., 2015), our inability to observe GPC mRNA in cells immediately following viral entry suggests that S antigenomic RNA packaged in virions is unable to be transcribed. Further, it suggests that GPC mRNAs are not packaged into viral particles, as has been suggested for Z mRNA (Salvato and Shimomaye, 1989).

An interesting observation from our study was that, despite infecting cells at an MOI of 0.1, ~65-90% of cells expressed one or more genes encoded on the S genomic RNA segment at 6 hpi. Because it takes ~ 8 h for an infected cell to make new infectious

progeny (Buchmeier et al., 1978; Dutko and Pfau, 1978; Lehmann-Grube, 1971; Lehmann-Grube et al., 1975), we were surprised to see such a high frequency of cells expressing these viral mRNAs at a time when the originally-infected cells could not yet have spread virus to additional uninfected cells in the monolayer. Notably, at this same 6 hpi time point, approximately 8% of cells expressed viral L mRNAs, which is consistent with the utilized MOI. This suggests that, within the viral stock, there may be a significant population of incomplete viral particles that possess the S segment but lack the L segment genomic RNA or a functional copy of this RNA. Considering that the genetic basis for how arenavirus DI particles block the propagation of infectious virus particles is unknown, these results may provide clues for future studies to define the mechanism at work.

A hallmark characteristic of LCMV infection is the ability to establish an asymptomtatic, persistent infection in reservoir rodents (Francis et al., 1987). Further, it is possible to recapitulate key aspects of this persistent infection in cell culture models of infection (Lehmann-Grube, 1967; Lehmann-Grube et al., 1969; Meyer et al., 2002; Oldstone and Buchmeier, 1982). One notable characteristic of cell culture models of LCMV infection is the cyclical rise and fall of release of infectious virus seen during persistence (Hotchin, 1974a; Hotchin et al., 1975; Lehmann-Grube, 1967; Lehmann-Grube et al., 1969; Staneck et al., 1972). Several models have been proposed to explain how LCMV restricts its spread to establish and maintain a noncytopathic persistent infection, both *in vitro* and *in vivo*. The first suggests that DI particles, which are produced in abundance by LCMV, can enter permissive host cells and interfere with the ability of

standard infectious virus particles to successfully infect and complete the viral life cycle (Burns and Buchmeier, 1993; Huang, 1973; Huang and Baltimore, 1970; Oldstone, 1998; Welsh et al., 1972). Hotchin proposed a second model that he termed cyclical, transient infection. In this model, cells infected with LCMV are initially productive in making infectious virus particles, but later become refractory to superinfection and ultimately clear virus, only to once again become susceptible to reinfection by the small number of cells that remain productively infected (Hotchin, 1973, 1974a, b; Hotchin et al., 1975). Southern and colleagues proposed a third model that was based upon the dynamics and genetic identity of viral RNA species profiled during acute and persistent infection. In particular, they demonstrated by Northern blot that LCMV RNAs (genome, antigenome, and mRNAs) accumulate to high levels during persistence, both *in vitro* and *in vivo* (Francis and Southern, 1988b; Meyer et al., 2002; Meyer and Southern, 1994, 1997). Further, they showed that a proportion of these genomic and antigenomic RNAs, but not mRNAs, contained short deletions in the untranslated regions at their termini (Meyer et al., 2002; Meyer and Southern, 1993, 1994, 1997). They proposed that these deleted RNAs were replication competent, but transcriptionally incompetent. These data suggest a model where, during persistence, viral protein expression and infectious virus production are inhibited due to the accumulation of high levels of transcriptionally defective genomic and antigenomic RNAs. Further, because these deleted RNAs were found in virions, it was proposed that they serve as the molecular basis for DI particle interference. Finally, it was proposed that these deleted RNAs can be repaired by the viral polymerase to initiate bursts

of productive replication/infectious virus production during persistence. This would support the cyclical aspect of Hotchin's model, but not the transience of infection as viral genetic material would not be cleared from infected cells. Each of these models, whether acting independently or in combination, would presumably restrict virus spread, allowing the virus to minimize its impact on host fitness while retaining its ability to propagate and ultimately maintain itself in nature.

In reality, it seems likely that a holistic model describing the establishment and maintenance of arenavirus persistence will incorporate elements of each model. The data in the current study, indeed, suggest elements of each could be important. Our observation that many cells lose then regain expression of viral RNAs at multiple time points during persistence strongly supports the hypothesis of coordinated cycles of viral clearance followed by reinfection. Hotchins et al. demonstrated a similar pattern using the expression of viral antigen and production of infectious virus as readouts (Hotchin, 1973, 1974a, b; Hotchin et al., 1975). One interpretation of our data is that the loss of antigen expression (and infectious virus production) seen in those studies was the result of cells completely clearing virus, including viral genetic material. Alternatively, it is possible that loss of viral antigen expression could have been due to the accumulation of transcriptionally-defective genomes in infected cells. Because our smFISH probe sets for encapsidated genomic and antigenomic RNAs lack the sensitivity seen by those that are specific for unencapsidated viral mRNAs, it is possible that some of the cells examined do in fact contain very low levels of terminally-deleted genomic or antigenomic RNAs. However, in this scenario, we

feel the subsequent cycles of viral RNA rescue in most cells would be unlikely if completely dependent on the repair of terminally truncated genomes through the addition of random non-templated bases to regenerate functional terminal untranslated regions. We think it more likely that the accumulation of transcriptionally non-functional genomes along with the polymerase inhibitory activity of the viral Z protein (Cornu and de la Torre, 2001, 2002; Kranzusch and Whelan, 2011; Lopez et al., 2001) both play a key role in negatively regulating viral transcription and replication following the peak of acute infection, providing an environment that permits cells to eliminate infection. The accumulation of terminally-deleted viral RNAs, if they are indeed the basis for DI particle interference with standard virus, could further work to preserve host fitness by driving the formation of DI particles to preserve nearby uninfected cells from infection. Reinfection of susceptible cells with virus from productively-infected reservoir cells within the population that express full length functional genome could restart the infection cycle as evidenced by the near 100% of cells expressing viral RNAs at multiple subsequent persistent time points. Being able to specifically visualize genomic and antigenomic RNAs with improved sensitivity by smFISH will be important to further define the exact mechanism employed by arenaviruses to restrict their spread and impact on host cells during persistent infection.

In summary, we have used fluorescence microscopy to visualize fluorescently-labeled arenavirus RNA molecules in infected cells. Further, we have described a flexible labeling, imaging, and image analysis pipeline that could be easily adapted to interrogate

the events of transcription or genomic replication of any RNA virus, particularly where it is critical to image and quantify RNA levels in hundreds to thousands of cells per experimental condition. We have taken advantage of this pipeline to gain new insights into the transcription and replication kinetics of LCMV RNAs over the course of infection that build upon previous studies. In particular, our data strongly support the transient, cyclical infection model originally proposed by Hotchin (Hotchin, 1973, 1974a, b; Hotchin et al., 1975) and suggest that, following a period of productive infection, cells can clear infection, including viral genetic material, before becoming susceptible to reinfection. Further, our data suggest that viral antigenomic RNA in virions may not be transcriptionally functional upon virus entry and that a significant fraction of virus particles may lack functional L genomic RNA. Our findings give new insights into longstanding questions about how viral RNA transcription and replication are regulated during infection and how viruses may establish a long-lived, persistent infection. Developing the ability to label genomic and antigenomic RNAs with greater sensitivity will be an important next step toward the construction of a quantitative model of the regulation of viral RNA replication and transcription over time with the goal of explaining the oscillatory behavior of viral RNA synthesis during persistence.

2.6. Materials and Methods

2.6.1. Cells and Viruses.

A549 (CCL-185) were obtained from American Type Culture Collection (ATCC, Manassas, VA). A549 cells were cultured in DMEM-F12 (11320-033, Thermo Fisher), containing 10% fetal bovine serum and 1% Penicillin-Streptomycin (15140-163, Thermo Fisher). LCMV Armstrong 53b was provided by J. L. Whitton (The Scripps Research institute, La Jolla, CA). A549 cells were infected with LCMV Arm53b at an MOI of 0.1 (Figure 2.5 to 2.6) or an MOI of 0.01 (Figure 2.1, 2.2, 2.4, 2.7, 2.8, and 2.9). For experiments examining late, persistent time points following infections, a T25 tissue culture flask of A549 cells was infected. The flask of infected cells was trypsinized and cells were plated on glass coverslips 24 hours prior to the reported time points where cover slips were fixed, stained, and imaged as described below (Figure 2.9). Remaining cells were diluted and re-plated in a T25 flask until 24 hours before the next examined time point where this process was repeated.

2.6.2. Single molecule RNA-FISH.

Cells were plated on 14 mm round #1 glass coverslips. Following infection, cells were briefly washed in room temperature DPBS (with Calcium and Magnesium) (14040133, Thermo Fisher) and fixed in 4% PFA in 1x PBS for 10 minutes at room temperature. Coverslips were washed twice in room temperature PBS and fixed again at -20° C with 70% ethanol for at least two hours. Coverslips were washed twice with 2x SSC (AM9770, Thermo Fisher) and washed once with 2x SSC and 10% Formamide (BP227,

Fisher Scientific). smFISH probes to different viral RNA species (Figure 2.1A) were designed using the Stellaris Probe Designer at https://www.biosearchtech.com/ (Table S2.2). Unlabeled smFISH probes had a 3' modified base with an amine functional group. Pools of 48 individual smFISH probes to a particular target RNA were combined at equimolar ratios and were covalently labeled with Cy3 (PA23001, GE Healthcare), AlexaFluor 568 (A20003, Thermo Fisher), or Cy5 (PA25001, GE Healthcare) as previously described (Zenklusen and Singer, 2010). Coverslips were placed face down on a 100 ul drop of hybridization mix containing 75 ng of smFISH probe dissolved in hybridization buffer composed of 10% dextran sulfate (D8906, Sigma-Aldrich), 2x SSC, and 10% Formamide. Hybridization occurred in a humidified chamber at 37° C overnight. Coverslips were washed twice in 2x SSC, 10% formamide at 37° C for 30 minutes. Coverslips were then washed once in 1x PBS. For cellular segmentation, cells were stained with HCS CellMask™ Green stain (H32714, Thermo Fisher) diluted at 50 ng/ml in PBS for 5 minutes at room temperature (note: this is significantly more dilute than recommended in the product information, but we found it necessary to prevent overstaining cells and thus to prevent spectral bleed through into the AlexaFluor 568 fluorescence channel). Nuclei were stained with 4', 6-diamidino-2-phenylindole hydrochloride 30 (DAPI) (D9542, Sigma-Aldrich) at 1 µg/ml in PBS for 5 minutes at room temperature. Cells were washed a final time in PBS, briefly washed in water, dried and mounted with ProLong Gold Antifade Reagent (P36934, Thermo Fisher).

2.6.3. Image Acquisition.

Wide-field fluorescent Z-stacks were acquired using a Nikon Ti Eclipse microscope with a 60 × 1.4 NA objective. Samples were illuminated with an LED light-source (Lumencor Spectra X light engine) with appropriate filter sets and images were captured with a Hamamatsu Orca flash 4.0 LT sCMOS camera. Z-stacks were captured at 300 nm increments, and the microscope was controlled by Nikon NIS Elements software. Captured ND2 images were converted to Tiffs using the open source Bio-formats tool kit (http://www.openmicroscopy.org/) (Goldberg et al., 2005).

2.6.4. Image Segmentation and Analysis.

DAPI and CellMask Green Z-stacks were projected using a focus-based projection method as previously described (Tsanov et al., 2016). Projected DAPI images were used for automatic nuclear segmentation in CellProfiler (Broad Institute) (Kamentsky et al., 2011) and served as the seed for automatic secondary cellular segmentation using the projected CellMask Green images (Figure 2.4A). Statistics including average pixel intensity within the regions defined by primary and secondary segmentation were extracted from maximum intensity projections of smFISH Z-stacks using CellProfiler (Figure 2.4B to D).

Single smFISH labeled RNAs were detected and localized in 3D using FISH-quant (Mueller et al., 2013). Briefly, smFISH Z-stacks were filtered using the "Dual Gaussian Filter" and spots were detected using the "Local Maximum" method. As a large number of acquired images required analysis, images were analyzed in "Batch Mode" with settings

determined to give low rates of false positive detections. The signal-to-noise ratio of different smFISH probe sets was determined as the average signal amplitude of identified smFISH spots in an individual cell divided by the standard deviation of the fluorescent signal in a region of the same cell where smFISH spots were absent (Figure 2.3).

Box and whisker plots were created using the ggplot2 package in R. The box represents the interquartile range of the data with the center line representing the median. Individual dots represent cells that are more than 1.5 times the interquartile range away from the median of the data.

2.7. Funding Information

We also gratefully acknowledge funding support from NIH grants T32 HL076122-10 (BRK), T32 AI055402 (CMZ), R21 AI088059 (JB), and P20RR021905 & P30GM118228 (Immunobiology and Infectious Disease COBRE awards) (JB). DZ is supported by the Canadian Institute for Health Research (Project Grant-366682), Fond de recherche du Quebec (Chercheur-boursier Junior 2), and the Canadian Foundation for Innovation. CZ, FM, and AS were supported by Institut Pasteur and the Fondation pour la Recherche Médicale (FRM). BRK was supported by a Chateaubriand fellowship from the Office for Science & Technology at the Embassy of France in the United States. The funders had no role in study design, data collection and analysis, decision to publish, or preparation of the manuscript.

2.8. Acknowledgments

We gratefully acknowledge J. Lindsay Whitton for providing us with LCMV strain Arm53b and Samir Rahman, Philippe Clerc, Christian Weber, and Sophie Abélanet for technical assistance. We thank Pablo Navarro and Jason Stumpff for graciously offering the use of their microscopy equipment and for providing their expertise and Jean-Michel Arbona and Wei Ouyang for helpful discussions.

2.9. Tables

Table 2.1. Ratio in the expression levels of viral mRNAs in individual infected cells.

	Time points	*Ratio NP mRNA and S antigenome /GPC mRNA and S genome (± SD)*	*Ratio NP mRNA and S antigenome /L mRNA and L antigenome (± SD)*
Early time points (hpi) MOI = 0.1	0.5	ND	ND
	1	ND	ND
	2	ND	ND
	3	ND	ND
	4[a]	4.3 ± 3.4	ND
	6[a]	6.0 ± 4.0	14.7 ± 9.5
	8	4.9 ± 4.1	14.8 ± 12.1
	10	5.6 ± 5.4	12.5 ± 9.7
	12	5.0 ± 4.9	10.8 ± 9.5
Peak time points (hpi) MOI = 0.01	12	4.6 ± 4.1	8.8 ± 6.7
	24	3.5 ± 3.4	14.8 ± 7.2
	36	2.3 ± 1.9	18.0 ± 12.8
	48	2.2 ± 1.2	28.7 ± 14.8
	60	2.9 ± 1.2	34.1 ± 13.3
	72	2.9 ± 1.1	30.1 ± 16.2
	96	4.0 ± 1.9	24.5 ± 13.4
Persistent time (dpi) MOI = 0.01	1.5	2.3 ± 1.6	10.2 ± 12.3
	4	4.3 ± 2.0	10.5 ± 10.4
	6	3.9 ± 2.4	4.9 ± 6.8
	8	1.0 ± 0.7	2.0 ± 3.0
	13	4.4 ± 2.8	24.1 ± 23.9
	16	1.8 ± 1.7	2.4 ± 3.5
	20	6.2 ± 3.7	28.1 ± 23.5
	23	3.2 ± 2.0	5.8 ± 7.3
	27	4.9 ± 4.2	2.7 ± 4.5
	30	4.0 ± 2.3	9.1 ± 8.9
	34	0.7 ± 1.2	2.2 ± 3.4
	37	4.5 ± 3.8	6.1 ± 9.1
	41	1.0 ± 1.3	7.3 ± 9.0

[a]Note that for time points prior to 8 hpi, genomic and antigenomic RNAs are not detectable by FISH probe sets with exclusive specificity for these RNAs (data not shown). Therefore, spots detected before 8 hpi are presumed to represent only the mRNAs, but not the genome or antigenome, recognized by each respective probe set. Spots detect at 8 hpi or later are presumed to be a mixture of all RNAs recognized by a particular probe set (e.g. mRNA and genome or antigenome).

2.10. Figures

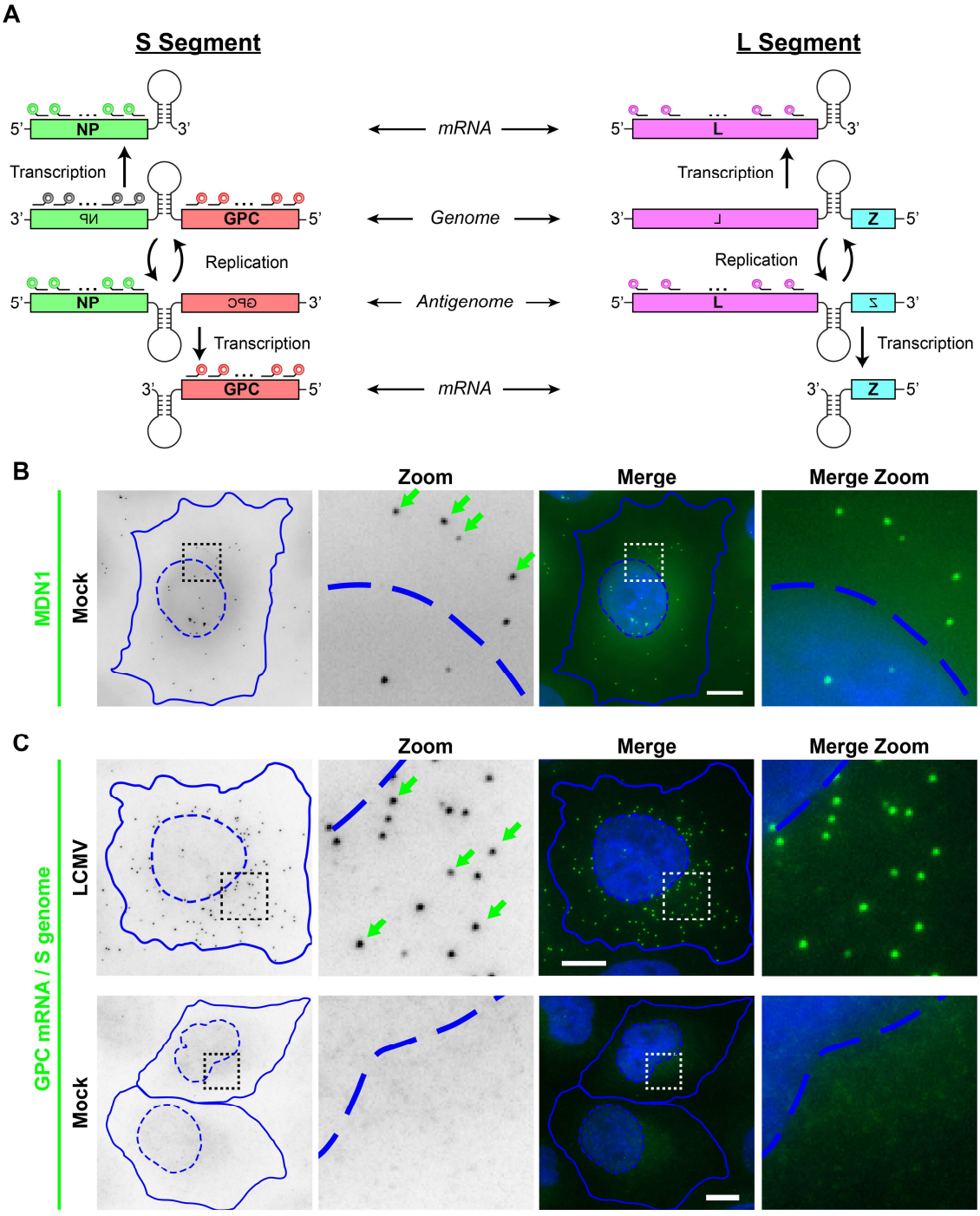
A
S Segment
L Segment
5'
NP
3'
mRNA
L
Transcription
Genome
Z
Replication
Antigenome
Transcription
mRNA
B
Zoom
Merge
Merge Zoom
MDN1
Mock
C
LCMV
GPC mRNA / S genome
Mock

Figure 2.1. LCMV RNA species can be specifically visualized using multiple, singly-labeled oligonucleotide smFISH probes.
(A) Overview of the scheme used by arenaviruses to transcribe and replicate their single-stranded, ambisense, bisegmented genome. smFISH probes that recognize the S segment genomic RNA are shown in gray, probes that recognize the S segment genome and GPC mRNA are shown in red, probes that recognize the S segment antigenome and NP mRNA are shown in green, and probes that recognize the L segment antigenome and L mRNA are shown in pink. smFISH probe sets consist of pools of 48 individual 20mer oligonucleotides each labeled with a single fluorophore at their 3' terminus. (B) Uninfected cells were stained with a control smFISH probe set specific to the cellular mRNA MDN1 labeled with Cy3. (C) Cells were either infected with LCMV at an MOI of 0.01 or, as a control, remained uninfected (mock). Cells were fixed at 24 hpi and stained with a Cy5-labeled smFISH probe set specific for S segment genomic RNA and GPC mRNA. Boxed regions of the cell are magnified and shown in columns labeled "Zoom". Green arrows indicate example smFISH stained spots most likely representing single labeled RNAs. Nuclear (hatched line) and cytoplasmic (solid line) boundaries are shown in blue. The same intensity levels for a particular probe set were applied to all images of mock- and LCMV-infected cells to permit comparisons. Scale bars are 10 μm.

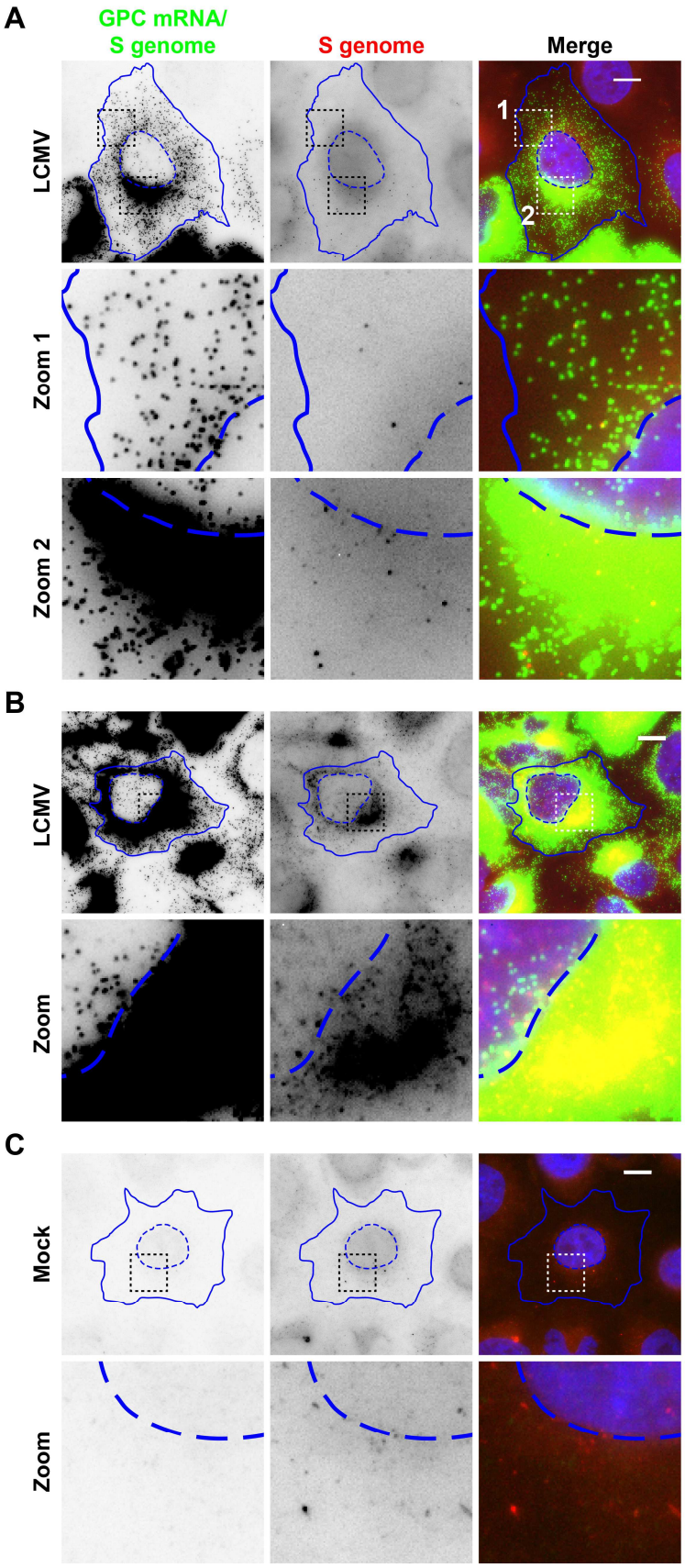
A
GPC mRNA/
S genome
S genome
Merge
LCMV
Zoom 1
Zoom 2
1
2
B
LCMV
Zoom
C
Mock
Zoom

Figure 2.2. smFISH probe sets recognizing viral mRNA species exhibit high signal-to-noise staining. Mock- or LCMV-infected cells (24 hr pi) were simultaneously stained with smFISH probe sets specific for either GPC mRNA and S genome (Cy5; green) or S genome only (AlexaFluor 568; red). Representative LCMV infected cells with moderate (A) or high (B) levels of viral RNA as well as a representative mock-infected cell (C) are displayed. Multiple Z stacks were acquired spanning the thickness of the cell and max intensity projections are displayed. Boxed regions of the cell are magnified and shown in rows labeled "Zoom". Nuclear (hatched line) and cytoplasmic (solid line) boundaries are shown in blue. (A to C) The same intensity levels for a particular probe set were applied to all images of mock- and LCMV-infected cells to permit comparisons. Scale bars are 10 μm.

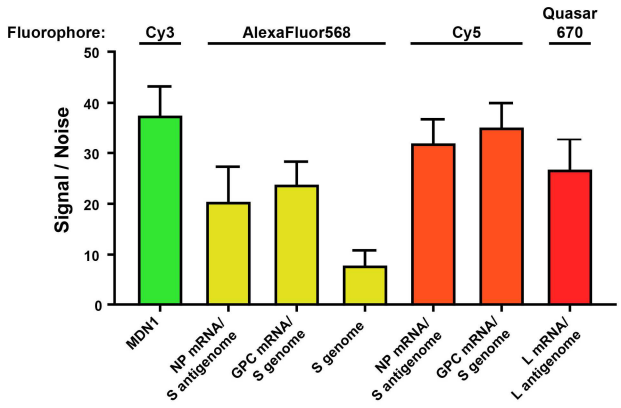

Figure 2.3. smFISH probe sets recognizing viral mRNA species exhibit high signal-to-noise staining
Signal-to-noise ratio of different smFISH probe sets labeled with the indicated fluorophores. Signal-to-noise ratio was calculated as average amplitude of detected smFISH spots divided by the standard deviation of signal in a region of the cell with no detected spots. The signal-to-noise ratio of 20 cells per smFISH probe set labeled with the indicated fluorophore was calculated, and the mean and standard deviation are graphed.

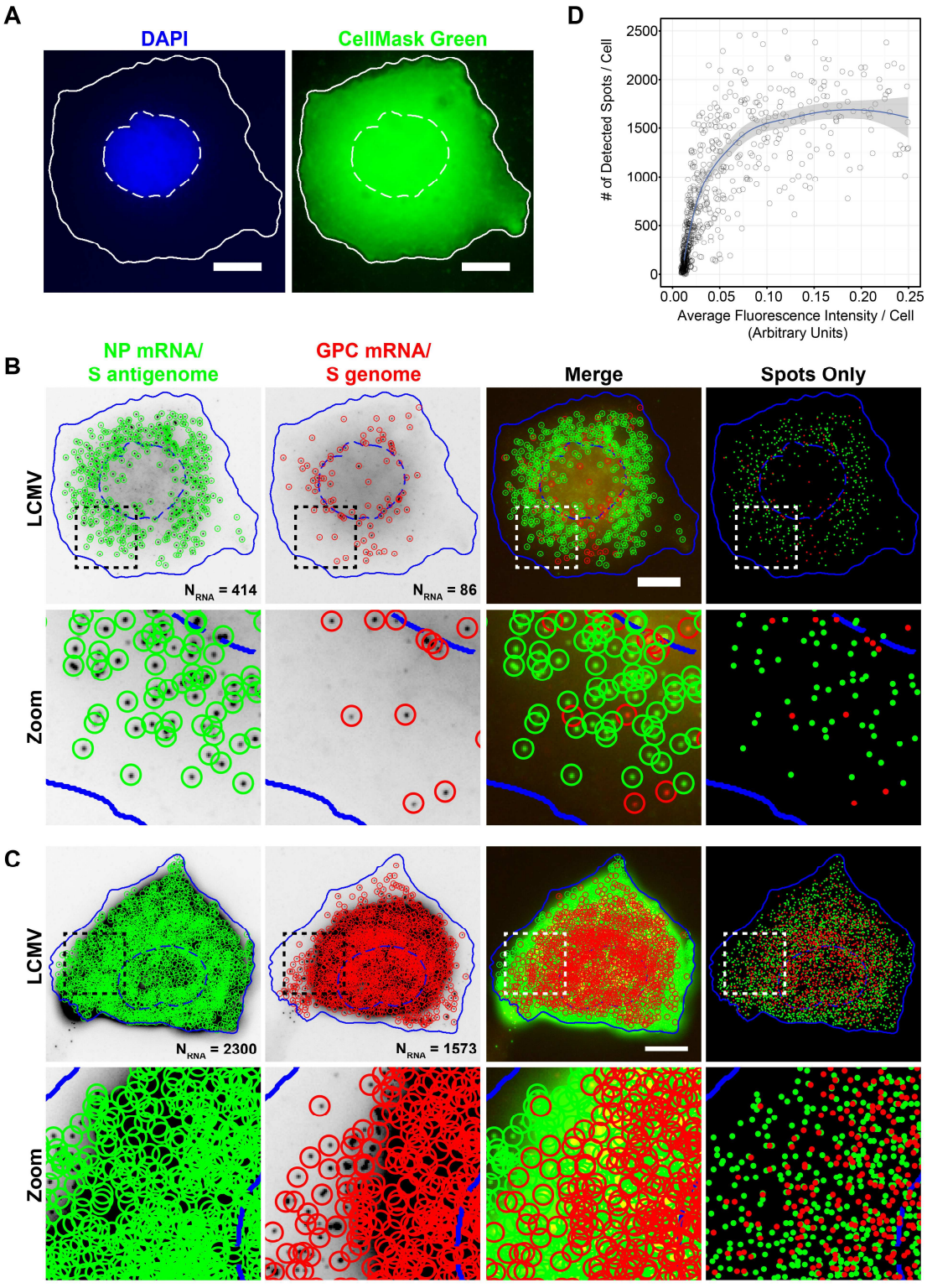
A
DAPI
CellMask Green
D
# of Detected Spots / Cell
2500
2000
1500
1000
500
0
0.00
0.05
0.10
0.15
0.20
0.25
Average Fluorescence Intensity / Cell
(Arbitrary Units)
B
NP mRNA/
S antigenome
GPC mRNA/
S genome
Merge
Spots Only
LCMV
Zoom
N_RNA = 414
N_RNA = 86
C
LCMV
Zoom
N_RNA = 2300
N_RNA = 1573

Figure 2.4. Automated detection and quantitation of LCMV RNAs labeled with spectrally distinct fluorophores.
(A) Cell nuclei and cytoplasms were automatically segmented using focus-based projections of DAPI (nuclei) or CellMask Green (cytoplasm) Z stacks acquired through the thickness of the cell. Note that pixel intensities of the CellMask Green projection displayed here have been log transformed to aid visualization. Nuclear (hatched line) and cytoplasmic (solid line) boundaries are shown in white. The scale bar is 10 μm.
(B and C) Maximum intensity projections of LCMV-infected cells were fixed 24 hpi and stained with smFISH probe sets to the NP mRNA/S antigenome (Cy5; green) and GPC mRNA/S genome (A568; red). The boxed region of each cell is magnified and shown in the row labeled "Zoom". Cells were segmented based on DAPI and CellMask Green staining (see panel A) and spots were detected and localized in 3D using FISH-quant. Individually detected RNAs are circled in green (NP mRNA/S antigenome) or red (GPC mRNA/S genome). The "Spots only" column shows only the position of detected spots in relation to the cell boundaries defined by segmentation. Nuclear (hatched line) and cytoplasmic (solid line) boundaries are shown in blue. The same intensity levels for a particular probe set were applied to both images of LCMV-infected cells to permit comparisons. The scale bar is 10 μm.
(D) Scatter plot shows the relationship between the fluorescence intensity in the smFISH channel in the maximum intensity projection of smFISH images and the number of smFISH spots detected by FISH-quant for LCMV-infected cells fixed 24 hpi and stained with the Cy5-labeled smFISH probes specific for NP mRNA/S antigenome.

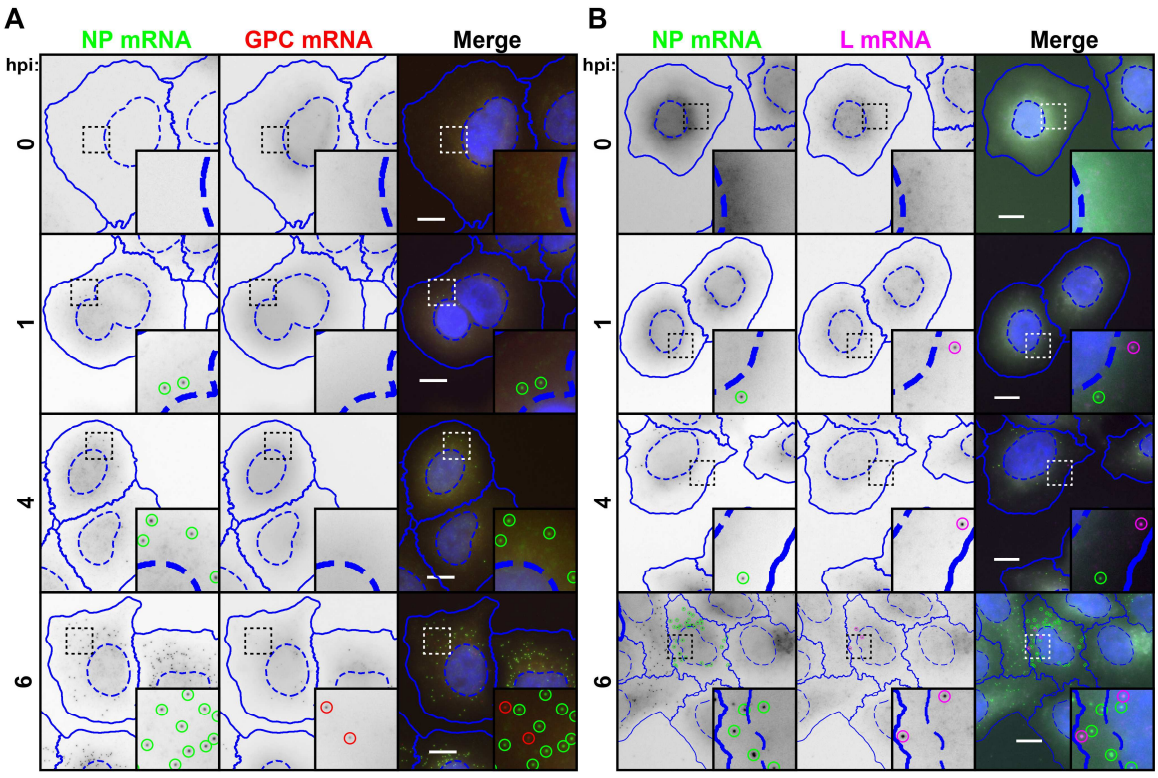

Figure 2.5. Transcription of NP and L genes is detectable soon following infection while GPC transcription exclusively occurs after a several hour lag.
Cells were infected with LCMV at an MOI of 0.1, fixed at various times following infection, and stained for NP mRNA (green) using a Cy5-labeled NP mRNA/S antigenome probe set, GPC mRNA (red) using an A568-labled GPC mRNA/S genome probe set (A) or NP mRNA (green) using an A568-labeled NP mRNA/S antigenome probe set and L mRNA (magenta) using a Quasar 670-labeled L mRNA/L antigenome probe set (B). Note that for the time points shown (less than 8 hpi), genomic and antigenomic RNAs are not detectable by smFISH probe sets with exclusive specificity for these RNAs (data not shown). Therefore, spots detected in this figure are presumed to represent only the mRNAs, but not the genome or antigenome, targeted by each respective probe set. Nuclear (hatched line) and cytoplasmic (solid line) boundaries as determined by Cell Profiler are shown in blue. Identified spots are outline by circles that are green for NP mRNA, red for GPC mRNA, and magenta for L mRNA. (A and B) The same intensity levels for a particular probe set were applied to all images of mock- and LCMV-infected cells across the time course to permit comparisons. Representative maximum intensity projections from 1 of 2 independent experiments are shown. Scale bar is 10 µm.

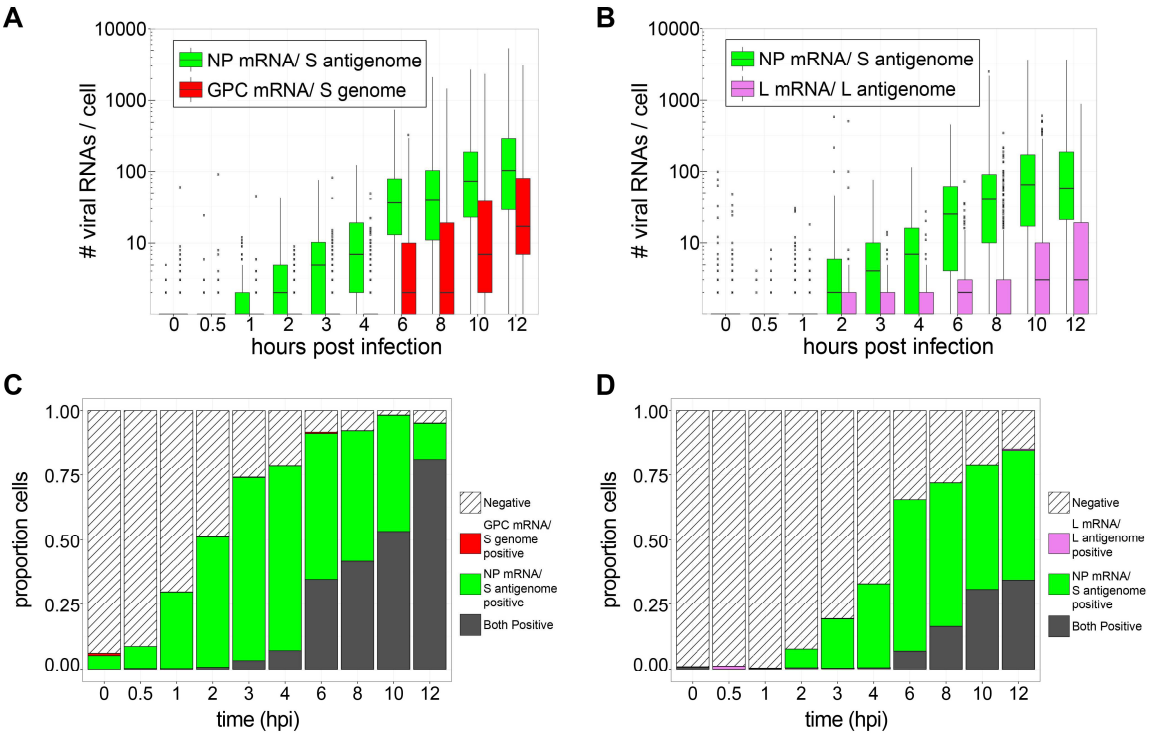

Figure 2.6. Transcription of NP and L genes is detectable immediately upon infection while GPC transcription exclusively occurs after a several hour lag.
Related to Figure 2.5. (A and B) Boxplots represent the number of viral RNAs detected in cells at early time points following infection with LCMV (see Figure 2.5). (C and D) Stacked bar graphs show the proportion of cells expressing RNAs detected by one, both, or neither viral RNA smFISH probe set. Between 620 and 1316 cells were examined at each time point (see Table S2.1 for exact numbers). In each case RNAs identified by specific probe sets are designated by color (green for NP mRNA/S antigenome probes, red for GPC mRNA/S genome probes, and magenta for L mRNA/L antigenome probes). Note that for time points prior to 8 hpi, genomic and antigenomic RNAs are not detectable by smFISH probe sets with exclusive specificity for these RNAs (data not shown). Therefore, spots detected before 8 hpi are presumed to represent only the mRNAs, but not the genome or antigenome, recognized by each respective probe set. Spots detected at 8 hpi or later are presumed to be a mixture of all RNAs recognized by a particular probe set (e.g. mRNA and genome or antigenome).

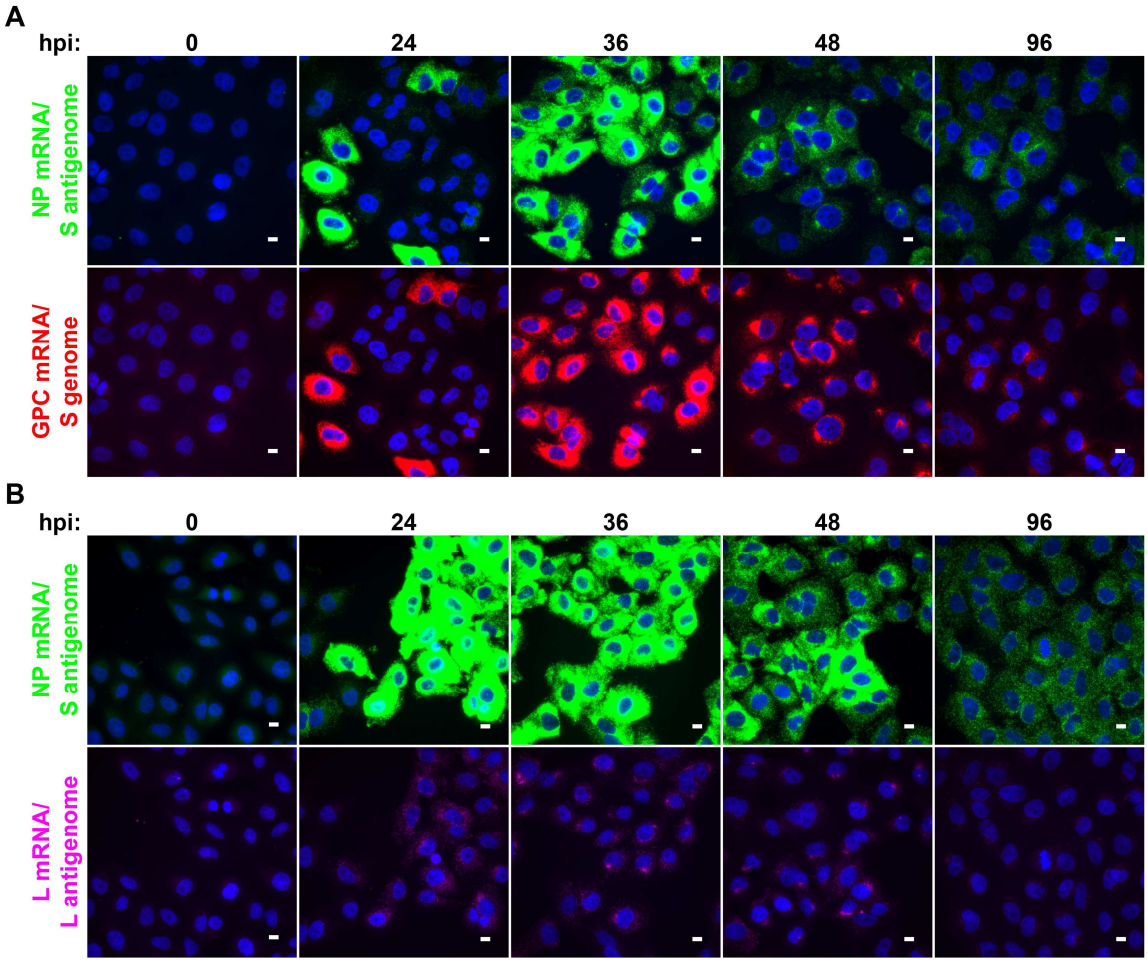

Figure 2.7. Peak viral RNA replication and transcription occurs 36 hpi and is slowly lost from infected cells over the following days.
Cells were infected with LCMV at an MOI of 0.01, fixed at various times following infection, and stained using smFISH probe sets specific for NP mRNA/S antigenome (Cy5; green) and GPC mRNA/S genome (A568; red) (A) or NP mRNA/S antigenome (A568; green) and L mRNA/L antigenome (Quasar 670; magenta) (B). (A and B) Representative maximum intensity projections of fields of infected cells at various time points from 1 of 2 independent experiments are shown. Each probe set is shown in its own row to highlight the difference in levels to which these RNAs accumulate. The same intensity levels for a particular probe set were applied to all images of mock- and LCMV-infected cells across the time course to permit comparisons. Scale bars = 10 μm.

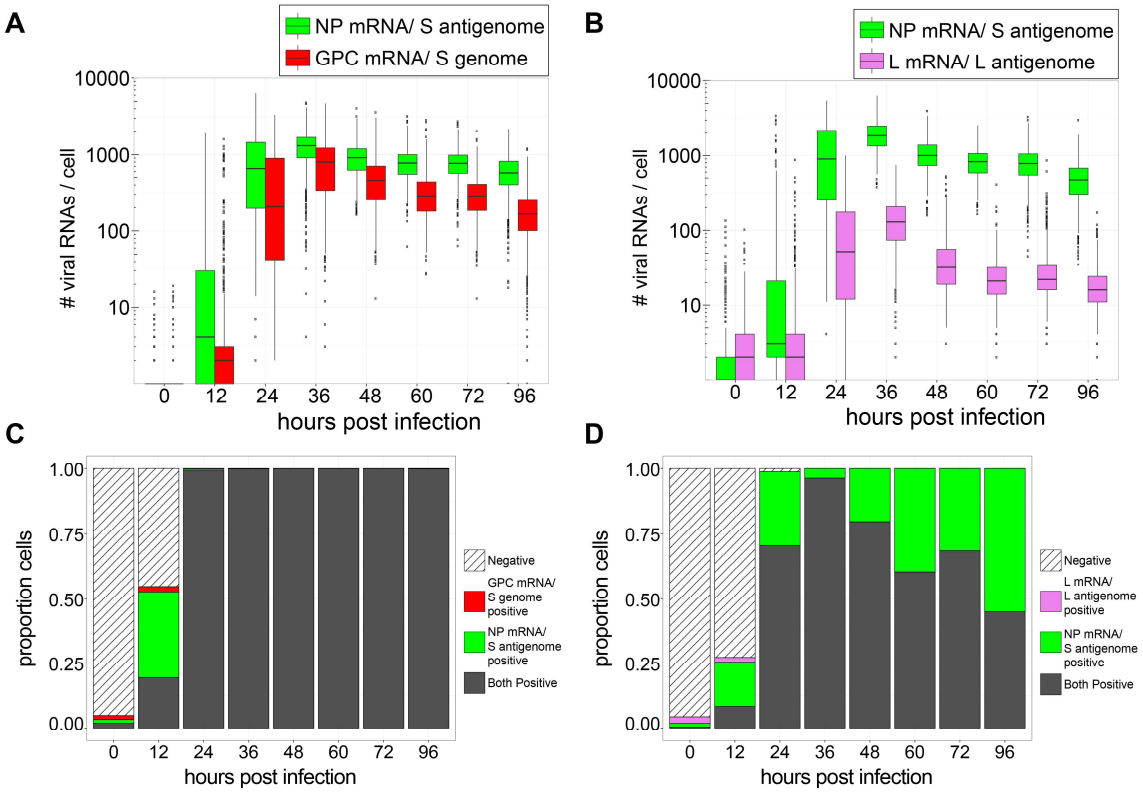

Figure 2.8. Peak viral RNA replication and transcription occurs 36 hpi and is slowly lost from infected cells over the following days.

Related to Figure 2.7. (A and B) Boxplots represent the number of mRNAs detected in cells at time points during the peak period of LCMV infection. (C and D) Stacked bar graph shows the proportion of cells expressing RNAs detected by one, both, or neither viral smFISH probe set. Between 480 and 1659 cells were examined at each time point (see Table S2.1 for exact numbers). RNAs identified by specific probe sets are designated by color (green for NP mRNA/S antigenome probes, red for GPC mRNA/S genome probes, and magenta for L mRNA/L antigenome probes).

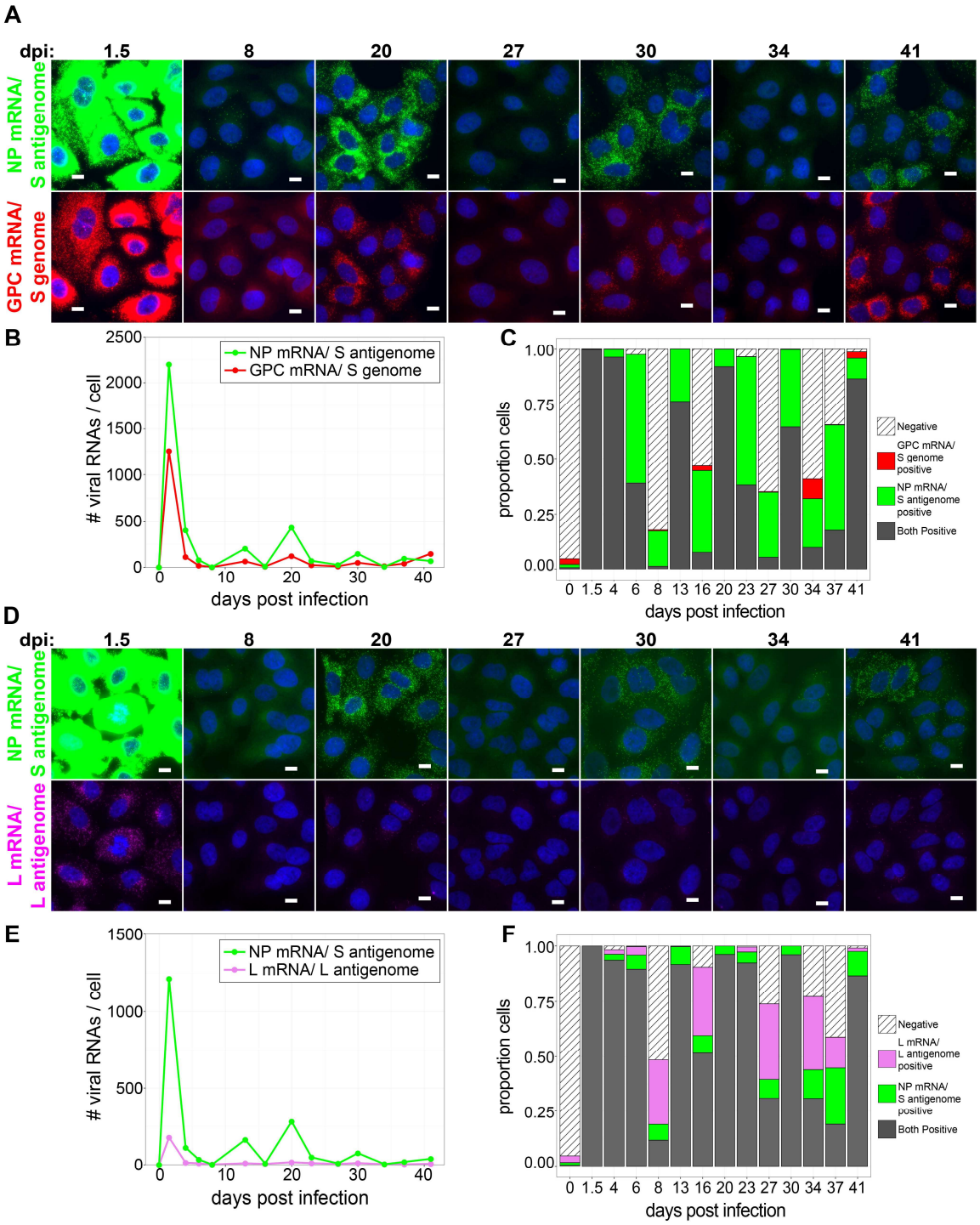

Figure 2.9. Cyclic periods of viral RNA production and viral RNA loss occur during persistence. Cells were infected with LCMV at an MOI of 0.01, fixed at the indicated time points following infection, and stained using smFISH probe sets specific for NP mRNA/S antigenome (Cy5; green) and GPC mRNA/S

genome (A568; red) (A) or NP mRNA/S antigenome (A568; green) and L mRNA/L antigenome (Quasar 670; magenta) (D). (A and D) Representative maximum intensity projections of fields of infected cells at various time points from 1 of 2 independent experiments are shown. Each probe set is shown in its own row to highlight the difference in levels to which these RNAs accumulate. The same intensity levels for a particular probe set were applied to all images of mock- and LCMV-infected cells across the time course to permit comparisons. Scale bar is 10 μm. (B and E) Line graphs show the average number of the indicated viral RNAs detected in cells at time points during the persistent phase of LCMV infection. (C and F) Stacked bar graph shows the proportion of cells expressing RNAs detected by one, both, or neither viral smFISH probe set. Between 316 and 1218 cells were examined at each time point (see Table S2.1 for exact numbers).

2.11. References

Auperin, D.D., Romanowski, V., Galinski, M., and Bishop, D.H. (1984b). Sequencing studies of pichinde arenavirus S RNA indicate a novel coding strategy, an ambisense viral S RNA. Journal of virology *52*, 897-904.

Buchmeier, M.J., de la Torre, J.C., and Peters, C.J. (2007). Arenaviridae: The Viruses and Their Replication. In Fields Virology, D.M. Knipe, P.M. Howley, D.E. Griffin, R.A. Lamb, M.A. Martin, B. Roizman, and S.E. Straus, eds. (Philadelphia: Wolters Kluwer Heath/Lippincott Williams & Wilkins), pp. 1791-1827.

Buchmeier, M.J., Elder, J.H., and Oldstone, M.B. (1978). Protein structure of lymphocytic choriomeningitis virus: identification of the virus structural and cell associated polypeptides. Virology *89*, 133-145.

Buchmeier, M.J., Welsh, R.M., Dutko, F.J., and Oldstone, M.B. (1980). The virology and immunobiology of lymphocytic choriomeningitis virus infection. Adv Immunol *30*, 275-331.

Buchmeier, M.J., and Zajac, A.J. (1999). Lymphocytic choriomeningitis virus. In Persistent viral infections, R. Ahmed, and I. Chen, eds. (Chichester ; New York: John Wiley & Sons), pp. x, 725 p.

Burns, J.W., and Buchmeier, M.J. (1993). Glycoproteins of the arenaviruses. In The Arenaviridae, M.S. Salvato, ed. (New York: Plenum Press), pp. 17-35.

Cornu, T.I., and de la Torre, J.C. (2001). RING finger Z protein of lymphocytic choriomeningitis virus (LCMV) inhibits transcription and RNA replication of an LCMV S-segment minigenome. Journal of virology *75*, 9415-9426.

Cornu, T.I., and de la Torre, J.C. (2002). Characterization of the arenavirus RING finger Z protein regions required for Z-mediated inhibition of viral RNA synthesis. Journal of virology *76*, 6678-6688.

Dutko, F.J., and Pfau, C.J. (1978). Arenavirus defective interfering particles mask the cell-killing potential of standard virus. The Journal of general virology *38*, 195-208.

Enria, D.A., Briggiler, A.M., and Sanchez, Z. (2008). Treatment of Argentine hemorrhagic fever. Antiviral Res *78*, 132-139.

Fischer, S.A., Graham, M.B., Kuehnert, M.J., Kotton, C.N., Srinivasan, A., Marty, F.M., Comer, J.A., Guarner, J., Paddock, C.D., DeMeo, D.L., Shieh, W.J., Erickson, B.R., Bandy, U., DeMaria, A., Jr., Davis, J.P., Delmonico, F.L., Pavlin, B., Likos, A., Vincent, M.J., Sealy, T.K., Goldsmith, C.S., Jernigan, D.B., Rollin, P.E., Packard, M.M., Patel, M.,

Rowland, C., Helfand, R.F., Nichol, S.T., Fishman, J.A., Ksiazek, T., Zaki, S.R., and Team, L.i.T.R.I. (2006). Transmission of lymphocytic choriomeningitis virus by organ transplantation. N Engl J Med *354*, 2235-2249.

Francis, S.J., and Southern, P.J. (1988a). Deleted viral RNAs and lymphocytic choriomeningitis virus persistence in vitro. The Journal of general virology *69 (Pt 8)*, 1893-1902.

Francis, S.J., and Southern, P.J. (1988b). Molecular analysis of viral RNAs in mice persistently infected with lymphocytic choriomeningitis virus. Journal of virology *62*, 1251-1257.

Francis, S.J., Southern, P.J., Valsamakis, A., and Oldstone, M.B. (1987). State of viral genome and proteins during persistent lymphocytic choriomeningitis virus infection. Current topics in microbiology and immunology *133*, 67-88.

Franze-Fernandez, M.T., Zetina, C., Iapalucci, S., Lucero, M.A., Bouissou, C., Lopez, R., Rey, O., Daheli, M., Cohen, G.N., and Zakin, M.M. (1987). Molecular structure and early events in the replication of Tacaribe arenavirus S RNA. Virus research *7*, 309-324.

Fuller-Pace, F.V., and Southern, P.J. (1988). Temporal analysis of transcription and replication during acute infection with lymphocytic choriomeningitis virus. Virology *162*, 260-263.

Fuller-Pace, F.V., and Southern, P.J. (1989). Detection of virus-specific RNA-dependent RNA polymerase activity in extracts from cells infected with lymphocytic choriomeningitis virus: in vitro synthesis of full-length viral RNA species. Journal of virology *63*, 1938-1944.

Goldberg, I.G., Allan, C., Burel, J.M., Creager, D., Falconi, A., Hochheiser, H., Johnston, J., Mellen, J., Sorger, P.K., and Swedlow, J.R. (2005). The Open Microscopy Environment (OME) Data Model and XML file: open tools for informatics and quantitative analysis in biological imaging. Genome Biol *6*, R47.

Haist, K., Ziegler, C., and Botten, J. (2015). Strand-Specific Quantitative Reverse Transcription-Polymerase Chain Reaction Assay for Measurement of Arenavirus Genomic and Antigenomic RNAs. PloS one *10*, e0120043.

Hotchin, J. (1973). Transient virus infection: spontaneous recovery mechanism of lymphocytic choriomeningitis virrus-infected cells. Nat New Biol *241*, 270-272.

Hotchin, J. (1974a). Cyclical phenomena in persistent virus infection. J Reticuloendothel Soc *15*, 304-311.

Hotchin, J. (1974b). The role of transient infection in arenavirus persistence. Prog Med Virol *18*, 81-93.

Hotchin, J., Kinch, W., Benson, L., and Sikora, E. (1975). Role of substrains in persistent lymphocytic choriomeningitis virus infection. Bull World Health Organ *52*, 457-463.

Huang, A.S. (1973). Defective interfering viruses. Annual review of microbiology *27*, 101-117.

Huang, A.S., and Baltimore, D. (1970). Defective viral particles and viral disease processes. Nature *226*, 325-327.

Kamentsky, L., Jones, T.R., Fraser, A., Bray, M.A., Logan, D.J., Madden, K.L., Ljosa, V., Rueden, C., Eliceiri, K.W., and Carpenter, A.E. (2011). Improved structure, function and compatibility for CellProfiler: modular high-throughput image analysis software. Bioinformatics *27*, 1179-1180.

Kranzusch, P.J., and Whelan, S.P. (2011). Arenavirus Z protein controls viral RNA synthesis by locking a polymerase-promoter complex. Proceedings of the National Academy of Sciences of the United States of America *108*, 19743-19748.

Lehmann-Grube, F. (1967). A carrier state of lymphocytic choriomeningitis virus in L cell cultures. Nature *213*, 770-773.

Lehmann-Grube, F. (1971). Lymphocytic choriomeningitis virus, Vol 10 (Wien: Springer-Verlag).

Lehmann-Grube, F., Martinez Peralta, L.M., Bruns, M., and Lohler, J. (1983). Persistent infection of mice with the lymphocytic choriomeningitis virus. In Virus-host interactions, receptors, persistence, and neurological diseases, H. Fraenkel-Conrat, and R.R. Wagner, eds. (New York: Plenum Press), pp. 43-103.

Lehmann-Grube, F., Popescu, M., Schaefer, H., and Gschwender, H.H. (1975). LCM virus infection of cells in vitro. Bull World Health Organ *52*, 443-456.

Lehmann-Grube, F., Slenczka, W., and Tees, R. (1969). A persistent and inapparent infection of L cells with the virus of lymphocytic choriomeningitis. The Journal of general virology *5*, 63-81.

Lopez, N., Jacamo, R., and Franze-Fernandez, M.T. (2001). Transcription and RNA replication of tacaribe virus genome and antigenome analogs require N and L proteins: Z protein is an inhibitor of these processes. Journal of virology *75*, 12241-12251.

McCormick, J.B., King, I.J., Webb, P.A., Scribner, C.L., Craven, R.B., Johnson, K.M., Elliott, L.H., and Belmont-Williams, R. (1986). Lassa fever. Effective therapy with ribavirin. N Engl J Med *314*, 20-26.

Meyer, B.J., de la Torre, J.C., and Southern, P.J. (2002). Arenaviruses: genomic RNAs, transcription, and replication. Current topics in microbiology and immunology *262*, 139-157.

Meyer, B.J., and Southern, P.J. (1993). Concurrent sequence analysis of 5' and 3' RNA termini by intramolecular circularization reveals 5' nontemplated bases and 3' terminal heterogeneity for lymphocytic choriomeningitis virus mRNAs. Journal of virology *67*, 2621-2627.

Meyer, B.J., and Southern, P.J. (1994). Sequence heterogeneity in the termini of lymphocytic choriomeningitis virus genomic and antigenomic RNAs. Journal of virology *68*, 7659-7664.

Meyer, B.J., and Southern, P.J. (1997). A novel type of defective viral genome suggests a unique strategy to establish and maintain persistent lymphocytic choriomeningitis virus infections. Journal of virology *71*, 6757-6764.

Mueller, F., Senecal, A., Tantale, K., Marie-Nelly, H., Ly, N., Collin, O., Basyuk, E., Bertrand, E., Darzacq, X., and Zimmer, C. (2013). FISH-quant: automatic counting of transcripts in 3D FISH images. Nature methods *10*, 277-278.

Oldstone, M.B. (1998). Viral persistence: mechanisms and consequences. Curr Opin Microbiol *1*, 436-441.

Oldstone, M.B., and Buchmeier, M.J. (1982). Restricted expression of viral glycoprotein in cells of persistently infected mice. Nature *300*, 360-362.

Polyak, S.J., Zheng, S., and Harnish, D.G. (1995b). Analysis of Pichinde arenavirus transcription and replication in human THP-1 monocytic cells. Virus research *36*, 37-48.

Raj, A., van den Bogaard, P., Rifkin, S.A., van Oudenaarden, A., and Tyagi, S. (2008). Imaging individual mRNA molecules using multiple singly labeled probes. Nature methods *5*, 877-879.

Salvato, M.S., and Shimomaye, E.M. (1989). The completed sequence of lymphocytic choriomeningitis virus reveals a unique RNA structure and a gene for a zinc finger protein. Virology *173*, 1-10.

Shivaprakash, M., Harnish, D., and Rawls, W. (1988). Characterization of temperature-sensitive mutants of Pichinde virus. Journal of virology *62*, 4037-4043.

Southern, P.J., Singh, M.K., Riviere, Y., Jacoby, D.R., Buchmeier, M.J., and Oldstone, M.B. (1987). Molecular characterization of the genomic S RNA segment from lymphocytic choriomeningitis virus. Virology *157*, 145-155.

Staneck, L.D., Trowbridge, R.S., Welsh, R.M., Wright, E.A., and Pfau, C.J. (1972). Arenaviruses: cellular response to long-term in vitro infection with parana and lymphocytic choriomeningitis viruses. Infect Immun *6*, 444-450.

Tsanov, N., Samacoits, A., Chouaib, R., Traboulsi, A.M., Gostan, T., Weber, C., Zimmer, C., Zibara, K., Walter, T., Peter, M., Bertrand, E., and Mueller, F. (2016). smiFISH and FISH-quant - a flexible single RNA detection approach with super-resolution capability. Nucleic Acids Res *44*, e165.

Welsh, R.M., O'Connell, C.M., and Pfau, C.J. (1972). Properties of defective lymphocytic choriomeningitis virus. The Journal of general virology *17*, 355-359.

Zenklusen, D., Larson, D.R., and Singer, R.H. (2008). Single-RNA counting reveals alternative modes of gene expression in yeast. Nat Struct Mol Biol *15*, 1263-1271.

Zenklusen, D., and Singer, R.H. (2010). Analyzing mRNA expression using single mRNA resolution fluorescent in situ hybridization. Methods Enzymol *470*, 641-659.

Ziegler, C.M., Eisenhauer, P., Bruce, E.A., Weir, M.E., King, B.R., Klaus, J.P., Krementsov, D.N., Shirley, D.J., Ballif, B.A., and Botten, J. (2016b). The Lymphocytic Choriomeningitis Virus Matrix Protein PPXY Late Domain Drives the Production of Defective Interfering Particles. PLoS pathogens *12*, e1005501.

2.12. Supplemental Tables

Table S2.1. Number of cells analyzed at each time point in selected Figures

	Number of cells analyzed per FISH probe set per time point in Figures 5 & 6	
Hours post infection	NP mRNA/ S antigenome GPC mRNA/ S genome	L mRNA/L antigenome NP mRNA/ S antigenome
0	752	634
1	759	659
2	1228	699
3	1316	748
4	1173	691
6	758	620
8	1037	645
10	940	629
12	1195	740
	Number of cells analyzed per FISH probe set per time point in Figures 7 & 8	
Hours post infection	NP mRNA/ S antigenome GPC mRNA/ S genome	L mRNA/L antigenome NP mRNA/ S antigenome
0	1119	760
12	733	494
24	757	480
36	731	565
48	789	585
60	719	494
72	886	713
96	1659	1064
	Number of cells analyzed per FISH probe set per time point in Figure 9	
Days post infection	NP mRNA/ S antigenome GPC mRNA/ S genome	L mRNA/L antigenome NP mRNA/ S antigenome
0	813	787
1.5	541	440
4	659	602
6	1130	649
8	955	787
13	649	316

16	1006	920
20	1181	902
23	997	903
27	1143	956
30	1046	874
34	1183	824
37	970	802
41	1218	926

Table S2.2. Full list and sequence of the FISH probes used in the current study

Target	Probe Sequence	Probe Name	Fluorophore
LCMV S Genome	tttagaggcccaaatgttgt	LCMV_S_Genome_1	AlexaFluor 568
LCMV S Genome	gctcccagatctgaaaactg	LCMV_S_Genome_2	AlexaFluor 568
LCMV S Genome	cactcatggactgcatcatt	LCMV_S_Genome_3	AlexaFluor 568
LCMV S Genome	tcgatgttgaaatgaccagg	LCMV_S_Genome_4	AlexaFluor 568
LCMV S Genome	ggactcacagaataggaagg	LCMV_S_Genome_5	AlexaFluor 568
LCMV S Genome	ccgatgacatcagaaagctt	LCMV_S_Genome_6	AlexaFluor 568
LCMV S Genome	atggttctaagctgtcaagg	LCMV_S_Genome_7	AlexaFluor 568
LCMV S Genome	tcgtcagttataggtgctct	LCMV_S_Genome_8	AlexaFluor 568
LCMV S Genome	gatcttgccgacctcttcaa	LCMV_S_Genome_9	AlexaFluor 568
LCMV S Genome	gattccaagtactcacacgg	LCMV_S_Genome_10	AlexaFluor 568
LCMV S Genome	ggaacccgttgatcaaaaac	LCMV_S_Genome_11	AlexaFluor 568
LCMV S Genome	cgggcagttcatacactttt	LCMV_S_Genome_12	AlexaFluor 568
LCMV S Genome	tgatccagtggaaatagcaa	LCMV_S_Genome_13	AlexaFluor 568
LCMV S Genome	caacgctcctacatggattg	LCMV_S_Genome_14	AlexaFluor 568
LCMV S Genome	tacagccagacaatgctttt	LCMV_S_Genome_15	AlexaFluor 568
LCMV S Genome	agaaacctgcagtcaattca	LCMV_S_Genome_16	AlexaFluor 568
LCMV S Genome	gcatgggaaaacacaacaat	LCMV_S_Genome_17	AlexaFluor 568
LCMV S Genome	gatggccatacatagcttgt	LCMV_S_Genome_18	AlexaFluor 568
LCMV S Genome	aaagtttgcctttcaggtga	LCMV_S_Genome_19	AlexaFluor 568
LCMV S Genome	caggaacccttatgaaaaca	LCMV_S_Genome_20	AlexaFluor 568
LCMV S Genome	ttgtttcagaccaagttggg	LCMV_S_Genome_21	AlexaFluor 568
LCMV S Genome	ggccaagagaaaactcaaca	LCMV_S_Genome_22	AlexaFluor 568
LCMV S Genome	gacctcttgaaggcagttct	LCMV_S_Genome_23	AlexaFluor 568
LCMV S Genome	ttttgatcaagccaagcaac	LCMV_S_Genome_24	AlexaFluor 568
LCMV S Genome	aactttagtcttggtgctgc	LCMV_S_Genome_25	AlexaFluor 568
LCMV S Genome	gtcatcactgaacagcagtc	LCMV_S_Genome_26	AlexaFluor 568
LCMV S Genome	tcttgaaaggctgaaagaca	LCMV_S_Genome_27	AlexaFluor 568
LCMV S Genome	ggcttgctttacacagtcaa	LCMV_S_Genome_28	AlexaFluor 568
LCMV S Genome	tcaatgacgttgtacaagcg	LCMV_S_Genome_29	AlexaFluor 568
LCMV S Genome	ctatggcttgtatggccaaa	LCMV_S_Genome_30	AlexaFluor 568
LCMV S Genome	aatcaatttggcacaatgcc	LCMV_S_Genome_31	AlexaFluor 568
LCMV S Genome	gggatgtgaaagactcatca	LCMV_S_Genome_32	AlexaFluor 568
LCMV S Genome	ttgggatgagaaagcctcag	LCMV_S_Genome_33	AlexaFluor 568
LCMV S Genome	gaccaaagatctcagatcct	LCMV_S_Genome_34	AlexaFluor 568
LCMV S Genome	gggaacttaacaacacagca	LCMV_S_Genome_35	AlexaFluor 568
LCMV S Genome	ccaggcttcaggggtatata	LCMV_S_Genome_36	AlexaFluor 568
LCMV S Genome	ccaagatcatgaggtctgaa	LCMV_S_Genome_37	AlexaFluor 568

LCMV S Genome	gctgaccttgagaagctgaa	LCMV_S_Genome_38	AlexaFluor 568
LCMV S Genome	cagtgcagaagaactgatgt	LCMV_S_Genome_39	AlexaFluor 568
LCMV S Genome	actgtacattctcttgtgga	LCMV_S_Genome_40	AlexaFluor 568
LCMV S Genome	gagactcagaagtctcaacc	LCMV_S_Genome_41	AlexaFluor 568
LCMV S Genome	aagagagatgacaaagacct	LCMV_S_Genome_42	AlexaFluor 568
LCMV S Genome	cttctctgaggtcagcaatg	LCMV_S_Genome_43	AlexaFluor 568
LCMV S Genome	ccaaccttctgaatgggttg	LCMV_S_Genome_44	AlexaFluor 568
LCMV S Genome	ggctgctgtcattaaggatg	LCMV_S_Genome_45	AlexaFluor 568
LCMV S Genome	gcagagcttcacatcagatg	LCMV_S_Genome_46	AlexaFluor 568
LCMV S Genome	cgcaagcattgagaagagaa	LCMV_S_Genome_47	AlexaFluor 568
LCMV S Genome	aggaagttaagagcttccaa	LCMV_S_Genome_48	AlexaFluor 568
LCMV NP mRNA/ S antigenome	ttggaagctcttaacttcct	LCMV_NP_mRNA_1	AlexaFluor 568 or Cy5
LCMV NP mRNA/ S antigenome	ttctcttctcaatgcttgcg	LCMV_NP_mRNA_2	AlexaFluor 568 or Cy5
LCMV NP mRNA/ S antigenome	catctgatgtgaagctctgc	LCMV_NP_mRNA_3	AlexaFluor 568 or Cy5
LCMV NP mRNA/ S antigenome	catccttaatgacagcagcc	LCMV_NP_mRNA_4	AlexaFluor 568 or Cy5
LCMV NP mRNA/ S antigenome	caacccattcagaaggttgg	LCMV_NP_mRNA_5	AlexaFluor 568 or Cy5
LCMV NP mRNA/ S antigenome	cattgctgacctcagagaag	LCMV_NP_mRNA_6	AlexaFluor 568 or Cy5
LCMV NP mRNA/ S antigenome	gttcttctgcactgagcctc	LCMV_NP_mRNA_7	AlexaFluor 568 or Cy5
LCMV NP mRNA/ S antigenome	aggtcagccgcaagagacat	LCMV_NP_mRNA_8	AlexaFluor 568 or Cy5
LCMV NP mRNA/ S antigenome	ctgaagcctggggcctttca	LCMV_NP_mRNA_9	AlexaFluor 568 or Cy5
LCMV NP mRNA/ S antigenome	tgtgttgttaagttccccat	LCMV_NP_mRNA_10	AlexaFluor 568 or Cy5
LCMV NP mRNA/ S antigenome	ctgagatctttggtctagtt	LCMV_NP_mRNA_11	AlexaFluor 568 or Cy5
LCMV NP mRNA/ S antigenome	tcatcccaactatctgtagg	LCMV_NP_mRNA_12	AlexaFluor 568 or Cy5
LCMV NP mRNA/ S antigenome	cttgcaccctgctgaggctt	LCMV_NP_mRNA_13	AlexaFluor 568 or Cy5
LCMV NP mRNA/ S antigenome	gatgagtctttcacatccca	LCMV_NP_mRNA_14	AlexaFluor 568 or Cy5
LCMV NP mRNA/ S antigenome	tgtgccaaattgattgttca	LCMV_NP_mRNA_15	AlexaFluor 568 or Cy5
LCMV NP mRNA/ S antigenome	aagccatagttagacttggc	LCMV_NP_mRNA_16	AlexaFluor 568 or Cy5
LCMV NP mRNA/ S antigenome	gtctgtgactgtttggccat	LCMV_NP_mRNA_17	AlexaFluor 568 or Cy5
LCMV NP mRNA/ S antigenome	ttgtacaacgtcattgagcg	LCMV_NP_mRNA_18	AlexaFluor 568 or Cy5
LCMV NP mRNA/ S antigenome	ttgactgtgtaaagcaagcc	LCMV_NP_mRNA_19	AlexaFluor 568 or Cy5
LCMV NP mRNA/ S antigenome	tgtctttcagcctttcaaga	LCMV_NP_mRNA_20	AlexaFluor 568 or Cy5
LCMV NP mRNA/ S antigenome	gcagcaccaagactaaagtt	LCMV_NP_mRNA_21	AlexaFluor 568 or Cy5
LCMV NP mRNA/ S antigenome	gttgcttggcttgatcaaaa	LCMV_NP_mRNA_22	AlexaFluor 568 or Cy5
LCMV NP mRNA/ S antigenome	gagaactgccttcaagaggt	LCMV_NP_mRNA_23	AlexaFluor 568 or Cy5
LCMV NP mRNA/ S antigenome	tgttgagttttctcttggcc	LCMV_NP_mRNA_24	AlexaFluor 568 or Cy5
LCMV NP mRNA/ S antigenome	cccaacttggtctgaaacaa	LCMV_NP_mRNA_25	AlexaFluor 568 or Cy5
LCMV NP mRNA/ S antigenome	tgttttcataagggttcctg	LCMV_NP_mRNA_26	AlexaFluor 568 or Cy5
LCMV NP mRNA/ S antigenome	tcacctgaaaggcaaacttt	LCMV_NP_mRNA_27	AlexaFluor 568 or Cy5
LCMV NP mRNA/ S antigenome	acaagctatgtatggccatc	LCMV_NP_mRNA_28	AlexaFluor 568 or Cy5

LCMV NP mRNA/ S antigenome	attgttgtgttttcccatgc	LCMV_NP_mRNA_29	AlexaFluor 568 or Cy5
LCMV NP mRNA/ S antigenome	gagttgactgcaggtttctc	LCMV_NP_mRNA_30	AlexaFluor 568 or Cy5
LCMV NP mRNA/ S antigenome	aggtggacctgctgctccag	LCMV_NP_mRNA_31	AlexaFluor 568 or Cy5
LCMV NP mRNA/ S antigenome	cattgtctggctgtagctta	LCMV_NP_mRNA_32	AlexaFluor 568 or Cy5
LCMV NP mRNA/ S antigenome	ctcccatgaggtcttttaaa	LCMV_NP_mRNA_33	AlexaFluor 568 or Cy5
LCMV NP mRNA/ S antigenome	caatccatgtaggagcgttg	LCMV_NP_mRNA_34	AlexaFluor 568 or Cy5
LCMV NP mRNA/ S antigenome	ttgctatttccactggatca	LCMV_NP_mRNA_35	AlexaFluor 568 or Cy5
LCMV NP mRNA/ S antigenome	aaaagtgtatgaactgcccg	LCMV_NP_mRNA_36	AlexaFluor 568 or Cy5
LCMV NP mRNA/ S antigenome	gtttttgatcaacgggttcc	LCMV_NP_mRNA_37	AlexaFluor 568 or Cy5
LCMV NP mRNA/ S antigenome	tgagtacttggaatcttgct	LCMV_NP_mRNA_38	AlexaFluor 568 or Cy5
LCMV NP mRNA/ S antigenome	agaggtcggcaagatccatg	LCMV_NP_mRNA_39	AlexaFluor 568 or Cy5
LCMV NP mRNA/ S antigenome	gtcaacccgggttgcgcatt	LCMV_NP_mRNA_40	AlexaFluor 568 or Cy5
LCMV NP mRNA/ S antigenome	cggaagagcacctataactg	LCMV_NP_mRNA_41	AlexaFluor 568 or Cy5
LCMV NP mRNA/ S antigenome	ttgacagcttagaaccatcc	LCMV_NP_mRNA_42	AlexaFluor 568 or Cy5
LCMV NP mRNA/ S antigenome	gctttctgatgtcatcggag	LCMV_NP_mRNA_43	AlexaFluor 568 or Cy5
LCMV NP mRNA/ S antigenome	ttcctattctgtgagtccag	LCMV_NP_mRNA_44	AlexaFluor 568 or Cy5
LCMV NP mRNA/ S antigenome	aacatcgataagcttaatgt	LCMV_NP_mRNA_45	AlexaFluor 568 or Cy5
LCMV NP mRNA/ S antigenome	tcgaagcttccctggtcatt	LCMV_NP_mRNA_46	AlexaFluor 568 or Cy5
LCMV NP mRNA/ S antigenome	tttcagatctgggagccttg	LCMV_NP_mRNA_47	AlexaFluor 568 or Cy5
LCMV NP mRNA/ S antigenome	cacaacatttgggcctctaa	LCMV_NP_mRNA_48	AlexaFluor 568 or Cy5
LCMV GPC mRNA/ S genome	agagcctcaaacattgtcac	LCMV_GPC_mRNA_1	AlexaFluor 568
LCMV GPC mRNA/ S genome	cacctcatcgatgatgtgag	LCMV_GPC_mRNA_2	AlexaFluor 568
LCMV GPC mRNA/ S genome	cgtgatcacgataagcacaa	LCMV_GPC_mRNA_3	AlexaFluor 568
LCMV GPC mRNA/ S genome	gcaaaattgtagacagcctt	LCMV_GPC_mRNA_4	AlexaFluor 568
LCMV GPC mRNA/ S genome	caatgcgaatatcccacagg	LCMV_GPC_mRNA_5	AlexaFluor 568
LCMV GPC mRNA/ S genome	cagccagaagtaggaaactg	LCMV_GPC_mRNA_6	AlexaFluor 568
LCMV GPC mRNA/ S genome	cttaagaccgtacatgccac	LCMV_GPC_mRNA_7	AlexaFluor 568
LCMV GPC mRNA/ S genome	ctcctttgtaaatgtcgggt	LCMV_GPC_mRNA_8	AlexaFluor 568
LCMV GPC mRNA/ S genome	actccactgacttaaattgg	LCMV_GPC_mRNA_9	AlexaFluor 568
LCMV GPC mRNA/ S genome	catggtcaggttcagatgtg	LCMV_GPC_mRNA_10	AlexaFluor 568
LCMV GPC mRNA/ S genome	gagttgttggctgaacatgc	LCMV_GPC_mRNA_11	AlexaFluor 568
LCMV GPC mRNA/ S genome	agaagtccccatactgatgt	LCMV_GPC_mRNA_12	AlexaFluor 568
LCMV GPC mRNA/ S genome	cattggtgaaggtcaattct	LCMV_GPC_mRNA_13	AlexaFluor 568
LCMV GPC mRNA/ S genome	cagattgcaaaagttgtgac	LCMV_GPC_mRNA_14	AlexaFluor 568
LCMV GPC mRNA/ S genome	ggctcgaaactatactcatg	LCMV_GPC_mRNA_15	AlexaFluor 568
LCMV GPC mRNA/ S genome	ttccctctgatactgaggtg	LCMV_GPC_mRNA_16	AlexaFluor 568
LCMV GPC mRNA/ S genome	ggatactgccttatagttgg	LCMV_GPC_mRNA_17	AlexaFluor 568
LCMV GPC mRNA/ S genome	ttatgccattgttgaagtcg	LCMV_GPC_mRNA_18	AlexaFluor 568
LCMV GPC mRNA/ S genome	gttctacactggctctgagc	LCMV_GPC_mRNA_19	AlexaFluor 568

LCMV GPC mRNA/ S genome	atctaggactctacctctga	LCMV_GPC_mRNA_20	AlexaFluor 568
LCMV GPC mRNA/ S genome	ccccgaaggcagttctaaac	LCMV_GPC_mRNA_21	AlexaFluor 568
LCMV GPC mRNA/ S genome	aggtggtcttgccatctgag	LCMV_GPC_mRNA_22	AlexaFluor 568
LCMV GPC mRNA/ S genome	gtattggtaactcgtctggc	LCMV_GPC_mRNA_23	AlexaFluor 568
LCMV GPC mRNA/ S genome	ccaaaaggacctgcatatgt	LCMV_GPC_mRNA_24	AlexaFluor 568
LCMV GPC mRNA/ S genome	ggaaaggagaatcctggaca	LCMV_GPC_mRNA_25	AlexaFluor 568
LCMV GPC mRNA/ S genome	agtgaagaacttagtcttct	LCMV_GPC_mRNA_26	AlexaFluor 568
LCMV GPC mRNA/ S genome	tgaatgtgcccgctagtctc	LCMV_GPC_mRNA_27	AlexaFluor 568
LCMV GPC mRNA/ S genome	ccctgaagagtctgacaaag	LCMV_GPC_mRNA_28	AlexaFluor 568
LCMV GPC mRNA/ S genome	gcaataaccacctggattct	LCMV_GPC_mRNA_29	AlexaFluor 568
LCMV GPC mRNA/ S genome	tgcagcaagaatcatccatt	LCMV_GPC_mRNA_30	AlexaFluor 568
LCMV GPC mRNA/ S genome	tgttcccgaaacacttaagc	LCMV_GPC_mRNA_31	AlexaFluor 568
LCMV GPC mRNA/ S genome	tacattgcatttcgcaactg	LCMV_GPC_mRNA_32	AlexaFluor 568
LCMV GPC mRNA/ S genome	tcaattagtcgcagcatgtc	LCMV_GPC_mRNA_33	AlexaFluor 568
LCMV GPC mRNA/ S genome	ttactcaaagcagccttgtt	LCMV_GPC_mRNA_34	AlexaFluor 568
LCMV GPC mRNA/ S genome	aagtgcaaggcagattctac	LCMV_GPC_mRNA_35	AlexaFluor 568
LCMV GPC mRNA/ S genome	tcaaagaattcactgttgtt	LCMV_GPC_mRNA_36	AlexaFluor 568
LCMV GPC mRNA/ S genome	agtggttcctcatcagtagt	LCMV_GPC_mRNA_37	AlexaFluor 568
LCMV GPC mRNA/ S genome	gtaattgcaatatggcaccc	LCMV_GPC_mRNA_38	AlexaFluor 568
LCMV GPC mRNA/ S genome	tgttctaggtaccaaaactt	LCMV_GPC_mRNA_39	AlexaFluor 568
LCMV GPC mRNA/ S genome	actagtttcgccggtctttg	LCMV_GPC_mRNA_40	AlexaFluor 568
LCMV GPC mRNA/ S genome	agtaagaaccattggtgaca	LCMV_GPC_mRNA_41	AlexaFluor 568
LCMV GPC mRNA/ S genome	tcactgaagtgggtctcatt	LCMV_GPC_mRNA_42	AlexaFluor 568
LCMV GPC mRNA/ S genome	atcggcttcctgttcgattt	LCMV_GPC_mRNA_43	AlexaFluor 568
LCMV GPC mRNA/ S genome	gcaggaagatgctgactaga	LCMV_GPC_mRNA_44	AlexaFluor 568
LCMV GPC mRNA/ S genome	cttttatgtgcctgtgtgtt	LCMV_GPC_mRNA_45	AlexaFluor 568
LCMV GPC mRNA/ S genome	tcctttgttggttaatcggt	LCMV_GPC_mRNA_46	AlexaFluor 568
LCMV GPC mRNA/ S genome	caccaggcaccttaaatgca	LCMV_GPC_mRNA_47	AlexaFluor 568
LCMV GPC mRNA/ S genome	cgtcttttccagacggtttt	LCMV_GPC_mRNA_48	AlexaFluor 568
LCMV L mRNA/L antigenome	ctctcatcctgttctatata	LCMV_L_mRNA_1	Quasar 670
LCMV L mRNA/L antigenome	tcccagaaagttgagtttct	LCMV_L_mRNA_2	Quasar 670
LCMV L mRNA/L antigenome	caatcagaaccattctgggt	LCMV_L_mRNA_3	Quasar 670
LCMV L mRNA/L antigenome	cagcgtgacagcaacttgag	LCMV_L_mRNA_4	Quasar 670
LCMV L mRNA/L antigenome	ttgtctgcactgtctatttc	LCMV_L_mRNA_5	Quasar 670
LCMV L mRNA/L antigenome	tgtttccacagacttatcgt	LCMV_L_mRNA_6	Quasar 670
LCMV L mRNA/L antigenome	tgtctatcagcttgtaacca	LCMV_L_mRNA_7	Quasar 670
LCMV L mRNA/L antigenome	caaaactggctggagtgctc	LCMV_L_mRNA_8	Quasar 670
LCMV L mRNA/L antigenome	ctgatgcatgccaatttgtt	LCMV_L_mRNA_9	Quasar 670
LCMV L mRNA/L antigenome	tggaactaatgtgacacccg	LCMV_L_mRNA_10	Quasar 670

LCMV L mRNA/L antigenome	gatagtagtcttcagggact	LCMV_L_mRNA_11	Quasar 670
LCMV L mRNA/L antigenome	ttttcatagagtccataccg	LCMV_L_mRNA_12	Quasar 670
LCMV L mRNA/L antigenome	attatgagttgacctcgcat	LCMV_L_mRNA_13	Quasar 670
LCMV L mRNA/L antigenome	ggcacatcctcataatttca	LCMV_L_mRNA_14	Quasar 670
LCMV L mRNA/L antigenome	atctcttctaaacctgctga	LCMV_L_mRNA_15	Quasar 670
LCMV L mRNA/L antigenome	gtttctctttaatttcccac	LCMV_L_mRNA_16	Quasar 670
LCMV L mRNA/L antigenome	cttcagggtttactttctga	LCMV_L_mRNA_17	Quasar 670
LCMV L mRNA/L antigenome	gagctcagagaattccttga	LCMV_L_mRNA_18	Quasar 670
LCMV L mRNA/L antigenome	tcatcactatcagcaaggtt	LCMV_L_mRNA_19	Quasar 670
LCMV L mRNA/L antigenome	ctccctgcttaatgttaaga	LCMV_L_mRNA_20	Quasar 670
LCMV L mRNA/L antigenome	taacatagagaggagcctct	LCMV_L_mRNA_21	Quasar 670
LCMV L mRNA/L antigenome	caactgtctccttctagtat	LCMV_L_mRNA_22	Quasar 670
LCMV L mRNA/L antigenome	tactatagcaacaacccacc	LCMV_L_mRNA_23	Quasar 670
LCMV L mRNA/L antigenome	aaagcttaccagcctatcat	LCMV_L_mRNA_24	Quasar 670
LCMV L mRNA/L antigenome	atgaactcctctttagtgct	LCMV_L_mRNA_25	Quasar 670
LCMV L mRNA/L antigenome	caccttctaaacacctttg	LCMV_L_mRNA_26	Quasar 670
LCMV L mRNA/L antigenome	agtccgtaatgctcgaaact	LCMV_L_mRNA_27	Quasar 670
LCMV L mRNA/L antigenome	tcagtgaatggtatgtggca	LCMV_L_mRNA_28	Quasar 670
LCMV L mRNA/L antigenome	atacattatcgggtgagctc	LCMV_L_mRNA_29	Quasar 670
LCMV L mRNA/L antigenome	gtgctgggttggaaattgta	LCMV_L_mRNA_30	Quasar 670
LCMV L mRNA/L antigenome	cttagtctagcaactgagct	LCMV_L_mRNA_31	Quasar 670
LCMV L mRNA/L antigenome	ctcacagaccctatttgatt	LCMV_L_mRNA_32	Quasar 670
LCMV L mRNA/L antigenome	attcttcagagtccagtttt	LCMV_L_mRNA_33	Quasar 670
LCMV L mRNA/L antigenome	ctccagtcttctggtataat	LCMV_L_mRNA_34	Quasar 670
LCMV L mRNA/L antigenome	atggagtagcaccttgaaga	LCMV_L_mRNA_35	Quasar 670
LCMV L mRNA/L antigenome	aattaaatgaccatccgggc	LCMV_L_mRNA_36	Quasar 670
LCMV L mRNA/L antigenome	ccttttaggatctgcataga	LCMV_L_mRNA_37	Quasar 670
LCMV L mRNA/L antigenome	tcggtgagacagtctttcaa	LCMV_L_mRNA_38	Quasar 670
LCMV L mRNA/L antigenome	gcattagcaacaatagggtc	LCMV_L_mRNA_39	Quasar 670
LCMV L mRNA/L antigenome	atttctctttgttgggttgg	LCMV_L_mRNA_40	Quasar 670
LCMV L mRNA/L antigenome	tatctgacactctgtacctg	LCMV_L_mRNA_41	Quasar 670
LCMV L mRNA/L antigenome	tccctcaacttatccattaa	LCMV_L_mRNA_42	Quasar 670
LCMV L mRNA/L antigenome	cttatacaccaccttctcag	LCMV_L_mRNA_43	Quasar 670
LCMV L mRNA/L antigenome	ggtctcctttgtgatcaaat	LCMV_L_mRNA_44	Quasar 670
LCMV L mRNA/L antigenome	caggagtgattgcttccttg	LCMV_L_mRNA_45	Quasar 670
LCMV L mRNA/L antigenome	gtgaatctcttcatttgctc	LCMV_L_mRNA_46	Quasar 670
LCMV L mRNA/L antigenome	tgctgacagtcaatttcttt	LCMV_L_mRNA_47	Quasar 670
LCMV L mRNA/L antigenome	ccagattaacacctggagtt	LCMV_L_mRNA_48	Quasar 670
MDN1 exon	tcgttcttggctgcgattaa	hsMDN1_exon_1	Cy3

MDN1 exon	taaggtactcaggacacact	hsMDN1_exon_2	Cy3
MDN1 exon	cacagtacagtccttatcca	hsMDN1_exon_3	Cy3
MDN1 exon	agcaaatccaaaaggagagg	hsMDN1_exon_4	Cy3
MDN1 exon	ttgaaagactggggatgtgt	hsMDN1_exon_5	Cy3
MDN1 exon	gcatctgaactctctaggaa	hsMDN1_exon_6	Cy3
MDN1 exon	gtgctcttcattcatacagg	hsMDN1_exon_7	Cy3
MDN1 exon	cctcaacctgaaatggatca	hsMDN1_exon_8	Cy3
MDN1 exon	aaaaccaaggccttctccaa	hsMDN1_exon_9	Cy3
MDN1 exon	aaagggagacttctggattg	hsMDN1_exon_10	Cy3
MDN1 exon	tcagacgaaacaagatgtcc	hsMDN1_exon_11	Cy3
MDN1 exon	accagcacataagacctaag	hsMDN1_exon_12	Cy3
MDN1 exon	gaagacttttgcagacagac	hsMDN1_exon_13	Cy3
MDN1 exon	acagcattctgagaagcaac	hsMDN1_exon_14	Cy3
MDN1 exon	tcctattggtccttccaaca	hsMDN1_exon_15	Cy3
MDN1 exon	cctgtcactgcagctaaata	hsMDN1_exon_16	Cy3
MDN1 exon	aagctggactttgagaagct	hsMDN1_exon_17	Cy3
MDN1 exon	acatctgtgcagcgatacat	hsMDN1_exon_18	Cy3
MDN1 exon	atatcctccagaaggatcca	hsMDN1_exon_19	Cy3
MDN1 exon	aagagctctccattctccaa	hsMDN1_exon_20	Cy3
MDN1 exon	aaatccaggtgccactttca	hsMDN1_exon_21	Cy3
MDN1 exon	caatttcctccacagctcaa	hsMDN1_exon_22	Cy3
MDN1 exon	atgactgtttagcggtcgat	hsMDN1_exon_23	Cy3
MDN1 exon	ccaggtgaattttggtccaa	hsMDN1_exon_24	Cy3
MDN1 exon	cagttctctcttatccaggt	hsMDN1_exon_25	Cy3
MDN1 exon	gtttctctccagtaagttgg	hsMDN1_exon_26	Cy3
MDN1 exon	gaactatcactccaagagtg	hsMDN1_exon_27	Cy3
MDN1 exon	aacttcttcaggtgcctgtt	hsMDN1_exon_28	Cy3
MDN1 exon	ctcaagggttggtcttttgt	hsMDN1_exon_29	Cy3
MDN1 exon	gggcaatcctattacaccaa	hsMDN1_exon_30	Cy3
MDN1 exon	ctcagaaagcattgctgtga	hsMDN1_exon_31	Cy3
MDN1 exon	gcttccaataacttctgcca	hsMDN1_exon_32	Cy3
MDN1 exon	tttgctgacacacactgcaa	hsMDN1_exon_33	Cy3
MDN1 exon	atggtagaggttttgccagt	hsMDN1_exon_34	Cy3
MDN1 exon	cctgtaatgtgagccaagta	hsMDN1_exon_35	Cy3
MDN1 exon	attgacaaccctcaaacggt	hsMDN1_exon_36	Cy3
MDN1 exon	gcaagtctgcagtatcactt	hsMDN1_exon_37	Cy3
MDN1 exon	atggtccaccggtttataac	hsMDN1_exon_38	Cy3
MDN1 exon	gtaagggtagccaaataagc	hsMDN1_exon_39	Cy3
MDN1 exon	aagagttcctcaaatgcctc	hsMDN1_exon_40	Cy3

MDN1 exon	gccccaagaacgtaaagttt	hsMDN1_exon_41	Cy3
MDN1 exon	ctgtctgtaacaggtctgaa	hsMDN1_exon_42	Cy3
MDN1 exon	ttagtctcaggagatcatgc	hsMDN1_exon_43	Cy3
MDN1 exon	agcagacttgtgtacatgct	hsMDN1_exon_44	Cy3
MDN1 exon	cactgtcttttccatccttg	hsMDN1_exon_45	Cy3
MDN1 exon	ccaaatgcttcccatttctc	hsMDN1_exon_46	Cy3
MDN1 exon	ttgggcatggttgagtctaa	hsMDN1_exon_47	Cy3
MDN1 exon	ctttacagcctgagctaatg	hsMDN1_exon_48	Cy3

CHAPTER 3:

VISUALIZATION OF THE LYMPHOCYTIC CHORIOMENINGITIS MAMMARENAVIRUS (LCMV) GENOME REVEALS THE EARLY ENDOSOME AS A POSSIBLE SITE FOR GENOME REPLICATION AND VIRAL PARTICLE PRE-ASSEMBLY

Benjamin R. King[1,2], Samuel Kellner[1], Philip L. Eisenhauer[1], Emily A. Bruce[1], Christopher M. Ziegler[1,2], Daniel Zenklusen[3], Jason Botten[1,4*]

[1]Department of Medicine, Division of Immunobiology, University of Vermont, Burlington, VT 05405, USA, [2]Cellular, Molecular, and Biomedical Sciences Graduate Program, University of Vermont, Burlington, VT 05405, USA, [3]Departement de Biochimie et Médecine Moléculaire, Université de Montréal, Montréal, QC H3T 1J4, Canada, [4]Department of Microbiology and Molecular Genetics, University of Vermont, Burlington, VT 05405, USA, *Corresponding author

Running title: LCMV genome replication and pre-assembly at the early endosome

3.1. Abstract

We report a fluorescence in situ hybridization (FISH) assay that allows the visualization of lymphocytic choriomeningitis mammarenavirus (LCMV) genomic RNAs in individual cells. We show that viral S segment genomic and antigenomic RNA, along with viral nucleoprotein, colocalize in subcellular structures we presume to be viral replication factories. These viral RNA structures are highly dynamic during acute infection, with the many small foci seen early coalescing into larger perinuclear foci later in infection. These late-forming perinuclear viral RNA aggregates are located near the cellular microtubule organizing center and colocalize with the early endosomal marker Rab5c and the viral glycoprotein in a proportion of infected cells. We propose that the virus is using the surface of a cellular membrane bound organelle as a site for the pre-assembly of viral components including genomic RNA and viral glycoprotein prior to their transport to the plasma membrane where new particles will bud.

3.2. Main Text

The major events of transcription and replication of the arenavirus genomic RNA are well understood at a population level (Figure 3.1A) (Fuller-Pace and Southern, 1988; Haist et al., 2015). However, technical limitations of Northern blot and quantitative RT-PCR have hindered our ability to examine these processes in individual cells and to visualize these events with subcellular resolution. Recent improvements in fluorescence in situ hybridization (FISH) technologies now permit the fluorescent labeling and microscopic visualization of RNA species at the single-cell and single-molecule level (Raj et al., 2008). This labeling strategy, relying on pools of fluorescently labeled 20mer oligonucleotide probes, allows visualization of target RNAs with a high signal-to-noise ratio and exquisite specificity (Raj et al., 2008). The replication dynamics of influenza A and Rift Valley Fever viruses (an orthomyxovirus and bunyavirus, respectively) have been examined using this RNA FISH labeling strategy, and have revealed subcellular sites of genomic RNA replication, assembly, and/or selectivity of genome recruitment into assembling particles (Chou et al., 2013; Lakdawala et al., 2014; Wichgers Schreur and Kortekaas, 2016).

Arenaviruses, like orthomyxoviruses and bunyaviruses, have a single-stranded, segmented, negative-sense RNA genome (Buchmeier et al., 2013). Previous work has suggested that the genomic RNA of Tacaribe virus (a New World arenavirus) associates with intracellular membranes (Baird et al., 2012). However, fluorescence microscopy visualizing the subcellular distribution of viral RNAs (nonspecifically-labeled with a chemically modified nucleotide) with various protein markers failed to identify the

subcellular compartment targeted by the virus (Baird et al., 2012). In the present study, we used pools of singly labeled FISH probes to specifically visualize the genomic RNA of lymphocytic choriomeningitis virus (LCMV), the prototypic mammarenavirus, with the goal to (i) define the dynamics of genomic RNA replication during the course of acute infection, (ii) characterize the subcellular localization of the genomic and antigenomic RNA, (iii) identify the membrane-bound compartment targeted by arenavirus genomic RNA, and (iv) describe how the virus may be taking advantage of this virus-targeted, intracellular compartment.

The arenaviruses have a bisegmented genome with each genomic segment encoding two genes in ambisense polarity (Buchmeier et al., 2013). The S genomic segment contains the negative-sense nucleoprotein (NP) gene and the pseudo-positive-sense glycoprotein precursor (GPC) gene (Figure 3.1A) (Buchmeier et al., 2013). The Stellaris Probe Designer tool (Biosearch Technologies, Inc.) was used to design custom pools of 3' amine oligo FISH probes that would specifically hybridize to the S genomic or S antigenomic RNAs (Figure 3.1A, Table S3.1). Probes were labeled post synthesis with Cy3 or Cy5 dyes and purified as described previously (Zenklusen and Singer, 2010). To follow the replication dynamics of the S genomic and S antigenomic RNAs, we infected A549 cells with LCMV at a MOI of 0.01, fixed infected cells as previously described (Raj et al., 2008) at the indicated times post-infection, and performed FISH hybridization with S genome and S antigenome probes as previously described (Castelnuovo et al., 2013). 3D datasets spanning the entire volume of the cells were acquired using a DeltaVision

restoration microscopy system (GE Healthcare), and images were deconvolved using softWoRx software. Bright signal was observed in cells infected with LCMV, but very little signal was detected in uninfected cells, confirming that FISH probes specifically recognize S genome and S antigenome (Figure 3.1B to C). As expected, RNA signal was mainly observed in the cytoplasm, where S genome and S antigenome concentrated in cytoplasmic foci of varying size, brightness, and subcellular localization (Figure 3.1B to C). It is known that genomic and antigenomic RNA is encapsidated by the viral NP (Buchmeier et al., 2013). Thus, we stained for both the viral NP and the S genome to confirm their colocalization. For joint protein and RNA staining, we combined the immunofluorescence and FISH staining protocols as previously described (Song et al., 2015). NP and S genome strongly colocalized in LCMV-infected cells (Figure 3.1D). The line scan of the two fluorescent signals (shown in the inset in Figure 3.1D) further confirms the colocalization between NP and S genome (Figure 3.1E).

Baird et al. (Baird et al., 2012) referred to foci of Tacaribe virus RNA colocalizing with viral NP as "replication-transcription complexes." With the ability to label bona fide arenavirus genomic and antigenomic RNA, we next wanted to profile the composition and dynamics of these viral replication complexes. We first asked whether S genome and S antigenome traffic to distinct subcellular locations or whether they remain associated in the same subcellular compartments. We therefore stained for both viral RNAs within the same cells and found that S genome and S antigenome exhibit strong colocalization, supporting

the idea that the genomic and antigenomic RNAs remain in close spatial proximity at the peak of acute infection (Figure 3.1F to G).

To explore the temporal evolution of viral replication complexes, we next infected A549 cells with LCMV, fixed cells at different time points post-infection, and stained for S genome and S antigenome (Figure 3.2). At 8 hours post-infection (h p.i.), S genome and S antigenome first become visible as small spots that are distributed throughout the cytoplasm, likely representing single viral genomes (Figure 3.2). Interestingly, few of these individual genome and anti-genome signal co-localize, suggesting that clustering of viral RNAs occur at a later stage during infection. At 12 and 24 h p.i., many cytoplasmic S genome/S antigenome foci are visible, and their size and intensity progressively increases, as well as the frequency of co-localization of genome and anti-genome signal (Figure 3.2). At 48 h p.i., in many cells, the multiple bright cytoplasmic foci coalesce into one or a few large aggregates located adjacent to the nucleus (Figure 3.2).

We were intrigued by the perinuclear localization of genomic RNA at the peak of acute infection and hypothesized that the arenavirus S genome RNA foci seen earlier in infection might be utilizing minus end-directed transport along microtubules to coalesce in larger structures near the cell's microtubule organizing center (MTOC). To test this, we stained cells for both gamma-tubulin (a marker of the MTOC) and S genome. Indeed, in most cases we found the perinuclear S genome aggregate was located immediately adjacent to the MTOC (Figure 3.3A). Previous observations that arenavirus ribonucleoprotein complexes copurified with cellular membranes (Baird et al., 2012), together with our

observation that perinuclear S genome aggregates concentrate near the MTOC, led us to postulate that the S genome could be localizing to endosomal membranes and taking advantage of this organelle's directed transport along microtubules (Nielsen et al., 1999). It was previously demonstrated that Rab5c, an early endosomal marker (Bucci et al., 1995), was required for the propagation of LCMV (Panda et al., 2011). Rab5c is a Rab GTPase, a family of proteins that play critical roles in establishment of vesicular identity, trafficking, and effector protein recruitment (Stenmark, 2009). Thus, we hypothesized that S genomic RNA may be localizing to Rab5c positive membranes to promote some aspect of the LCMV life cycle. To test this, we stained cells infected with LCMV for either 24 or 48 hours with an antibody specifically recognizing Rab5c and with FISH probes specific for S genome. Notably, at 48 h p.i., in a subset of cells, we observed increased levels of Rab5c and a perinuclear redistribution of this protein that resulted in strong colocalization with viral genome (Figure 3.3B to D). However, the colocalization of S genome appeared highly time-dependent as no colocalization was observed at 24 h p.i. (Figure 3B to D). These data suggest that Rab5c may play an important role late in the LCMV life cycle, complementing previous work showing the importance of Rab5 for arenavirus entry (Martinez et al., 2009; Rojek et al., 2008). Furthermore, our observation of Rab5c's involvement in the replication of arenaviral RNA is intriguing in light of other studies showing Rab5c as a cellular dependency factor for the replication of Zika virus, a flavivirus (Savidis et al., 2016).

Our finding that Rab5c colocalizes with LCMV RNA was somewhat surprising given that previous work by Baird et al. did not observe any colocalization of Tacaribe

virus replication-transcription complexes with endosomal markers, including Rab5a, which is closely related to Rab5c (Baird et al., 2012; Bucci et al., 1995). The previous studies of Tacaribe virus examined a single time point after infection. Given the temporal specificity of the Rab5c-LCMV RNA association observed in the current study, it is possible that New World arenaviruses like Tacaribe do associate with endosomal markers, but that a kinetic study would be required to uncover such a result. Alternatively, it is possible that individual arenaviruses utilize different host machinery for genome replication and virus assembly. Indeed, related studies in our laboratory have demonstrated that replication of LCMV, but not the New World arenavirus Junín Candid #1, is impaired following siRNA silencing of Rab5c (C. M. Ziegler, P. Eisenhauer, J. A. Kelly, L. N. Dang, V. Beganovic, E. A. Bruce, B. R. King, D. J. Shirley, M. E. Weir, B. A. Ballif, and J. Botten, unpublished results). This result, which confirms the previously demonstrated importance of Rab5c for LCMV propagation (Panda et al., 2011), suggests that Old World arenaviruses such as LCMV, but not those of the New World lineage, are uniquely dependent upon Rab5c for successful completion of the life cycle. Further studies will be required to determine the extent to which Rab5c and other proteins in the Rab GTPase family are utilized by genetically diverse arenaviruses.

It is known that arenaviruses bud from the plasma membrane of infected cells (Buchmeier et al., 2007). Why, then, would LCMV S genome concentrate on the surface of Rab5c positive vesicular structures in infected cells? One possibility is that these structures represent sites where different viral components pre-assemble before being

trafficked together to the plasma membrane for budding. Indeed, it has been suggested that influenza A virus uses Rab11-positive membranes for trafficking of viral ribonucleoproteins to the plasma membrane (Amorim et al., 2011; Eisfeld et al., 2011; Momose et al., 2011). To test this possibility in the current system, we stained for another LCMV structural protein, its glycoprotein (GPC) (monoclonal antibody 33.6 (Weber and Buchmeier, 1988)), and S genome at 12, 24, and 48 h p.i.. We found that at 48 h p.i., in most cells, there was a high degree of colocalization between GPC and S genome (Figure 3.3E to G). As with Rab5c, the colocalization between these two viral components was variable at different stages of infection, and little colocalization was observed at earlier time points (Figure 3.3E to G). As no direct NP-GPC interaction has been reported in the literature, GPC recruitment to encapsidated S genomic RNA would likely be dependent on the presence of the viral matrix protein, Z, which has been shown to interact with both NP and GPC (Capul et al., 2007; Eichler et al., 2004).

In summary, we describe the use of single-molecule resolution RNA FISH to specifically visualize LCMV S genome and S antigenome during the course of acute infection. For the first time, we reveal that the S genome and antigenome largely colocalize in the same subcellular structures during acute infection. Viral genomic RNA is highly dynamic during the course of acute infection with many dim genomic RNA foci, likely representing individual viral genomes, progressively increasing in intensity and eventually coalescing into larger perinuclear structures, which, in many cells, appear to colocalize with the early endosomal marker Rab5c –shown by us and others to have a

critical role in supporting the LCMV life cycle (Panda et al., 2011) (C. M. Ziegler, P. Eisenhauer, J. A. Kelly, L. N. Dang, V. Beganovic, E. A. Bruce, B. R. King, D. J. Shirley, M. E. Weir, B. A. Ballif, and J. Botten, unpublished results). We propose LCMV is using this intracellular membrane as a scaffold for genome replication and possibly pre-assembly of viral components prior to being trafficked to the plasma membrane where they will bud as infectious virions.

3.3. Funding Information

This publication was made possible by NIH Grant Numbers 5 P30 RR032135 from the COBRE Program of the National Center for Research Resources and 8 P30 GM103498 from the National Institute of General Medical Sciences. We also gratefully acknowledge funding support from NIH grants T32 HL076122-10 (BRK), T32 AI055402 (CMZ), R21 AI088059 (JB), and P20RR021905 & P30GM118228 (Immunobiology and Infectious Disease COBRE awards) (JB). DZ is supported by the Canadian Institute for Health Research (Project Grant-366682), Fond de recherche du Quebec (Chercheur-boursier Junior 2), and the Canadian Foundation for Innovation.

3.4. Acknowledgements

For providing key reagents, we gratefully acknowledge Jason Stumpff (gamma tubulin antibody), Michael Buchmeier (antibodies 1-1.3 and 33.6), and J. Lindsay Whitton (LCMV). We thank Samir Rahman and Todd Clason for technical assistance.

3.5. Figures

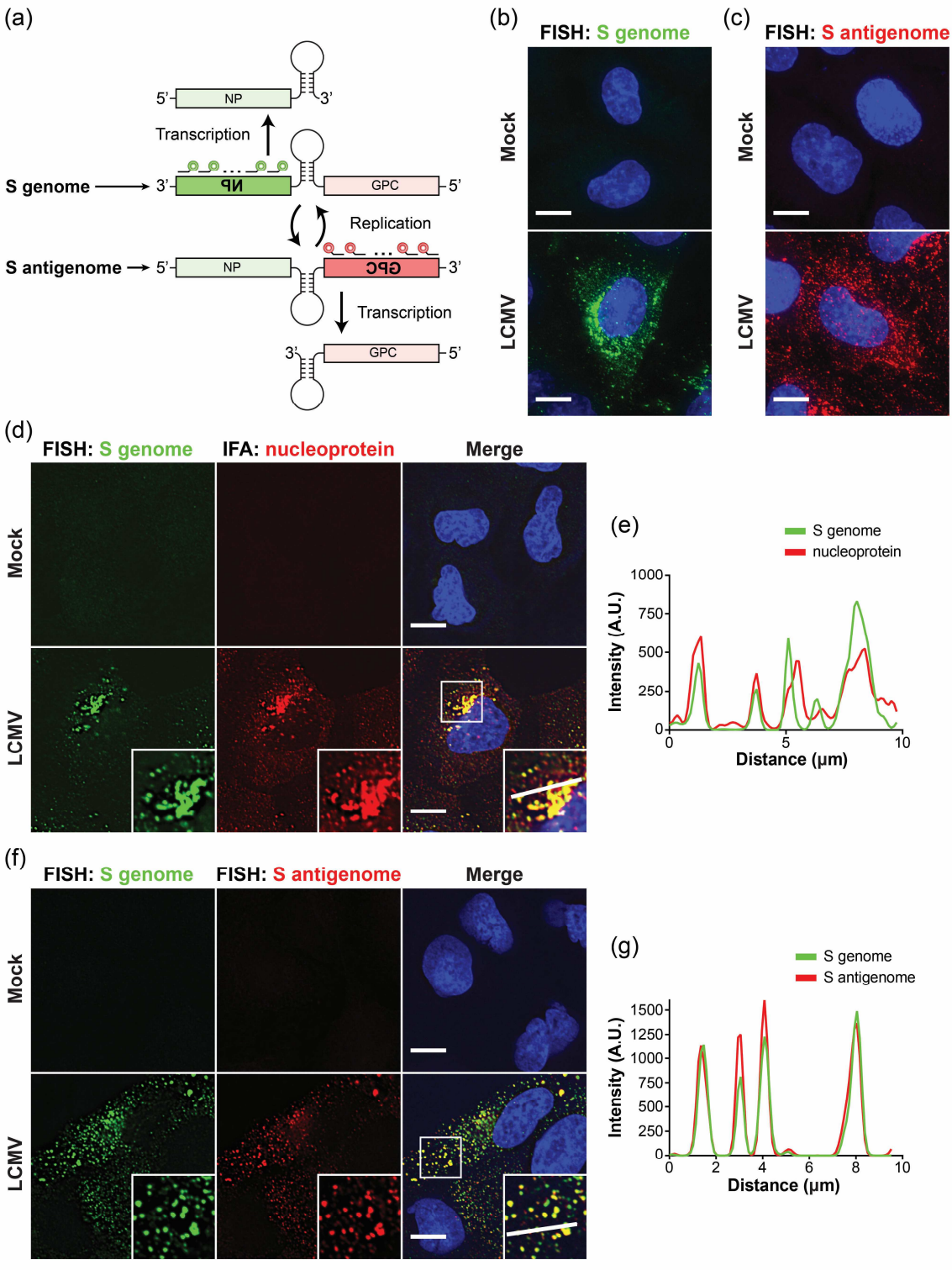
(a)
5'
NP
3'
Transcription
S genome
3'
NP
GPC
5'
Replication
S antigenome
5'
NP
GPC
3'
Transcription
3'
GPC
5'
(b)
FISH: S genome
Mock
LCMV
(c)
FISH: S antigenome
Mock
LCMV
(d)
FISH: S genome
IFA: nucleoprotein
Merge
Mock
LCMV
(e)
S genome
nucleoprotein
Intensity (A.U.)
1000
750
500
250
0
0
5
10
Distance (μm)
(f)
FISH: S genome
FISH: S antigenome
Merge
Mock
LCMV
(g)
S genome
S antigenome
Intensity (A.U.)
1500
1250
1000
750
500
250
0
0
2
4
6
8
10
Distance (μm)

Figure 3.1. Visualization of S genome and antigenomic RNAs by multiple, singly-labeled FISH probes.
(A) Diagram showing the transcription and replication scheme of the LCMV S genomic RNA. Briefly, S genome serves as the template for the viral polymerase to generate full-length, antigenome replicative intermediates. S genome and S antigenome serve as templates for transcription of the NP and GPC mRNAs, respectively. FISH probe sets (each containing 48 individual 20mer probes bearing a single fluorophore at their 3' terminus) were used to specifically visualize either the S genomic or S antigenomic RNA.
(B) Maximum intensity projection of either mock- or LCMV-infected cells (48 h p.i.) stained with S genome FISH probes labeled with Cy3.
(C) Maximum intensity projection of either mock- or LCMV-infected cells (48 h p.i.) stained with S antigenome FISH probes labeled with Cy3.
(D) Single Z stack of either mock- or LCMV-infected cells (48 h p.i.) stained for S genome (Cy5) and LCMV nucleoprotein (1-1.3 (from M. Buchmeier, University of California Irvine) [primary antibody] as previously described (King et al., 2017); goat, anti-mouse AlexaFluor 488) [secondary antibody]).
(E) Fluorescence line scan of S genome and NP signals along the line indicated in the inset of the merged image in (d).
(F) Single Z stack of either mock- or LCMV-infected cells (48 h p.i.) stained with S genome (Cy5) and S antigenome (Cy3) FISH probes.
(G) Fluorescence line scan of S genome and S antigenome signals along the line indicated in the inset of the merged image in (f). Scale bar = 10 μm.

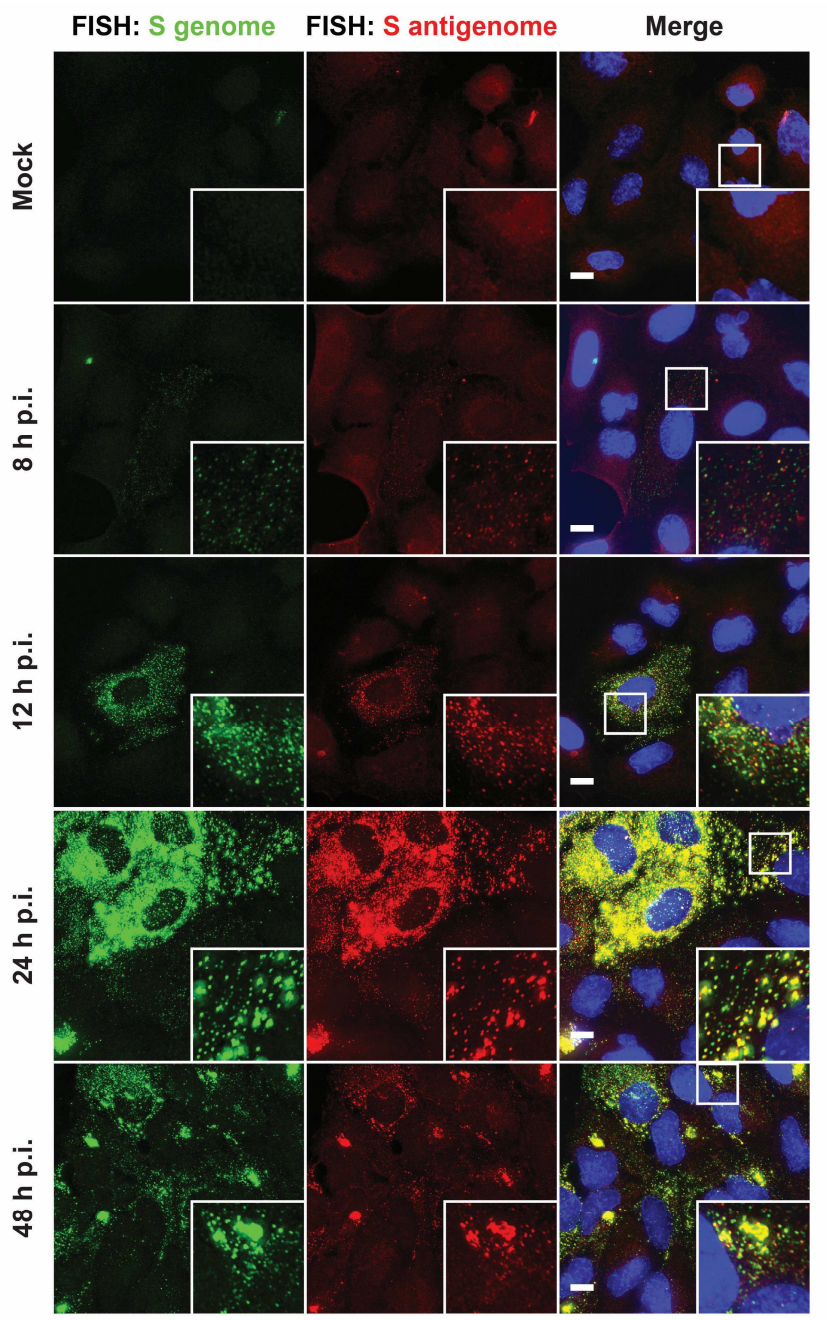

Figure 3.2. Dynamics of S genome and S antigenome during acute LCMV infection.
Cells were infected with LCMV at an MOI of 0.01 or not (mock) and fixed at multiple time points following infection. Maximum intensity projections of cells stained with S genome (Cy5) and S antigenome (Cy3) FISH probes are presented. Scale bar = 10 μm.

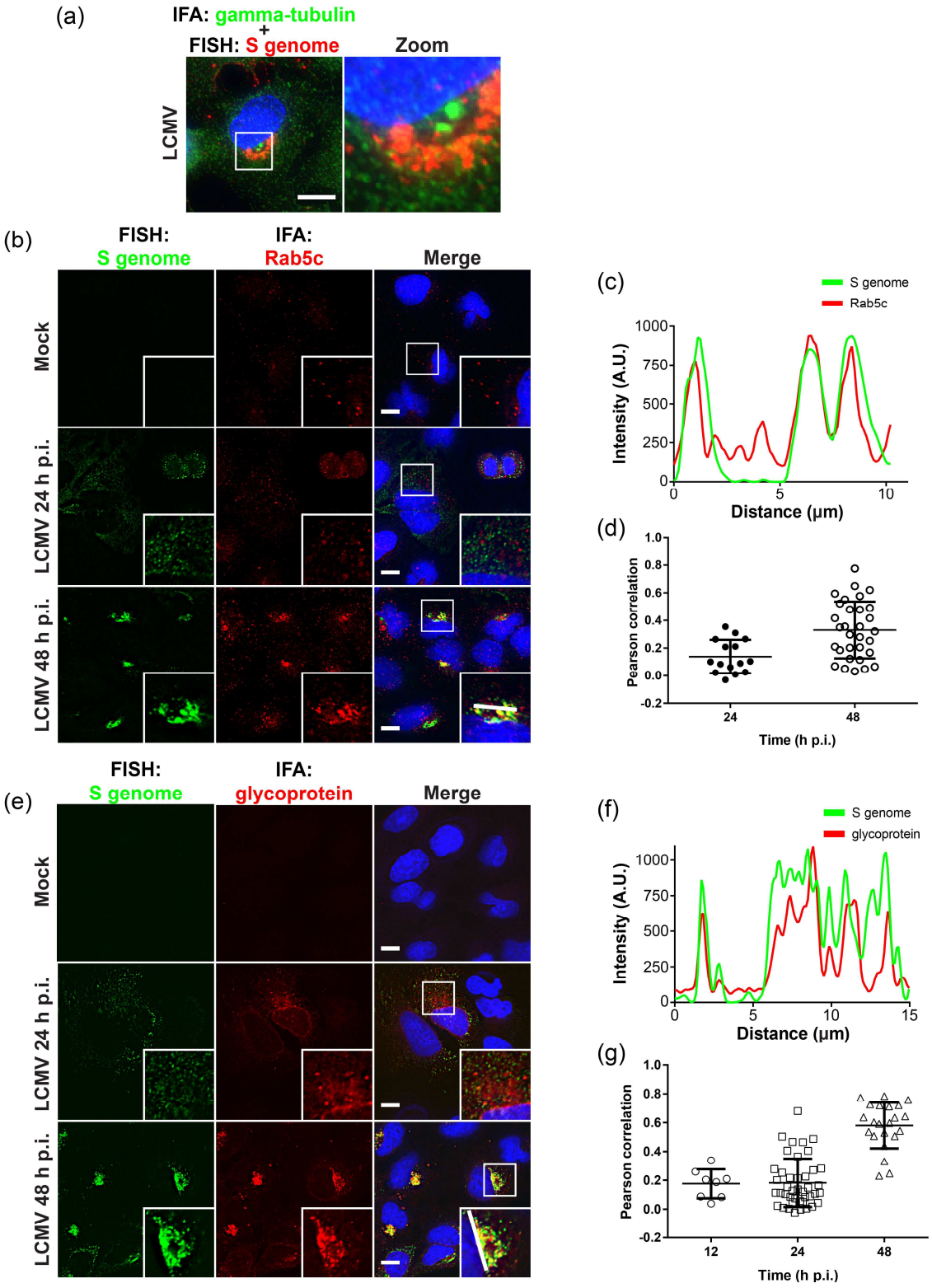
(a)
IFA: gamma-tubulin
+
FISH: S genome
Zoom
LCMV
(b)
FISH:
S genome
IFA:
Rab5c
Merge
Mock
LCMV 24 h p.i.
LCMV 48 h p.i.
(c)
S genome
Rab5c
Intensity (A.U.)
1000
750
500
250
0
0
5
10
Distance (µm)
(d)
Pearson correlation
1.0
0.8
0.6
0.4
0.2
0.0
-0.2
24
48
Time (h p.i.)
(e)
FISH:
S genome
IFA:
glycoprotein
Merge
Mock
LCMV 24 h p.i.
LCMV 48 h p.i.
(f)
S genome
glycoprotein
Intensity (A.U.)
1000
750
500
250
0
0
5
10
15
Distance (µm)
(g)
Pearson correlation
1.0
0.8
0.6
0.4
0.2
0.0
-0.2
12
24
48
Time (h p.i.)

Figure 3.3. LCMV S segment genome selectively colocalizes with Rab5c and viral glycoprotein later during acute infection.
(A) At 48 h p.i., perinuclear S genome aggregates localize near the microtubule organizing center (MTOC) as visualized by gamma-tubulin (GTU-88, Sigma-Aldrich [primary]; goat, anti-mouse AlexaFluor 488) [secondary]) and S genome (Cy5-labeled FISH probes). A maximum intensity projection of a representative cell is shown.
(B) Single Z stack of either mock- or LCMV-infected cells at the indicated time points after infection were stained for S genome (Cy5-labeled FISH probes) and Rab5c (sc-365667, Santa Cruz Biotechnology [primary]; goat, anti-rabbit AlexaFluor 488) [secondary]).
(C) Fluorescence line scan of S genome and Rab5c along the line indicated in the inset of the merged image at 48 h p.i. (b) is shown.
(D) The Pearson's correlation coefficient between S genome and Rab5c fluorescence signal in individual infected cells at either 24 or 48 h p.i. was calculated in softWoRx software and the scores of individual cells were graphed.
(E) Single Z stacks of either mock- or LCMV-infected cells that were stained for S genome (Cy5-labeled FISH probes) and viral glyocoprotein (GPC) (mouse anti-GPC, 33.6 (from M. Buchmeier, University of California Irvine) [primary] at 1:500; goat, anti-mouse AlexaFluor 488) [secondary]) are shown.
(F) Fluorescence line scan of S genome and GPC along the line indicated in the inset of the merged image at 48 h p.i. (e) is shown.
(g) The Pearson's correlation coefficient between S genome and GPC fluorescence signal in individual infected cells at either 12, 24, or 48 h p.i. was calculated in softWoRx software and the scores of individual cells were graphed.

3.6. References

Amorim, M.J., Bruce, E.A., Read, E.K., Foeglein, A., Mahen, R., Stuart, A.D., and Digard, P. (2011). A Rab11- and microtubule-dependent mechanism for cytoplasmic transport of influenza A virus viral RNA. Journal of virology *85*, 4143-4156.

Baird, N.L., York, J., and Nunberg, J.H. (2012). Arenavirus infection induces discrete cytosolic structures for RNA replication. Journal of virology *86*, 11301-11310.

Bucci, C., Lutcke, A., Steele-Mortimer, O., Olkkonen, V.M., Dupree, P., Chiariello, M., Bruni, C.B., Simons, K., and Zerial, M. (1995). Co-operative regulation of endocytosis by three Rab5 isoforms. FEBS Lett *366*, 65-71.

Buchmeier, M.J., de la Torre, J.C., and Peters, C.J. (2007). Arenaviridae: The Viruses and Their Replication. In Fields Virology, D.M. Knipe, P.M. Howley, D.E. Griffin, R.A. Lamb, M.A. Martin, B. Roizman, and S.E. Straus, eds. (Philadelphia: Wolters Kluwer Heath/Lippincott Williams & Wilkins), pp. 1791-1827.

Buchmeier, M.J., de la Torre, J.C., and Peters, C.J. (2013). Arenaviridae. In Fields Virology, D.M. Knipe, P.M. Howley, J.I. Cohen, D.E. Griffin, R.A. Lamb, M.A. Martin, V.R. Racaniello, and B. Roizman, eds. (Philadelphia, PA: Wolters Kluwer Heath/Lippincott Williams & Wilkins), pp. 1283-1303.

Capul, A.A., Perez, M., Burke, E., Kunz, S., Buchmeier, M.J., and de la Torre, J.C. (2007). Arenavirus Z-glycoprotein association requires Z myristoylation but not functional RING or late domains. Journal of virology *81*, 9451-9460.

Castelnuovo, M., Rahman, S., Guffanti, E., Infantino, V., Stutz, F., and Zenklusen, D. (2013). Bimodal expression of PHO84 is modulated by early termination of antisense transcription. Nat Struct Mol Biol *20*, 851-858.

Chou, Y.Y., Heaton, N.S., Gao, Q., Palese, P., Singer, R.H., and Lionnet, T. (2013). Colocalization of different influenza viral RNA segments in the cytoplasm before viral budding as shown by single-molecule sensitivity FISH analysis. PLoS pathogens *9*, e1003358.

Eichler, R., Strecker, T., Kolesnikova, L., ter Meulen, J., Weissenhorn, W., Becker, S., Klenk, H.D., Garten, W., and Lenz, O. (2004). Characterization of the Lassa virus matrix protein Z: electron microscopic study of virus-like particles and interaction with the nucleoprotein (NP). Virus research *100*, 249-255.

Eisfeld, A.J., Kawakami, E., Watanabe, T., Neumann, G., and Kawaoka, Y. (2011). RAB11A is essential for transport of the influenza virus genome to the plasma membrane. Journal of virology *85*, 6117-6126.

Fuller-Pace, F.V., and Southern, P.J. (1988). Temporal analysis of transcription and replication during acute infection with lymphocytic choriomeningitis virus. Virology *162*, 260-263.

Haist, K., Ziegler, C., and Botten, J. (2015). Strand-Specific Quantitative Reverse Transcription-Polymerase Chain Reaction Assay for Measurement of Arenavirus Genomic and Antigenomic RNAs. PloS one *10*, e0120043.

King, B.R., Hershkowitz, D., Eisenhauer, P.L., Weir, M.E., Ziegler, C.M., Russo, J., Bruce, E.A., Ballif, B.A., and Botten, J. (2017). A Map of the Arenavirus Nucleoprotein-Host Protein Interactome Reveals that Junin Virus Selectively Impairs the Antiviral Activity of Double-Stranded RNA-Activated Protein Kinase (PKR). Journal of virology *91*.

Lakdawala, S.S., Wu, Y., Wawrzusin, P., Kabat, J., Broadbent, A.J., Lamirande, E.W., Fodor, E., Altan-Bonnet, N., Shroff, H., and Subbarao, K. (2014). Influenza a virus assembly intermediates fuse in the cytoplasm. PLoS pathogens *10*, e1003971.

Martinez, M.G., Forlenza, M.B., and Candurra, N.A. (2009). Involvement of cellular proteins in Junin arenavirus entry. Biotechnology journal *4*, 866-870.

Momose, F., Sekimoto, T., Ohkura, T., Jo, S., Kawaguchi, A., Nagata, K., and Morikawa, Y. (2011). Apical transport of influenza A virus ribonucleoprotein requires Rab11-positive recycling endosome. PloS one *6*, e21123.

Nielsen, E., Severin, F., Backer, J.M., Hyman, A.A., and Zerial, M. (1999). Rab5 regulates motility of early endosomes on microtubules. Nature cell biology *1*, 376-382.

Panda, D., Das, A., Dinh, P.X., Subramaniam, S., Nayak, D., Barrows, N.J., Pearson, J.L., Thompson, J., Kelly, D.L., Ladunga, I., and Pattnaik, A.K. (2011). RNAi screening reveals requirement for host cell secretory pathway in infection by diverse families of negative-strand RNA viruses. Proceedings of the National Academy of Sciences of the United States of America *108*, 19036-19041.

Raj, A., van den Bogaard, P., Rifkin, S.A., van Oudenaarden, A., and Tyagi, S. (2008). Imaging individual mRNA molecules using multiple singly labeled probes. Nature methods *5*, 877-879.

Rojek, J.M., Sanchez, A.B., Nguyen, N.T., de la Torre, J.C., and Kunz, S. (2008). Different mechanisms of cell entry by human-pathogenic Old World and New World arenaviruses. Journal of virology *82*, 7677-7687.

Savidis, G., McDougall, W.M., Meraner, P., Perreira, J.M., Portmann, J.M., Trincucci, G., John, S.P., Aker, A.M., Renzette, N., Robbins, D.R., Guo, Z., Green, S., Kowalik, T.F.,

and Brass, A.L. (2016). Identification of Zika Virus and Dengue Virus Dependency Factors using Functional Genomics. Cell Rep *16*, 232-246.

Song, T., Zheng, Y., Wang, Y., Katz, Z., Liu, X., Chen, S., Singer, R.H., and Gu, W. (2015). Specific interaction of KIF11 with ZBP1 regulates the transport of beta-actin mRNA and cell motility. Journal of cell science *128*, 1001-1010.

Stenmark, H. (2009). Rab GTPases as coordinators of vesicle traffic. Nat Rev Mol Cell Biol *10*, 513-525.

Weber, E.L., and Buchmeier, M.J. (1988). Fine mapping of a peptide sequence containing an antigenic site conserved among arenaviruses. Virology *164*, 30-38.

Wichgers Schreur, P.J., and Kortekaas, J. (2016). Single-Molecule FISH Reveals Non-selective Packaging of Rift Valley Fever Virus Genome Segments. PLoS pathogens *12*, e1005800.

Zenklusen, D., and Singer, R.H. (2010). Analyzing mRNA expression using single mRNA resolution fluorescent in situ hybridization. Methods Enzymol *470*, 641-659.

3.7. Supplemental Table

Table S3.1. Full list and sequence of the FISH probes used in the current study.

Target	Probe Name	Probe Sequence (5' to 3')
LCMV S Genome	Genome 1	tttagaggcccaaatgttgt
LCMV S Genome	Genome 2	gctcccagatctgaaaactg
LCMV S Genome	Genome 3	cactcatggactgcatcatt
LCMV S Genome	Genome 4	tcgatgttgaaatgaccagg
LCMV S Genome	Genome 5	ggactcacagaataggaagg
LCMV S Genome	Genome 6	ccgatgacatcagaaagctt
LCMV S Genome	Genome 7	atggttctaagctgtcaagg
LCMV S Genome	Genome 8	tcgtcagttataggtgctct
LCMV S Genome	Genome 9	gatcttgccgacctcttcaa
LCMV S Genome	Genome 10	gattccaagtactcacacgg
LCMV S Genome	Genome 11	ggaacccgttgatcaaaaac
LCMV S Genome	Genome 12	cgggcagttcatacactttt
LCMV S Genome	Genome 13	tgatccagtggaaatagcaa
LCMV S Genome	Genome 14	caacgctcctacatggattg
LCMV S Genome	Genome 15	tacagccagacaatgctttt
LCMV S Genome	Genome 16	agaaacctgcagtcaattca
LCMV S Genome	Genome 17	gcatgggaaaacacaacaat
LCMV S Genome	Genome 18	gatggccatacatagcttgt
LCMV S Genome	Genome 19	aaagtttgcctttcaggtga
LCMV S Genome	Genome 20	caggaacccttatgaaaaca
LCMV S Genome	Genome 21	ttgtttcagaccaagttggg
LCMV S Genome	Genome 22	ggccaagagaaaactcaaca
LCMV S Genome	Genome 23	gacctcttgaaggcagttct
LCMV S Genome	Genome 24	ttttgatcaagccaagcaac
LCMV S Genome	Genome 25	aactttagtcttggtgctgc
LCMV S Genome	Genome 26	gtcatcactgaacagcagtc
LCMV S Genome	Genome 27	tcttgaaaggctgaaagaca
LCMV S Genome	Genome 28	ggcttgctttacacagtcaa
LCMV S Genome	Genome 29	tcaatgacgttgtacaagcg
LCMV S Genome	Genome 30	ctatggcttgtatggccaaa
LCMV S Genome	Genome 31	aatcaatttggcacaatgcc
LCMV S Genome	Genome 32	gggatgtgaaagactcatca
LCMV S Genome	Genome 33	ttgggatgagaaagcctcag
LCMV S Genome	Genome 34	gaccaaagatctcagatcct
LCMV S Genome	Genome 35	gggaacttaacaacacagca

LCMV S Genome	Genome 36	ccaggcttcaggggtatata
LCMV S Genome	Genome 37	ccaagatcatgaggtctgaa
LCMV S Genome	Genome 38	gctgaccttgagaagctgaa
LCMV S Genome	Genome 39	cagtgcagaagaactgatgt
LCMV S Genome	Genome 40	actgtacattctcttgtgga
LCMV S Genome	Genome 41	gagactcagaagtctcaacc
LCMV S Genome	Genome 42	aagagagatgacaaagacct
LCMV S Genome	Genome 43	cttctctgaggtcagcaatg
LCMV S Genome	Genome 44	ccaaccttctgaatgggttg
LCMV S Genome	Genome 45	ggctgctgtcattaaggatg
LCMV S Genome	Genome 46	gcagagcttcacatcagatg
LCMV S Genome	Genome 47	cgcaagcattgagaagagaa
LCMV S Genome	Genome 48	aggaagttaagagcttccaa
LCMV S Antigenome	Antigenome 1	ggtgtaaaaaccgtctggaa
LCMV S Antigenome	Antigenome 2	accgattaaccaacaaagga
LCMV S Antigenome	Antigenome 3	ataaaaggtggctcatgtcc
LCMV S Antigenome	Antigenome 4	ctagtcagcatcttcctgca
LCMV S Antigenome	Antigenome 5	gatgttttccacatctgcat
LCMV S Antigenome	Antigenome 6	ccctagcattgatggacctt
LCMV S Antigenome	Antigenome 7	aacaggaagccgataacatg
LCMV S Antigenome	Antigenome 8	aaatgagacccacttcagtg
LCMV S Antigenome	Antigenome 9	gcttgtcaccaatggttctt
LCMV S Antigenome	Antigenome 10	gaaactagtgtccccaagtg
LCMV S Antigenome	Antigenome 11	acctagaacatgcaaagacc
LCMV S Antigenome	Antigenome 12	gggtgccatattgcaattac
LCMV S Antigenome	Antigenome 13	actactgatgaggaaccact
LCMV S Antigenome	Antigenome 14	gtagaatctgccttgcactt
LCMV S Antigenome	Antigenome 15	aggctgctttgagtaagttc
LCMV S Antigenome	Antigenome 16	gctgcgactaattgactaca
LCMV S Antigenome	Antigenome 17	tcatgatgccgaattctgtg
LCMV S Antigenome	Antigenome 18	cagttgcgaaatgcaatgta
LCMV S Antigenome	Antigenome 19	gcttaagtgtttcgggaaca
LCMV S Antigenome	Antigenome 20	aatggatgattcttgctgca
LCMV S Antigenome	Antigenome 21	agaatccaggtggttattgc
LCMV S Antigenome	Antigenome 22	acattcacctggactttgtc
LCMV S Antigenome	Antigenome 23	tcttcactaggagactagcg
LCMV S Antigenome	Antigenome 24	tctcctttcccaagagaaga
LCMV S Antigenome	Antigenome 25	acatatgcaggtccttttgg
LCMV S Antigenome	Antigenome 26	atagaacctgggaaaaccac

LCMV S Antigenome	Antigenome 27	gccagacgagttaccaatac
LCMV S Antigenome	Antigenome 28	atgtttagaactgccttcgg
LCMV S Antigenome	Antigenome 29	agtgtagaaccttcagaggt
LCMV S Antigenome	Antigenome 30	ctcagatcgacaaagtgctc
LCMV S Antigenome	Antigenome 31	cagtatcctgcgacttcaac
LCMV S Antigenome	Antigenome 32	tcagagggaactccaactat
LCMV S Antigenome	Antigenome 33	tagtttcgagcctacacctc
LCMV S Antigenome	Antigenome 34	tttgaccacacactcatgag
LCMV S Antigenome	Antigenome 35	ttttgcaatctgacctctgc
LCMV S Antigenome	Antigenome 36	agaattgaccttcaccaatg
LCMV S Antigenome	Antigenome 37	acatcagtatggggacttct
LCMV S Antigenome	Antigenome 38	gcatgttcagccaacaactc
LCMV S Antigenome	Antigenome 39	cacatctgaacctgaccatg
LCMV S Antigenome	Antigenome 40	ccaatttaagtcagtggagt
LCMV S Antigenome	Antigenome 41	acccgacatttacaaaggag
LCMV S Antigenome	Antigenome 42	gtggcatgtacggtcttaag
LCMV S Antigenome	Antigenome 43	cagtttcctacttctggctg
LCMV S Antigenome	Antigenome 44	cctgtgggatattcgcattg
LCMV S Antigenome	Antigenome 45	aaggctgtctacaattttgc
LCMV S Antigenome	Antigenome 46	ttgtgcttatcgtgatcacg
LCMV S Antigenome	Antigenome 47	ctcacatcatcgatgaggtg
LCMV S Antigenome	Antigenome 48	gtgacaatgtttgaggctct

CHAPTER 4:

A MAP OF THE ARENAVIRUS NUCLEOPROTEIN-HOST PROTEIN INTERACTOME REVEALS THAT JUNÍN VIRUS SELECTIVELY IMPAIRS THE ANTIVIRAL ACTIVITY OF DOUBLE-STRANDED RNA-ACTIVATED PROTEIN KINASE (PKR)

Benjamin R. King[1,2], Dylan Hershkowitz[1], Philip L. Eisenhauer[1], Marion E. Weir[3,#], Christopher M. Ziegler[1,2], Joanne Russo[1,§], Emily A. Bruce[1], Bryan A. Ballif[3], Jason Botten[1,4*]

[1]Department of Medicine, Division of Immunobiology, [2]Cellular, Molecular, and Biomedical Sciences Graduate Program, [3]Department of Biology, [4]Department of Microbiology and Molecular Genetics, University of Vermont, Burlington, VT 05405, USA, [#]Current address: Cell Signaling Technology, Beverly, MA, 01915, [§]Current address: Department of Integrative Physiology and Pathobiology, Tufts University School of Medicine, Boston, MA 02111, *Corresponding author

Running Title: Junín virus antagonizes the antiviral activity of PKR

4.1. Abstract

Arenaviruses are enveloped negative-strand RNA viruses that cause significant human disease. Encoding only four proteins to accomplish the viral life cycle, each arenavirus protein likely plays unappreciated accessory roles during infection. Here, we used immunoprecipitation and mass spectrometry to identify human proteins that interact with the nucleoprotein (NP) of the Old World arenavirus lymphocytic choriomeningitis (LCMV) and the New World arenavirus Junín Candid #1 (JUNV). Bioinformatic analysis of the identified protein partners of NP revealed that host translation appears to be a key biological process engaged during infection. In particular, NP associates with the dsRNA-activated protein kinase (PKR), a well-characterized antiviral protein that inhibits cap-dependent protein translation initiation via phosphorylation of eIF2α. JUNV infection leads to increased expression of PKR as well as its redistribution to viral replication and transcription factories. Further, phosphorylation of PKR, which is a prerequisite for its ability to phosphorylate eIF2α, is readily induced by JUNV. However, JUNV prevents this pool of activated PKR from phosphorylating eIF2α, even following exposure to the synthetic dsRNA poly(I:C), a potent PKR agonist. This blockade of PKR function was highly specific as LCMV was unable to similarly inhibit eIF2α phosphorylation. JUNV's ability to antagonize the antiviral activity of PKR appears to be complete as silencing of PKR expression had no impact on viral propagation. In summary, we have provided a detailed map of the host machinery engaged by the arenavirus NP and identified an antiviral pathway that is subverted by JUNV.

4.2. Importance

Arenaviruses are important human pathogens for which FDA-approved vaccines do not exist and effective antiviral therapeutics are needed. Design of antiviral treatment options and elucidation of the mechanistic basis of disease pathogenesis will depend on an increased basic understanding of these viruses and, in particular, their interactions with host cell machinery. Identifying host proteins critical for the viral life cycle and/or pathogenesis represents a useful strategy to uncover new drug targets. This study, for the first time, reveals the extensive human protein interactome of the arenavirus nucleoprotein and uncovers a potent antiviral host protein that is neutralized during Junín virus infection. In so doing, we have gained further insight into the interplay between the virus and the host innate immune response and provided an important dataset for the field.

4.3. Introduction

The arenaviruses are a family of enveloped RNA viruses that can cause severe human disease. In particular, several family members, including Lassa virus (LASV) and Junín virus (JUNV), cause hemorrhagic fever syndromes (Buchmeier et al., 2007). Additionally, lymphocytic choriomeningitis virus (LCMV), which has a global distribution, is an underappreciated human pathogen that represents a significant teratogenic threat to developing fetuses and is a danger to immunosuppressed populations (Buchmeier et al., 2007; Fischer et al., 2006). There are currently no FDA-approved vaccines to prevent arenavirus infection and effective antiviral treatments are limited (Enria et al., 2008; McCormick et al., 1986). Several of the arenaviruses require biosafety level (BSL)-4 containment and are designated as Select Agents and potential bioterrorism threats (Botten et al., 2013). This highlights the critical need for new prevention and treatment options for these dangerous viruses, and the successful development of a next generation antiviral therapeutic will depend on an improved understanding of the basic biology of the arenavirus life cycle.

Arenaviruses have a single-stranded, bisegmented negative-sense RNA genome. Each genomic RNA segment contains 2 open reading frames arranged in an ambisense fashion (Buchmeier et al., 2001). The virus encodes only 4 proteins: the nucleoprotein (NP) and glycoprotein (GPC) on the S genomic segment and the RNA-dependent RNA polymerase (L) and viral matrix protein (Z) on the L genomic segment (Buchmeier et al., 2001). These four viral proteins are sufficient to achieve all of the steps of the viral life cycle. Nevertheless, it is likely that each is highly multifunctional and relies upon

interactions with multiple host proteins to facilitate key steps of the viral life cycle and/or to subvert an effective host immune response.

The canonical role of the arenavirus NP is to encapsidate the viral genomic RNA and aid the viral polymerase in the process of genome replication (Buchmeier et al., 2001). NP also acts to prevent the induction of type I IFN via its ability to degrade dsRNA substrates that could activate cytoplasmic RIG-I like receptors (Hastie et al., 2011a; Qi et al., 2010). Work by other groups has already demonstrated the ability of the arenavirus NP to engage in protein-protein interactions with host cellular proteins. However, only a few host factors engaged by NP are known and the functional importance of these interactions necessitates further investigation. Among the Old World arenaviruses, it was demonstrated that ALIX/AIP1, an endosomal sorting complex required for transport (ESCRT) associated protein, associates with NP and is necessary for the efficient recruitment of NP into Z-induced virus like particles (Shtanko et al., 2011). LCMV NP has been shown to interact with IKKε, which contributes to its repression of type I IFN induction (Pythoud et al., 2012). Keratin 1, also an interacting partner of LCMV NP, is important for the virus's ability to spread from cell to cell (Labudova et al., 2009). The New World arenavirus JUNV NP was shown to associate with eIF4A and eIF4GI, and these interactions were important for translation of viral mRNAs (Linero et al., 2013). Last, JUNV NP was shown to interact with hnRNP A/B proteins, which were required for viral propagation (Maeto et al., 2011). While a small number of cellular proteins have been shown to interact and/or colocalize with the arenavirus NP, a large-scale mapping of the host cellular interactome of NP is

necessary to fully appreciate the multifunctional role that this viral protein plays during the viral life cycle.

Besides our appreciation of NP's role in interfering with type I IFN induction and its interaction with a handful of cellular proteins, little is known about the additional accessory role(s) NP may play in the infected cells and how these may be affected by its interaction with host proteins. To address this gap in our knowledge, we mapped the cellular protein interactome of the arenavirus NP using LCMV, an Old World arenavirus member, and the New World JUNV strain Candid #1 (Goni et al., 2006). Our studies revealed that the arenavirus NP interacts with an extensive array of cellular proteins. In particular, host protein translation appears to be a major cellular function targeted by the arenavirus NP. We identified that the double-stranded RNA-activated protein kinase (PKR), an important antiviral effector, interacts with both the JUNV and LCMV NP. We show that, despite becoming highly activated during JUNV infection, PKR is unable to carry out its canonical antiviral function, which is to phosphorylate eIF2α and trigger a global shutdown of cap-dependent translation. LCMV similarly activates PKR but, unlike JUNV, appears unable to fully suppress PKR's kinase activity as transient eIF2α phosphorylation occurs during LCMV infection. Nevertheless, the replication of both viruses was unaffected by PKR silencing suggesting that arenaviruses have developed strategies to neutralize this critical arm of the host innate immune response.

4.4. Results

4.4.1. Identification of human proteins that associate with the arenavirus nucleoprotein.

Viruses hijack cellular factors to complete necessary steps of their life cycle and/or to evade the host immune response. Thus, discovering these host factors has the potential to identify drug targets or help illuminate cellular pathways targeted by the virus. To identify the cellular protein partners of the arenavirus NP, we employed a strategy in which human cells (A549 or HEK 293T) were first infected with either the Old World arenavirus LCMV strain Armstrong 53b or the New World arenavirus JUNV strain Candid #1 (hereafter referred to as JUNV) (Figure 4.1A). Following establishment of acute infection, each NP and its associated cellular protein partners were immunoprecipitated from cell lysates using an NP-specific monoclonal antibody. The immune complexes were separated by SDS-PAGE, and stained with Coomassie blue to allow visualization of the captured NP (bait) as well as its interacting host proteins (the prey) (Figure 4.1B to E). The stained SDS-PAGE gels were cut into sections, and the proteins contained in each section were digested with trypsin and extracted for subsequent liquid chromatography tandem mass spectrometry (LC-MS/MS). Identified proteins were considered valid interactors in a given run when i) 2 or more unique tryptic peptides were detected from a particular protein in the infected sample but not the mock control or ii) when a minimum of five-fold more total tryptic peptides was detected from a particular protein in the infected sample compared to the mock control. Using these criteria, we identified 509 human proteins that associated

with JUNV NP and 348 that associated with LCMV NP in at least one experiment (Figure 4.1F and Table S4.1). Of these proteins, 275 had a conserved interaction with JUNV NP and LCMV NP (Figure 4.1F). Additionally, there was a high degree of reproducibility when comparing the interacting host proteins between the 2 human cell lines, HEK 293T and A549, where 83% of interacting proteins identified in HEK 293T cells were also observed in A549 cells (Figure 4.1G). Thus, this data set represents the first large-scale map of the arenavirus NP-human protein interactome.

4.4.2. Cellular processes targeted by the arenavirus NP.

We were especially interested in the 275 proteins that exhibited a conserved interaction with both JUNV NP and LCMV NP as these could represent fundamental and highly conserved aspects of arenavirus biology. Indeed, conserved hits for both viruses were, on average, identified by more spectral counts than those of JUNV NP or LCMV NP alone (Figure 4.2A). Because the strongest interactors were likely those identified by multiple tryptic peptides, we examined in greater detail the "strong interactors" which were in the top 25% of all interacting host proteins by spectral counts (Figure 4.2A and Table 4.1). However, it should be noted that the mass spectrometry approach used in this study is semi-quantitative. It is possible that a strong, specific interacting cellular protein may not be detected at all or only at very low levels for technical reasons. Nevertheless, to better characterize the subset of proteins detected by the highest number spectral counts, we used the NIH DAVID functional annotation and gene-enrichment tool (Huang et al., 2009a, b) to identify functional groups of proteins that may be over-represented in our dataset. Of

the annotation clusters identified within this group, protein translation was the top process engaged by the arenavirus NP (Figure 4.2B), suggesting that this may be a key cellular process regulated by the virus during infection. Two important host protein partners involved in translation were eukaryotic translation initiation factor 2 subunit alpha, eIF2α, a translation initiation factor critical for the cap-dependent assembly of the 43S ribosomal preinitiation complex (Garcia et al., 2007), and the double-stranded RNA-activated protein kinase, PKR, which can lead to arrest of cellular translation in response to viral infection via phosphorylation of eIF2α (Garcia et al., 2007) (Table 4.1 and S4.1). In addition, NIH DAVID analysis on the subset of proteins interacting with only the JUNV NP or the LCMV NP revealed functional processes of nucleotide binding or organelle/nuclear lumen being engaged by the respective NPs (Figure 4.2D and E). Functional categories enriched in this "strong interactor" subset were very similar to those categories represented by the dataset as a whole (Figure 4.2B and C).

4.4.3. Biochemical validation of the interaction between cellular proteins and arenavirus NPs.

We next chose a subset of the identified host proteins and attempted to further validate their association with a particular arenavirus NP via immunoprecipitation and Western blot. This subset of proteins included PKR, eIF2α, and Ras GTPase-activating protein-binding protein 1 (G3BP1) (proteins involved in translation); splicing factor, proline- and glutamine-rich (SFPQ) (part of several top clusters identified by the DAVID analysis including RNA processing, binding, and stability); and apoptosis-inducing factor

1, mitochondrial (AIFM1) (the most abundantly detected interacting partner of JUNV NP and identified as being part of the organelle/nuclear lumen cluster by the DAVID analysis). Each protein, with the exception of AIFM1, co-immunoprecipitated as prey with NP (bait) from cells infected with JUNV or LCMV (Figure 4.3A, lane 3; Figure 4.3B, lane 3). AIFM1 interacted specifically with JUNV NP but not LCMV NP while eIF2α interacted weakly with LCMV NP compared to JUNV NP. Reciprocally, PKR, G3BP1, and AIFM1, when serving as bait for immunoprecipitation from JUNV or LCMV-infected lysates, were each able to co-precipitate both viral NPs, but JUNV NP interacted more strongly with both AIFM1 and PKR when compared to LCMV NP (Figure 4.3C to H). Finally, we addressed whether this subset of host proteins could associate with an arenavirus NP in the absence of other viral proteins or the full viral genome. G3BP1, eIF2α, AIFM1, and SFPQ interact with Lassa virus, LCMV, and JUNV NP (expressed via plasmid in HEK 293T cells) while PKR only associates with JUNV NP (Figure 4.4A). Notably, the strength of interaction between each host protein and a particular NP was variable (Figure 4.4A). Additionally, immunoprecipitation of PKR and AIFM1 from transfected HEK 293T cells was able to co-precipitate each of arenaviral NPs tested (Figure 4.4B and C).

4.4.4. PKR and G3BP1 colocalize with JUNV NP.

We next used fluorescence microscopy to determine whether PKR and G3BP1 were recruited to the replication and transcription factories of JUNV or LCMV. In JUNV-infected cells, at 72 hours post-infection (hpi), the majority of the cells were infected, and NP formed large, perinuclear puncta in most cells (Figure 4.5A). At 48 hpi in LCMV-

infected cells, most cells were infected and displayed a variable pattern of cytoplasmic NP staining. LCMV NP concentrated into puncta that were either small and scattered through the cytoplasm or large and located near the nucleus (Figure 4.5B). In the setting of JUNV infection, total PKR signal increased compared to mock cells (Figure 4.5A). While PKR staining was cytoplasmic in both infected and uninfected cells, JUNV infection resulted in a relocalization and concentration of PKR in JUNV NP-containing puncta (Figure 4.5A, see fluorescence intensity profiles). This was specific to JUNV as PKR protein levels were not upregulated in LCMV-infected cells and PKR remained diffusely localized, without specifically colocalizing with LCMV NP (Figure 4.5B, see fluorescence intensity profiles). This finding is consistent with biochemical evidence suggesting that PKR has a stronger association with JUNV NP compared to LCMV NP (Figure 4.3C and D and 4.4A).

G3BP1 generally displayed a diffuse cytoplasmic staining pattern in uninfected cells (Figure 4.6), although some minority of uninfected cells spontaneously displayed distinct cytoplasmic puncta of G3BP1 staining in presumed stress granule structures (Figure 4.6A). Similar to PKR, a portion of the cytoplasmic G3BP1 concentrated in JUNV NP puncta (Figure 4.6A, see fluorescence intensity profiles). In LCMV-infected cells, G3BP1 maintained a predominantly diffuse cytoplasmic staining pattern with slight enrichment at NP puncta (Figure 4.6B, see fluorescence intensity profiles).

Collectively, these experiments further validate the biological interaction of PKR and G3BP1 with JUNV NP and define these host proteins as components/markers of

presumptive viral replication and transcription factories. Further, they show the specificity of the NP-PKR interaction for JUNV.

4.4.5. PKR is activated following JUNV infection but does not phosphorylate eIF2α.

Because of the importance of PKR as an antiviral innate immune mediator (Garcia et al., 2007) and the specificity of the interaction with the JUNV NP (Figure 4.3C and D, 4.4A, and 4.5), we next sought to functionally characterize the importance of this interaction in the context of both New World and Old World arenavirus infections. Over a time course of acute infection, cellular protein lysates were probed for phospho-PKR (T446), a phosphorylation site in the activation loop and a marker of activated PKR. We also probed for phospho-eIF2α (S51), the target of PKR's kinase activity and a marker of global translational shutdown. Both expression and phosphorylation of PKR were strongly induced late in infection with JUNV, yet there was no concomitant increase in the phosphorylation of PKR's target, eIF2α, at these time points (Figure 4.7A to C). In LCMV-infected cells, overall PKR levels did not increase but there was an induction of phosphorylation of PKR at 36 and 48 hpi. However, in contrast to JUNV, there was a small yet significant increase in the phosphorylation of eIF2α at these time points (Figure 4.7D to F). This suggested an ability of JUNV to prevent activated PKR from phosphorylating its target eIF2α.

4.4.6. JUNV infection blocks poly(I:C)-induced phosphorylation of eIF2α.

The observation that PKR was highly activated (phosphorylated) in JUNV-infected cells, yet this activated PKR failed to phosphorylate eIF2α, suggested that the virus was

evading this innate surveillance pathway. To determine whether we could overcome the ability of the virus to block active PKR from phosphorylating eIF2α, we transfected cells with poly(I:C), a synthetic dsRNA analog that strongly activates PKR (Garcia et al., 2007). When comparing mock-cells that had been transfected with lipofectamine but no poly(I:C) (vehicle control) to those transfected with increasing quantities of poly(I:C), phosphorylation of PKR was effectively induced by increasing concentrations of poly(I:C) (Figure 4.8A, B, E, and F). In JUNV-infected cells, there were already high levels of phospho-PKR (Figure 4.8A and B). However, transfection with poly(I:C) further increased the induction of PKR phosphorylation (Figure 4.8A and B). In mock-infected cells, the increased PKR phosphorylation following poly(I:C) transfection led to increased phosphorylation of eIF2α (Figure 4.8A, C, E, and G). However, there was no increase in the phosphorylation of eIF2α in JUNV-infected cells (Figure 4.8A and C). In LCMV-infected cells, phosphorylation of PKR could be further induced following poly(I:C) transfection (Figure 4.8E and F). However, this active PKR was able to phosphorylate eIF2α and there was no difference between phospho-eIF2α in mock-infected and LCMV-infected cells following poly(I:C) transfection (Figure 4.8E and G). Thus, JUNV appears to specifically block activated PKR from phosphorylating its downstream target, eIF2α.

4.4.7. JUNV selectively blocks PKR's functionality.

Though activated PKR's canonical target is eIF2α, PKR can also activate alternate signaling pathways. Among these alternate pathways is the activation of NF-κB signaling (Zamanian-Daryoush et al., 2000), through an incompletely defined pathway. While the

exact mechanism is unclear, it is known that IκB is degraded following PKR activation and that this allows the nuclear translocation of the NF-κB transcription factor, and subsequent expression of NF-κB responsive genes (Zamanian-Daryoush et al., 2000). To determine whether this alternate PKR signaling pathway remained functional in cells expressing arenavirus NPs, we also probed cellular protein lysates for IκB to see if it was degraded following poly(I:C) transfection as would be expected. We saw that whether cells were uninfected or infected with JUNV or LCMV, they were able to efficiently degrade IκB following transfection with poly(I:C), suggesting that this alternate PKR signaling function remains intact (Figure 4.8A, D, E, and H). An alternate possibility is that the observed IκB degradation could be the result of signaling downstream of other innate immune sensors capable of responding to dsRNA such as TLR3, RIG-I, or MDA5 (Kawai and Akira, 2008).

4.4.8. Translational profile of cells infected with JUNV or LCMV.

We wanted to examine whether eIF2α phosphorylation observed in LCMV- but not JUNV-infected cells (Figure 4.7 and 4.8) was functionally correlated with repression of global translation in these cells. To assess rates of active translation, we utilized a newly described assay to examine protein translation levels in individual cells infected with either LCMV or JUNV (David et al., 2012; Schmidt et al., 2009). At various time points following infection, cells were pulse-labeled with puromycin, which is covalently incorporated into growing peptide chains. Nascent peptides were detected with a puromycin-specific monoclonal antibody, and were visualized by confocal microscopy. Mock-infected cells were labeled with puromycin to determine normal translation rates

whereas mock-infected cells that were pre-treated with sodium arsenite were labeled to determine protein production levels in a repressed translational state (Figure 4.9A to D). While cells infected with either LCMV or JUNV exhibited reduced rates of translation compared to uninfected cells, the biological importance of this subtle decrease is unclear as the majority of cells maintained translation rates that were in the "normal range" observed in mock-infected cells (Figure 4.9A to D). However, at intermediate time points following infection with LCMV (24-36 hpi), there was a significant increase in cells exhibiting translation rates that were highly reduced compared to mock-infected cells (Figure 4.9A, C, and E). A similar pattern was not observed in JUNV-infected cells (Figure 4.9B, D, and E). These data further support the observations shown in Figures 4.7 and 4.8 that LCMV is more sensitive than JUNV to PKR-dependent phosphorylation of eIF2α. Importantly, these experiments demonstrate that, in most instances, JUNV and LCMV are capable of infecting host cells without inducing a potent global shutdown of translation, despite highly activating PKR.

4.4.9. Replication of influenza A virus lacking expression of the NS1 protein is rescued by siRNA knockdown of PKR.

We wanted to examine whether arenavirus growth would be affected by the knockdown of PKR by siRNA. In order to validate our siRNA knockdowns, we infected siRNA treated cells with an influenza A virus (strain Pan-delNS1) lacking expression of the nonstructural protein NS1, a well-documented PKR antagonist (Bergmann et al., 2000; Hatada et al., 1999), to demonstrate that we were able to effectively knockdown PKR

expression to a level that could functionally rescue the replication of this highly PKR-sensitive virus. Protein levels of PKR were greatly reduced in cells transfected with a PKR-specific siRNA compared to a scrambled, non-targeting control siRNA (Figure 4.10A). As expected, the level of viral nucleoprotein in cells and the quantity of released infectious virus by cells infected with the wild type parental strain Pan/99 were unaffected by PKR knockdown (Figure 4.10A to C). However, when cells were infected with the mutant Pan-delNS1, viral nucleoprotein was expressed at higher levels (~eight fold) and significantly more (~six-fold) infectious virus was released from cells where PKR had been knocked down following siRNA transfection (Figure 4.10A to C). Together these results show that our knockdown of PKR by siRNA is sufficient to rescue a PKR-sensitive virus.

4.4.10. JUNV's antagonism of PKR's antiviral activity is complete.

We next wished to test whether PKR, which appears unable to phosphorylate its downstream substrate, eIF2α, during JUNV infection (Figure 4.7A and C), could still exert an antiviral effect on the propagation of JUNV. Additionally, we were curious if knockdown of PKR could improve the replication of LCMV by preventing the activation of eIF2α (Figure 4.7 and 4.8) and the transient translation repression (Figure 4.9) observed during LCMV infection. To do so, we measured the levels of NP produced in infected cells (Figure 4.11A, B, D, and E) and infectious virus released from cells (Figure 4.11C and F) treated with siRNAs to silence PKR expression. Despite nearly complete knockdown of PKR with either of two distinct PKR-specific siRNAs (Figure 4.11A and D), release of infectious JUNV and LCMV virus was not impacted when compared to cells treated with

a scrambled, nonspecific siRNA (Figure 4.11C and F). Levels of JUNV NP were similarly unaffected by the knockdown of PKR (Figure 4.11B). LCMV NP levels were slightly increased when PKR was knocked down with one of the two PKR specific siRNAs (Figure 4.11E). This result suggests that JUNV is capable of completely neutralizing the antiviral actions of PKR and further that PKR is not fundamentally required for the efficient propagation of JUNV. On the other hand, while eIF2α is activated and translation is repressed during LCMV infection, knockdown of PKR had no effect on the release of infectious LCMV virus and a modest effect on production of viral NP, which we believe to represent the transience of PKR's restriction on LCMV infection.

4.5. Discussion

The small size of the arenavirus proteome suggests that each viral protein is highly multifunctional. One strategy to identify additional accessory roles for these proteins is to identify the host machinery they engage during infection. In this study, we conducted a large-scale mapping of the human cellular interactome of the Old World and New World arenavirus NP. While the identified interactome was complex, a large percentage of the cellular protein partners were shared among Old World and New World NPs (Figure 4.1F). Bioinformatic analysis revealed a significant enrichment in proteins involved in protein translation, including the antiviral protein PKR (Figure 4.2 and Table 4.1). Our studies demonstrate that JUNV, despite activating PKR during infection (Figure 4.7A and B), selectively and potently inhibits PKR's ability to phosphorylate its downstream substrate,

eIF2α (Figure 4.7A and C and 4.8A and C), and subsequently interfere with viral propagation (Figure 4.11C).

PKR is one of four cellular kinases able to phosphorylate eIF2α and thus globally shut down cap-dependent translation in response to viral infection (Donnelly et al., 2013). This type I IFN-stimulated protein consists of two domains: an N terminal domain that contains two double-stranded RNA binding motifs and a C terminal kinase domain. In non-stressed cells, monomeric PKR is expressed at low basal levels. Upon exposure to a dsRNA ligand, the N terminal domain binds the dsRNA, PKR dimerizes, and each PKR subunit trans autophosphorylates at T446 and T451. Phosphorylation of these residues leads to full activation of PKR, which is then able to phosphorylate eIF2α at S51, leading to cap-dependent translation shutdown (Figure 4.12) (Garcia et al., 2007; Zhang et al., 2001).

A key finding of our proteomics studies was that both JUNV and LCMV NP interact with PKR. However, our follow-up biochemical validation (Figure 4.3 and 4.4) and immunofluorescence microscopy studies (Figure 4.5) suggest that this interaction may be more biologically-relevant for JUNV NP than LCMV NP. We demonstrate that PKR is strongly activated in cells infected with JUNV or LCMV (Figure 4.7) and even more so in infected cells that are transfected with the PKR agonist poly(I:C) (Figure 4.8). Nevertheless, this active PKR is only able to phosphorylate eIF2α in LCMV-infected cells as eIF2α phosphorylation by active PKR is strongly blunted in JUNV-infected cells (Figure 4.7 and 4.8). This effect is recapitulated in experiments measuring rates of translation in infected cells (Figure 4.9), where the majority of cells infected with JUNV or LCMV

maintain normal rates of translation throughout the course of infection. However, at 36 hpi, a significant proportion of LCMV infected cells enter a state of translation repression (Figure 4.9E), which happens to coincide with the spike in observed eIF2α phosphorylation observed by Western blot (Figure 4.7D and F). Interestingly, this effect of translation repression appears transient as the proportion of LCMV-infected cells with normal levels of translation recovers by 48 hpi (Figure 4.9A, C, and E). The finding that siRNA silencing of PKR, while sufficient to rescue the PKR-sensitive virus IAV Pan-delNS1 (Figure 4.10), had no effect on the JUNV life cycle (Figure 4.11A to C) and minimal to no effect on that of LCMV (Figure 4.11D to F) suggests that these viruses are both resistant to PKR's antiviral activity. The observation that LCMV remains resistant to PKR is surprising in light of the previous findings of this paper and could reflect both the transience of PKR's ability to control LCMV infection and/or the fact that LCMV possesses complementary mechanisms to inhibit PKR activity. A final possibility is that PKR could play a proviral role in the context of arenavirus infection as has previously been described for hepatitis C virus (Arnaud et al., 2010; Garaigorta and Chisari, 2009). Though, we consider this possiblity unlikely as PKR knockdown did not reduce the fitness of JUNV or LCMV (Figure 4.11).

Because protein translation is an absolutely critical process for the production of new viral components, many viruses, including those that rely on cap-dependent translation, have evolved mechanisms to interfere with the canonical antiviral role of PKR (Reineke and Lloyd, 2013). For example, the dsDNA poxvirus, vaccinia, expresses the E3L

protein, which prevents PKR from binding to dsRNA (Chang et al., 1992; Langland and Jacobs, 2002). The paramyxovirus measles, a negative strand RNA virus, antagonizes PKR activation via its nonstructural protein C, which negatively regulates the production of viral dsRNA intermediates during infection (Toth et al., 2009). In A549 cells, it was shown that the paramyxovirus respiratory syncytial virus (RSV) antagonizes PKR activity via its N protein, which binds PKR and decreases its ability to bind eIF2α thus shielding it from PKR's kinase activity (Groskreutz et al., 2010). Another report confirmed that RSV infection leads to the activation of PKR but that it also leads to significant phosphorylation of eIF2α in HEp-2 cells (Lindquist et al., 2011). The discrepancy between these two studies may be due to cell type-specific expression of protein phosphatase 2 – the enzyme responsible for dephosphorylating eIF2α. The nonstructural protein 1 (NS1) of the orthomyxovirus influenza A directly interacts with PKR and appears to interfere with its ability to bind dsRNA and become activated (Li et al., 2006; Lu et al., 1995). A common theme from these examples is that PKR antagonism represents a common strategy employed by diverse viruses, but the means by which they accomplish this feat is similarly variable. Among the viruses cited herein, the ability of JUNV to prevent eIF2α phosphorylation is most similar to that previously described for RSV as in both cases PKR becomes activated but is unable to phosphorylate eIF2α (Figure 4.7, 4.8, and 4.12) (Groskreutz et al., 2010).

The exact mechanism used by JUNV to antagonize PKR's ability to phosphorylate eIF2α remains unclear. Our studies suggest that NP itself, as well as its ability to interact

with the cellular factors PKR and eIF2α, may be critical. Indeed, in a related study, Linero et al. demonstrated that acute JUNV infection or expression of JUNV NP alone is sufficient to prevent eIF2α phosphorylation and the subsequent formation of cellular stress granules (SGs) following exposure to the oxidative stressor sodium arsenite (Linero et al., 2011). Phosphorylaton of eIF2α is a key event in driving the nucleation of SGs, which contain stalled cellular mRNAs and their associated translation initiation factors and are associated with inhibition of cap-dependent translation in response to various cellular stresses, including virus infection (Thomas et al., 2011). Sodium arsenite is thought to induce SG formation via activation of PKR and/or heme-regulated inhibitor (McEwen et al., 2005; Patel et al., 2000), which ultimately phosphorylate eIF2α. Therefore, if sodium arsenite drives eIF2α phosphorylation via PKR, NP may similarly block PKR's ability to phosphorylate eIF2α in response to both oxidative stress (sodium arsenite) and dsRNA intermediates (poly(I:C)).

JUNV has also been shown to block SG formation in response to challenge with the ER stressors DTT or thapsigargin, both of which lead to the phosphorylation of eIF2α via activation of protein kinase-like endoplasmic reticulum kinase (PERK), but not PKR (Harding et al., 2000; Harding et al., 1999). Paradoxically, despite failing to drive SG formation in JUNV-infected cells, both DTT and thapsigargin potently induced the phosphorylation of eIF2α in these same cells (Linero et al., 2011). We identified G3BP1, another cellular protein critical for the nucleation of stress granules (Tourriere et al., 2003), as an interacting partner of JUNV and LCMV NP (Figure 4.3A, B, G, and H and 4.4A and

Table S4.1). Further, a related study demonstrated that G3BP1 colocalizes with the arenavirus Tacaribe NP during infection (Baird et al., 2012). It is possible that JUNV NP can prevent SG nucleation despite the presence of phosphorylated eIF2α by interfering with key SG proteins such as G3BP1. Indeed, several other SG proteins were identified as partners of arenavirus NPs in our study, including eIF3 components, G3BP2, PABC, and several small ribosomal subunit proteins (Table S4.1 and S4.2) (Anderson and Kedersha, 2008; Buchan and Parker, 2009).

In addition to the antagonism of PKR's antiviral function reported here, arenaviruses have been shown to interfere with other innate immune pathways responsible for antiviral defense, including the RIG-I/MAVS pathway that drives type I IFN production. In particular, the arenavirus NP has been shown to associate with IKKε and block its ability to phosphorylate/activate IRF3, which is required for type I IFN production (Pythoud et al., 2012). LCMV NP has also been shown to block NFκB activition (Rodrigo et al., 2012). The arenavirus NP further antagonizes the type I IFN response via its 3' to 5' exonuclease activity that limits the availability of viral dsRNA replicative intermediates for recognition by the RIG-I/MAVS pathway (Hastie et al., 2011a; Qi et al., 2010). Notably, our results would suggest that NP cannot clear all of these dsRNA intermediates as we presume these are driving the activation of PKR during infection. Intriguingly, arenaviruses appear highly selective in their antagonism of these innate immune pathways. For example, Pythoud et al. demonstrated that despite blocking RIG-I/MAVS-dependent type I IFN production, LCMV leaves MAVS-dependent apoptosis fully functional

(Pythoud et al., 2015). Likewise, we report here that JUNV can block activated PKR from phosphorylating eIF2α (Figure 4.7A and C and 4.8A and C), yet leaves this phosphorylated form of PKR capable of inducing the degradation IκB in response to poly(I:C) (Figure 4.8A and D), which is a key step upstream of NFκB activation (Garcia et al., 2007; Zamanian-Daryoush et al., 2000), though we recommend caution in the interpretation of this finding as other innate immune sensors are also able to the activate NFκB in response to stimulation with dsRNA ligands (Kawai and Akira, 2008). These examples of selective antagonism suggest that arenaviruses have co-evolved with their reservoir rodents so that arenavirus-infected cells within the host, while unable to respond to the infecting arenavirus, can still mount an effective antimicrobial response against other enviromental pathogens to ensure the fitness and survival of the host.

The cellular protein partners of the arenavirus NP identified in this study may provide clues to advance our understanding of how these viruses hijack host cell machinery to facilitate the viral life cycle. Importantly, each protein partner represents a candidate target for future antiviral screening. For example, several host proteins that interact with NP and are required for viral propagation were validated in our study, including hnRNPA1 and hnRNPA2B1 (Maeto et al., 2011), as well as eIF4A and eIF4G, which are components of the eIF4F translation initiation complex (Baird et al., 2012; Linero et al., 2013) (Table 4.1). Also consistent with these previous studies, eIF4E, the cap-binding component of the eIF4F complex, was not detected in our work, supporting the hypothesis that JUNV and other New World arenavirus NPs can replace the cap-binding function of eIF4E to facilitate

translation of viral mRNAs (Linero et al., 2013). Finally, 8 additional host proteins identified in our screen – COPA, DDX60L, EIF3A, EIF3G, FAU, FBL, HNRNPK, and NOP56 (Table S4.1) – had previously been shown to be required for LCMV and VSV replication (Panda et al., 2011). Our results suggest these proteins may be critical for viral propagation due to their interaction with the LCMV NP. These examples highlight the feasibility and the utility of using a proteomics-based approach to identify antiviral targets.

In summary, we have provided the first detailed map of the human proteins engaged by the arenavirus NP and also highlighted host processes that are likely important for arenavirus propagation and/or pathogenesis. This information will serve as a useful resource to guide future studies investigating the importance of arenavirus-host interactions and defining additional functions of NP. By showing that JUNV can selectively block the canonical antiviral role of PKR, we have advanced our understanding of the seemingly multifaceted strategy employed by arenaviruses to curtail an effective innate immune response. Important questions to address in the future will include dissecting the specific mechanism used by JUNV to inihibit PKR's antiviral activity as well as to fully interrogate the importance of the remaining cellular interacting proteins identified in the proteomics screen.

4.6. Materials and Methods

4.6.1. Cells and viruses.

HEK 293T/17 cells (CRL-11268) and A549 (CCL-185) were procured from American Type Culture Collection (ATCC, Manassas, VA). Vero E6 cells were generously given by J. L. Whitton (The Scripps Research institute, La Jolla, CA). HEK 293T/17 cells were cultured in Dulbecco's Modified Eagle Medium (DMEM) (11965-118) containing 10% fetal bovine serum, 1% Penicillin-Streptomycin (15140-163), 1% MEM Non-Essential Amino Acids Solution (11140-050), 1% HEPES Buffer Solution (15630-130), and 1% GlutaMAX (35050-061) purchased from Thermo Fisher Scientific (Waltham, MA). A549 cells were cultured in DMEM-F12 (11320-033, Thermo Fisher), supplemented with 10% fetal bovine serum, and 1% Penicillin-Streptomycin. Vero E6 cells were maintained in DMEM, containing 10% fetal bovine serum, 1% Penicillin-Streptomycin, and 1% HEPES Buffer Solution. JUNV strain Candid #1 was generously provided by R. Tesh (The University of Texas Medical Branch at Galveston) and M. J. Buchmeier (University of California, Irvine). LCMV Armstrong 53b was obtained from J. L. Whitton. Titers of LCMV and JUNV were performed by standard plaque assay on Vero E6 cells. Recombinant influenza A/Panama/2007/99 (Pan/99) wild type virus and recombinant influenza A Panama/2007/99 ΔNS1 (Pan-delNS1) virus were generously provided by T. Wolff (Robert Koch-Institut, Berlin) (Matthaei et al., 2013). Cells were infected with IAV at an MOI of 1 after being washed with serum-free media. Infected cells were cultured in serum-free DMEM containing 1ug/ml TPCK Trypsin (T1426, Sigma-Aldrich) and 0.14%

BSA. Titers of IAV Pan/99 were determined by standard plaque assay on MDCK cells using a low-viscosity overlay (0.5x DMEM, 0.5ug/ml TPCK Trypsin, 0.07% BSA, 1.2% Avicel (RC591, FMC Biopolymer)) (Matrosovich et al., 2006). Titers of IAV Pan-delNS1 were determined by immunological focus assay on MDCK cells essentially as described in (Battegay et al., 1991) using a low-viscosity overlay and an IAV NP monoclonal antibody (ab20343, Abcam, at 1:5,000).

4.6.2. Immunoprecipitations and affinity purifications.

Cells were scraped into the media following infection or transfection, pelleted, washed with cold PBS, and gently lysed on ice in 25 mM Tris-HCL, pH 7.6 containing 1% Triton X-100 (T9284, Sigma-Aldrich, St. Louis, MO), 0.5% Nonidet P-40 IGEPAL CA-630 (198596, MP Biomedicals, Solon, OH), 140 mM NaCl, 1 mM calcium chloride (21115, Sigma-Aldrich), and a Complete Mini EDTA-Free Protease Inhibitor Cocktail tablet (04693159001, Roche Applied Science). Cell lysates were clarified of insoluble material by centrifugation at 10,000 rpm at 4°C. To pre-clear proteins non-specifically interacting with the magnetic Protein G beads (Dynabeads Protein G beads, 10004D, Thermo Fisher), beads were added to lysate and incubated on a rotating platform for 15 minutes at 4°C. Appropriate antibody was added to cell lysates and incubated for 2 hours at 4°C. Magnetic Protein G beads were added to lysates and incubated for 1 hour at 4°C. The beads were washed 4 times with ice cold lysis buffer to remove nonspecific proteins. Bound protein was stripped from the beads into 1x Laemmli Buffer, 5% β-mercaptoethanol by heating at 100°C for 5 minutes. Immunoprecipitated proteins were separated by SDS-

PAGE as described below. Antibodies used for immunoprecipitations are as follows: JUNV NP (KA03-AA01, BEI Resources), LCMV NP (1.1.3 and 24A, generously provided by M. J. Buchmeier) (Buchmeier et al., 1981), AIF (sc-9416, Santa Cruz), G3BP1 (A302-033A, Bethyl), and PKR (Y117, Abcam).

Affinity purification of biotinylated viral NPs was performed as follows. Viral NPs were cloned into a modified pCAGGS plasmid and carried a C-terminal HA epitope tag, the tobacco etch virus (TEV) protease cleavage site, and a biotin acceptor peptide. Viral NPs were biotinylated when cotransfected with the plasmid BirA, which expresses a bacterial biotin ligase. As a control to validate the specificity of the protein-protein interaction, cells were transfected with an empty vector along with BirA. Cells were lysed as described above. Biotinylated proteins were captured by incubating cleared lysate with magnetic streptavidin beads (Dynabeads MyOne Streptavidin T1, 65602, Thermo Fisher) at 4°C for 2.5 hours. Beads were washed 4 times with cold lysis buffer, and interacting proteins were stripped from beads into 1x Laemmli buffer containing 5% β-mercaptoethanol by heating at 100°C for 5 minutes.

4.6.3. Mass Spectrometry.

To define the cellular protein interactome of JUNV NP and LCMV NP, A549 or HEK 293T cells were infected with either JUNV C#1 or LCMV Armstrong 53b. Following infection, the viral NPs were immunoprecipitated (as described above) along with associated cellular proteins. After denaturation, the immune complexes were separated by SDS-PAGE on Novex 4-20% Tris-Glycine polyacrylamide gels. Gels were Coomassie

stained (0.02% Brilliant Blue R (B7920, Sigma-Aldrich) in 32% methanol, 22% acetic acid) at room temperature overnight. Gels were destained for 6-8 hours in a solution containing 30% methanol and 10% acetic acid. Each lane was cut out of the gel in 13 (JUNV NP) or 15 (LCMV NP) slices (cut maps available upon request). In-gel trypsin digestion of proteins was performed with Sequencing Grade Modified Trypsin (V5111, Promega, Madison, WI at 6 ng/μL) in 50 mM ammonium bicarbonate overnight at 37°C as previously reported (Ballif et al., 2006). Peptides were extracted from the digested gel slices with 50% acetonitrile (MeCN) and 2.5% formic acid (FA) and dried using a vacuum centrifuge. Dried peptides were resuspended in 2.5% MeCN and 2.5% FA and loaded onto a 12 cm reverse-phase Magic C18 microcapillary column (5 μm, 200 Å, Michrom Bioresources, Inc., Auburn, CA) utilizing a MicroAS autosampler (Thermo Scientific, Pittsburgh, PA). Peptides were eluted with a 5-35% MeCN (0.15% FA) gradient using a Surveyor Pump Plus HPLC (Thermo Scientific) over 40 min, after a 15min isocratic loading with 2.5% MeCN and 0.15% FA. An LTQ-XL linear ion trap mass spectrometer (Thermo Scientific) was used to acquire mass spectra of eluted peptides over the entire run using 10 MS/MS scans following each survey scan. Raw data were searched against the human IPI forward and reverse concatenated databases using SEQUEST software allowing a 2 Da mass tolerance for peptide matches. Cysteine residues were required to have a static increase in 71.0 Da for acylamide adduction. A 16.0 Da differential modification on methionine residues was permitted. Host proteins were accepted as legitimate NP protein partners if they were identified by 2 or more unique tryptic peptides in samples infected

with either JUNV or LCMV but not in the corresponding uninfected control. Alternatively, proteins were included if there was a 5-fold higher quantity of total tryptic peptides that were detected for a particular human protein from a viral infected sample compared to the sample from the corresponding uninfected control. Using these filters, the false discovery rate of peptides was less than 1%.

Bioinformatic analysis of cellular protein partners was performed with the NIH DAVID functional annotation tool (Version 6.7; https://david.ncifcrf.gov/) (Huang et al., 2009a, b).

4.6.4. SDS-PAGE and Western Blot.

Novex 4-20% Tris-Glycine polyacrylamide gels or NuPAGE™ Novex™ 4-12% Bis-Tris Midi Protein Gels (WG1402BOX, Thermo Scientific) were used to separate protein lysates by SDS-PAGE. MOPS SDS Running Buffer (NP0001, Thermo Scientific) was used with the NuPage Bis-Tris polyacrylamide gels. Protein was transferred from gels onto nitrocellulose membranes using the iBlot Gel Transfer Device and the iBlot Transfer Stack nitrocellulose membranes (IB3010-01, Thermo Scientific). Membranes were blocked with 5% milk in PBS for 1 hour at room temperature. Primary antibodies and secondary antibodies were diluted in PBS containing 5% milk, 3% FBS, and 0.05% Nonidet P-40 IGEPAL CA-630). Blots were incubated in diluted primary antibody overnight at 4°C. Primary antibodies used for Western blot were: PKR (sc-707, Santa Cruz, at 1:1000), IκBα (9242, Cell Signaling, at 1:1000), rabbit anti-actin (A2066, Sigma Aldrich, at 1:5000), mouse anti-actin (A5441, Sigma Aldrich, at 1:5000), SFPQ (NB100-

61044, Novus, at 1:2500), eIF2α (sc-11386, Santa Cruz, at 1:1000), p-eIF2α S51 (3398, Cell Signaling, at 1:1000), G3BP1 (A302-033A, Bethyl, at 1:2500), AIF (sc-9416, Santa Cruz, at 1:1000), p-PKR T446 (E120, Abcam, at 1:1000), anti-JUNV NP (NA05-AG12, BEI-Resources, at 1:200), anti-LCMV NP (2165, M. J. Buchmeier, at 1:10,000), and IAV NP (ab20343, Abcam, at 1:1,000). Unbound primary antibody was washed from blots by 3 consecutive washes in Western wash solution (PBS with 0.5% Nonidet P-40 IGEPAL CA-630). Blots were incubated with diluted secondary antibody for 2 hours at room temperature: goat anti-mouse (H+L) (71045-3, Novagen, at 1:10,000), goat anti-mouse (light chain only) (AP200P, Millipore, at 1:10,000), goat anti-rabbit (H+L) (111-035-045, Jackson, at 1:10,000), mouse anti-rabbit (light chain only) (211-032-171, at 1:10,000), or rabbit anti-goat peroxidase (401515, Calbiochem, at 1:10,000). Finally, blots were washed 3 more times with Western wash before developing with chemiluminescent substrate (either Pierce ECL Western Blotting Substrate (32109), SuperSignal West Pico (34080) or Femto (34096) Chemiluminescent Substrate, Thermo Scientific). Alternately, blots were probed with fluorescently labeled secondary antibodies: IRDye 800CW goat anti-rabbit IgG (H+L) (926-32211, LI-COR, at 1:20,000), IRDye 800CW goat anti-mouse IgG (H+L) (926- 32210, LI-COR, at 1:20,000), IRDye 680RD goat anti-mouse IgG (H+L) (926-68070, LICOR, at 1:20,000), and IRDye 680RD goat anti-rabbit IgG (H+L) (926-68071, LICOR, at 1:20,000) and visualized with an Odyssey Infrared Imaging System (LI-COR Biosciences, Lincoln, NE).

4.6.5. Plasmids and transfection.

To validate the interaction of identified cellular proteins, the arenaviral NPs were subcloned into a modified pCAGGS expression vector as previously described (Cornillez-Ty et al., 2009; Klaus et al., 2013). This vector expresses an NP fusion protein containing 3 C-terminal elements: a hemagglutinin (HA) epitope tag (YPYDVPDYA), the tobacco etch virus (TEV) protease cleavage site (ENLYFQG), and a 23 amino acid biotin acceptor peptide (BAP) (MASSLRQILDSQKMEWRSNAGGS). The BAP sequence can be biotinylated when cells are cotransfected with a plasmid that encodes the bacterial biotin ligase BirA, and the biotinylated NP can be affinity purified as described (Cornillez-Ty et al., 2009; Klaus et al., 2013). The NP sequences subcloned into the pCAGGS expression vector were (for each NP, an NCBI Gene Identifier number and a Protein Locus number are listed): LASV strain Josiah (NC_004296, NP_694869), LCMV Armstrong 53b (DQ408671, ABD73126), and JUNV strain Candid 1 (HQ126699, AEB32437). Transfection of HEK 293T cells was done using Polyethylenimine (PEI) (23966, Polysciences, Inc., Warrington, PA) (5 µg of PEI (10010049, Thermo Fisher) per 1 µg DNA).

4.6.6. Confocal Microscopy.

The localization of the viral NP and cellular proteins in JUNV- or LCMV-infected A549 cells was visualized by confocal microscopy. A549 cells were seeded onto #1.5 12 mm glass cover slips (12-545-81, Thermo Scientific). The day after seeding, cells were infected or not (mock) with JUNV at an MOI of 0.1 or LCMV at an MOI of 0.01. Cells

were fixed 48 or 72 hr after infection with 4% PFA (15714, Electron Microscopy Sciences) in 1x PBS. Cells were permeabilized in PBS with 0.1% Triton X-100 and 1% BSA and then blocked in PBS containing 3% BSA for 30 minutes at room temperature.

Cells were incubated with a primary antibody diluted in 1% BSA in 1x PBS at room temperature for 1 hour. NA05-AG12 (mouse) to detect JUNV NP was diluted at 1:100, 1.1.3 (mouse) for LCMV NP was diluted 1:500, anti-PKR antibody (rabbit monoclonal, Y117, Abcam) was diluted 1:100, and anti-G3BP1 (A302-033A, Bethyl) was diluted 1:100. Coverslips were washed 4 times in 1x PBS at room temperature. Coverslips were incubated with secondary antibody diluted in 1% BSA in 1x PBS for 30 minutes at room temperature. Secondary antibodies were Alexa Fluor 488-conjugated goat anti-mouse IgG (H+L) (A-11029, Thermo Scientific) (1:800) and Alexa Fluor 647-conjugated goat anti-rabbit IgG (H+L) (A-21245, Thermo Scientific) (1:800). Coverslips were washed 3 times in PBS, stained with 4', 6-diamidino-2-phenylindole hydrochloride 30 (DAPI) (D9542, Sigma Aldrich), and washed a final time in PBS, and mounted onto glass slides using ProLong Gold Antifade Reagent (P36934, Thermo Fisher). Confocal microscopy was performed with a Zeiss LSM 510 Laser Scanning Confocal Microscope. Images were acquired with a 63X objective lens with a numerical aperture of 1.4. Images were acquired at 1.0 Airy unit for the Alexa Fluor 647 dye. Pinhole diameter for the DAPI and Alexa Fluor 488 channels were set accordingly.

4.6.7. Puromycylation of nascent polypeptides.

To label newly-synthesized peptides in infected cells growing on glass coverslips, cells were incubated for 5 minutes at 37°C in puromycylation media: DMEM/F12, 10% FBS, 1% Pen-Strep supplemented with 91 μM puromycin (P8833, Sigma-Aldrich) and 208 μM emetine (E2375, Sigma-Aldrich) as previously described (David et al., 2012). As a negative control, some cells were pretreated with complete media containing 500 μM Sodium Arsenite (1.06277, Sigma-Aldrich) for 15 minutes at 37°C before labeling with puromycylation media. Following the labeling reaction, cells were briefly washed with cold DPBS (with calcium and magnesium) (14040133, Thermo Fisher). Cells were washed with cold permeabilization buffer (50 mM Tris HCl, 5 mM MgCl2, 25 mM KCl, 0.015% Digitonin (D141, Sigma-Aldrich)) to remove free puromycin before being fixed in 3% PFA in 1x PBS for 15 minutes at room temperature. Cells were prepared for confocal microscopy as described above. LCMV NP was labeled with the 1.1.3 antibody (at 6.8 μg/ml), and JUNV NP was labeled with the NA05 antibody (at 10 μg/ml), with both antibodies directly conjugated to Alexa Fluor 488 (Thermo Fisher).Puromycin was detected with the monoclonal antibody 12D10 directly conjugated to Alexa Fluor® 647 (at 1 ug/ml, MABE343-AF647, Sigma-Aldrich). Puromycin levels were quantitated in individual cells with a customized image analysis pipeline in CellProfiler (Broad Institute) (Kamentsky et al., 2011).

4.6.8. Poly(I:C) transfections.

For a single well in a six well plate, 0 μg, 0.5 μg, or 5 μg of poly(I:C) (P0913, Sigma Aldrich) was added to 125 μL Opti-Mem Media (31985070, Thermo Fisher) and mixed well. 3 μL of Lipofectamine 2000 (11668019, Thermo Fisher) was added to a second tube containing 125 μL Opti-Mem and mixed gently. The solution containing poly(I:C) was added to the solution containing Lipofectamine 2000, mixed gently, and incubated at room temperature for 10 minutes. Media was aspirated from the wells and replaced with 2 ml of fresh warm complete A549 media. The poly(I:C)/Lipofetamine transfection mix was added dropwise to the well. The transfected cells were incubated at 37°C for 6 hours at which time cells were lysed and analyzed by Western blot.

4.6.9. siRNA.

siRNAs were reverse transfected in A549 cells in a 12 well plate format as follows. To 100 μL of Opti-Mem, 2 μL of Lipofectamine RNAi Max (13778075, Thermo Fisher) was added and mixed gently. To another 100 μL of Opti-Mem, 12 pmoles of siRNA was added and mixed. The siRNA-containing solution was added to the lipofectamine-containing solution and allowed to incubate at room temperature for 5 minutes. 200 μL of this mixture were added to an empty well of a 12 well plate. Next, 40,000 A549 cells in 1 ml of complete A549 media were added to the Opti-MEM/siRNA-containing well and incubated at 37°C. Two days post-transfection, the media was replaced with fresh prewarmed complete A549 media. siRNA-transfected A549 cells were infected 72 hours post-siRNA transfection. Silencer Select siRNAs were used for knockdown experiments:

Silencer Select Negative Control No. 1 siRNA: “siSCR” (4390843, Thermo Fisher), “siPKR-1” (s11185, 4390824, Thermo Fisher) (Figure 4.10 and 4.11), and “siPKR-2” (s229501, 4392420, Thermo Fisher) (Figure 4.11).

4.6.10. Statistics.

Statistical analyses were performed in GraphPad software. Two-way ANOVA with post-hoc Tukey’s multiple comparisons test was used for Figure 4.8. One-way ANOVA with Dunnett’s multiple comparisons test was used for Figures 4.7, 4.9C, 4.9D, and 4.11. One-way ANOVA with Tukey’s multiple comparisons test was used for Figure 4.9E. Unpaired two-tailed Student’s T-test was used for Figure 4.10.

4.7. Funding Information

The authors gratefully acknowledge NIH grants T32 HL076122-10 (BRK), T32 AI055402 (CMZ), R21 AI088059 (JB), and P20RR021905 (Immunobiology and Infectious Disease COBRE) (JB). Additionally, the mass spectrometry analysis was supported by the Vermont Genetics Network through NIH grant 8P20GM103449 from the INBRE program and of the NIGMS (BAB and MEW). The funders had no role in study design, data collection and analysis, decision to publish, or preparation of the manuscript.

4.8. Acknowledgments

We thank the UVM Immunobiology Group for insightful discussions. We are grateful to Drs. Michael Buchmeier, J. Lindsay Whitton, Bob Tesh, and Thorsten Wolff for providing critical reagents as described in the Materials and Methods. We acknowledge the work of Jamie Kelly and Sarah Girome in help with experiments. We thank the UVM Neuroscience Imaging and Physiology Core and the UVM Microscopy Imaging Center for microscopy and imaging support. Confocal microscopy was performed on a Zeiss 510 META laser scanning confocal microscope supported by NIH Award Number 1S10RR019246 from the National Center for Research Resources.

4.9. Tables

Table 4.1. The top 25% most abundantly detected conserved protein partners of JUNV C#1 and LCMV Armstrong 53b NP.

Gene symbol, description, and IPI ID for the most abundantly detected host protein partners of the arenavirus NP are listed below. The most abundant interactors were defined as those having the highest average number of spectral counts (total peptides) from the JUNV (n=8 independent experiments) or LCMV (n=4 independent experiments) mass spectrometry.

Gene symbol	Gene Description	IPI ID	Peptide spectral counts	
			JUNV	LCMV
AIFM1	programmed cell death 8 (apoptosis-inducing factor)	IPI00000690	89	3
ASPH	aspartate beta-hydroxylase	IPI00294834	23	8
CCT6A	chaperonin containing TCP1, subunit 6A (zeta 1)	IPI00027626	43	3
CCT7	chaperonin containing TCP1, subunit 7 (eta)	IPI00018465	40	4
CKAP4	cytoskeleton-associated protein 4	IPI00141318	22	9
CKAP5	cytoskeleton associated protein 5	IPI00028275	13	12
CLTC	clathrin, heavy polypeptide (Hc)	IPI00024067	19	18
DDX3X	DEAD (Asp-Glu-Ala-Asp) box polypeptide 3, X-linked	IPI00215637	18	18
DDX5	DEAD (Asp-Glu-Ala-Asp) box polypeptide 5	IPI00017617	12	24
DHX9	DEAH-Box Helicase 9	IPI00844578	32	27
EEF1A2	eukaryotic translation elongation factor 1 alpha 2	IPI00014424	16	8
FLNA	filamin A, alpha (actin binding protein 280)	IPI00302592	16	77
FLNB	filamin B, beta (actin binding protein 278)	IPI00289334	13	21
HADHA	hydroxyacyl-Coenzyme A dehydrogenase/3-ketoacyl-Coenzyme A thiolase/enoyl-Coenzyme A hydratase (trifunctional protein), alpha subunit	IPI00031522	22	15
HIST2H2BE	histone 2, H2be	IPI00003935	8	39
HNRNPA1	heterogeneous nuclear ribonucleoprotein A1	IPI00215965	13	16
HNRNPA2B1	heterogeneous nuclear ribonucleoprotein A2/B1	IPI00396378	17	12
HNRNPA2B1	heterogeneous nuclear ribonucleoprotein A2/B1	IPI00386854	3	27
HNRNPK	heterogeneous nuclear ribonucleoprotein K	IPI00216049	24	15
HNRNPM	heterogeneous nuclear ribonucleoprotein M	IPI00171903	25	32
HNRNPU	heterogeneous nuclear ribonucleoprotein U (scaffold attachment factor A)	IPI00479217	15	12
HSPA8	heat shock 70kDa protein 8	IPI00003865	31	18
IGF2BP1	insulin-like growth factor 2 mRNA binding protein 1	IPI00008557	20	19
ILF2	interleukin enhancer binding factor 2, 45kDa	IPI00005198	12	19
IQGAP1	IQ motif containing GTPase activating protein 1	IPI00009342	14	20
KIAA1618	chromosome 17 open reading frame 27	IPI00642126	76	3
LMNA	lamin A/C	IPI00021405	31	105
MAP1B	microtubule-associated protein 1B	IPI00008868	14	10
MATR3	matrin 3	IPI00017297	12	20
MOV10	Mov10, Moloney leukemia virus 10, homolog (mouse)	IPI00444452	17	16
MYBBP1A	MYB binding protein (P160) 1a	IPI00005024	28	6
MYO1B	myosin IB	IPI00376344	10	30
MYO1C	myosin IC	IPI00010418	27	55
MYO6	myosin VI	IPI00008455	9	18
NCL	nucleolin	IPI00183526	22	17
NCL	nucleolin	IPI00444262	22	13
NPM1	anaplastic lymphoma kinase (Ki-1)	IPI00220740	14	26
PABPC1	poly(A) binding protein, cytoplasmic 1	IPI00008524	29	39
PARP1	poly (ADP-ribose) polymerase family, member 1	IPI00449049	24	30
PLEC1	plectin 1, intermediate filament binding protein 500kDa	IPI00014898	55	307
PKR	Double Stranded RNA Activated Protein Kinase (eukaryotic translation initiation factor 2-alpha kinase 2)	IPI00019463	18	7
PRKDC	protein kinase, DNA-activated, catalytic polypeptide	IPI00296337	60	46

RPL10A	ribosomal protein L10a	IPI00412579	15	12
RPL12	ribosomal protein L12	IPI00024933	15	11
RPL13P12	ribosomal Protein L13 pseudogene 12	IPI00397611	13	13
RPL23	ribosomal protein L23	IPI00010153	14	19
RPL23A	ribosomal protein L23a	IPI00021266	12	15
RPL3	ribosomal protein L3	IPI00550021	19	14
RPL4	ribosomal protein L4	IPI00003918	20	9
RPL5	ribosomal protein L5	IPI00000494	22	17
RPL6	ribosomal protein L6	IPI00329389	25	28
RPL7	ribosomal protein L7	IPI00030179	14	18
RPL7A	ribosomal protein L7a	IPI00299573	16	17
RPLP0	ribosomal protein, large, P0	IPI00008530	39	31
RPLP2	ribosomal protein, large, P2	IPI00008529	22	15
RPS18	ribosomal protein S18	IPI00013296	12	14
RPS19	ribosomal protein S19	IPI00215780	9	21
RPS3	ribosomal protein S3	IPI00011253	14	31
RPS3A	ribosomal protein S3A	IPI00419880	11	20
RPS4X	ribosomal protein S4, X-linked	IPI00217030	13	22
RRBP1	ribosome binding protein 1 homolog 180kDa (dog)	IPI00215743	40	6
SFPQ	splicing factor proline/glutamine-rich (polypyrimidine tract binding protein associated)	IPI00010740	17	16
SLC25A5	solute carrier family 25 (mitochondrial carrier; adenine nucleotide translocator), member 5	IPI00007188	27	27
TMPO	thymopoietin	IPI00030131	9	43
TMPO	thymopoietin	IPI00216230	4	34
TUBB2C	tubulin, beta 2C	IPI00007752	14	8
XRCC5	X-ray repair complementing defective repair in Chinese hamster cells 5 (double-strand-break rejoining; Ku autoantigen, 80kDa)	IPI00220834	14	13
XRCC6	X-ray repair complementing defective repair in Chinese hamster cells 6 (Ku autoantigen, 70kDa)	IPI00644712	15	18

4.10. Figures

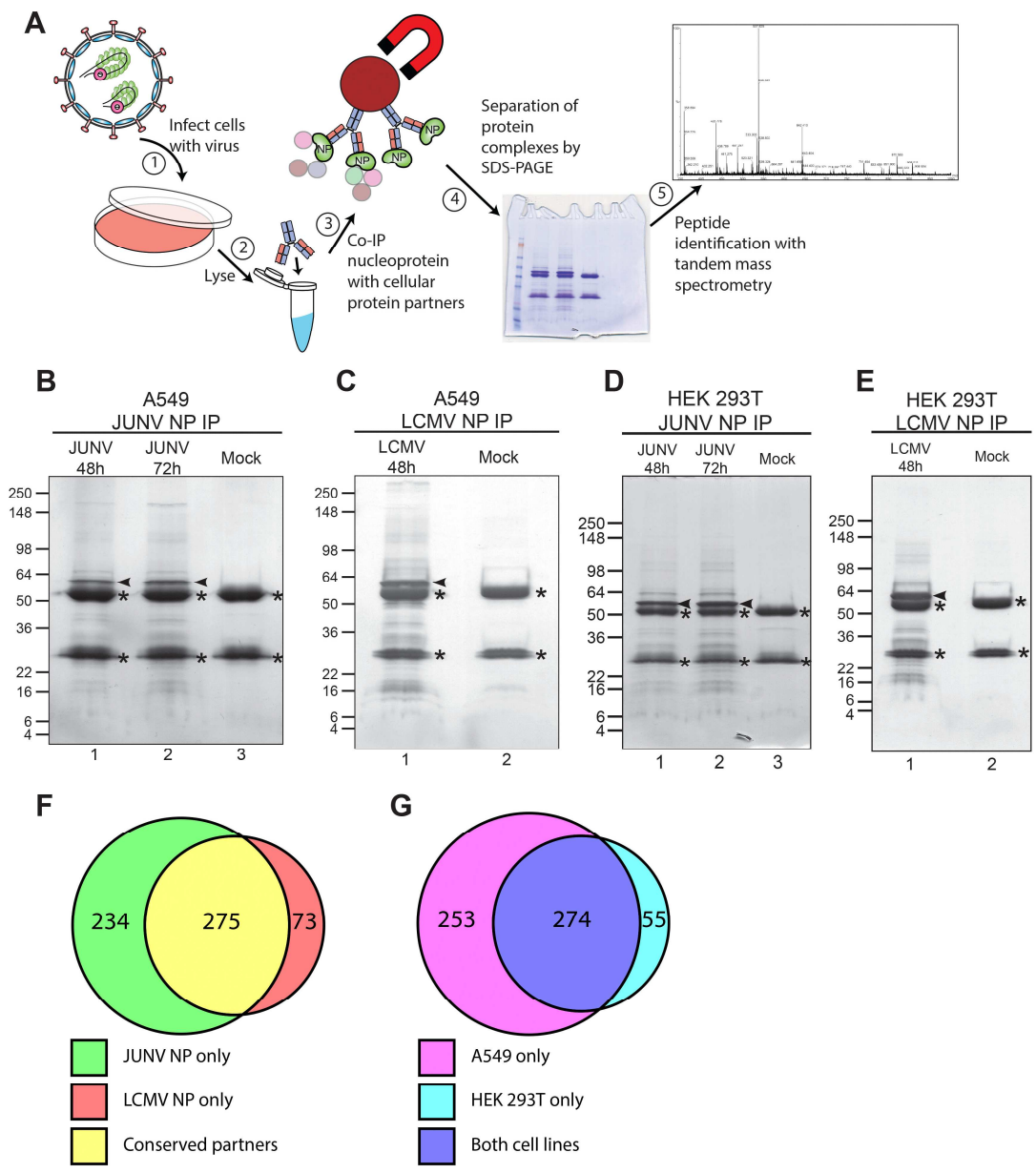

Figure 4.1. Identification of human proteins that associate with the arenavirus nucleoprotein. (A) Overview of experimental approach to identify human cellular protein partners of the arenavirus nucleoprotein in the context of infected cells. A549 or HEK 293T cells were infected with either JUNV Candid #1, LCMV Armstrong 53b, or uninfected (mock). Cells were lysed and NP was immunoprecipitated with monoclonal antibodies. The immunoprecipitated fractions were separated by SDS-PAGE and lanes were cut into multiple slices. Proteins were digested with trypsin, peptides were extracted from each slice, and proteins were identified by tandem-mass spectrometry. (B-E) Representative Coomassie-stained gels of immunoprecipitated NP from (B) JUNV- or mock-infected A549 cells (C) LCMV- or mock-infected A549

cells (D) JUNV- or mock-infected HEK 293T cells, or (E) LCMV- or mock-infected HEK 293T cells. Immunoprecipitated NP is indicated by an arrowhead in each gel. Background bands composed of IgG heavy and light chains are denoted with asterisks. (F) Venn diagram representing the number of host proteins interacting with JUNV NP, LCMV NP, or both. (G) Venn diagram representing the number of host protein partners (of either JUNV or LCMV NP) identified in A549 cells, HEK 293T cells, or both. The Coomassie gels shown in panels (B-E) are representative of 2 independent experiments.

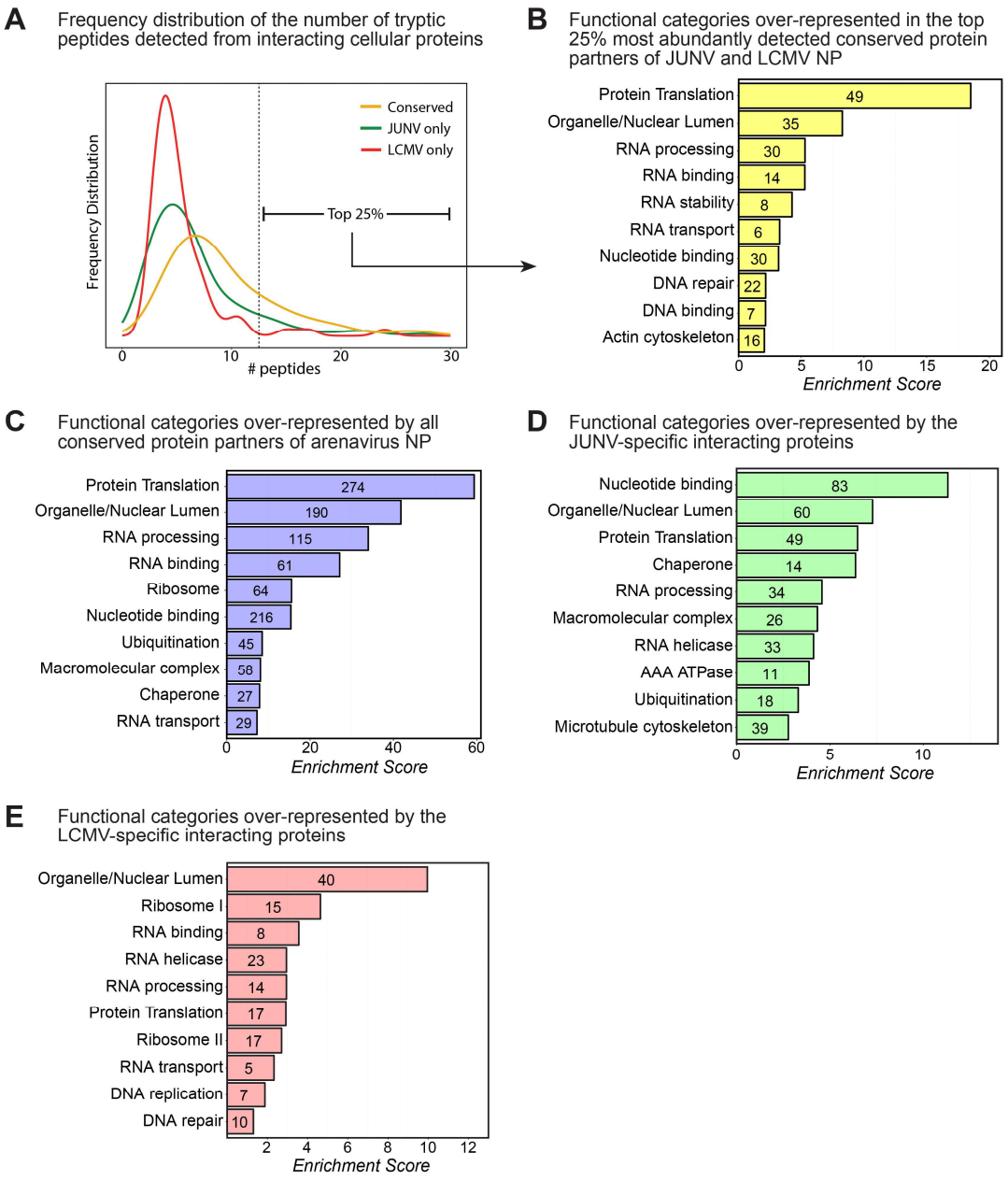

Figure 4.2. Bioinformatic analysis of host protein partners of the arenavirus NP.
(A) A frequency distribution histogram showing the number of individually identified peptides per protein for host proteins interacting with JUNV NP only, LCMV NP only, or both viral NPs (conserved). Vertical dashed line indicates the threshold above which the 25% most abundant conserved interacting proteins were detected. (B) A bioinformatics NIH DAVID functional annotation clustering analysis showing the most highly enriched biological function categories represented in the list of the 25% most abundantly detected and conserved interacting proteins (n= 69) displayed in Table 4.1. (C) A bioinformatics NIH DAVID functional annotation clustering analysis showing the most highly enriched biological function categories represented in the entire list of interacting proteins (n= 582). (D) NIH DAVID analysis on the subset of

proteins displaying specific interactions with only the JUNV NP (n=234). (E) NIH DAVID analysis on the subset of proteins displaying specific interactions with only the LCMV NP (n=73). For panels (A-E), interacting human proteins that were detected in at least 1 of the 2 independent experiments for JUNV in either A549 or HEK 293T cells and/or 1 of the 2 independent experiments for LCMV in either A549 or HEK 293T cells were used for bioinformatic analysis.

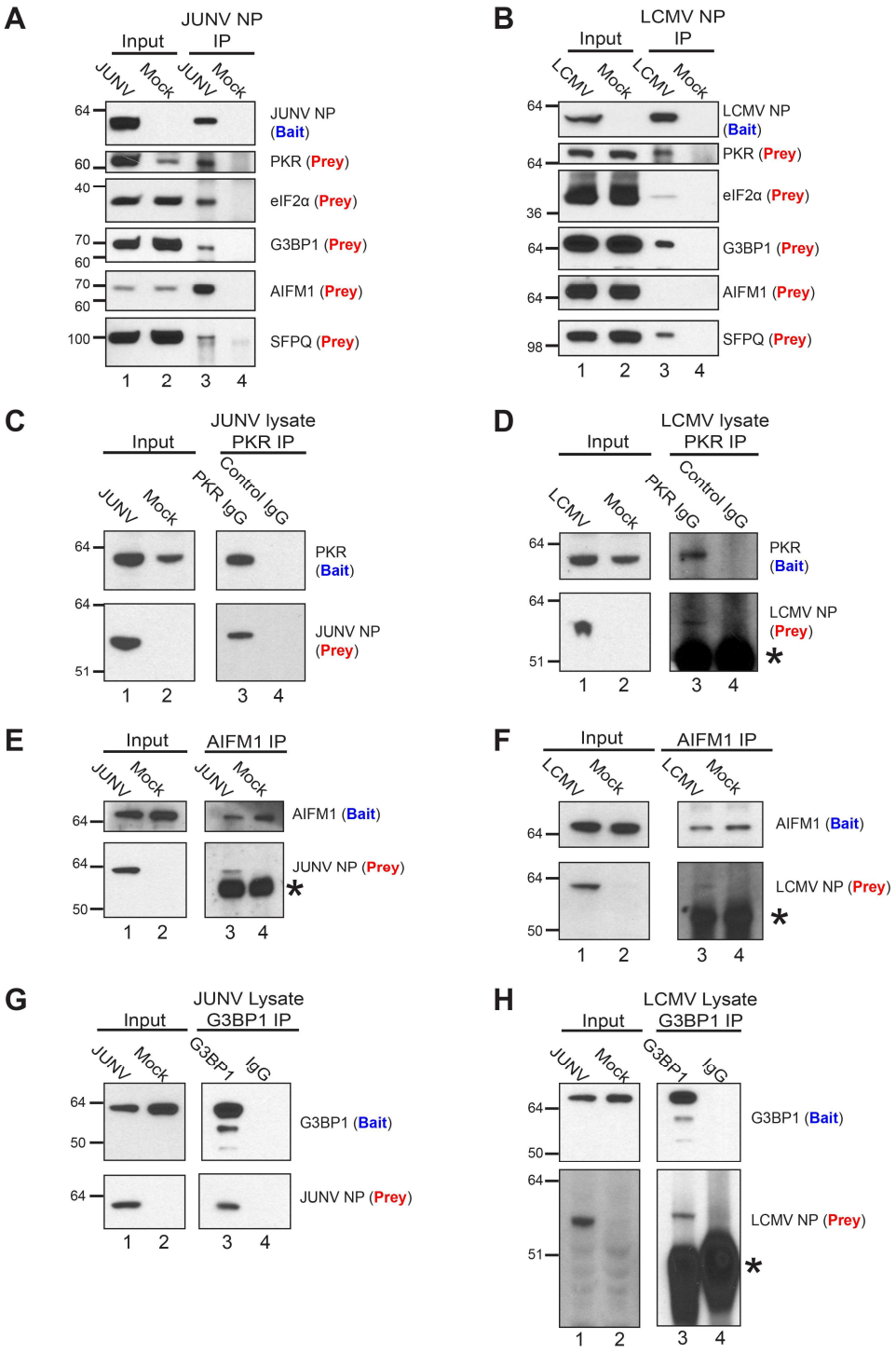
A
JUNV NP
Input
IP
JUNV
Mock
JUNV
Mock
64
JUNV NP (Bait)
60
PKR (Prey)
40
eIF2α (Prey)
70
60
G3BP1 (Prey)
70
60
AIFM1 (Prey)
100
SFPQ (Prey)
1 2 3 4
B
LCMV NP
Input
IP
LCMV
Mock
LCMV
Mock
64
LCMV NP (Bait)
64
PKR (Prey)
36
eIF2α (Prey)
64
G3BP1 (Prey)
64
AIFM1 (Prey)
98
SFPQ (Prey)
1 2 3 4
C
JUNV lysate
Input
PKR IP
JUNV
Mock
PKR IgG
Control IgG
64
PKR (Bait)
64
51
JUNV NP (Prey)
1 2 3 4
D
LCMV lysate
Input
PKR IP
LCMV
Mock
PKR IgG
Control IgG
64
PKR (Bait)
64
51
LCMV NP (Prey)
*
1 2 3 4
E
Input
AIFM1 IP
JUNV
Mock
JUNV
Mock
64
AIFM1 (Bait)
64
50
JUNV NP (Prey)
*
1 2 3 4
F
Input
AIFM1 IP
LCMV
Mock
LCMV
Mock
64
AIFM1 (Bait)
64
50
LCMV NP (Prey)
*
1 2 3 4
G
JUNV Lysate
Input
G3BP1 IP
JUNV
Mock
G3BP1
IgG
64
50
G3BP1 (Bait)
64
JUNV NP (Prey)
1 2 3 4
H
LCMV Lysate
Input
G3BP1 IP
JUNV
Mock
G3BP1
IgG
64
50
G3BP1 (Bait)
64
51
LCMV NP (Prey)
*
1 2 3 4

Figure 4.3. Biochemical validation of the interaction between cellular proteins and arenavirus NPs in infected cells.
(A) JUNV NP (bait) was immunoprecipitated from lysates of A549 cells infected (JUNV) or not (mock) with JUNV, and associated cellular proteins (prey) were detected by Western blot. (B) LCMV NP (bait) was immunoprecipitated from lysates of A549 cells infected (LCMV) or not (mock) with LCMV Armstrong 53b, and associated cellular proteins (prey) were detected by Western blot. (C and D) A549 cells were infected with JUNV (C) or LCMV (D), or uninfected (mock); at 72 hpi (JUNV) or 48 hpi (LCMV), immunoprecipitations from infected lysates were performed using either a monoclonal antibody to the C terminus of PKR (bait) or a species-matched control IgG, and associated JUNV NP (C) or LCMV NP (D) prey were detected by Western blot. (E and F) AIFM1 (bait) was immunoprecipitated from lysates of A549 cells infected or not (mock) with JUNV (E) or LCMV Armstrong 53b (F) using an AIFM1-specific polyclonal antibody and AIFM1 (bait) and associated NP (prey) were detected by Western blot. (G and H) G3BP1 (bait) was immunoprecipitated from lysates of A549 cells infected with JUNV (72 hpi) (G) or LCMV Armstrong 53b (48 hpi) (H) using either a polyclonal antibody to G3BP1 (bait) or a control rabbit IgG, and G3BP1 (bait) and associated NP (prey) were detected by Western blot. Protein bands composed of the IgG heavy chain in (D, E, F, and H) are denoted with an asterisk. Data are representative of 2 (A and B)), 4 (C), 5 (D), or 1 (E-H) independent experiments.

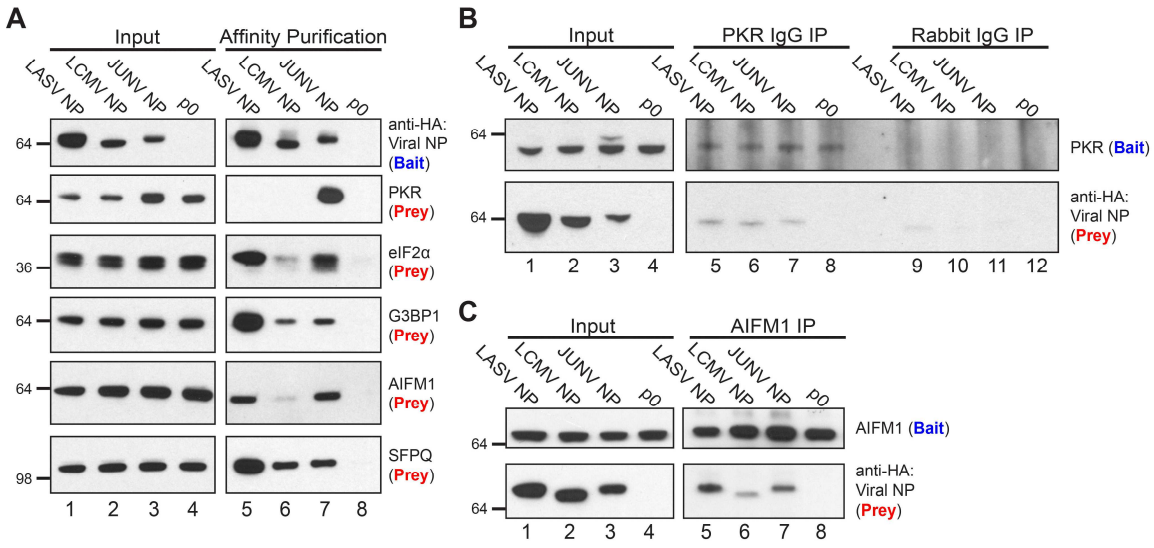

Figure 4.4. Biochemical validation of interactions between arenavirus NPs expressed from plasmid and endogenous host proteins.
(A) HEK 293T cells were co-transfected with a plasmid encoding each respective arenavirus NP with a C-terminal HA epitope tag, the TEV cleavage site, and a biotin acceptor peptide, along with a second plasmid that encodes BirA, a bacterial biotin ligase, to ensure biotinylation of the viral NPs. As a control, cells were co-transfected with the BirA plasmid and an empty vector (p0). Biotinylated NPs and associated host proteins were affinity purified from cell lysates (input) using magnetic streptavidin beads and captured proteins were detected by Western blot. (B and C) HEK 293T cells were transfected with a plasmid encoding each respective arenavirus NP with a C-terminal HA epitope tag, the TEV cleavage site, and a biotin acceptor peptide or, as a control, an empty vector (p0). (B) PKR (bait) was immunoprecipitated with a monoclonal antibody to the C terminus of PKR or with an irrelevant rabbit IgG. PKR (bait) and associated viral NP (prey) were detected by Western blot. (C) AIFM1 (bait) was immunoprecipitated with a polyclonal antibody. AIFM1 (bait) and associated viral NP (prey) were detected by Western blot. Data are representative of 2 (A), 3 (B), or 2 (C) independent experiments.

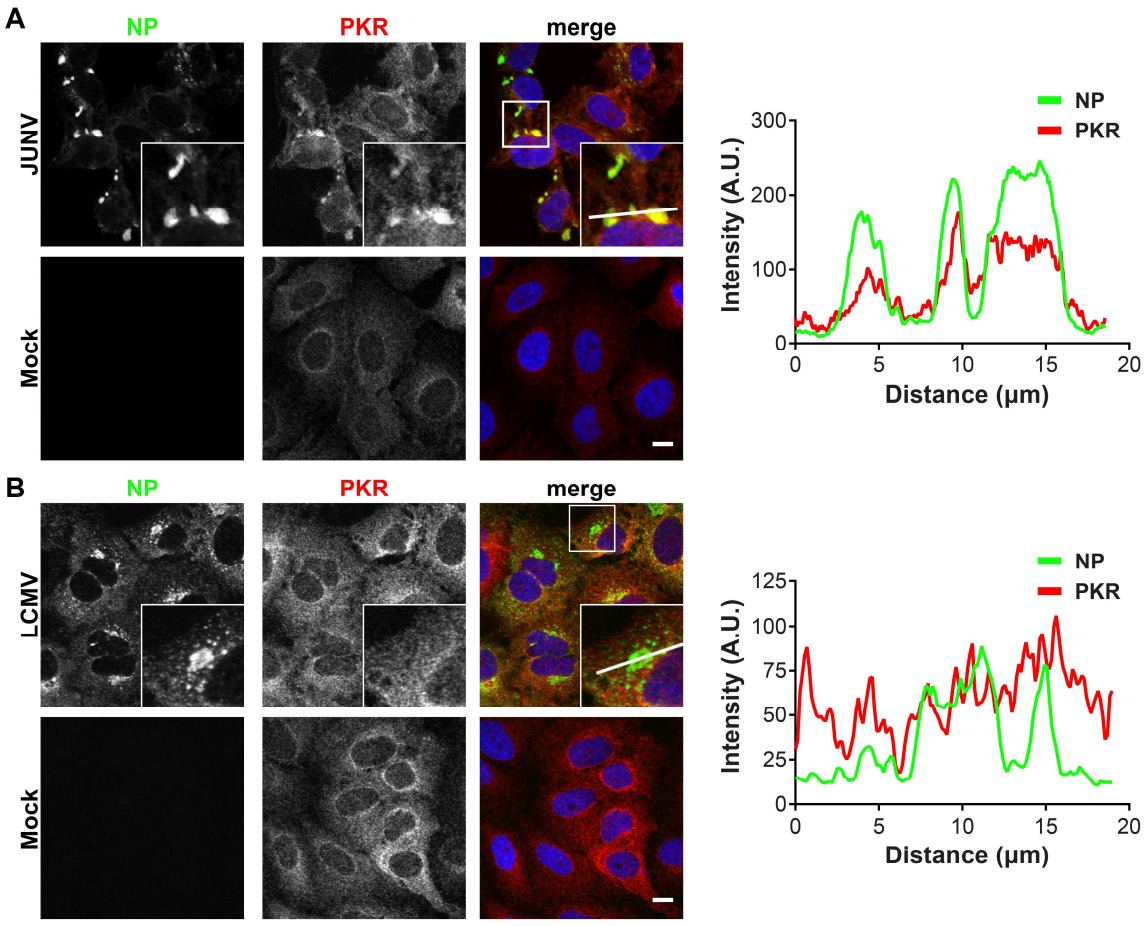

Figure 4.5. PKR colocalizes with JUNV but not LCMV NP.
A549 cells were (A) infected (JUNV) or not (mock) with JUNV and fixed at 72 hpi (n=5) or (B) infected (LCMV) or not (mock) with LCMV Arm53b and fixed at 48 hpi (n=4). Cells were stained for NP (green) and PKR (red) and visualized by confocal immunofluorescence microscopy. Inset shows higher magnification of the boxed areas. A fluorescence plot profile is included to show NP and PKR signal intensity along the white line indicated in the magnified region in the merge panel from either JUNV or LCMV infected cells. Scale bar = 10μm.

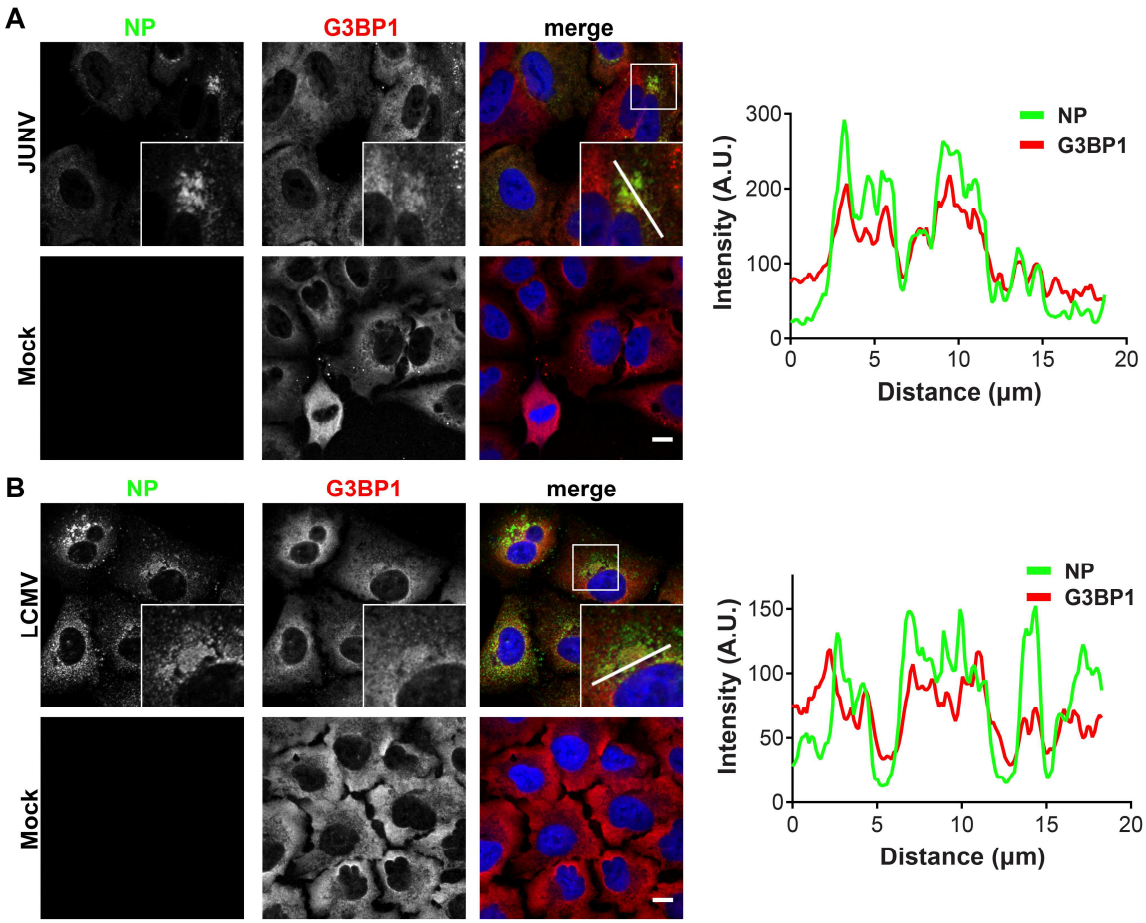

Figure 4.6. G3BP1 colocalizes with JUNV and LCMV NP.
A549 cells were (A) infected (JUNV) or not (mock) with JUNV and fixed at 72 hpi (n=1) or (B) infected (LCMV) or not (mock) with LCMV Arm53b and fixed at 48 hpi (n=1). Cells were stained for NP (green) and G3BP1 (red) and visualized by confocal immunofluorescence microscopy. Inset shows higher magnification of the boxed areas. A fluorescence plot profile is included to show NP and G3BP1 signal intensity along the white line indicated in the magnified region in the merge panel from either JUNV or LCMV infected cells. Scale bar = 10μm.

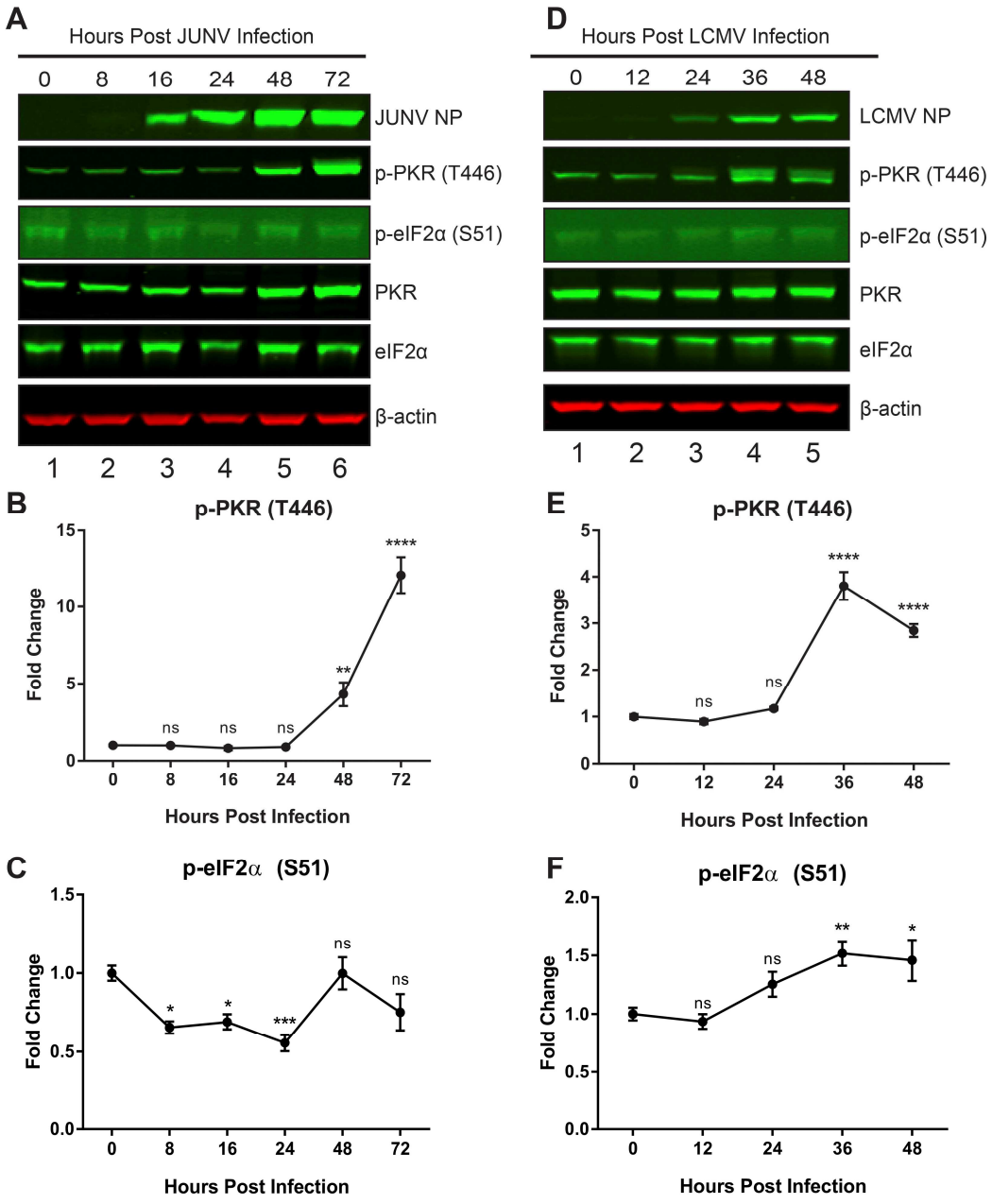

Figure 4.7. PKR is activated following JUNV infection but cannot phosphorylate eIF2α.
A549 cells were infected with JUNV (A-C) or LCMV (D-F). Infected cell lysates were collected during a time course of acute infection. Viral NPs, phosphorylated PKR (T446), total PKR, phosphorylated eIF2α (S51), total eIF2α, and β-actin were visualized by Western blot (A and D). Phosphorylated PKR (B and E) and phosphorylated eIF2α (C and F) were quantified, and compared using one-way ANOVA. Data are presented as mean fold change ± SEM from 2 independent experiments featuring 3 technical replicates per experiment. ns – not significant, P>0.05; *, P≤0.05; **, P≤0.01; ***, P≤0.001; ****, P≤0.0001

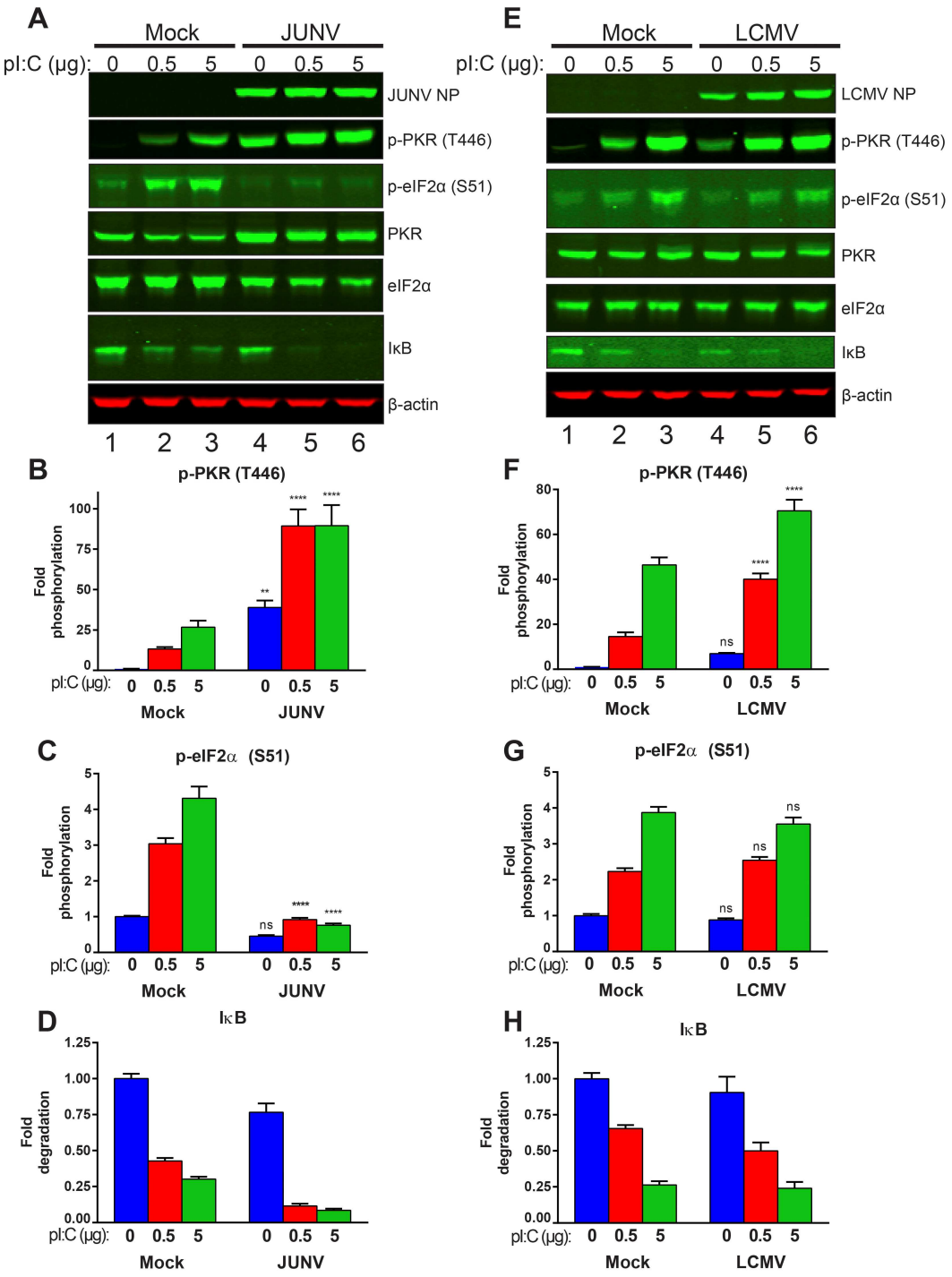

Figure 4.8. JUNV infection blocks poly(I:C)-induced phosphorylation of eIF2α.
A549 cells infected with either JUNV (A-D) or LCMV (E-H) or uninfected (mock) were transfected with the indicated quantities of poly(I:C) to induce PKR activation. Viral NPs, phosphorylated PKR (T446), total

PKR, phosphorylated eIF2α (S51), total eIF2α, IκB, and β-actin were visualized by Western blot (A and E). Phosphorylated PKR (B and F), phosphorylated eIF2α (C and G), and IκB (D and H) were quantified, and compared using two-way ANOVA. Data are presented as mean fold change ± SEM from 2 independent experiments featuring 3 technical replicates per experiment. ns – not significant, $P>0.05$; *, $P\leq0.05$; **, $P\leq0.01$; ***, $P\leq0.001$; ****, $P\leq0.0001$

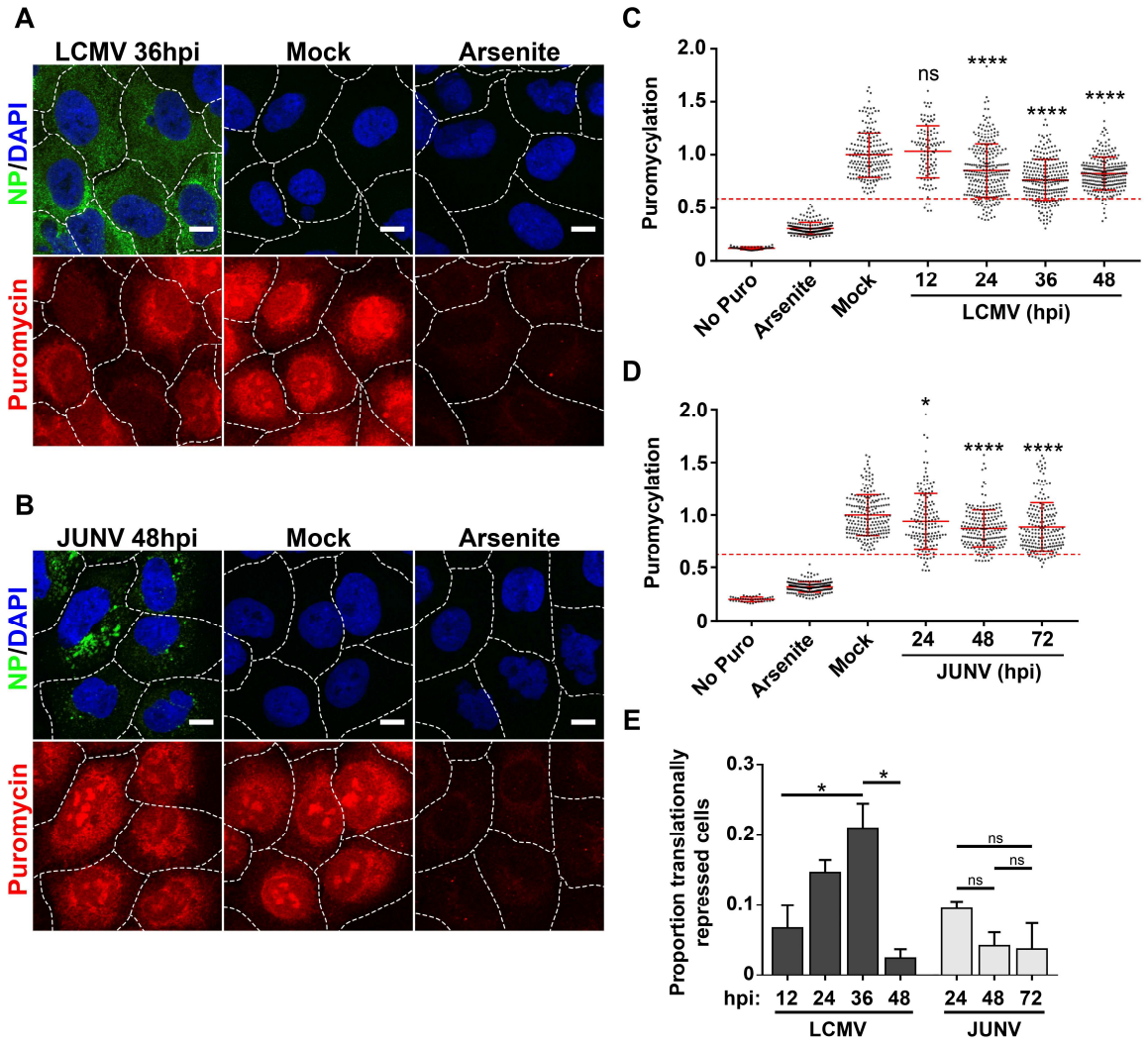

Figure 4.9. Translational profile of cells infected with JUNV or LCMV.
(A and B) Cells were either infected with LCMV (A) (n=2) or JUNV (B) (n=2), mock-infected, or treated with 500 µM Sodium Arsenite, and rates of translation were assessed by labeling newly synthesized peptides with puromycin. (C and D) Puromycin levels were quantitated in individual cells receiving no puromycin, mock-infected cells labeled with puromycin, mock-infected cells treated with Sodium Arsenite prior to puromycin labeling, or in cells infected with LCMV(C) or JUNV (D) at different time points following infection. Each individual cell was normalized to the mean level of puromycylation of mock-infected cells. The puromycin labeling of individual cells is represented by single dots, the mean puromycin labeling is represented by a solid red horizontal line in each condition, red error bars represent ± SD and were compared between mock and each time point by one-way ANOVA. A red dashed line, which represents the threshold for translational repression, was set as the mean level of puromycylation in mock-infected cells labeled with puromycin minus (1.96*SD). (C) No Puro, n=44 cells; Arsenite, n=194 cells; Mock, n=191 cells; LCMV 12h, n=113 cells; LCMV 24h, n=276 cells; LCMV 36h, n=260 cells; LCMV 48h, n=269 cells. (D) No Puro, n=40 cells; Arsenite, n=205 cells; Mock, n=215 cells; JUNV 24h, n=161 cells; JUNV 48h, n=198 cells; JUNV 72h, n=205 cells. (E) The proportion of individual cells that fall below the translational repression

threshold in each condition were compared with one-way ANOVA. Though all possible comparisons between LCMV-infected cultures at different times post-infection in panel (E) were made, for clarity, only significant differences are shown. In panels (A) and (B), the borders between adjacent cells are represented by dashed white lines. Scale bar = 10μm. ns – not significant, $P>0.05$; *, $P\leq0.05$; ****, $P\leq0.0001$.

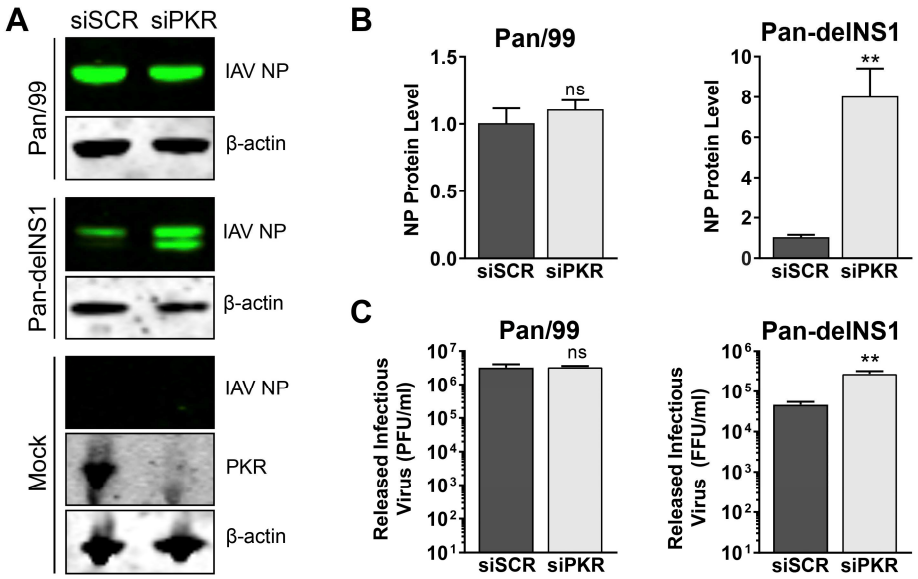

Figure 4.10. Loss of functional PKR enhances growth of mutant delNS1 but not WT influenza A virus. A549 cells were transfected with a non-targeting scrambled siRNA (siSCR) or with a PKR-specific siRNA. Three days following siRNA transfection, cells were infected with either WT influenza A virus (IAV) Pan/99, a mutant IAV that does not express NS1 (Pan-delNS1), or mock-infected, and supernatants and cellular protein lysates were collected at 16 hpi. Protein levels of IAV nucleoprotein (NP) were detected by Western blot (A) and quantified, normalized to β-actin levels, and normalized to the mean of levels of NP in siSCR transfected cells (B). PKR expression in mock-infected cells was visualized by Western blot to confirm knockdown (A). The quantities of infectious virus in the supernatants was determined by plaque assay (for IAV Pan/99) or by focus assay (for IAV Pan-delNS1) (C). The effect of PKR knockdown on viral NP levels as well as released infectious virus was determined using a two-tailed, unpaired T-test (B and C). Data are presented as mean plaque forming units (PFU)/ml ± SEM or mean focus forming units (FFU)/ml ± SEM from 2 independent experiments featuring 2 technical replicates per experiment. ns – not significant, $P>0.05$; **, $P\leq0.01$

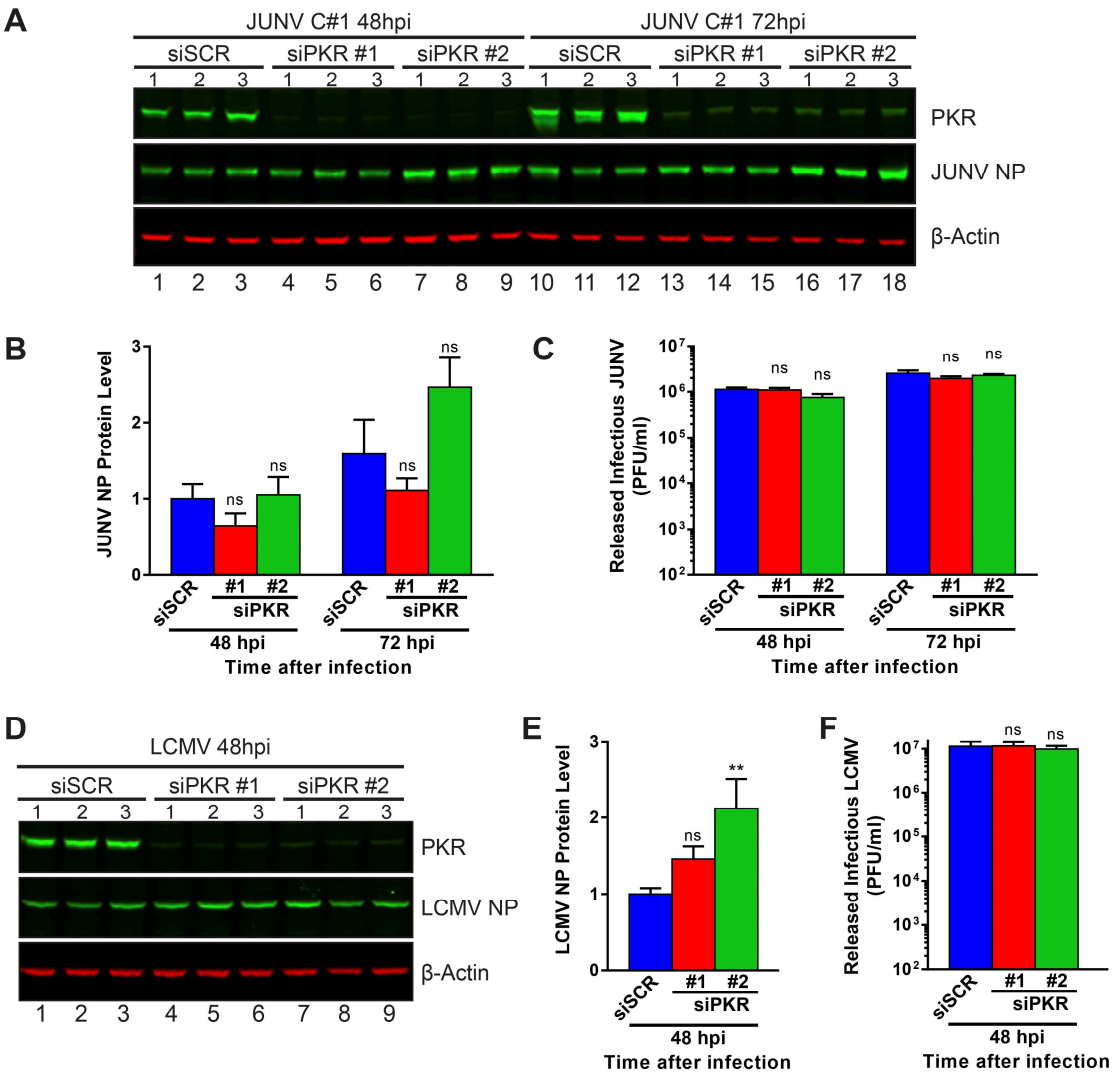

Figure 4.11. Loss of functional PKR does not impact arenavirus propagation.
A549 cells were transfected with a non-targeting scrambled siRNA (siSCR) or with one of two PKR-specific siRNAs (siPKR #1, siPKR #2). Three days after siRNA transfection, cells were infected with JUNV (A-C) or LCMV (D-F), and supernatants and cellular protein lysates were collected at 48 (JUNV and LCMV) and 72 hpi (JUNV only). Protein levels of PKR and viral NP were visualized by Western blot (A and D). NP protein levels were quantified, normalized to β-actin levels, and normalized to the mean of levels of NP in siSCR transfected cells at 48hpi and were compared by one-way ANOVA (B and E). The quantities of infectious virus in the supernatants were determined by plaque assay and were compared by one-way ANOVA (C and F). Data are presented as mean ± SEM from 2 independent experiments featuring 3 technical replicates per experiment. Data are presented as mean PFU/ml ± SEM from 2 independent experiments featuring 3 technical replicates per experiment in panels A to C (JUNV) or 3 independent experiments featuring 3 technical replicates per experiment in panels D to F (LCMV). ns – not significant, $P>0.05$; **, $P\leq0.01$

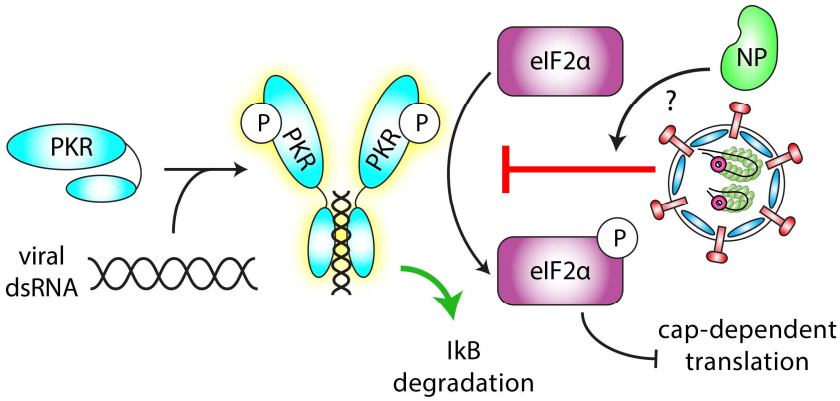

Figure 4.12. JUNV infection blocks PKR's antiviral activity.
Inactive PKR exists in an unphosphorylated, monomeric form. Upon binding a dsRNA ligand with its N-terminal dsRNA binding domains, PKR dimerizes and undergoes an autophosphorylation event (at T446 and T451). This activated form of PKR phosphorylates eIF2α at serine 51, which leads to a global cap-dependent translation shutdown. The results of this study show that PKR is able to become phosphorylated in cells infected with JUNV but is deficient in its ability to phosphorylate its target eIF2α. We hypothesize that the viral NP may be responsible for blocking this step as it was shown to interact with both PKR and eIF2α. Other functions of active PKR such as the activation of NF-κB (as assayed by IκB degradation) remain intact.

4.11. References

Anderson, P., and Kedersha, N. (2008). Stress granules: the Tao of RNA triage. Trends Biochem Sci *33*, 141-150.

Arnaud, N., Dabo, S., Maillard, P., Budkowska, A., Kalliampakou, K.I., Mavromara, P., Garcin, D., Hugon, J., Gatignol, A., Akazawa, D., Wakita, T., and Meurs, E.F. (2010). Hepatitis C virus controls interferon production through PKR activation. PloS one *5*, e10575.

Baird, N.L., York, J., and Nunberg, J.H. (2012). Arenavirus infection induces discrete cytosolic structures for RNA replication. Journal of virology *86*, 11301-11310.

Ballif, B.A., Cao, Z., Schwartz, D., Carraway, K.L., 3rd, and Gygi, S.P. (2006). Identification of 14-3-3epsilon substrates from embryonic murine brain. J Proteome Res *5*, 2372-2379.

Battegay, M., Cooper, S., Althage, A., Banziger, J., Hengartner, H., and Zinkernagel, R.M. (1991). Quantification of lymphocytic choriomeningitis virus with an immunological focus assay in 24- or 96-well plates. J Virol Methods *33*, 191-198.

Bergmann, M., Garcia-Sastre, A., Carnero, E., Pehamberger, H., Wolff, K., Palese, P., and Muster, T. (2000). Influenza virus NS1 protein counteracts PKR-mediated inhibition of replication. Journal of virology *74*, 6203-6206.

Botten, J., King, B., Klaus, J., and Ziegler, C. (2013). Pathogenic Old World Arenaviruses. In Viral Hemorrhagic Fevers, S.K. Singh, and D. Ruzek, eds. (Boca Raton, Florida: CRC Press), pp. 233-259.

Buchan, J.R., and Parker, R. (2009). Eukaryotic stress granules: the ins and outs of translation. Molecular cell *36*, 932-941.

Buchmeier, M.J., Bowen, M.D., and Peters, C.J. (2001). *Arenaviridae*: The viruses and their replication. In Fields Virology, H.P.M. Knipe D. M., Griffin D. E., Lamb R. A., Martin M. A., Roizman B., Straus S. E., ed. (Philadelphia, PA: Lippincott Williams & Wilkins), pp. 1635-1668.

Buchmeier, M.J., de la Torre, J.C., and Peters, C.J. (2007). Arenaviridae: The Viruses and Their Replication. In Fields Virology, D.M. Knipe, P.M. Howley, D.E. Griffin, R.A. Lamb, M.A. Martin, B. Roizman, and S.E. Straus, eds. (Philadelphia: Wolters Kluwer Heath/Lippincott Williams & Wilkins), pp. 1791-1827.

Buchmeier, M.J., Lewicki, H.A., Tomori, O., and Oldstone, M.B. (1981). Monoclonal antibodies to lymphocytic choriomeningitis and pichinde viruses: generation, characterization, and cross-reactivity with other arenaviruses. Virology *113*, 73-85.

Chang, H.W., Watson, J.C., and Jacobs, B.L. (1992). The E3L gene of vaccinia virus encodes an inhibitor of the interferon-induced, double-stranded RNA-dependent protein kinase. Proceedings of the National Academy of Sciences of the United States of America *89*, 4825-4829.

Cornillez-Ty, C.T., Liao, L., Yates, J.R., 3rd, Kuhn, P., and Buchmeier, M.J. (2009). Severe acute respiratory syndrome coronavirus nonstructural protein 2 interacts with a host protein complex involved in mitochondrial biogenesis and intracellular signaling. Journal of virology *83*, 10314-10318.

David, A., Dolan, B.P., Hickman, H.D., Knowlton, J.J., Clavarino, G., Pierre, P., Bennink, J.R., and Yewdell, J.W. (2012). Nuclear translation visualized by ribosome-bound nascent chain puromycylation. The Journal of cell biology *197*, 45-57.

Donnelly, N., Gorman, A.M., Gupta, S., and Samali, A. (2013). The eIF2alpha kinases: their structures and functions. Cell Mol Life Sci *70*, 3493-3511.

Enria, D.A., Briggiler, A.M., and Sanchez, Z. (2008). Treatment of Argentine hemorrhagic fever. Antiviral Res *78*, 132-139.

Fischer, S.A., Graham, M.B., Kuehnert, M.J., Kotton, C.N., Srinivasan, A., Marty, F.M., Comer, J.A., Guarner, J., Paddock, C.D., DeMeo, D.L., Shieh, W.J., Erickson, B.R., Bandy, U., DeMaria, A., Jr., Davis, J.P., Delmonico, F.L., Pavlin, B., Likos, A., Vincent, M.J., Sealy, T.K., Goldsmith, C.S., Jernigan, D.B., Rollin, P.E., Packard, M.M., Patel, M., Rowland, C., Helfand, R.F., Nichol, S.T., Fishman, J.A., Ksiazek, T., Zaki, S.R., and Team, L.i.T.R.I. (2006). Transmission of lymphocytic choriomeningitis virus by organ transplantation. N Engl J Med *354*, 2235-2249.

Garaigorta, U., and Chisari, F.V. (2009). Hepatitis C virus blocks interferon effector function by inducing protein kinase R phosphorylation. Cell host & microbe *6*, 513-522.

Garcia, M.A., Meurs, E.F., and Esteban, M. (2007). The dsRNA protein kinase PKR: virus and cell control. Biochimie *89*, 799-811.

Goni, S.E., Iserte, J.A., Ambrosio, A.M., Romanowski, V., Ghiringhelli, P.D., and Lozano, M.E. (2006). Genomic features of attenuated Junin virus vaccine strain candidate. Virus genes *32*, 37-41.

Groskreutz, D.J., Babor, E.C., Monick, M.M., Varga, S.M., and Hunninghake, G.W. (2010). Respiratory Syncytial Virus Limits alpha Subunit of Eukaryotic Translation

Initiation Factor 2 (eIF alpha) Phosphorylation to Maintain Translation and Viral Replication. Journal of Biological Chemistry *285*, 24023-24031.

Harding, H.P., Zhang, Y., Bertolotti, A., Zeng, H., and Ron, D. (2000). Perk is essential for translational regulation and cell survival during the unfolded protein response. Molecular cell *5*, 897-904.

Harding, H.P., Zhang, Y., and Ron, D. (1999). Protein translation and folding are coupled by an endoplasmic-reticulum-resident kinase. Nature *397*, 271-274.

Hastie, K.M., Kimberlin, C.R., Zandonatti, M.A., MacRae, I.J., and Saphire, E.O. (2011a). Structure of the Lassa virus nucleoprotein reveals a dsRNA-specific 3' to 5' exonuclease activity essential for immune suppression. Proceedings of the National Academy of Sciences of the United States of America *108*, 2396-2401.

Hatada, E., Saito, S., and Fukuda, R. (1999). Mutant influenza viruses with a defective NS1 protein cannot block the activation of PKR in infected cells. Journal of virology *73*, 2425-2433.

Huang, D.W., Sherman, B.T., and Lempicki, R.A. (2009a). Bioinformatics enrichment tools: paths toward the comprehensive functional analysis of large gene lists. Nucleic Acids Res *37*, 1-13.

Huang, D.W., Sherman, B.T., and Lempicki, R.A. (2009b). Systematic and integrative analysis of large gene lists using DAVID bioinformatics resources. Nat Protoc *4*, 44-57.

Kamentsky, L., Jones, T.R., Fraser, A., Bray, M.A., Logan, D.J., Madden, K.L., Ljosa, V., Rueden, C., Eliceiri, K.W., and Carpenter, A.E. (2011). Improved structure, function and compatibility for CellProfiler: modular high-throughput image analysis software. Bioinformatics *27*, 1179-1180.

Kawai, T., and Akira, S. (2008). Toll-like receptor and RIG-I-like receptor signaling. Ann N Y Acad Sci *1143*, 1-20.

Klaus, J.P., Eisenhauer, P., Russo, J., Mason, A.B., Do, D., King, B., Taatjes, D., Cornillez-Ty, C., Boyson, J.E., Thali, M., Zheng, C., Liao, L., Yates, J.R., 3rd, Zhang, B., Ballif, B.A., and Botten, J.W. (2013). The intracellular cargo receptor ERGIC-53 is required for the production of infectious arenavirus, coronavirus, and filovirus particles. Cell host & microbe *14*, 522-534.

Labudova, M., Tomaskova, J., Skultety, L., Pastorek, J., and Pastorekova, S. (2009). The nucleoprotein of lymphocytic choriomeningitis virus facilitates spread of persistent infection through stabilization of the keratin network. Journal of virology *83*, 7842-7849.

Langland, J.O., and Jacobs, B.L. (2002). The role of the PKR-inhibitory genes, E3L and K3L, in determining vaccinia virus host range. Virology *299*, 133-141.

Li, S., Min, J.Y., Krug, R.M., and Sen, G.C. (2006). Binding of the influenza A virus NS1 protein to PKR mediates the inhibition of its activation by either PACT or double-stranded RNA. Virology *349*, 13-21.

Lindquist, M.E., Mainou, B.A., Dermody, T.S., and Crowe, J.E., Jr. (2011). Activation of protein kinase R is required for induction of stress granules by respiratory syncytial virus but dispensable for viral replication. Virology *413*, 103-110.

Linero, F., Welnowska, E., Carrasco, L., and Scolaro, L. (2013). Participation of eIF4F complex in Junin virus infection: blockage of eIF4E does not impair virus replication. Cellular microbiology *15*, 1766-1782.

Linero, F.N., Thomas, M.G., Boccaccio, G.L., and Scolaro, L.A. (2011). Junin virus infection impairs stress-granule formation in Vero cells treated with arsenite via inhibition of eIF2alpha phosphorylation. The Journal of general virology *92*, 2889-2899.

Lu, Y., Wambach, M., Katze, M.G., and Krug, R.M. (1995). Binding of the influenza virus NS1 protein to double-stranded RNA inhibits the activation of the protein kinase that phosphorylates the elF-2 translation initiation factor. Virology *214*, 222-228.

Maeto, C.A., Knott, M.E., Linero, F.N., Ellenberg, P.C., Scolaro, L.A., and Castilla, V. (2011). Differential effect of acute and persistent Junin virus infections on the nucleo-cytoplasmic trafficking and expression of heterogeneous nuclear ribonucleoproteins type A and B. The Journal of general virology *92*, 2181-2190.

Matrosovich, M., Matrosovich, T., Garten, W., and Klenk, H.D. (2006). New low-viscosity overlay medium for viral plaque assays. Virol J *3*, 63.

Matthaei, M., Budt, M., and Wolff, T. (2013). Highly pathogenic H5N1 influenza A virus strains provoke heterogeneous IFN-alpha/beta responses that distinctively affect viral propagation in human cells. PloS one *8*, e56659.

McCormick, J.B., King, I.J., Webb, P.A., Scribner, C.L., Craven, R.B., Johnson, K.M., Elliott, L.H., and Belmont-Williams, R. (1986). Lassa fever. Effective therapy with ribavirin. N Engl J Med *314*, 20-26.

McEwen, E., Kedersha, N., Song, B., Scheuner, D., Gilks, N., Han, A., Chen, J.J., Anderson, P., and Kaufman, R.J. (2005). Heme-regulated inhibitor kinase-mediated phosphorylation of eukaryotic translation initiation factor 2 inhibits translation, induces stress granule formation, and mediates survival upon arsenite exposure. The Journal of biological chemistry *280*, 16925-16933.

Panda, D., Das, A., Dinh, P.X., Subramaniam, S., Nayak, D., Barrows, N.J., Pearson, J.L., Thompson, J., Kelly, D.L., Ladunga, I., and Pattnaik, A.K. (2011). RNAi screening reveals requirement for host cell secretory pathway in infection by diverse families of negative-strand RNA viruses. Proceedings of the National Academy of Sciences of the United States of America *108*, 19036-19041.

Patel, C.V., Handy, I., Goldsmith, T., and Patel, R.C. (2000). PACT, a stress-modulated cellular activator of interferon-induced double-stranded RNA-activated protein kinase, PKR. The Journal of biological chemistry *275*, 37993-37998.

Pythoud, C., Rodrigo, W.W., Pasqual, G., Rothenberger, S., Martinez-Sobrido, L., de la Torre, J.C., and Kunz, S. (2012). Arenavirus nucleoprotein targets interferon regulatory factor-activating kinase IKKepsilon. Journal of virology *86*, 7728-7738.

Pythoud, C., Rothenberger, S., Martinez-Sobrido, L., de la Torre, J.C., and Kunz, S. (2015). Lymphocytic Choriomeningitis Virus Differentially Affects the Virus-Induced Type I Interferon Response and Mitochondrial Apoptosis Mediated by RIG-I/MAVS. Journal of virology *89*, 6240-6250.

Qi, X., Lan, S., Wang, W., Schelde, L.M., Dong, H., Wallat, G.D., Ly, H., Liang, Y., and Dong, C. (2010). Cap binding and immune evasion revealed by Lassa nucleoprotein structure. Nature *468*, 779-783.

Reineke, L.C., and Lloyd, R.E. (2013). Diversion of stress granules and P-bodies during viral infection. Virology *436*, 255-267.

Rodrigo, W.W., Ortiz-Riano, E., Pythoud, C., Kunz, S., de la Torre, J.C., and Martinez-Sobrido, L. (2012). Arenavirus nucleoproteins prevent activation of nuclear factor kappa B. Journal of virology *86*, 8185-8197.

Schmidt, E.K., Clavarino, G., Ceppi, M., and Pierre, P. (2009). SUnSET, a nonradioactive method to monitor protein synthesis. Nature methods *6*, 275-277.

Shtanko, O., Watanabe, S., Jasenosky, L.D., Watanabe, T., and Kawaoka, Y. (2011). ALIX/AIP1 is required for NP incorporation into Mopeia virus Z-induced virus-like particles. Journal of virology *85*, 3631-3641.

Thomas, M.G., Loschi, M., Desbats, M.A., and Boccaccio, G.L. (2011). RNA granules: the good, the bad and the ugly. Cellular signalling *23*, 324-334.

Toth, A.M., Devaux, P., Cattaneo, R., and Samuel, C.E. (2009). Protein Kinase PKR Mediates the Apoptosis Induction and Growth Restriction Phenotypes of C Protein-Deficient Measles Virus. Journal of virology *83*, 961-968.

Tourriere, H., Chebli, K., Zekri, L., Courselaud, B., Blanchard, J.M., Bertrand, E., and Tazi, J. (2003). The RasGAP-associated endoribonuclease G3BP assembles stress granules. The Journal of cell biology *160*, 823-831.

Zamanian-Daryoush, M., Mogensen, T.H., DiDonato, J.A., and Williams, B.R. (2000). NF-kappaB activation by double-stranded-RNA-activated protein kinase (PKR) is mediated through NF-kappaB-inducing kinase and IkappaB kinase. Molecular and cellular biology *20*, 1278-1290.

Zhang, F., Romano, P.R., Nagamura-Inoue, T., Tian, B., Devert, T.E., Mathews, M.B., Ozato, K., and Hinnebusch, A.G. (2001). Binding of double-stranded RNA to protein kinase PKR is required for dimerization and promotes critical autophosphorylation events in the activation loop. Journal of Biological Chemistry *276*, 24946-24958.

4.12. Supplemental Tables

Table S4.1. Complete list of cellular proteins that were detected as interacting with the JUNV or LCMV NP.
The average number of spectral counts (total peptides) detected by mass spectrometry from host proteins that associated with the JUNV NP in A549 cells (n=4) or HEK 293T cells (n=4); or with the LCMV NP in A549 cells (n=2) or HEK 293T cells (n=2).

Gene symbol	Gene Description	IPI id	Peptide Spectral Count			
			JUNV		LCMV	
			A549	HEK 293T	A549	HEK 293T
ABCF1	ATP-binding cassette, sub-family F (GCN20), member 1	IPI00013495	5.3	0.0	0.0	4.0
ABCF2	ATP-binding cassette, sub-family F (GCN20), member 2	IPI00005045	3.0	1.0	0.0	3.5
ACAD11	acyl-Coenzyme A dehydrogenase family, member 11	IPI00420065	0.0	1.8	0.0	0.0
ACIN1	apoptotic chromatin condensation inducer 1	IPI00007334	0.0	0.5	0.0	0.0
ACTA2	actin, alpha 2, smooth muscle, aorta	IPI00008603	0.0	3.5	0.0	0.0
ACTB	actin, beta	IPI00021439	20.0	0.0	0.0	0.0
ACTBL2	similar to RIKEN cDNA 4732495G21 gene	IPI00003269	3.8	1.0	0.0	0.0
ADAR	adenosine deaminase, RNA-specific	IPI00025057	6.3	2.8	4.0	0.0
AGRN	agrin	IPI00374563	4.0	0.0	0.0	0.0
AHNAK	AHNAK nucleoprotein (desmoyokin)	IPI00021812	1.8	0.0	13.0	0.0
AIFM1	programmed cell death 8 (apoptosis-inducing factor)	IPI00000690	75.8	101.5	0.0	1.5
AIMP1	small inducible cytokine subfamily E, member 1 (endothelial monocyte-activating)	IPI00006252	0.0	2.5	0.0	1.5
AIMP2	JTV1 gene	IPI00011916	0.0	0.0	3.0	0.0
AK2	adenylate kinase 2	IPI00172460	0.0	1.5	0.0	0.0
AKR1B10	aldo-keto reductase family 1, member B10 (aldose reductase)	IPI00105407	2.0	0.0	0.0	0.0
AKR1C2	aldo-keto reductase family 1, member C2 (dihydrodiol dehydrogenase 2; bile acid binding protein; 3-alpha hydroxysteroid dehydrogenase, type III)	IPI00005668	2.5	0.0	5.0	0.0
ANXA1	annexin A1	IPI00218918	11.5	0.0	0.0	0.0
ANXA2	annexin A2	IPI00418169	9.3	0.0	0.0	0.0
ANXA2P2	Putative annexin A2-like protein	IPI00334627	20.5	0.0	0.0	0.0
AP1B1	adaptor-related protein complex 1, beta 1 subunit	IPI00328257	5.8	0.0	1.5	1.5
AP2A1	adaptor-related protein complex 2, alpha 1 subunit	IPI00256684	5.5	0.0	1.5	0.0
AP2A2	adaptor-related protein complex 2, alpha 2 subunit	IPI00016621	3.8	0.0	3.5	0.0
AP2B1	adaptor related protein complex 2, beta 1 subunit	IPI00784156	4.3	0.0	0.0	0.0
ASPH	aspartate beta-hydroxylase	IPI00294834	11.3	0.0	7.5	0.0
ATAD3A	ATPase family, AAA domain containing 3A	IPI00295992	0.0	2.3	1.5	2.0

ATAD3B	ATPase family, AAA domain containing 3B	IPI00045921	1.3	2.0	0.0	4.0
ATAD3B	ATPase family, AAA domain containing 3B	IPI00178879	0.0	1.3	0.0	0.0
ATP1A1	ATPase, Na+/K+ transporting, alpha 1 polypeptide	IPI00006482	0.0	0.5	0.0	0.0
ATP2A2	ATPase, Ca++ transporting, cardiac muscle, slow twitch 2	IPI00177817	5.0	0.0	0.0	0.0
ATP5A1	ATP synthase, H+ transporting, mitochondrial F1 complex, alpha subunit 1, cardiac muscle	IPI00440493	1.8	0.0	0.0	0.0
ATP5C1	ATP synthase, H+ transporting, mitochondrial F1 complex, gamma polypeptide 1	IPI00395769	5.5	0.0	3.5	0.0
ATP5J2	ATP synthase, H+ transporting, mitochondrial F0 complex, subunit F2	IPI00219291	2.3	0.0	0.0	0.0
ATP5L	ATP synthase, H+ transporting, mitochondrial F0 complex, subunit G	IPI00027448	2.8	0.0	0.0	0.0
ATXN2L	ataxin 2-like	IPI00456359	1.3	0.8	3.5	2.0
BANF1	barrier to autointegration factor 1	IPI00026087	2.0	0.0	0.0	1.5
BAT2	HLA-B associated transcript 2	IPI00010700	0.0	6.0	0.0	0.0
BAT2D1	BAT2 domain containing 1	IPI00083708	1.0	3.8	2.0	0.0
BRI3BP	BRI3 binding protein	IPI00103599	2.0	0.0	0.0	0.0
BUB3	BUB3 budding uninhibited by benzimidazoles 3 homolog (yeast)	IPI00013468	3.8	0.0	2.5	0.0
BXDC2	brix domain containing 2	IPI00181728	2.8	0.0	0.0	0.0
C14orf156	chromosome 14 open reading frame 156	IPI00009922	0.0	0.0	1.5	0.0
C14orf166	chromosome 14 open reading frame 166	IPI00006980	0.8	0.0	10.5	5.0
C16orf80	gene trap locus 3 (mouse)	IPI00001655	0.0	0.0	2.5	0.0
C19orf66	hypothetical protein FLJ11286	IPI00167592	1.8	0.0	0.0	0.0
C1orf57	chromosome 1 open reading frame 57	IPI00031570	0.0	3.8	0.0	0.0
C1QBP	complement component 1, q subcomponent binding protein	IPI00014230	1.5	2.8	5.0	0.0
C22orf28	hypothetical protein HSPC117	IPI00550689	2.8	0.0	2.0	0.0
CAD	carbamoyl-phosphate synthetase 2, aspartate transcarbamylase, and dihydroorotase	IPI00301263	6.8	1.0	0.0	0.0
CALM1;CALM3;CALM2	calmodulin 2 (phosphorylase kinase, delta)	IPI00075248	0.0	0.0	1.5	0.0
CAPRIN1	cell cycle associated protein 1	IPI00783872	7.3	14.5	11.5	9.5
CAPZA1	capping protein (actin filament) muscle Z-line, alpha 1	IPI00005969	0.5	0.0	0.0	0.0
CBX1	chromobox homolog 1 (HP1 beta homolog Drosophila)	IPI00010320	0.0	0.0	2.0	0.0
CCDC124	hypothetical protein BC013949	IPI00060627	0.0	0.0	1.5	3.5
CCT2	chaperonin containing TCP1, subunit 2 (beta)	IPI00297779	27.8	12.8	0.0	0.0
CCT3	chaperonin containing TCP1, subunit 3 (gamma)	IPI00290770	66.8	29.5	0.0	0.0
CCT5	chaperonin containing TCP1, subunit 5 (epsilon)	IPI00010720	54.5	19.3	0.0	0.0

CCT6A	chaperonin containing TCP1, subunit 6A (zeta 1)	IPI00027626	52.8	23.0	1.5	0.0
CCT7	chaperonin containing TCP1, subunit 7 (eta)	IPI00018465	56.0	24.3	2.0	0.0
CCT8	chaperonin containing TCP1, subunit 8 (theta)	IPI00302925	54.0	21.5	0.0	0.0
CENPV	proline rich 6	IPI00376481	0.0	0.0	3.0	0.0
CEP170	centrosomal protein 170kDa	IPI00186194	1.5	1.0	0.0	0.0
CHCHD4	coiled-coil-helix-coiled-coil-helix domain containing 4	IPI00177428	9.8	7.0	0.0	0.0
CIRBP	cold inducible RNA binding protein	IPI00180954	0.0	0.0	0.0	1.5
CKAP4	cytoskeleton-associated protein 4	IPI00141318	25.3	1.8	9.0	0.0
CKAP5	cytoskeleton associated protein 5	IPI00028275	11.5	11.0	11.5	0.0
CLASP1	cytoplasmic linker associated protein 1	IPI00396279	1.5	1.3	0.0	0.0
CLASP2	cytoplasmic linker associated protein 2	IPI00024382	1.3	0.8	2.0	0.0
CLTC	clathrin, heavy polypeptide (Hc)	IPI00024067	9.3	0.0	9.0	0.0
CNOT1	CCR4-NOT transcription complex, subunit 1	IPI00166010	0.0	5.3	0.0	0.0
CNP	2',3'-cyclic nucleotide 3' phosphodiesterase	IPI00220993	2.3	0.0	0.0	0.0
COL18A1	collagen, type XVIII, alpha 1	IPI00022822	0.8	0.0	0.0	0.0
COL1A2	collagen, type I, alpha 2	IPI00304962	0.0	3.8	0.0	0.0
COPA	coatomer protein complex, subunit alpha	IPI00295857	0.8	0.0	0.0	0.0
CORO1C	coronin 1C	IPI00798401	0.0	0.0	10.5	0.0
CPSF6	cleavage and polyadenylation specific factor 6, 68kDa	IPI00012998	3.0	0.0	0.0	0.0
CROP	cisplatin resistance-associated overexpressed protein	IPI00107745	0.0	0.0	2.5	0.0
CSDA	cold shock domain protein A	IPI00031801	5.5	0.0	6.0	0.0
CSDE1	cold shock domain containing E1, RNA-binding	IPI00470891	1.3	0.0	0.0	0.0
CSNK1A1L	casein kinase 1, alpha 1-like	IPI00167096	0.0	0.0	2.0	0.0
CTNND1	catenin (cadherin-associated protein), delta 1	IPI00182469	2.5	0.0	0.0	0.0
DAP3	death associated protein 3	IPI00018120	3.3	0.0	0.0	0.0
DDX1	DEAD (Asp-Glu-Ala-Asp) box polypeptide 1	IPI00293655	8.0	2.5	15.0	15.5
DDX17	DEAD (Asp-Glu-Ala-Asp) box polypeptide 17	IPI00023785	8.0	7.3	0.0	7.0
DDX21	DEAD (Asp-Glu-Ala-Asp) box polypeptide 21	IPI00015953	10.3	7.3	6.5	4.0
DDX23	DEAD (Asp-Glu-Ala-Asp) box polypeptide 23	IPI00006725	2.8	1.0	0.0	0.0
DDX24	DEAD (Asp-Glu-Ala-Asp) box polypeptide 24	IPI00006987	2.5	0.0	0.0	0.0
DDX3X	DEAD (Asp-Glu-Ala-Asp) box polypeptide 3, X-linked	IPI00215637	19.0	3.3	17.0	9.5
DDX3Y;LOC100130220	DEAD (Asp-Glu-Ala-Asp) box polypeptide 3, Y-linked	IPI00293616	1.5	0.0	0.0	0.0
DDX46	DEAD (Asp-Glu-Ala-Asp) box polypeptide 46	IPI00329791	1.3	0.0	2.5	0.0
DDX5	DEAD (Asp-Glu-Ala-Asp) box polypeptide 5	IPI00017617	14.5	8.5	13.0	10.5
DDX50	DEAD (Asp-Glu-Ala-Asp) box polypeptide 50	IPI00031554	0.0	0.0	0.0	2.0
DDX54	DEAD (Asp-Glu-Ala-Asp) box polypeptide 54	IPI00152510	2.3	0.0	0.0	0.0
DDX6	DEAD (Asp-Glu-Ala-Asp) box polypeptide 6	IPI00030320	0.0	0.0	0.0	1.5

DDX60	hypothetical protein FLJ20035	IPI00217606	6.0	0.0	0.0	0.0
DDX60L	DEAD-Box Helicase 60-Like	IPI00853133	2.5	0.0	0.0	0.0
DECR1	2,4-dienoyl CoA reductase 1, mitochondrial	IPI00003482	3.3	2.0	3.5	0.0
DERA	2-deoxyribose-5-phosphate aldolase homolog (C. elegans)	IPI00219677	9.3	0.0	0.0	0.0
DHX15	DEAH (Asp-Glu-Ala-His) box polypeptide 15	IPI00396435	8.8	4.3	2.5	2.5
DHX29	DEAH (Asp-Glu-Ala-His) box polypeptide 29	IPI00217413	5.3	5.5	3.0	0.0
DHX30	DEAH (Asp-Glu-Ala-His) box polypeptide 30	IPI00164906	0.0	0.5	0.0	0.0
DHX30	DEAH (Asp-Glu-Ala-His) box polypeptide 30	IPI00411733	4.0	8.0	8.5	6.5
DHX36	DEAH (Asp-Glu-Ala-His) box polypeptide 36	IPI00027415	4.8	2.8	2.0	4.5
DHX57	DEAH (Asp-Glu-Ala-Asp/His) box polypeptide 57	IPI00168885	1.8	0.0	0.0	0.0
DHX9	DEAH (Asp-Glu-Ala-His) box polypeptide 9	IPI00844578	34.5	28.8	20.5	6.0
DIMT1L	dimethyladenosine transferase	IPI00004459	0.0	0.0	2.0	1.5
DNAJA1	DnaJ (Hsp40) homolog, subfamily A, member 1	IPI00012535	0.0	0.0	0.0	1.5
DNAJA3	DnaJ (Hsp40) homolog, subfamily A, member 3	IPI00179187	1.0	0.0	1.5	1.5
DNAJC13	DnaJ (Hsp40) homolog, subfamily C, member 13	IPI00307259	4.5	0.8	2.5	0.0
DOCK6	dedicator of cytokinesis 6	IPI00184772	1.5	0.0	0.0	0.0
DOCK7	dedicator of cytokinesis 7	IPI00183572	0.0	0.8	0.0	0.0
DPM1	dolichyl-phosphate mannosyltransferase polypeptide 1, catalytic subunit	IPI00022018	0.0	0.0	0.0	2.0
DRG1	developmentally regulated GTP binding protein 1	IPI00031836	8.3	0.0	4.5	5.0
DSP	desmoplakin	IPI00013933	4.8	2.8	0.0	0.0
DYNC1H1	dynein, cytoplasmic 1, heavy chain 1	IPI00456969	4.5	2.5	0.0	0.0
EBNA1BP2	EBNA1 binding protein 2	IPI00745955	0.5	0.0	0.0	0.0
ECT2	epithelial cell transforming 2	IPI00748143	1.3	0.0	0.0	0.0
EDC4	autoantigen	IPI00376317	0.0	1.0	0.0	0.0
EEF1A1	chemokine (C-C motif) receptor 5	IPI00025447	6.5	2.0	0.0	0.0
EEF1A2	eukaryotic translation elongation factor 1 alpha 2	IPI00014424	11.8	0.0	4.0	0.0
EEF1E1	eukaryotic translation elongation factor 1 epsilon 1	IPI00003588	0.0	0.0	0.0	2.5
EFTUD2	elongation factor Tu GTP binding domain containing 2	IPI00003519	1.8	1.0	7.0	0.0
EIF2AK2	eukaryotic translation initiation factor 2-alpha kinase 2	IPI00019463	17.0	1.3	7.0	3.0
EIF2S1	eukaryotic translation initiation factor 2, subunit 1 alpha, 35kDa	IPI00219678	12.0	2.3	10.5	3.5
EIF2S2	eukaryotic translation initiation factor 2, subunit 2 beta, 38kDa	IPI00021728	0.0	0.0	2.5	2.0
EIF3A	eukaryotic translation initiation factor 3, subunit 10 theta, 150/170kDa	IPI00029012	2.5	1.5	5.5	0.0

EIF3B	eukaryotic translation initiation factor 3, subunit 9 eta, 116kDa	IPI00396370	0.0	0.0	2.0	0.0
EIF3CL;EIF3C	eukaryotic translation initiation factor 3, subunit 8, 110kDa	IPI00016910	0.0	0.0	2.0	0.0
EIF3F	eukaryotic translation initiation factor 3, subunit 5 epsilon, 47kDa	IPI00654777	0.8	0.0	0.0	3.0
EIF3G	eukaryotic translation initiation factor 3, subunit 4 delta, 44kDa	IPI00290460	0.8	0.0	0.0	0.0
EIF3L	eukaryotic translation initiation factor 3, subunit 6 interacting protein	IPI00465233	0.0	1.3	0.0	2.5
EIF4A1;SNORA67	eukaryotic translation initiation factor 4A, isoform 1	IPI00025491	0.0	0.0	1.5	0.0
EIF4A3	DEAD (Asp-Glu-Ala-Asp) box polypeptide 48	IPI00009328	0.0	0.0	0.0	2.0
EIF4B	eukaryotic translation initiation factor 4B	IPI00012079	1.3	0.0	0.0	0.0
EIF4G1	eukaryotic translation initiation factor 4 gamma, 1	IPI00220365	0.8	0.8	5.5	0.0
EIF4G1	eukaryotic translation initiation factor 4 gamma, 1	IPI00386533	2.5	1.3	2.5	0.0
EIF4G3	eukaryotic translation initiation factor 4 gamma, 3	IPI00328268	0.0	0.5	0.0	0.0
EIF5A2	eukaryotic translation initiation factor 5A2	IPI00006935	1.0	0.0	0.0	0.0
EIF5B	eukaryotic translation initiation factor 5B	IPI00299254	10.0	10.5	6.5	0.0
ELAVL1	ELAV (embryonic lethal, abnormal vision, Drosophila)-like 1 (Hu antigen R)	IPI00301936	4.0	3.8	14.0	10.0
EMD	emerin (Emery-Dreifuss muscular dystrophy)	IPI00032003	1.8	2.5	14.5	2.0
EMG1	EMG1 nucleolar protein homolog (S. cerevisiae)	IPI00025347	0.0	0.0	2.5	0.0
EPPK1	epiplakin 1	IPI00010951	0.8	0.0	9.5	0.0
EPRS	glutamyl-prolyl-tRNA synthetase	IPI00013452	9.3	11.3	5.5	2.5
ERLIN1	SPFH domain family, member 1	IPI00007940	2.3	0.0	0.0	0.0
EWSR1	Ewing sarcoma breakpoint region 1	IPI00009841	0.0	0.0	0.0	1.5
EXOSC10	exosome component 10	IPI00009464	2.8	0.8	1.5	0.0
EXOSC6	exosome component 6	IPI00073602	0.0	1.8	0.0	0.0
EXOSC9	exosome component 9	IPI00029697	1.0	0.0	0.0	0.0
FAM120A	chromosome 9 open reading frame 10	IPI00039626	6.3	0.0	11.5	4.0
FAM164A	chromosome 8 open reading frame 70	IPI00329753	0.5	0.0	0.0	0.0
FAM83H	family with sequence similarity 83 member H	IPI00784320	0.0	0.0	4.0	0.0
FAM91A1	family with sequence similarity 91, member A1	IPI00152671	1.0	0.0	0.0	0.0
FARSA	phenylalanine-tRNA synthetase-like, alpha subunit	IPI00031820	0.0	1.8	0.0	0.0
FARSB	phenylalanine-tRNA synthetase-like, beta subunit	IPI00300074	3.3	2.5	1.5	3.0
FASN	fatty acid synthase	IPI00026781	1.5	0.0	0.0	0.0
FAU	Finkel-Biskis-Reilly murine sarcoma virus (FBR-MuSV) ubiquitously expressed (fox derived); ribosomal protein S30	IPI00019770	3.3	0.0	0.0	0.0

FBL	fibrillarin	IPI00025039	1.5	0.0	3.5	0.0
FLNA	filamin A, alpha (actin binding protein 280)	IPI00302592	11.8	0.0	38.5	0.0
FLNB	filamin B, beta (actin binding protein 278)	IPI00289334	6.5	0.0	10.5	0.0
FLNC	filamin C, gamma (actin binding protein 280)	IPI00178352	3.8	0.0	0.0	0.0
FMR1	fragile X mental retardation 1	IPI00215720	3.3	5.8	0.0	6.5
FUS	fusion (involved in t(12;16) in malignant liposarcoma)	IPI00221354	0.0	1.3	0.0	0.0
FXR1	fragile X mental retardation, autosomal homolog 1	IPI00016249	4.8	2.0	4.0	3.5
FXR2	fragile X mental retardation, autosomal homolog 2	IPI00016250	0.0	5.0	0.0	4.5
G3BP1	Ras-GTPase-activating protein SH3-domain-binding protein	IPI00012442	8.3	6.8	10.5	12.0
G3BP2	Ras-GTPase activating protein SH3 domain-binding protein 2	IPI00009057	1.5	3.5	0.0	6.0
G6PD	glucose-6-phosphate dehydrogenase	IPI00216008	2.8	0.0	0.0	0.0
GCN1L1	GCN1 general control of amino-acid synthesis 1-like 1 (yeast)	IPI00001159	3.3	0.8	0.0	0.0
GIGYF2	trinucleotide repeat containing 15	IPI00647635	0.0	0.5	0.0	0.0
GNB2L1	guanine nucleotide binding protein (G protein), beta polypeptide 2-like 1	IPI00641950	1.3	3.3	0.0	0.0
GNL3	guanine nucleotide binding protein-like 3 (nucleolar)	IPI00003886	2.0	4.5	0.0	5.0
GRWD1	glutamate-rich WD repeat containing 1	IPI00027831	3.0	0.0	0.0	0.0
GTF2I	general transcription factor II, i	IPI00054042	2.8	0.0	2.0	0.0
GTF3C1	general transcription factor IIIC, polypeptide 1, alpha 220kDa	IPI00414481	0.5	0.0	0.0	0.0
GTPBP1	GTP binding protein 1	IPI00010463	0.0	1.3	0.0	0.0
GTPBP4	GTP binding protein 4	IPI00385042	4.3	0.0	0.0	2.0
H1FX	H1 histone family, member X	IPI00021924	5.5	0.0	4.5	2.0
H2AFV	H2A histone family, member V	IPI00018278	3.8	0.0	0.0	5.0
H2AFY	H2A histone family, member Y	IPI00059366	3.0	0.0	8.0	0.0
HADHA	hydroxyacyl-Coenzyme A dehydrogenase/3-ketoacyl-Coenzyme A thiolase/enoyl-Coenzyme A hydratase (trifunctional protein), alpha subunit	IPI00031522	24.3	8.0	15.0	0.0
HADHB	hydroxyacyl-Coenzyme A dehydrogenase/3-ketoacyl-Coenzyme A thiolase/enoyl-Coenzyme A hydratase (trifunctional protein), beta subunit	IPI00022793	2.0	0.0	0.0	0.0
HDLBP	high density lipoprotein binding protein (vigilin)	IPI00022228	3.8	1.0	5.5	0.0
HERC5	hect domain and RLD 5	IPI00008821	1.3	1.3	0.0	0.0
HIST1H1C	histone 1, H1c	IPI00217465	3.3	1.5	0.0	0.0

HIST1H4J;HIST1H4E;HIST1H4H;HIST1H4K;HIST2H4A;HIST1H4D;HIST1H4F;HIST2H4B;HIST1H4C;HIST1H4B;HIST1H4I;HIST1H4L;HIST1H4A;HIST4H4	histone 2, H4	IPI00453473	8.3	0.0	0.0	0.0
HIST2H2BE	histone 2, H2be	IPI00003935	0.0	2.0	32.5	6.0
HNRNPA0	heterogeneous nuclear ribonucleoprotein A0	IPI00011913	2.3	0.0	8.5	2.0
HNRNPA1	heterogeneous nuclear ribonucleoprotein A1	IPI00215965	14.0	8.5	10.0	5.5
HNRNPA2B1	heterogeneous nuclear ribonucleoprotein A2/B1	IPI00386854	0.8	1.8	15.5	11.0
HNRNPA2B1	heterogeneous nuclear ribonucleoprotein A2/B1	IPI00396378	5.5	11.0	7.0	4.5
HNRNPA3	heterogeneous nuclear ribonucleoprotein A3	IPI00419373	7.5	5.8	12.0	4.0
HNRNPAB	heterogeneous nuclear ribonucleoprotein A/B	IPI00106509	4.5	3.5	4.0	0.0
HNRNPC	heterogeneous nuclear ribonucleoprotein C (C1/C2)	IPI00216592	9.3	2.8	10.5	3.0
HNRNPCL1	heterogeneous nuclear ribonucleoprotein C-like 1	IPI00027569	4.5	0.0	0.0	3.0
HNRNPD	heterogeneous nuclear ribonucleoprotein D (AU-rich element RNA binding protein 1, 37kDa)	IPI00028888	3.8	4.0	2.0	3.5
HNRNPF	heterogeneous nuclear ribonucleoprotein F	IPI00003881	2.8	0.0	8.5	3.0
HNRNPH1	heterogeneous nuclear ribonucleoprotein H1 (H)	IPI00013881	0.0	0.0	2.5	0.0
HNRNPH3	heterogeneous nuclear ribonucleoprotein H3 (2H9)	IPI00013877	2.0	0.0	7.5	0.0
HNRNPK	heterogeneous nuclear ribonucleoprotein K	IPI00216049	23.5	6.0	19.5	3.5
HNRNPL	heterogeneous nuclear ribonucleoprotein L	IPI00027834	2.5	1.8	7.5	4.0
HNRNPM	heterogeneous nuclear ribonucleoprotein M	IPI00171903	30.0	7.8	12.5	19.0
HNRNPR	heterogeneous nuclear ribonucleoprotein R	IPI00012074	6.8	2.0	6.5	4.5
HNRNPU	heterogeneous nuclear ribonucleoprotein U (scaffold attachment factor A)	IPI00479217	19.5	11.3	9.0	9.0
HNRNPUL1	heterogeneous nuclear ribonucleoprotein U-like 1	IPI00013070	11.3	2.8	4.5	2.5
HNRNPUL2	heterogeneous nuclear ribonucleoprotein U-like 2	IPI00456887	3.3	0.0	0.0	0.0
HNRPDL	heterogeneous nuclear ribonucleoprotein D-like	IPI00011274	2.3	2.3	3.5	2.0
HP1BP3	heterochromatin protein 1, binding protein 3	IPI00640417	2.0	0.0	0.0	0.0
HRNR	hornerin	IPI00398625	2.0	0.0	0.0	0.0
HSD17B12	hydroxysteroid (17-beta) dehydrogenase 12	IPI00007676	3.0	2.3	0.0	0.0
HSP90AA1	heat shock protein 90kDa alpha (cytosolic), class A member 1	IPI00382470	3.0	1.5	0.0	0.0
HSPA1A;HSPA1B	heat shock 70kDa protein 1A	IPI00304925	7.8	0.0	0.0	5.0
HSPA1L	heat shock 70kDa protein 7 (HSP70B)	IPI00301277	4.8	2.3	4.0	5.5
HSPA2	heat shock 70kDa protein 2	IPI00007702	1.5	0.0	0.0	0.0

HSPA5	heat shock 70kDa protein 5 (glucose-regulated protein, 78kDa)	IPI00003362	0.0	0.0	4.0	4.0
HSPA8	heat shock 70kDa protein 8	IPI00003865	31.0	0.0	19.5	8.0
HSPD1	heat shock protein family D (Hsp60) member 1	IPI00784154	2.8	0.0	0.0	0.0
IARS	isoleucine-tRNA synthetase	IPI00644127	3.3	2.0	5.5	2.5
IFI16	interferon, gamma-inducible protein 16	IPI00003443	2.8	0.0	0.0	0.0
IFIT3	interferon-induced protein with tetratricopeptide repeats 3	IPI00024254	1.0	0.0	0.0	0.0
IGF2BP1	insulin-like growth factor 2 mRNA binding protein 1	IPI00008557	19.8	21.0	17.0	21.5
IGF2BP2	insulin-like growth factor 2 mRNA binding protein 2	IPI00179713	4.0	2.5	0.0	4.0
IGF2BP3	insulin-like growth factor 2 mRNA binding protein 3	IPI00165467	3.0	1.0	3.0	6.5
IGF2BP3	insulin-like growth factor 2 mRNA binding protein 3	IPI00658000	7.3	6.3	10.0	9.5
IGLC1;IGLV1-44;IGLV1-40;IGLV3-21;IGLV2-11;IGLV2-14;IGL@;IGLC2;IGLC3	immunoglobulin lambda constant 1 (Mcg marker)	IPI00154742	3.8	0.0	0.0	0.0
ILF2	interleukin enhancer binding factor 2, 45kDa	IPI00005198	12.8	11.3	7.5	11.5
ILF3	interleukin enhancer binding factor 3, 90kDa	IPI00219330	14.5	8.5	10.5	16.0
ILK-2;CCT4	chaperonin containing TCP1, subunit 4 (delta)	IPI00302927	44.0	17.0	0.0	0.0
IMMT	inner membrane protein, mitochondrial (mitofilin)	IPI00009960	2.5	1.3	1.5	0.0
IMP3	IMP3, U3 small nucleolar ribonucleoprotein, homolog (yeast)	IPI00019488	0.0	0.0	2.0	0.0
IPO7	importin 7	IPI00007402	2.5	1.0	0.0	0.0
IQGAP1	IQ motif containing GTPase activating protein 1	IPI00009342	13.8	0.0	19.5	0.0
ISG15	interferon, alpha-inducible protein (clone IFI-15K)	IPI00375631	14.0	0.0	0.0	0.0
KARS	lysyl-tRNA synthetase	IPI00014238	1.5	1.8	0.0	3.0
KHDRBS1	KH domain containing, RNA binding, signal transduction associated 1	IPI00008575	0.8	1.8	0.0	4.0
KIAA0020	pumilio RNA binding family member 3	IPI00791325	0.8	0.0	4.0	0.0
KIAA1618	KIAA1618	IPI00217287	22.0	0.0	0.0	0.0
KIAA1618	KIAA1618	IPI00218094	19.5	0.0	0.0	0.0
KIAA1618	chromosome 17 open reading frame 27	IPI00642126	76.3	0.0	1.5	0.0
KIAA1967	KIAA1967	IPI00182757	3.0	0.0	0.0	0.0
KIF2A	kinesin heavy chain member 2	IPI00010368	3.0	0.0	0.0	0.0
KIFC1	kinesin family member C1	IPI00306400	0.0	2.5	0.0	0.0
KPNB1	karyopherin (importin) beta 1	IPI00001639	4.3	1.5	4.0	0.0
KTN1	kinectin 1 (kinesin receptor)	IPI00328753	2.0	0.0	0.0	0.0
LACTB	lactamase, beta	IPI00294186	5.8	0.0	2.5	0.0

LAMA5	laminin subunit alpha 5	IPI00783665	5.3	0.0	0.0	0.0
LAMB1	laminin, beta 1	IPI00013976	3.0	0.0	0.0	0.0
LAMC1	laminin, gamma 1 (formerly LAMB2)	IPI00298281	2.5	0.0	0.0	0.0
LARP1	La ribonucleoprotein domain family, member 1	IPI00185919	11.0	7.8	14.5	8.0
LARP4	La ribonucleoprotein domain family, member 4	IPI00043638	0.0	0.0	0.0	1.5
LARP4B	La ribonucleoprotein domain family member 4B	IPI00827634	1.0	0.0	0.0	3.5
LARS	leucyl-tRNA synthetase	IPI00103994	0.0	2.5	2.0	1.5
LBA1	tetratricopeptide repeat and ankyrin repeat containing 1	IPI00847543	1.8	0.0	0.0	0.0
LEMD2	LEM domain containing 2	IPI00168336	0.0	0.0	8.5	0.0
LIG3	ligase III, DNA, ATP-dependent	IPI00000156	0.0	1.0	7.0	0.0
LMNA	lamin A/C	IPI00021405	23.0	0.0	52.5	0.0
LMNB1	lamin B1	IPI00217975	1.3	0.8	13.0	0.0
LOC26010	DNA polymerase-transactivated protein 6	IPI00023532	4.8	0.0	0.0	0.0
LOC442497;SLC3A2	solute carrier family 3 (activators of dibasic and neutral amino acid transport), member 2	IPI00027493	6.0	0.0	0.0	0.0
LOC652595		IPI00183920	1.3	0.0	0.0	1.5
LRPPRC	leucine rich pentatricopeptide repeat containing	IPI00783271	7.8	2.8	15.5	0.0
LRRC59	leucine rich repeat containing 59	IPI00396321	8.3	2.3	10.0	4.5
LUC7L2	LUC7-like 2 (S. cerevisiae)	IPI00006932	1.5	0.0	0.0	2.0
MACF1	microtubule-actin crosslinking factor 1	IPI00256861	3.0	0.0	0.0	0.0
MAP1B	microtubule-associated protein 1B	IPI00008868	13.8	0.0	5.0	0.0
MAP4	microtubule-associated protein 4	IPI00220113	0.0	3.5	5.0	3.0
MAP4	microtubule-associated protein 4	IPI00396171	2.5	0.0	0.0	0.0
MAP7	microtubule-associated protein 7	IPI00020771	8.5	0.0	0.0	0.0
MARS	methionine-tRNA synthetase	IPI00008240	0.0	2.0	0.0	5.0
MATR3	matrin 3	IPI00017297	7.5	7.8	13.0	7.0
MCM3	MCM3 minichromosome maintenance deficient 3 (S. cerevisiae)	IPI00013214	1.0	0.0	0.0	0.0
MDN1	MDN1, midasin homolog (yeast)	IPI00167941	0.0	0.8	0.0	0.0
MKI67	antigen identified by monoclonal antibody Ki-67	IPI00004233	0.0	0.0	2.5	0.0
MKI67IP	MKI67 (FHA domain) interacting nucleolar phosphoprotein	IPI00154590	0.0	0.0	3.5	0.0
MOV10	Mov10, Moloney leukemia virus 10, homolog (mouse)	IPI00444452	14.0	20.8	10.5	21.5
MPRIP	myosin phosphatase-Rho interacting protein	IPI00166518	2.3	1.5	6.5	0.0
MRPL11	mitochondrial ribosomal protein L11	IPI00007001	0.0	0.0	1.5	0.0
MRPS22	mitochondrial ribosomal protein S22	IPI00013146	0.0	0.0	1.5	0.0
MRPS27	mitochondrial ribosomal protein S27	IPI00022002	1.3	0.0	0.0	0.0
MRPS9	mitochondrial ribosomal protein S9	IPI00641924	2.8	0.0	0.0	0.0

MRTO4	chromosome 1 open reading frame 33	IPI00106491	0.0	0.0	2.0	1.5
MSH2	mutS homolog 2, colon cancer, nonpolyposis type 1 (E. coli)	IPI00017303	1.5	0.0	0.0	0.0
MSH6	mutS homolog 6 (E. coli)	IPI00106847	3.3	0.5	3.0	0.0
MSI2	musashi homolog 2 (Drosophila)	IPI00073713	0.0	0.0	0.0	2.0
MTDH	metadherin	IPI00328715	1.8	0.0	0.0	0.0
MTUS1	mitochondrial tumor suppressor 1	IPI00428447	1.8	0.0	0.0	0.0
MVP	major vault protein	IPI00000105	1.3	0.0	0.0	0.0
MX1	myxovirus (influenza virus) resistance 1, interferon-inducible protein p78 (mouse)	IPI00167949	2.8	0.0	0.0	0.0
MYBBP1A	MYB binding protein (P160) 1a	IPI00005024	32.5	22.5	7.5	2.0
MYH10	myosin, heavy polypeptide 10, non-muscle	IPI00397526	12.5	5.3	0.0	0.0
MYH9	myosin, heavy polypeptide 9, non-muscle	IPI00019502	144.8	2.0	0.0	0.0
MYL12B	myosin regulatory light chain MRLC2	IPI00033494	6.8	0.0	0.0	0.0
MYL6;MYL6B	myosin, light polypeptide 6, alkali, smooth muscle and non-muscle	IPI00335168	6.5	0.0	0.0	0.0
MYL9	myosin, light polypeptide 9, regulatory	IPI00030929	5.3	0.0	0.0	0.0
MYO1B	myosin IB	IPI00376344	10.0	0.0	29.5	0.0
MYO1C	myosin IC	IPI00010418	27.5	6.5	27.5	0.0
MYO1D	myosin ID	IPI00329719	0.0	3.0	1.5	0.0
MYO1E	myosin IE	IPI00329672	3.0	0.0	3.5	0.0
MYO6	myosin VI	IPI00008455	0.0	2.3	9.0	0.0
MYO9B	myosin IXB	IPI00306933	0.5	0.0	0.0	0.0
NACA	nascent-polypeptide-associated complex alpha polypeptide	IPI00023748	3.3	0.0	0.0	0.0
NAT10	N-acetyltransferase 10	IPI00300127	0.0	0.0	2.0	0.0
NCBP1	nuclear cap binding protein subunit 1, 80kDa	IPI00019380	4.3	1.0	4.5	9.0
NCL	nucleolin	IPI00183526	29.8	15.0	19.0	14.5
NCL	nucleolin	IPI00444262	25.3	12.8	9.5	16.5
NME4	non-metastatic cells 4, protein expressed in	IPI00012972	2.3	0.0	0.0	0.0
NMNAT1	nicotinamide nucleotide adenylyltransferase 1	IPI00009726	0.0	0.8	0.0	0.0
NOL6	nucleolar protein family 6 (RNA-associated)	IPI00152890	0.0	0.0	2.0	0.0
NOM1	nucleolar protein with MIF4G domain 1	IPI00145593	1.8	0.0	0.0	0.0
NONO	non-POU domain containing, octamer-binding	IPI00304596	2.5	6.8	5.5	0.0
NOP2	nucleolar protein 1, 120kDa	IPI00294891	8.8	2.3	5.0	0.0
NOP56	nucleolar protein 5A (56kDa with KKE/D repeat)	IPI00411937	0.0	0.0	3.5	0.0
NOP58	nucleolar protein NOP5/NOP58	IPI00006379	2.5	0.0	2.0	0.0
NPM1	anaplastic lymphoma kinase (Ki-1)	IPI00220740	12.0	5.3	15.5	10.5
NSUN2	NOL1/NOP2/Sun domain family, member 2	IPI00306369	5.3	0.0	0.0	0.0

NUFIP2	nuclear fragile X mental retardation protein interacting protein 2	IPI00002349	0.0	0.0	2.0	3.0
NUMA1	nuclear mitotic apparatus protein 1	IPI00006196	0.5	0.0	0.0	0.0
NUP133	nucleoporin 133kDa	IPI00291200	0.0	0.0	2.0	0.0
OAS2	2'-5'-oligoadenylate synthetase 2, 69/71kDa	IPI00217049	2.0	0.0	0.0	0.0
OAS3	2'-5'-oligoadenylate synthetase 3, 100kDa	IPI00002405	16.8	0.0	0.0	0.0
OGDH	oxoglutarate (alpha-ketoglutarate) dehydrogenase (lipoamide)	IPI00098902	3.8	0.0	0.0	0.0
PA2G4	proliferation-associated 2G4, 38kDa	IPI00299000	0.0	1.3	0.0	0.0
PABPC1	poly(A) binding protein, cytoplasmic 1	IPI00008524	35.8	21.5	39.5	38.5
PABPC4	poly(A) binding protein, cytoplasmic 4 (inducible form)	IPI00012726	6.3	3.5	7.0	13.5
PARP1	poly (ADP-ribose) polymerase family, member 1	IPI00449049	20.0	15.5	24.0	20.5
PARP9	poly (ADP-ribose) polymerase family, member 9	IPI00027803	0.5	0.0	0.0	0.0
PCBP2	poly(rC) binding protein 2	IPI00012066	0.0	0.0	0.0	3.5
PDCD11	programmed cell death 11	IPI00400922	0.0	0.0	3.0	0.0
PELP1	proline, glutamic acid and leucine rich protein 1	IPI00006702	0.8	3.0	0.0	0.0
PFDN2	prefoldin subunit 2	IPI00006052	2.5	0.0	0.0	0.0
PFKP	phosphofructokinase, platelet	IPI00009790	0.0	0.0	2.0	0.0
PGAM5	phosphoglycerate mutase family member 5	IPI00063242	3.3	1.8	5.5	3.0
PGAM5	phosphoglycerate mutase family member 5	IPI00788907	2.5	0.0	0.0	0.0
PHB2	prohibitin 2	IPI00027252	1.0	0.0	0.0	0.0
PLEC1	plectin 1, intermediate filament binding protein 500kDa	IPI00014898	67.5	1.5	153.5	0.0
PNO1	putatative 28 kDa protein	IPI00024524	0.0	0.0	1.5	0.0
POLRMT	polymerase (RNA) mitochondrial (DNA directed)	IPI00298738	2.5	0.0	2.0	0.0
PPIB	peptidylprolyl isomerase B (cyclophilin B)	IPI00646304	0.0	0.0	2.0	0.0
PPP1CC	protein phosphatase 1, catalytic subunit, gamma isoform	IPI00005705	0.0	0.8	0.0	0.0
PPP1R12A	protein phosphatase 1, regulatory (inhibitor) subunit 12A	IPI00183002	0.0	0.0	1.5	0.0
PRDX1	peroxiredoxin 1	IPI00000874	0.0	0.0	4.0	0.0
PRIC285	peroxisomal proliferator-activated receptor A interacting complex 285	IPI00249304	24.0	2.5	0.0	0.0
PRKDC	protein kinase, DNA-activated, catalytic polypeptide	IPI00296337	76.5	43.0	46.0	0.0
PRKRA	protein kinase, interferon-inducible double stranded RNA dependent activator	IPI00021167	0.0	1.8	0.0	0.0
PRPF40A	pre-mRNA processing factor 40 homolog A	IPI00337385	0.0	0.5	0.0	0.0
PRPF8	PRP8 pre-mRNA processing factor 8 homolog (yeast)	IPI00007928	1.8	2.0	3.5	0.0
PRPH	peripherin	IPI00013164	0.0	0.0	2.5	0.0

PSMC5	proteasome (prosome, macropain) 26S subunit, ATPase, 5	IPI00023919	1.3	0.0	0.0	0.0
PSPC1	paraspeckle component 1	IPI00103525	0.0	1.0	0.0	0.0
PTBP1	polypyrimidine tract binding protein 1	IPI00179964	6.3	8.3	10.5	0.0
PTCD3	pentatricopeptide repeat domain 3	IPI00783302	0.5	0.0	0.0	0.0
PTK2	PTK2 protein tyrosine kinase 2	IPI00012885	1.0	0.0	0.0	0.0
PTPLAD1	protein tyrosine phosphatase-like A domain containing 1	IPI00008998	4.0	0.0	3.0	0.0
PTRF	polymerase I and transcript release factor	IPI00176903	6.3	0.0	0.0	0.0
PURA	purine-rich element binding protein A	IPI00023591	0.0	0.5	3.0	2.5
PYGM	phosphorylase, glycogen; muscle (McArdle syndrome, glycogen storage disease type V)	IPI00218130	1.3	0.0	0.0	0.0
QARS	glutaminyl-tRNA synthetase	IPI00026665	1.0	0.0	1.5	3.5
RAI14	retinoic acid induced 14	IPI00292953	2.8	2.0	11.0	0.0
RALY	RNA binding protein, autoantigenic (hnRNP-associated with lethal yellow homolog (mouse))	IPI00011268	0.5	0.0	3.5	0.0
RANBP2	RAN binding protein 2	IPI00221325	0.0	0.0	2.5	0.0
RARS	arginyl-tRNA synthetase	IPI00004860	2.8	3.5	1.5	2.5
RBM14;RBM4	RNA binding motif protein 14	IPI00013174	0.0	5.0	3.0	4.5
RBM25	RNA binding motif protein 25	IPI00004273	0.5	0.0	0.0	0.0
RBM28	RNA binding motif protein 28	IPI00304187	2.5	0.0	0.0	0.0
RBM39	RNA-binding region (RNP1, RRM) containing 2	IPI00163505	3.5	1.8	0.0	3.0
RBMX	RNA binding motif protein, X-linked	IPI00304692	0.8	0.0	0.0	0.0
RECQL	RecQ protein-like (DNA helicase Q1-like)	IPI00178431	1.3	0.0	0.0	0.0
RFC1	replication factor C (activator 1) 1, 145kDa	IPI00375358	0.0	1.5	0.0	0.0
RFC2	replication factor C (activator 1) 2, 40kDa	IPI00017412	0.0	0.0	2.0	0.0
RFC4	replication factor C (activator 1) 4, 37kDa	IPI00017381	3.3	0.0	2.5	0.0
RFC5	replication factor C (activator 1) 5, 36.5kDa	IPI00031514	1.5	0.0	0.0	0.0
RIF1	RAP1 interacting factor homolog (yeast)	IPI00293845	0.0	0.0	3.5	0.0
RNF213	ring finger protein 213	IPI00470478	12.8	0.0	0.0	0.0
RPA1	replication protein A1, 70kDa	IPI00020127	0.0	2.5	13.0	2.5
RPA2	replication protein A2, 32kDa	IPI00013939	0.0	0.0	5.5	0.0
RPL10A	ribosomal protein L10a	IPI00412579	6.8	20.0	6.0	5.5
RPL10L	ribosomal protein L10-like	IPI00064765	0.0	0.0	3.0	0.0
RPL10P16	ribosomal protein L10 pseudogene 16	IPI00374260	2.0	0.0	0.0	0.0
RPL11	ribosomal protein L11	IPI00376798	5.5	2.5	0.0	0.0
RPL12	ribosomal protein L12	IPI00024933	18.8	10.5	5.0	11.0
RPL13	ribosomal protein L13	IPI00465361	7.3	1.0	6.5	4.5
RPL13A	ribosomal protein L13a	IPI00304612	5.8	1.0	2.0	3.5

RPL13P12	ribosomal protein L13 pseudogene 12	IPI00397611	9.0	9.8	9.5	9.5
RPL14	ribosomal protein L14	IPI00555744	3.0	0.0	0.0	0.0
RPL15	ribosomal protein L15	IPI00470528	0.0	6.0	8.0	4.0
RPL18	ribosomal protein L18	IPI00215719	13.5	11.3	9.0	7.5
RPL18A	ribosomal protein L18a	IPI00026202	5.8	1.8	9.5	3.0
RPL19	ribosomal protein L19	IPI00025329	6.8	2.5	4.5	0.0
RPL21P19;RPL21;RPL21P16	ribosomal protein L21	IPI00247583	10.0	8.3	8.5	6.0
RPL22	ribosomal protein L22	IPI00219153	0.0	1.3	0.0	0.0
RPL23	ribosomal protein L23	IPI00010153	7.3	6.8	15.5	12.5
RPL23A	ribosomal protein L23a	IPI00021266	14.3	8.8	11.0	12.0
RPL24	ribosomal protein L24	IPI00306332	6.3	7.5	7.5	4.5
RPL26L1	ribosomal protein L26-like 1	IPI00007144	6.0	4.8	8.0	7.0
RPL27	ribosomal protein L27	IPI00219155	10.3	2.8	4.0	4.0
RPL27A	ribosomal protein L27a	IPI00456758	5.3	4.0	0.0	0.0
RPL28	ribosomal protein L28	IPI00182533	5.0	2.3	0.0	0.0
RPL3	ribosomal protein L3	IPI00550021	19.3	18.0	15.0	13.0
RPL30	ribosomal protein L30	IPI00219156	12.8	6.0	11.0	13.5
RPL31	ribosomal protein L31	IPI00026302	5.5	4.0	0.0	0.0
RPL34	ribosomal protein L34	IPI00219160	4.3	1.5	5.5	4.0
RPL35	ribosomal protein L35	IPI00412607	2.0	3.3	3.5	3.0
RPL35A	ribosomal protein L35a	IPI00029731	7.8	6.3	3.5	4.0
RPL36	ribosomal protein L36	IPI00216237	6.8	1.8	5.5	5.5
RPL36AL	ribosomal protein L36a-like	IPI00056494	1.0	0.0	0.0	0.0
RPL37A	ribosomal protein L37a	IPI00414860	0.0	1.8	0.0	0.0
RPL38	ribosomal protein L38	IPI00215790	6.3	0.0	0.0	0.0
RPL4	ribosomal protein L4	IPI00003918	27.8	12.3	9.0	9.0
RPL5	ribosomal protein L5	IPI00000494	15.5	11.8	13.5	11.5
RPL6	ribosomal protein L6	IPI00329389	22.8	27.8	26.5	29.0
RPL7;RPL7P32	ribosomal protein L7	IPI00030179	15.5	11.8	17.5	18.5
RPL7A	ribosomal protein L7a	IPI00299573	17.5	15.0	17.5	8.5
RPL7AP27		IPI00075558	2.5	1.8	0.0	0.0
RPL7L1	ribosomal protein L7-like 1	IPI00456940	0.0	0.0	2.5	0.0
RPL8	ribosomal protein L8	IPI00012772	8.0	3.8	8.5	6.0
RPL9	ribosomal protein L9	IPI00031691	1.8	3.8	14.5	7.0
RPLP0	ribosomal protein, large, P0	IPI00008530	40.3	37.0	29.0	32.0
RPLP1	ribosomal protein, large, P1	IPI00008527	7.0	2.5	0.0	4.0
RPLP2	ribosomal protein, large, P2	IPI00008529	22.8	20.8	6.5	8.0

RPN1	ribophorin I	IPI00025874	2.3	0.0	2.0	0.0
RPS10	ribosomal protein S10	IPI00008438	4.3	1.8	0.0	7.0
RPS11	ribosomal protein S11	IPI00025091	5.3	0.0	4.5	3.0
RPS13	ribosomal protein S13	IPI00221089	12.0	6.3	11.5	6.5
RPS14	ribosomal protein S14	IPI00026271	7.5	2.3	9.5	6.0
RPS15	ribosomal protein S15	IPI00479058	1.0	0.0	2.0	0.0
RPS15A	ribosomal protein S15a	IPI00221091	6.0	3.5	6.5	4.0
RPS16	ribosomal protein S16	IPI00221092	9.0	4.8	16.5	15.5
RPS17	ribosomal protein S17	IPI00221093	5.8	1.8	10.5	0.0
RPS18;LOC100130553	ribosomal protein S18	IPI00013296	16.8	5.0	16.0	11.0
RPS19	ribosomal protein S19	IPI00215780	10.8	5.5	22.0	19.5
RPS2	ribosomal protein S2	IPI00013485	7.3	4.3	14.5	14.0
RPS20	ribosomal protein S20	IPI00012493	0.8	0.0	5.5	6.0
RPS23	ribosomal protein S23	IPI00218606	8.0	0.0	9.0	5.0
RPS24	ribosomal protein S24	IPI00029750	8.8	4.8	12.5	5.5
RPS25	ribosomal protein S25	IPI00012750	3.8	0.0	0.0	8.0
RPS27	ribosomal protein S27	IPI00397358	0.5	0.0	3.5	0.0
RPS27	ribosomal protein S27 (metallopanstimulin 1)	IPI00513971	0.0	0.0	2.5	0.0
RPS28	ribosomal protein S28	IPI00719622	0.0	0.0	3.5	0.0
RPS3	ribosomal protein S3	IPI00011253	20.3	7.3	33.5	28.5
RPS3A	ribosomal protein S3A	IPI00419880	15.3	4.5	22.0	8.5
RPS4X	ribosomal protein S4, X-linked	IPI00217030	18.0	8.3	25.5	17.5
RPS5	ribosomal protein S5	IPI00008433	0.0	0.5	4.0	0.0
RPS6	ribosomal protein S6	IPI00021840	8.0	4.0	9.0	6.0
RPS7	ribosomal protein S7	IPI00013415	1.3	6.8	8.5	5.5
RPS7P4		IPI00008293	1.5	0.0	3.5	1.5
RPS8	ribosomal protein S8	IPI00216587	10.3	7.3	8.0	4.5
RPS9	ribosomal protein S9	IPI00221088	3.0	5.5	19.5	8.0
RPSAP12	ribosomal protein SA pseudogene 12	IPI00398958	3.3	0.0	2.0	0.0
RRBP1	ribosome binding protein 1 homolog 180kDa (dog)	IPI00215743	55.3	4.8	6.0	0.0
RRP12	KIAA0690	IPI00101186	1.8	0.0	0.0	0.0
RSL1D1	ribosomal L1 domain containing 1	IPI00008708	0.5	0.0	0.0	0.0
S100A10	S100 calcium binding protein A10 (annexin II ligand, calpactin I, light polypeptide (p11))	IPI00183695	2.8	0.0	0.0	0.0
SAMD9	sterile alpha motif domain containing 9	IPI00217018	1.5	0.0	0.0	0.0
SAMHD1	SAM domain and HD domain 1	IPI00294739	2.3	0.5	0.0	0.0
SEMG1	semenogelin I	IPI00023020	7.0	0.0	0.0	0.0

SEMG2	semenogelin II	IPI00025415	2.5	0.0	0.0	0.0
SERBP1	SERPINE1 mRNA binding protein 1	IPI00410693	4.8	5.0	4.5	0.0
SF3A1	splicing factor 3a, subunit 1, 120kDa	IPI00017451	0.5	1.0	1.5	0.0
SF3B1	splicing factor 3b, subunit 1, 155kDa	IPI00026089	2.8	0.0	3.5	0.0
SF3B2	splicing factor 3b, subunit 2, 145kDa	IPI00221106	2.8	0.0	1.5	0.0
SFPQ	splicing factor proline/glutamine-rich (polypyrimidine tract binding protein associated)	IPI00010740	9.8	23.5	8.0	8.0
SFRS1	splicing factor, arginine/serine-rich 1 (splicing factor 2, alternate splicing factor)	IPI00215884	9.8	5.0	13.0	7.0
SFRS2	splicing factor, arginine/serine-rich 2	IPI00005978	3.0	0.0	0.0	1.5
SFRS3	splicing factor, arginine/serine-rich 3	IPI00010204	2.3	0.0	0.0	2.5
SFRS5	splicing factor, arginine/serine-rich 5	IPI00012341	2.5	0.0	0.0	0.0
SFRS6	splicing factor, arginine/serine-rich 6	IPI00012345	0.0	1.5	0.0	0.0
SFRS7	splicing factor, arginine/serine-rich 7, 35kDa	IPI00003377	3.5	2.5	4.0	4.0
SFXN1	sideroflexin 1	IPI00009368	0.0	2.5	0.0	0.0
SGPL1	sphingosine-1-phosphate lyase 1	IPI00099463	1.0	0.0	0.0	0.0
SKIV2L2	superkiller viralicidic activity 2-like 2 (S. cerevisiae)	IPI00647217	2.3	0.0	0.0	1.5
SLC25A1	solute carrier family 25 (mitochondrial carrier; citrate transporter), member 1	IPI00294159	1.3	0.0	0.0	0.0
SLC25A11	solute carrier family 25 (mitochondrial carrier; oxoglutarate carrier), member 11	IPI00219729	1.5	6.0	2.0	2.5
SLC25A12	solute carrier family 25 (mitochondrial carrier, Aralar), member 12	IPI00386271	1.0	0.0	0.0	0.0
SLC25A13	solute carrier family 25, member 13 (citrin)	IPI00007084	2.8	5.0	1.5	1.5
SLC25A3	solute carrier family 25 (mitochondrial carrier; phosphate carrier), member 3	IPI00022202	7.0	4.0	2.0	0.0
SLC25A5	solute carrier family 25 (mitochondrial carrier; adenine nucleotide translocator), member 5	IPI00007188	30.8	17.0	27.0	0.0
SLC25A6	solute carrier family 25 (mitochondrial carrier; adenine nucleotide translocator), member 4	IPI00291467	7.3	0.0	7.5	0.0
SLC2A1	solute carrier family 2 (facilitated glucose transporter), member 1	IPI00220194	0.8	0.0	0.0	0.0
SMARCA1	SWI/SNF related, matrix associated, actin dependent regulator of chromatin, subfamily a, member 1	IPI00216046	0.0	0.0	4.5	0.0
SMARCA5	SWI/SNF related, matrix associated, actin dependent regulator of chromatin, subfamily a, member 5	IPI00297211	0.0	0.0	1.5	0.0
SMC1A	SMC1 structural maintenance of chromosomes 1-like 1 (yeast)	IPI00291939	0.0	1.3	2.0	0.0

SMC2	SMC2 structural maintenance of chromosomes 2-like 1 (yeast)	IPI00007927	2.0	1.0	0.0	0.0
SMC3	chondroitin sulfate proteoglycan 6 (bamacan)	IPI00219420	0.0	0.0	6.5	0.0
SMC4	SMC4 structural maintenance of chromosomes 4-like 1 (yeast)	IPI00328298	1.8	1.3	0.0	0.0
SMCHD1	structural maintenance of chromosomes flexible hinge domain containing 1	IPI00465022	1.0	0.0	0.0	0.0
SND1	staphylococcal nuclease domain containing 1	IPI00140420	0.5	0.0	0.0	1.5
SNORA7A;RPL32	ribosomal protein L32	IPI00395998	5.0	0.0	0.0	0.0
SNRNP200	activating signal cointegrator 1 complex subunit 3-like 1	IPI00168235	0.0	2.5	0.0	0.0
SNRNP200	activating signal cointegrator 1 complex subunit 3-like 1	IPI00420014	2.3	1.3	3.0	0.0
SNRPD1	small nuclear ribonucleoprotein D1 polypeptide 16kDa	IPI00302850	0.0	0.0	0.0	2.5
SNRPD2	small nuclear ribonucleoprotein D2 polypeptide 16.5kDa	IPI00017963	2.8	0.0	0.0	3.5
SNRPE	small nuclear ribonucleoprotein polypeptide E	IPI00029266	1.5	0.0	0.0	0.0
SNRPG	small nuclear ribonucleoprotein polypeptide G	IPI00016572	1.5	0.0	2.0	0.0
SPATS2	spermatogenesis associated, serine-rich 2	IPI00329345	2.3	0.0	0.0	0.0
SPTAN1	spectrin, alpha, non-eythrocytic 1	IPI00744706	2.3	0.0	12.0	0.0
SPTBN1	spectrin, beta, non-erythrocytic 1	IPI00005614	1.8	0.0	13.5	0.0
SQRDL	sulfide quinone reductase-like (yeast)	IPI00009634	1.8	0.0	0.0	0.0
SRP14	signal recognition particle 14kDa (homologous Alu RNA binding protein)	IPI00293434	3.3	0.0	6.5	2.0
SRP9;SRP9L1	signal recognition particle 9kDa	IPI00216125	0.5	0.0	0.0	0.0
SRPK1	SFRS protein kinase 1	IPI00290439	0.0	0.0	0.0	3.5
SRPK2	SFRS protein kinase 2	IPI00333420	0.8	0.0	0.0	0.0
SRRM1	serine/arginine repetitive matrix 1	IPI00328293	1.0	0.0	0.0	0.0
SRRM2	serine/arginine repetitive matrix 2	IPI00782992	2.5	10.0	4.5	7.0
SRRT	ARS2 protein	IPI00220038	3.0	0.0	0.0	0.0
SSB	Sjogren syndrome antigen B (autoantigen La)	IPI00009032	1.8	0.0	0.0	3.0
SSBP1	single-stranded DNA binding protein 1	IPI00029744	0.0	0.0	14.0	1.5
SSRP1	structure specific recognition protein 1	IPI00005154	6.3	3.0	0.0	0.0
STAT1	signal transducer and activator of transcription 1, 91kDa	IPI00030781	0.8	0.0	0.0	0.0
STAU1	staufen, RNA binding protein, homolog 1 (Drosophila)	IPI00000001	1.0	0.5	0.0	0.0
STRAP	serine/threonine kinase receptor associated protein	IPI00294536	1.0	0.0	0.0	0.0
STT3B	STT3, subunit of the oligosaccharyltransferase complex, homolog B (S. cerevisiae)	IPI00152377	1.0	0.0	0.0	0.0
SUB1	SUB1 homolog (S. cerevisiae)	IPI00221222	3.0	1.8	0.0	0.0
SUPT16H	suppressor of Ty 16 homolog (S. cerevisiae)	IPI00026970	8.5	7.5	0.0	0.0
SYNCRIP	synaptotagmin binding, cytoplasmic RNA interacting protein	IPI00018140	12.3	3.3	11.5	13.5

TAF15	TAF15 RNA polymerase II, TATA box binding protein (TBP)-associated factor, 68kDa	IPI00020194	0.5	0.0	0.0	0.0
TARDBP	TAR DNA binding protein	IPI00025815	1.8	0.0	0.0	0.0
TBCB	cytoskeleton associated protein 1	IPI00293126	1.0	0.0	0.0	0.0
TBL2	transducin (beta)-like 2	IPI00000948	4.0	0.0	1.5	0.0
TCOF1	Treacher Collins-Franceschetti syndrome 1	IPI00165041	4.3	0.5	0.0	0.0
TCP1	t-complex 1	IPI00290566	70.8	36.0	0.0	0.0
TEX10	testis expressed sequence 10	IPI00549664	0.0	0.0	0.0	2.0
TFAM	transcription factor A, mitochondrial	IPI00020928	0.0	0.0	3.0	0.0
TGM2	transglutaminase 2 (C polypeptide, protein-glutamine-gamma-glutamyltransferase)	IPI00294578	5.0	0.0	0.0	0.0
THOC2	THO complex 2	IPI00158615	0.0	0.0	1.5	0.0
THOC4	THO complex 4	IPI00328840	2.0	0.0	0.0	2.5
THOC6	THO complex 6 homolog (Drosophila)	IPI00301252	0.0	0.0	2.0	0.0
THRAP3	thyroid hormone receptor associated protein 3	IPI00104050	0.0	2.0	0.0	0.0
TIMM50	translocase of inner mitochondrial membrane 50 homolog (yeast)	IPI00418497	3.3	0.0	0.0	0.0
TJP1	tight junction protein 1 (zona occludens 1)	IPI00216219	2.3	0.0	9.0	0.0
TMCO1	transmembrane and coiled-coil domains 1	IPI00026111	1.8	0.0	0.0	0.0
TMOD3	tropomodulin 3 (ubiquitous)	IPI00005087	1.3	0.0	0.0	0.0
TMPO	thymopoietin	IPI00030131	4.3	0.0	43.0	0.0
TMPO	thymopoietin	IPI00216230	1.8	0.0	34.0	0.0
TNFAIP2	tumor necrosis factor, alpha-induced protein 2	IPI00304866	2.0	0.0	0.0	0.0
TOP1	topoisomerase (DNA) I	IPI00413611	5.0	1.5	0.0	3.0
TOP2A	topoisomerase (DNA) II alpha 170kDa	IPI00178667	0.0	0.0	12.0	0.0
TOP2B	topoisomerase (DNA) II beta 180kDa	IPI00027280	0.0	0.0	7.5	0.0
TPM1	tropomyosin 1 (alpha)	IPI00000230	5.0	0.0	0.0	0.0
TRAM1	translocation associated membrane protein 1	IPI00219111	10.8	0.0	0.0	0.0
TRIM21	tripartite motif-containing 21	IPI00018971	26.0	2.8	0.0	0.0
TRIM25	tripartite motif-containing 25	IPI00029629	9.3	0.0	0.0	0.0
TRIM28	tripartite motif-containing 28	IPI00438229	3.3	0.0	0.0	0.0
TRIP12	thyroid hormone receptor interactor 12	IPI00032342	2.0	0.0	2.0	0.0
TROVE2	TROVE domain family, member 2	IPI00019450	2.0	2.5	2.5	2.0
TSR1	TSR1, 20S rRNA accumulation, homolog (yeast)	IPI00292894	6.3	0.0	4.5	2.5
TUBA1C	tubulin, alpha 6	IPI00166768	10.0	0.0	0.0	0.0
TUBA4A	tubulin, alpha 1 (testis specific)	IPI00007750	9.0	5.0	0.0	0.0
TUBB	tubulin, beta	IPI00011654	8.5	4.5	0.0	0.0
TUBB1	tubulin, beta 1	IPI00006510	1.8	0.8	2.5	0.0

TUBB2C	tubulin, beta 2C	IPI00007752	7.8	13.5	4.0	0.0
TUFM	Tu translation elongation factor, mitochondrial	IPI00027107	7.5	0.0	2.5	1.5
TXN	thioredoxin	IPI00216298	9.8	14.8	0.0	0.0
U2AF1	U2(RNU2) small nuclear RNA auxiliary factor 1	IPI00005613	3.5	0.0	0.0	0.0
U2AF2	U2 (RNU2) small nuclear RNA auxiliary factor 2	IPI00031556	4.3	3.8	0.0	0.0
UBC;RPS27A; UBB	ribosomal protein S27a	IPI00179330	7.5	1.5	13.0	0.0
UBTF	upstream binding transcription factor, RNA polymerase I	IPI00014533	2.5	0.0	0.0	1.5
UGDH	UDP-glucose dehydrogenase	IPI00031420	2.3	0.0	0.0	0.0
UNC45B	unc-45 homolog B (C. elegans)	IPI00217428	0.8	0.0	0.0	0.0
UPF1	UPF1 regulator of nonsense transcripts homolog (yeast)	IPI00034049	1.8	2.5	12.5	5.0
UQCRC2	ubiquinol-cytochrome c reductase core protein II	IPI00305383	3.5	0.0	0.0	0.0
USP10	ubiquitin specific peptidase 10	IPI00291946	1.3	3.0	6.5	7.0
USP39	ubiquitin specific peptidase 39	IPI00419844	0.0	0.0	0.0	2.5
UTP20;LOC653877	UTP20, small subunit (SSU) processome component, homolog (yeast)	IPI00004970	0.5	0.0	1.5	0.0
VIM	vimentin	IPI00418471	0.0	8.3	0.0	0.0
VRK1	vaccinia related kinase 1	IPI00019640	0.0	0.0	2.0	0.0
XPO1	exportin 1 (CRM1 homolog, yeast)	IPI00298961	0.5	1.0	0.0	0.0
XPOT	exportin, tRNA (nuclear export receptor for tRNAs)	IPI00306290	1.0	1.3	0.0	0.0
XRCC1	X-ray repair complementing defective repair in Chinese hamster cells 1	IPI00002564	0.0	0.0	1.5	0.0
XRCC5	X-ray repair complementing defective repair in Chinese hamster cells 5 (double-strand-break rejoining; Ku autoantigen, 80kDa)	IPI00220834	10.5	3.8	16.5	10.0
XRCC6	X-ray repair complementing defective repair in Chinese hamster cells 6 (Ku autoantigen, 70kDa)	IPI00644712	15.0	6.8	24.0	12.0
XRN2	5'-3' exoribonuclease 2	IPI00100151	12.8	1.5	6.5	2.0
YBX1	Y box binding protein 1	IPI00031812	9.0	2.0	5.0	4.0
YTHDC2	YTH domain containing 2	IPI00010200	2.5	1.0	1.5	0.0
YWHAQ	tyrosine 3-monooxygenase/tryptophan 5-monooxygenase activation protein, theta polypeptide	IPI00018146	2.3	0.0	0.0	0.0
ZC3H4		IPI00187011	2.0	0.0	0.0	0.0
ZC3HAV1	zinc finger CCCH-type, antiviral 1	IPI00332936	10.5	0.0	2.5	2.0
ZC3HAV1	zinc finger CCCH-type, antiviral 1	IPI00410067	1.5	0.0	0.0	0.0
ZCCHC3	zinc finger, CCHC domain containing 3	IPI00011550	0.0	0.0	0.0	5.5
ZNFX1	zinc finger, NFX1-type containing 1	IPI00165981	3.3	0.0	0.0	0.0
-	keratin 8-like 1	IPI00017870	2.3	0.0	21.0	0.0

-		IPI00069693	4.3	0.0	3.5	0.0
-		IPI00176692	3.8	0.0	0.0	4.0
-		IPI00394699	9.3	3.0	5.0	7.0

Table S4.2. Stress granule proteins that interact with arenavirus NP.
Cellular proteins with a known association with stress granules are listed, including the multiple ribosomal S proteins (RPS) that are constituents of the small ribosomal subunit.

Gene Symbol	Gene Description	IPI ID
CAPRIN1	Cell Cycle Associated Protein 1	IPI00783872
DDX6	DEAD (Asp-Glu-Ala-Asp) box polypeptide 6	IPI00030320
EIF3A	eukaryotic translation initiation factor 3, subunit 10 theta, 150/170kDa	IPI00029012
EIF3B	eukaryotic translation initiation factor 3, subunit 9 eta, 116kDa	IPI00396370
EIF3CL;EIF3C	eukaryotic translation initiation factor 3, subunit 8, 110kDa	IPI00016910
EIF3F	eukaryotic translation initiation factor 3, subunit 5 epsilon, 47kDa	IPI00654777
EIF3G	eukaryotic translation initiation factor 3, subunit 4 delta, 44kDa	IPI00290460
EIF3L	eukaryotic translation initiation factor 3, subunit 6 interacting protein	IPI00465233
EIF4A1;SNORA67	eukaryotic translation initiation factor 4A, isoform 1	IPI00025491
EIF4A3	DEAD (Asp-Glu-Ala-Asp) box polypeptide 48	IPI00009328
EIF4G1	eukaryotic translation initiation factor 4 gamma, 1	IPI00220365
EIF4G3	eukaryotic translation initiation factor 4 gamma, 3	IPI00328268
ELAVL1	ELAV (embryonic lethal, abnormal vision, Drosophila)-like 1 (Hu antigen R)	IPI00301936
FXR1	fragile X mental retardation, autosomal homolog 1	IPI00016249
FXR2	fragile X mental retardation, autosomal homolog 2	IPI00016250
G3BP1	Ras-GTPase-activating protein SH3-domain-binding protein	IPI00012442
G3BP2	Ras-GTPase activating protein SH3 domain-binding protein 2	IPI00009057
GNB2L1	guanine nucleotide binding protein (G protein), beta polypeptide 2-like 1	IPI00641950
PABPC1	poly(A) binding protein, cytoplasmic 1	IPI00008524
PABPC4	poly(A) binding protein, cytoplasmic 4 (inducible form)	IPI00012726
RPS10	ribosomal protein S10	IPI00008438
RPS11	ribosomal protein S11	IPI00025091
RPS13	ribosomal protein S13	IPI00221089
RPS14	ribosomal protein S14	IPI00026271
RPS15	ribosomal protein S15	IPI00479058
RPS15A	ribosomal protein S15a	IPI00221091
RPS16	ribosomal protein S16	IPI00221092
RPS17	ribosomal protein S17	IPI00221093
RPS18;LOC100130553	ribosomal protein S18	IPI00013296
RPS19	ribosomal protein S19	IPI00215780
RPS2	ribosomal protein S2	IPI00013485
RPS20	ribosomal protein S20	IPI00012493
RPS23	ribosomal protein S23	IPI00218606
RPS24	ribosomal protein S24	IPI00029750

RPS25	ribosomal protein S25	IPI00012750
RPS27	ribosomal protein S27 (metallopanstimulin 1)	IPI00513971
RPS27	ribosomal protein S27	IPI00397358
RPS28	ribosomal protein S28	IPI00719622
RPS3	ribosomal protein S3	IPI00011253
RPS3A	ribosomal protein S3A	IPI00419880
RPS4X	ribosomal protein S4, X-linked	IPI00217030
RPS5	ribosomal protein S5	IPI00008433
RPS6	ribosomal protein S6	IPI00021840
RPS7	ribosomal protein S7	IPI00013415
RPS7P4	ribosomal protein S7 pseudogene 4	IPI00008293
RPS8	ribosomal protein S8	IPI00216587
RPS9	ribosomal protein S9	IPI00221088
STAU1	staufen, RNA binding protein, homolog 1 (Drosophila)	IPI00000001
YBX1	Y box binding protein 1	IPI00031812

CHAPTER 5: SUMMARY OF FINDINGS AND FUTURE DIRECTIONS

5.1. Arenvirus genome transcription and replication

How viruses establish long lived persistent infections in their rodent hosts has been an important question motivating researchers since the discovery of this key feature of arenavirus infections. The methods researchers took toward examining these questions evolved along with cell culture and molecular biology technologies over time. Early work spearheaded by Hotchin *et al.* during the late 1960's and 1970's used cell culture models and measured viral release from infected cells as a primary metric of active infection. Tracking release of infectious particles from infected cultures and from individual cells isolated from those cultures over time led to the emergence of a model whereby arenavirus persistence was hypothesized to be repeated cycles of transient infections of individual cells within a large population of cells (Hotchin, 1973, 1974a, b).

During the 1980's and 1990's with the advent of more advanced molecular biology, gene cloning, and nucleic acid sequencing technologies, it became possible to probe the genetic events of arenavirus infection more directly. It was found that the arenaviruses had a bi-segmented, single-stranded, negative-sense genome (Leung et al., 1977). Researchers discovered that the arenaviruses possessed an interesting "ambisense" coding strategy where each genomic RNA segment encodes two genes but in opposite polarity (Auperin et al., 1984b; Salvato and Shimomaye, 1989; Southern et al., 1987). This suggested that these viruses to control the relative timing of specific gene expression events based on the polarity of the viral genes on the genomic RNA that would be delivered to

newly infected cells, which was subsequently demonstrated in cells infected with TCRV (Franze-Fernandez et al., 1987). It was shown that purified virus packaged both genomic and antigenomic RNA (Franze-Fernandez et al., 1987). Further, it was shown that smaller than expected genomic RNAs appear in infected cells over time, suggesting that viral RNAs may accumulate deletions following the initial phase of acute infection (Francis and Southern, 1988a, b).

These initial experiments led to the systematic exploration of the genetic nature of persistence in both *in vitro* and *in vivo* models of infection primarily by Southern *et al*. in the 1980's and 1990's. They observed that viral RNA is maintained in persistently infected mouse tissue and in persistently infected cell culture (Francis and Southern, 1988a, b). They suggested that the genetic signature of reduced arenavirus replication during persistence was due to the appearance of short deletions in the 3' and 5' UTR regions of the viral genomic RNAs, and that these deletions selectively inhibited gene transcription but permitted genome replication (Meyer and Southern, 1994). Lastly, they proposed that terminal deletions could be repaired by the viral polymerase leading to a rescue of viral genome that was both transcription and replication competent, thus allowing productive infection of cells to reset (Meyer and Southern, 1997). With this new data, the field seems to have largely forgotten the original work by Hotchin *et al*., with more recent reviews of the subject making no mention of his work on persistence, and focus instead on the work of Southern *et al*. to explain the mechanism by which infected cells become persistently infected (Labudova et al., 2016).

We were not convinced that the genetic model put forth by Southern *et al*. told the whole story for two primary reasons. First, Southern *et al*. suggest that persistently infected cells maintain high levels of genomic material during persistence and the expression of this genetic material is regulated by the presence or absence of terminal deletions that can be repaired. However, this does not completely match observations from the work of Hotchin *et al*., which showed that the vast majority of individual cells cloned from persistently infected cultures did not produce infectious virus (Hotchin, 1973). Second, Southern *et al*. suggest a repair mechanism of the genomic terminal deletions (from 2-38 base pairs in length) relying solely on addition of random non-templated nucleotides (Meyer and Southern, 1997). While, it is possible that this method could repair very short deletions of just a few lost bases, the probability that a viral polymerase could correctly repair longer deletions becomes vanishingly improbable. We thus hypothesized that neither the hypotheses of Hotchin or Southern were complete and that recent improvements in fluorescence in situ hybridization (FISH) permitting the labeling of single RNA molecules could bring these two models of persistence into harmony.

The work presented in Chapter 2 leveraged cutting-edge single-molecule RNA FISH (smFISH) and a high-throughput imaging and analysis pipeline to follow the kinetics of genome transcription and replication in single cells during a time course of infection from one hour to several weeks following initial infection. This work allowed us to confirm previous data showing the temporal separation between the expression of the viral NP and GPC genes providing further appreciation for the ability of this ambisense coding strategy

to temporally control viral gene expression programs (Franze-Fernandez et al., 1987). Further, though previous work indicated that S antigenomic RNA was packaged in LCMV virions, we never detected expression of GPC in the initial hours following infection suggesting that if antigenome is packaged in infectious virions, this RNA is transcriptionally incompetent upon initial RNP release into the cytoplasm of the newly infected cells (Franze-Fernandez et al., 1987). Additionally, data from Chapter 2 suggest that a subpopulation of viral particles do not package the L segment. This observation could suggest that recruitment of viral genetic material into budding virions is not a highly regulated process and virions packaging various suites of encapsidated RNAs could occur as has recently been demonstrated to be the case for Rift Valley fever virus using a similar smFISH approach (Wichgers Schreur and Kortekaas, 2016).

Strikingly, when we imaged thousands of individual cells from persistently infected cells over time, we noted that, at some time points in the persistent phase, the majority of cells in the population had no detectable viral RNAs and at other time points, close to 100% of cells in the population had detectable viral RNAs. Moreover, the transition between these states occurred cyclically over time similar the cycles of release of infectious virus during persistence as previously reported in the literature (Lehmann-Grube et al., 1969). This suggested to us that the model of Hotchin appears to be correct, and individual cells experience cyclic self-limited transient infections during persistence. While we do not question the veracity of the results of Southern *et al*., we suggest that the terminal deletions that occur in genomes during persistence most likely are a mechanism

employed by the virus to limit its own transcription and replication within a cell and to eventually clear active infection. We think it more likely that these cells become re-infected from virus produced by reservoir cells containing viral genomic RNA with intact 3' and 5' UTRs than the alternative where genomes in each persistently infected cell are repaired by the viral L polymerase through the addition of random non-templated bases.

A serious limitation of the study presented in Chapter 2 was the poor signal-to-noise ratio (SNR) of the FISH probe sets that were designed to specifically hybridize to the genomic (but not the viral mRNAs). This fact led us to use probe sets that targeted the viral mRNAs along with their respective genomic or antigenomic RNA species. The strength of this approach is that we can simultaneously visualize a greater range of viral RNA species in single infected cells. However, we lose the ability to definitively know the identity of the RNAs we are visualizing. Future work to improve the binding sensitivity of genome specific FISH probe sets would be worthwhile. We hypothesized that encapsidation of viral genomic and antigenomic RNA by nucleoprotein could prevent probe access and limit probe sensitivity. If this is the case, we believe that performing a brief protease digestion of fixed cells prior to FISH staining, as has previously been reported (Buxbaum et al., 2014), could allow us to overcome this technical barrier. The added insight gained from this would improve our ability to quantitatively characterize the rates of genome replication and even allow us to estimate rates of genome degradation. These data would be instrumental for the creation of a mathematical model describing the genetic events of arenavirus infection, a tool that could be invaluable to help predict how various mutations

to the viral L polymerase, Z protein, or NP (all known regulators of the viral gene expression program) could affect the kinetics of viral growth and/or alter the propensity of the virus to establish persistent infection.

5.2. Arenavirus Replication Complexes

As obligate intracellular parasites, viruses are unable to replicate independently of a host cell. It is becoming increasingly clear that a range of viruses create specific niches at subcellular sites to facilitate various steps of their life cycle (den Boon et al., 2010; Novoa et al., 2005a). Though comparatively little is known about how negative-strand viruses take advantage of cellular compartments, there are a few notable recent examples in the literature (Bruce et al., 2010; Novoa et al., 2005b). For example, it was shown that Influenza A virus (IAV) is dependent on Rab11 positive recycling endosomes for optimal replication (Amorim et al., 2011; Eisfeld et al., 2011). Two independent groups used smFISH to demonstrate that the Rab11 positive recycling endosome is a site where the different viral genomic segments assemble and are transported to the plasma membrane (Chou et al., 2013; Lakdawala et al., 2014).

We were motivated to explore what role membrane bound compartments may play in facilitating the life cycle of the prototypic arenavirus LCMV by several key findings: (i) the observation that IAV, a negative-strand virus with a segmented RNA genome, intimately relies upon a cellular membrane bound organelle, (ii) that the arenavirus NP localizes to defined punctate structures in the cytoplasm of infected cells (Baird et al., 2012; Knopp et al., 2015), and (iii) that arenaviral RNPs copurify with cellular

membrane (Baird et al., 2012). In Chapter 3, we used smFISH probe sets to specifically label and visualize S segment genomic and antigenomic RNA in cells acutely infected with LCMV. Viral genomic RNA localized in defined cytoplasmic foci whose size, brightness, and subcellular localization evolved over the course of acute infection. We confirmed that these cytoplasmic foci were sites of active viral replication by demonstrating the colocalization of S genomic RNA with S antigenomic RNA, its replicative complementary intermediate, and nucleoprotein, which encapsidates the genomic and antigenomic RNA. Taking advantage of a previously published siRNA screen showing that Rab5c was required for optimal LCMV growth (Panda et al., 2011), we showed that LCMV S genome concentrates at Rab5c positive early endosomal membranes in a proportion of infected cells. Thus, to address the question of how the virus may benefit from concentrating its genetic material at this endosomal membrane, we examined whether the virus was recruiting other viral structural components to this site. Indeed, we showed, that in a portion of infected cells there was a high degree of colocalization between the viral S genome and viral glycoprotein, suggesting that the virus may be utilizing intracellular membrane bound compartments as sites for the assembly of nascent viral components before being transported to the plasma membrane where budding occurs, a finding that contradicts the current dogma of arenavirus assembly.

Obvious next steps to confirm and extend these findings are to fully define all of the viral components that may be assembled at the intracellular sites identified in Chapter 3 and to characterize the mechanisms they use to traffic to the plasma membrane. Indeed,

elements of this work are currently underway. We have shown that the viral Z protein strongly colocalizes with Rab5c positive endosomes in a subpopulation of LCMV infected cells (C. M. Ziegler, E. A. Bruce, B. R. King, and J. Botten, Unpublished Data) providing some evidence that all the viral components pre-assemble intracellularly. Additionally, we have observed that disruption of the microtubule cytoskeleton by treating cells with nocodazole results in a dramatic redistribution of viral components in infected cells (B. R. King and J. Botten, Unpublished Data). However, infectious viral output is unaffected following microtubule disruption suggesting that the virus may employ redundant intracellular transport mechanisms permitting intracellular viral assembly and trafficking as has also recently been reported for IAV (Nturibi et al., 2017). It will be important to further explore the role of microtubules in trafficking and, additionally, to consider actin-dependent pathways as alternative routes the virus may take to reach the plasma membrane. To better understand the role played by Rab5c in promoting these processes, infection of cells should be performed in cells stably transduced with a drug-inducible dominant negative Rab5c. Imaging the localization of the different viral components following the disruption of Rab5c function will be highly informative and should include the Rab5a and Rab5b isoforms to determine the specificity of this pathway. Furthermore, immunogold EM studies to examine the ultrastructural detail of viral replication complexes in the cytoplasm of infected cells will provide additional critical insights.

5.3. The NP host-protein interactome

In addition to its canonical role of encapsidation of the viral single-stranded RNA genome, over the past years NP's multifunctional nature has become clear. Structural investigations have yielded insight into how the viral NP is able to bind viral RNA and has also revealed a C terminal domain with a previously unrecognized 3' to 5' exonuclease activity (Hastie et al., 2011a; Qi et al., 2010; Zhang et al., 2013). This has provided the first mechanistic explanation of how the arenavirus NP is able to inhibit the activation of the host type I IFN response. Other documented roles played by NP in the arenavirus life cycle are interaction with viral Z protein (Levingston Macleod et al., 2011; Ortiz-Riano et al., 2011), important for the recruitment of viral RNPs into budding virions (Levingston Macleod et al., 2011), regulation of apoptosis (Wolff et al., 2013a), modulation of innate immunity signaling (Pythoud et al., 2012; Rodrigo et al., 2012), and regulation of cellular translation by preventing the induction of stress granules in infected cells (Linero et al., 2011). By playing such diverse roles, in the life cycle, we had hypothesized that virus must interact with a wide range of cellular proteins, and that these protein-protein interactions would facilitate these, and potentially, as yet, undescribed steps of the viral life cycle.

In Chapter 4, we performed tandem mass spectrometry to identify the host cellular protein partners of the Old World arenavirus LCVM NP and the New World arenavirus JUNV. Here we established the first wide-scale interactome map of the host cell machinery engaged by diverse arenaviruses during infection, giving us an unprecedented view of the diverse biological functions performed by NP. Bioinformatic analysis of this protein-protein interaction map suggested that host cellular translation was a major

biological function that was highly associated with NP. This was fascinating in view of the observation that JUNV NP is able to prevent the assembly of stress granules in response to cellular stress in viral infected cells and cells ectopically expressing NP (Linero et al., 2011). Mining the data set for master regulators of cellular translation, we identified the eIF2α kinase PKR, a cytoplasmic sensor of dsRNA (most often a result of viral infection) that phosphorylates eIF2α and leads to global translation arrests.

The identification of this cellular factor led us to functionally characterize the NP-PKR interaction and the PKR signaling pathway in infected cells. We found that the NP-PKR interaction appeared to be stronger for JUNV NP than for LCMV NP. Additionally, we found that while PKR was activated in JUNV infected cells, it was unable to phosphorylate eIF2α, and translation rates remained normal. On the other hand, the weaker LCMV NP-PKR interaction was not as robust at interfering with PKR's activity. This result is interesting considering studies showing divergence in the ability of the Old World and New World NP's ability to prevent robust induction of type I IFN. LASV and LCMV NP were both shown to strongly inhibit the expression of type I IFN (Hastie et al., 2011a; Martinez-Sobrido et al., 2009; Martinez-Sobrido et al., 2007; Qi et al., 2010). However, JUNV, in one study, did not exhibit the same exonuclease activity (Zhang et al., 2013) and poorly inhibits type I IFN induction (Huang et al., 2012). This data fits with the model of PKR inhibition revealed in our study. We conjecture that because JUNV NP is unable to prevent the induction of type I IFN, it must develop additional strategies to limit the antiviral activity of individual IFN stimulated genes (e.g. PKR) to promote viral growth in

infected cells. The imperative of Old World arenavirus (e.g. LASV or LCMV) NP to inhibit the activity of various interferon stimulated genes may be relaxed as the expression of these genes remains low.

Moreover, the identification of PKR as a functionally important host protein partner of JUNV NP was interesting in light of the work showing that stress granule induction is inhibited in JUVN infected cells and in cells expressing JUNV NP (Linero et al., 2011). The large-scale map of arenavirus NP and host cellular protein interactions from this study has allowed us to hypothesize that the interaction between JUNV NP and PKR may be the mechanism utilized by the virus to maintain normal rates of translation in cells experiencing stress that would normally lead to the phosphorylation of eIF2α and the formation of stress granules.

The conclusion of Chapter 4 that JUNV NP is able to inhibit the activity of PKR has also been explored recently by Huang *et al.* (Huang et al., 2017). They show that infection with wild type JUNV strain Romero leads to both activation of PKR and eIF2α phosphorylation, in contrast to our result showing no eIF2α phosphorylation (Huang et al., 2017). Nevertheless, the authors demonstrated that in PKR deficient cells, WT JUNV replication was marginally impaired, suggesting that active PKR is not playing an antiviral role in New World arenavirus infections and may even be beneficial for viral growth (Huang et al., 2017). Additional work is needed to reconcile the results of our two studies and to explore the possibility that NP's engagement with PKR may be one mechanism by which JUNV C#1 is attenuated.

Beyond the ability of arenaviruses to modulate host cellular translation, this work has provided an important data set to the field that will serve as an important hypothesis generating tool in the future. Another tantalizing question that have emerged from our data, but remain to be tested in more detail, is how JUNV NP is involved in the balance between apoptosis initiation versus its inhibition. Interestingly, the most abundantly detected cellular protein partner of JUNV NP was apoptosis inducing factor 1 (AIFM1), which is released from the mitochondria following stress and is translocated to the nucleus where it is involved in nuclear fragmentation during the apoptotic program (Lipton and Bossy-Wetzel, 2002). It remains to be explored how this interaction may be critical in regulating the precarious balancing act between cell survival and apoptosis noted in studies of JUNV infected cells (Kolokoltsova et al., 2014; Wolff et al., 2013a).

5.4. Conclusion

In conclusion, I have had the opportunity to explore a broad range of questions related to the arenavirus life cycle during my dissertation. The principle that unifies the diverse projects described herein is how the virus utilizes specific subcellular niches and cellular machinery to promote effective viral transcription, replication, and additional steps of the virus life cycle. The work we have performed has allowed us to revisit long standing conflicting hypotheses of persistence, to develop new paradigms of how arenaviruses may rely on cellular organelles to promote assembly, and identify additional ways in which arenaviruses hijack cellular machinery to avoid an effective innate immune response. It is our hope that the conclusions of this work and the future studies it inspires will lead to the

development of novel antiviral therapeutics that can be used to better treat these devastating infections that touch so many people around the world.

5.5. References

Amorim, M.J., Bruce, E.A., Read, E.K., Foeglein, A., Mahen, R., Stuart, A.D., and Digard, P. (2011). A Rab11- and microtubule-dependent mechanism for cytoplasmic transport of influenza A virus viral RNA. Journal of virology *85*, 4143-4156.

Auperin, D.D., Romanowski, V., Galinski, M., and Bishop, D.H. (1984b). Sequencing studies of pichinde arenavirus S RNA indicate a novel coding strategy, an ambisense viral S RNA. Journal of virology *52*, 897-904.

Baird, N.L., York, J., and Nunberg, J.H. (2012). Arenavirus infection induces discrete cytosolic structures for RNA replication. Journal of virology *86*, 11301-11310.

Bruce, E.A., Digard, P., and Stuart, A.D. (2010). The Rab11 pathway is required for influenza A virus budding and filament formation. Journal of virology *84*, 5848-5859.

Buxbaum, A.R., Wu, B., and Singer, R.H. (2014). Single beta-actin mRNA detection in neurons reveals a mechanism for regulating its translatability. Science *343*, 419-422.

Chou, Y.Y., Heaton, N.S., Gao, Q., Palese, P., Singer, R.H., and Lionnet, T. (2013). Colocalization of different influenza viral RNA segments in the cytoplasm before viral budding as shown by single-molecule sensitivity FISH analysis. PLoS pathogens *9*, e1003358.

den Boon, J.A., Diaz, A., and Ahlquist, P. (2010). Cytoplasmic viral replication complexes. Cell host & microbe *8*, 77-85.

Eisfeld, A.J., Kawakami, E., Watanabe, T., Neumann, G., and Kawaoka, Y. (2011). RAB11A is essential for transport of the influenza virus genome to the plasma membrane. Journal of virology *85*, 6117-6126.

Francis, S.J., and Southern, P.J. (1988a). Deleted viral RNAs and lymphocytic choriomeningitis virus persistence in vitro. The Journal of general virology *69 (Pt 8)*, 1893-1902.

Francis, S.J., and Southern, P.J. (1988b). Molecular analysis of viral RNAs in mice persistently infected with lymphocytic choriomeningitis virus. Journal of virology *62*, 1251-1257.

Franze-Fernandez, M.T., Zetina, C., Iapalucci, S., Lucero, M.A., Bouissou, C., Lopez, R., Rey, O., Daheli, M., Cohen, G.N., and Zakin, M.M. (1987). Molecular structure and early events in the replication of Tacaribe arenavirus S RNA. Virus research *7*, 309-324.

Hastie, K.M., Kimberlin, C.R., Zandonatti, M.A., MacRae, I.J., and Saphire, E.O. (2011a). Structure of the Lassa virus nucleoprotein reveals a dsRNA-specific 3' to 5' exonuclease activity essential for immune suppression. Proceedings of the National Academy of Sciences of the United States of America *108*, 2396-2401.

Hotchin, J. (1973). Transient virus infection: spontaneous recovery mechanism of lymphocytic choriomeningitis virrus-infected cells. Nat New Biol *241*, 270-272.

Hotchin, J. (1974a). Cyclical phenomena in persistent virus infection. J Reticuloendothel Soc *15*, 304-311.

Hotchin, J. (1974b). The role of transient infection in arenavirus persistence. Prog Med Virol *18*, 81-93.

Huang, C., Kolokoltsova, O.A., Mateer, E.J., Koma, T., and Paessler, S. (2017). Highly pathogenic New World arenavirus infection activates the pattern recognition receptor PKR without attenuating virus replication in human cells. Journal of virology.

Huang, C., Kolokoltsova, O.A., Yun, N.E., Seregin, A.V., Poussard, A.L., Walker, A.G., Brasier, A.R., Zhao, Y., Tian, B., de la Torre, J.C., and Paessler, S. (2012). Junin virus infection activates the type I interferon pathway in a RIG-I-dependent manner. PLoS Negl Trop Dis *6*, e1659.

Knopp, K.A., Ngo, T., Gershon, P.D., and Buchmeier, M.J. (2015). Single nucleoprotein residue modulates arenavirus replication complex formation. mBio *6*, e00524-00515.

Kolokoltsova, O.A., Grant, A.M., Huang, C., Smith, J.K., Poussard, A.L., Tian, B., Brasier, A.R., Peters, C.J., Tseng, C.T., de la Torre, J.C., and Paessler, S. (2014). RIG-I enhanced interferon independent apoptosis upon Junin virus infection. PloS one *9*, e99610.

Labudova, M., Pastorek, J., and Pastorekova, S. (2016). Lymphocytic choriomeningitis virus: ways to establish and maintain non-cytolytic persistent infection. Acta Virol *60*, 15-26.

Lakdawala, S.S., Wu, Y., Wawrzusin, P., Kabat, J., Broadbent, A.J., Lamirande, E.W., Fodor, E., Altan-Bonnet, N., Shroff, H., and Subbarao, K. (2014). Influenza a virus assembly intermediates fuse in the cytoplasm. PLoS pathogens *10*, e1003971.

Lehmann-Grube, F., Slenczka, W., and Tees, R. (1969). A persistent and inapparent infection of L cells with the virus of lymphocytic choriomeningitis. The Journal of general virology *5*, 63-81.

Leung, W.C., Ghosh, H.P., and Rawls, W.E. (1977). Strandedness of Pichinde virus RNA. Journal of virology *22*, 235-237.

Levingston Macleod, J.M., D'Antuono, A., Loureiro, M.E., Casabona, J.C., Gomez, G.A., and Lopez, N. (2011). Identification of two functional domains within the arenavirus nucleoprotein. Journal of virology *85*, 2012-2023.

Linero, F.N., Thomas, M.G., Boccaccio, G.L., and Scolaro, L.A. (2011). Junin virus infection impairs stress-granule formation in Vero cells treated with arsenite via inhibition of eIF2alpha phosphorylation. The Journal of general virology *92*, 2889-2899.

Lipton, S.A., and Bossy-Wetzel, E. (2002). Dueling activities of AIF in cell death versus survival: DNA binding and redox activity. Cell *111*, 147-150.

Martinez-Sobrido, L., Emonet, S., Giannakas, P., Cubitt, B., Garcia-Sastre, A., and de la Torre, J.C. (2009). Identification of amino acid residues critical for the anti-interferon activity of the nucleoprotein of the prototypic arenavirus lymphocytic choriomeningitis virus. Journal of virology *83*, 11330-11340.

Martinez-Sobrido, L., Giannakas, P., Cubitt, B., Garcia-Sastre, A., and de la Torre, J.C. (2007). Differential inhibition of type I interferon induction by arenavirus nucleoproteins. Journal of virology *81*, 12696-12703.

Meyer, B.J., and Southern, P.J. (1994). Sequence heterogeneity in the termini of lymphocytic choriomeningitis virus genomic and antigenomic RNAs. Journal of virology *68*, 7659-7664.

Meyer, B.J., and Southern, P.J. (1997). A novel type of defective viral genome suggests a unique strategy to establish and maintain persistent lymphocytic choriomeningitis virus infections. Journal of virology *71*, 6757-6764.

Novoa, R.R., Calderita, G., Arranz, R., Fontana, J., Granzow, H., and Risco, C. (2005a). Virus factories: associations of cell organelles for viral replication and morphogenesis. Biology of the cell / under the auspices of the European Cell Biology Organization *97*, 147-172.

Novoa, R.R., Calderita, G., Cabezas, P., Elliott, R.M., and Risco, C. (2005b). Key Golgi factors for structural and functional maturation of bunyamwera virus. Journal of virology *79*, 10852-10863.

Nturibi, E., Bhagwat, A.R., Coburn, S., Myerburg, M.M., and Lakdawala, S.S. (2017). Intracellular Colocalization of Influenza Viral RNA and Rab11A Is Dependent upon Microtubule Filaments. Journal of virology *91*.

Ortiz-Riano, E., Cheng, B.Y., de la Torre, J.C., and Martinez-Sobrido, L. (2011). The C-Terminal Region of Lymphocytic Choriomeningitis Virus Nucleoprotein Contains Distinct

and Segregable Functional Domains Involved in NP-Z Interaction and Counteraction of the Type I Interferon Response. Journal of virology *85*, 13038-13048.

Panda, D., Das, A., Dinh, P.X., Subramaniam, S., Nayak, D., Barrows, N.J., Pearson, J.L., Thompson, J., Kelly, D.L., Ladunga, I., and Pattnaik, A.K. (2011). RNAi screening reveals requirement for host cell secretory pathway in infection by diverse families of negative-strand RNA viruses. Proceedings of the National Academy of Sciences of the United States of America *108*, 19036-19041.

Pythoud, C., Rodrigo, W.W., Pasqual, G., Rothenberger, S., Martinez-Sobrido, L., de la Torre, J.C., and Kunz, S. (2012). Arenavirus nucleoprotein targets interferon regulatory factor-activating kinase IKKepsilon. Journal of virology *86*, 7728-7738.

Qi, X., Lan, S., Wang, W., Schelde, L.M., Dong, H., Wallat, G.D., Ly, H., Liang, Y., and Dong, C. (2010). Cap binding and immune evasion revealed by Lassa nucleoprotein structure. Nature *468*, 779-783.

Rodrigo, W.W., Ortiz-Riano, E., Pythoud, C., Kunz, S., de la Torre, J.C., and Martinez-Sobrido, L. (2012). Arenavirus nucleoproteins prevent activation of nuclear factor kappa B. Journal of virology *86*, 8185-8197.

Salvato, M.S., and Shimomaye, E.M. (1989). The completed sequence of lymphocytic choriomeningitis virus reveals a unique RNA structure and a gene for a zinc finger protein. Virology *173*, 1-10.

Southern, P.J., Singh, M.K., Riviere, Y., Jacoby, D.R., Buchmeier, M.J., and Oldstone, M.B. (1987). Molecular characterization of the genomic S RNA segment from lymphocytic choriomeningitis virus. Virology *157*, 145-155.

Wichgers Schreur, P.J., and Kortekaas, J. (2016). Single-Molecule FISH Reveals Non-selective Packaging of Rift Valley Fever Virus Genome Segments. PLoS pathogens *12*, e1005800.

Wolff, S., Becker, S., and Groseth, A. (2013a). Cleavage of the Junin virus nucleoprotein serves a decoy function to inhibit the induction of apoptosis during infection. Journal of virology *87*, 224-233.

Zhang, Y., Li, L., Liu, X., Dong, S., Wang, W., Huo, T., Guo, Y., Rao, Z., and Yang, C. (2013). Crystal structure of Junin virus nucleoprotein. The Journal of general virology *94*, 2175-2183.

COMPREHENSIVE BIBLIOGRAPHY

Ambrosio, A., Saavedra, M., Mariani, M., Gamboa, G., and Maiza, A. (2011). Argentine hemorrhagic fever vaccines. Hum Vaccin *7*, 694-700.

Amorim, M.J., Bruce, E.A., Read, E.K., Foeglein, A., Mahen, R., Stuart, A.D., and Digard, P. (2011). A Rab11- and microtubule-dependent mechanism for cytoplasmic transport of influenza A virus viral RNA. Journal of virology *85*, 4143-4156.

Anderson, P., and Kedersha, N. (2008). Stress granules: the Tao of RNA triage. Trends Biochem Sci *33*, 141-150.

Armstrong, C., and Dickens, P.F. (1935). Benign Lymphocytic Choriomeningitis (Acute Aseptic Meningitis): A New Disease Entity. Public Health Reports *50*, 831-842.

Armstrong, C., and Lillie, R.D. (1934). Experimental Lymphocytic Choriomeningitis of Monkeys and Mice Produced by a Virus Encountered in Studies of the 1933 St. Louis Encephalitis Epidemic. Public Health Reports *49*, 1019-1027.

Armstrong, C., and Wooley, J.G. (1935). Studies on the Origin of a Newly Discovered Virus Which Causes Lymphocytic Choriomeningitis in Experimental Animals. Public Health Reports *50*, 537-541.

Arnaud, N., Dabo, S., Maillard, P., Budkowska, A., Kalliampakou, K.I., Mavromara, P., Garcin, D., Hugon, J., Gatignol, A., Akazawa, D., Wakita, T., and Meurs, E.F. (2010). Hepatitis C virus controls interferon production through PKR activation. PloS one *5*, e10575.

Auperin, D., Dimock, K., Cash, P., Rawls, W.E., Leung, W.C., and Bishop, D.H. (1982a). Analyses of the genomes of prototype pichinde arenavirus and a virulent derivative of Pichinde Munchique: evidence for sequence conservation at the 3' termini of their viral RNA species. Virology *116*, 363-367.

Auperin, D.D., Compans, R.W., and Bishop, D.H. (1982b). Nucleotide sequence conservation at the 3' termini of the virion RNA species of New World and Old World arenaviruses. Virology *121*, 200-203.

Auperin, D.D., Galinski, M., and Bishop, D.H. (1984a). The sequences of the N protein gene and intergenic region of the S RNA of pichinde arenavirus. Virology *134*, 208-219.

Auperin, D.D., Romanowski, V., Galinski, M., and Bishop, D.H. (1984b). Sequencing studies of pichinde arenavirus S RNA indicate a novel coding strategy, an ambisense viral S RNA. Journal of virology *52*, 897-904.

Baird, N.L., York, J., and Nunberg, J.H. (2012). Arenavirus infection induces discrete cytosolic structures for RNA replication. Journal of virology *86*, 11301-11310.

Ballif, B.A., Cao, Z., Schwartz, D., Carraway, K.L., 3rd, and Gygi, S.P. (2006). Identification of 14-3-3epsilon substrates from embryonic murine brain. J Proteome Res *5*, 2372-2379.

Battegay, M., Cooper, S., Althage, A., Banziger, J., Hengartner, H., and Zinkernagel, R.M. (1991). Quantification of lymphocytic choriomeningitis virus with an immunological focus assay in 24- or 96-well plates. J Virol Methods *33*, 191-198.

Bausch, D.G., Hadi, C.M., Khan, S.H., and Lertora, J.J. (2010). Review of the literature and proposed guidelines for the use of oral ribavirin as postexposure prophylaxis for Lassa fever. Clin Infect Dis *51*, 1435-1441.

Bergmann, M., Garcia-Sastre, A., Carnero, E., Pehamberger, H., Wolff, K., Palese, P., and Muster, T. (2000). Influenza virus NS1 protein counteracts PKR-mediated inhibition of replication. Journal of virology *74*, 6203-6206.

Bodewes, R., Raj, V.S., Kik, M.J., Schapendonk, C.M., Haagmans, B.L., Smits, S.L., and Osterhaus, A.D. (2014). Updated phylogenetic analysis of arenaviruses detected in boid snakes. Journal of virology *88*, 1399-1400.

Bonthius, D.J. (2009). Lymphocytic choriomeningitis virus: a prenatal and postnatal threat. Adv Pediatr *56*, 75-86.

Bonthius, D.J. (2012). Lymphocytic choriomeningitis virus: an underrecognized cause of neurologic disease in the fetus, child, and adult. Semin Pediatr Neurol *19*, 89-95.

Botten, J., King, B., Klaus, J., and Ziegler, C. (2013). Pathogenic Old World Arenaviruses. In Viral Hemorrhagic Fevers, S.K. Singh, and D. Ruzek, eds. (Boca Raton, Florida: CRC Press), pp. 233-259.

Bruce, E.A., Digard, P., and Stuart, A.D. (2010). The Rab11 pathway is required for influenza A virus budding and filament formation. Journal of virology *84*, 5848-5859.

Brunotte, L., Kerber, R., Shang, W., Hauer, F., Hass, M., Gabriel, M., Lelke, M., Busch, C., Stark, H., Svergun, D.I., Betzel, C., Perbandt, M., and Gunther, S. (2011). Structure of the Lassa virus nucleoprotein revealed by X-ray crystallography, small-angle X-ray scattering, and electron microscopy. The Journal of biological chemistry *286*, 38748-38756.

Bucci, C., Lutcke, A., Steele-Mortimer, O., Olkkonen, V.M., Dupree, P., Chiariello, M., Bruni, C.B., Simons, K., and Zerial, M. (1995). Co-operative regulation of endocytosis by three Rab5 isoforms. FEBS Lett *366*, 65-71.

Buchan, J.R., and Parker, R. (2009). Eukaryotic stress granules: the ins and outs of translation. Molecular cell *36*, 932-941.

Buchmeier, M.J. (2002). Arenaviruses: protein structure and function. Current topics in microbiology and immunology *262*, 159-173.

Buchmeier, M.J., Bowen, M.D., and Peters, C.J. (2001). *Arenaviridae*: The viruses and their replication. In Fields Virology, H.P.M. Knipe D. M., Griffin D. E., Lamb R. A., Martin M. A., Roizman B., Straus S. E., ed. (Philadelphia, PA: Lippincott Williams & Wilkins), pp. 1635-1668.

Buchmeier, M.J., de la Torre, J.C., and Peters, C.J. (2007). Arenaviridae: The Viruses and Their Replication. In Fields Virology, D.M. Knipe, P.M. Howley, D.E. Griffin, R.A. Lamb, M.A. Martin, B. Roizman, and S.E. Straus, eds. (Philadelphia: Wolters Kluwer Heath/Lippincott Williams & Wilkins), pp. 1791-1827.

Buchmeier, M.J., de la Torre, J.C., and Peters, C.J. (2013). Arenaviridae. In Fields Virology, D.M. Knipe, P.M. Howley, J.I. Cohen, D.E. Griffin, R.A. Lamb, M.A. Martin, V.R. Racaniello, and B. Roizman, eds. (Philadelphia, PA: Wolters Kluwer Heath/Lippincott Williams & Wilkins), pp. 1283-1303.

Buchmeier, M.J., Elder, J.H., and Oldstone, M.B. (1978). Protein structure of lymphocytic choriomeningitis virus: identification of the virus structural and cell associated polypeptides. Virology *89*, 133-145.

Buchmeier, M.J., Lewicki, H.A., Tomori, O., and Oldstone, M.B. (1981). Monoclonal antibodies to lymphocytic choriomeningitis and pichinde viruses: generation, characterization, and cross-reactivity with other arenaviruses. Virology *113*, 73-85.

Buchmeier, M.J., Welsh, R.M., Dutko, F.J., and Oldstone, M.B. (1980). The virology and immunobiology of lymphocytic choriomeningitis virus infection. Adv Immunol *30*, 275-331.

Buchmeier, M.J., and Zajac, A.J. (1999). Lymphocytic choriomeningitis virus. In Persistent viral infections, R. Ahmed, and I. Chen, eds. (Chichester ; New York: John Wiley & Sons), pp. x, 725 p.

Burns, J.W., and Buchmeier, M.J. (1991). Protein-protein interactions in lymphocytic choriomeningitis virus. Virology *183*, 620-629.

Burns, J.W., and Buchmeier, M.J. (1993). Glycoproteins of the arenaviruses. In The Arenaviridae, M.S. Salvato, ed. (New York: Plenum Press), pp. 17-35.

Burri, D.J., da Palma, J.R., Kunz, S., and Pasquato, A. (2012). Envelope glycoprotein of arenaviruses. Viruses *4*, 2162-2181.

Buxbaum, A.R., Wu, B., and Singer, R.H. (2014). Single beta-actin mRNA detection in neurons reveals a mechanism for regulating its translatability. Science *343*, 419-422.

Capul, A.A., Perez, M., Burke, E., Kunz, S., Buchmeier, M.J., and de la Torre, J.C. (2007). Arenavirus Z-glycoprotein association requires Z myristoylation but not functional RING or late domains. Journal of virology *81*, 9451-9460.

Carnec, X., Baize, S., Reynard, S., Diancourt, L., Caro, V., Tordo, N., and Bouloy, M. (2011). Lassa virus nucleoprotein mutants generated by reverse genetics induce a robust type I interferon response in human dendritic cells and macrophages. Journal of virology *85*, 12093-12097.

Carter, M.F., Biswal, N., and Rawls, W.E. (1973). Characterization of nucleic acid of pichinde virus. Journal of virology *11*, 61-68.

Carter, M.F., Biswal, N., and Rawls, W.E. (1974). Polymerase activity of Pichinde virus. Journal of virology *13*, 577-583.

Casabona, J.C., Levingston Macleod, J.M., Loureiro, M.E., Gomez, G.A., and Lopez, N. (2009). The RING domain and the L79 residue of Z protein are involved in both the rescue of nucleocapsids and the incorporation of glycoproteins into infectious chimeric arenavirus-like particles. Journal of virology *83*, 7029-7039.

Castelnuovo, M., Rahman, S., Guffanti, E., Infantino, V., Stutz, F., and Zenklusen, D. (2013). Bimodal expression of PHO84 is modulated by early termination of antisense transcription. Nat Struct Mol Biol *20*, 851-858.

Chan, Y.K., and Gack, M.U. (2016). Viral evasion of intracellular DNA and RNA sensing. Nature reviews. Microbiology *14*, 360-373.

Chang, H.W., Watson, J.C., and Jacobs, B.L. (1992). The E3L gene of vaccinia virus encodes an inhibitor of the interferon-induced, double-stranded RNA-dependent protein kinase. Proceedings of the National Academy of Sciences of the United States of America *89*, 4825-4829.

Charrel, R.N., Coutard, B., Baronti, C., Canard, B., Nougairede, A., Frangeul, A., Morin, B., Jamal, S., Schmidt, C.L., Hilgenfeld, R., Klempa, B., and de Lamballerie, X. (2011).

Arenaviruses and hantaviruses: from epidemiology and genomics to antivirals. Antiviral Res *90*, 102-114.

Charrel, R.N., and de Lamballerie, X. (2003). Arenaviruses other than Lassa virus. Antiviral Res *57*, 89-100.

Charrel, R.N., and de Lamballerie, X. (2010). Zoonotic aspects of arenavirus infections. Vet Microbiol *140*, 213-220.

Charrel, R.N., de Lamballerie, X., and Emonet, S. (2008). Phylogeny of the genus Arenavirus. Curr Opin Microbiol *11*, 362-368.

Charrel, R.N., Lemasson, J.J., Garbutt, M., Khelifa, R., De Micco, P., Feldmann, H., and de Lamballerie, X. (2003). New insights into the evolutionary relationships between arenaviruses provided by comparative analysis of small and large segment sequences. Virology *317*, 191-196.

Chou, Y.Y., Heaton, N.S., Gao, Q., Palese, P., Singer, R.H., and Lionnet, T. (2013). Colocalization of different influenza viral RNA segments in the cytoplasm before viral budding as shown by single-molecule sensitivity FISH analysis. PLoS pathogens *9*, e1003358.

Cornillez-Ty, C.T., Liao, L., Yates, J.R., 3rd, Kuhn, P., and Buchmeier, M.J. (2009). Severe acute respiratory syndrome coronavirus nonstructural protein 2 interacts with a host protein complex involved in mitochondrial biogenesis and intracellular signaling. Journal of virology *83*, 10314-10318.

Cornu, T.I., and de la Torre, J.C. (2001). RING finger Z protein of lymphocytic choriomeningitis virus (LCMV) inhibits transcription and RNA replication of an LCMV S-segment minigenome. Journal of virology *75*, 9415-9426.

Cornu, T.I., and de la Torre, J.C. (2002). Characterization of the arenavirus RING finger Z protein regions required for Z-mediated inhibition of viral RNA synthesis. Journal of virology *76*, 6678-6688.

D'Antuono, A., Loureiro, M.E., Foscaldi, S., Marino-Buslje, C., and Lopez, N. (2014). Differential contributions of tacaribe arenavirus nucleoprotein N-terminal and C-terminal residues to nucleocapsid functional activity. Journal of virology *88*, 6492-6505.

David, A., Dolan, B.P., Hickman, H.D., Knowlton, J.J., Clavarino, G., Pierre, P., Bennink, J.R., and Yewdell, J.W. (2012). Nuclear translation visualized by ribosome-bound nascent chain puromycylation. The Journal of cell biology *197*, 45-57.

den Boon, J.A., and Ahlquist, P. (2010). Organelle-like membrane compartmentalization of positive-strand RNA virus replication factories. Annual review of microbiology *64*, 241-256.

den Boon, J.A., Diaz, A., and Ahlquist, P. (2010). Cytoplasmic viral replication complexes. Cell host & microbe *8*, 77-85.

Donnelly, N., Gorman, A.M., Gupta, S., and Samali, A. (2013). The eIF2alpha kinases: their structures and functions. Cell Mol Life Sci *70*, 3493-3511.

Dutko, F.J., and Pfau, C.J. (1978). Arenavirus defective interfering particles mask the cell-killing potential of standard virus. The Journal of general virology *38*, 195-208.

Eichler, R., Strecker, T., Kolesnikova, L., ter Meulen, J., Weissenhorn, W., Becker, S., Klenk, H.D., Garten, W., and Lenz, O. (2004). Characterization of the Lassa virus matrix protein Z: electron microscopic study of virus-like particles and interaction with the nucleoprotein (NP). Virus research *100*, 249-255.

Eisfeld, A.J., Kawakami, E., Watanabe, T., Neumann, G., and Kawaoka, Y. (2011). RAB11A is essential for transport of the influenza virus genome to the plasma membrane. Journal of virology *85*, 6117-6126.

Ellenberg, P., Edreira, M., Lozano, M., and Scolaro, L. (2002). Synthesis and expression of viral antigens in Vero cells persistently infected with Junin virus. Archives of virology *147*, 1543-1557.

Ellenberg, P., Edreira, M., and Scolaro, L. (2004). Resistance to superinfection of Vero cells persistently infected with Junin virus. Archives of virology *149*, 507-522.

Emonet, S., Lemasson, J.J., Gonzalez, J.P., de Lamballerie, X., and Charrel, R.N. (2006). Phylogeny and evolution of old world arenaviruses. Virology *350*, 251-257.

Enria, D.A., Briggiler, A.M., and Sanchez, Z. (2008). Treatment of Argentine hemorrhagic fever. Antiviral Res *78*, 132-139.

Farber, F.E., and Rawls, W.E. (1975). Isolation of ribosome-like sturctures from Pichinde virus. The Journal of general virology *26*, 21-31.

Fehling, S.K., Lennartz, F., and Strecker, T. (2012). Multifunctional nature of the arenavirus RING finger protein Z. Viruses *4*, 2973-3011.

Ferron, F., Weber, F., de la Torre, J.C., and Reguera, J. (2017). Transcription and replication mechanisms of Bunyaviridae and Arenaviridae L proteins. Virus research *234*, 118-134.

Findlay, G.M., Alcock, N.S., and Stern, R.O. (1936). The Virus Ætiology Of One Form Of Lymphocytic Meningitis. Lancet *227*, 650-654.

Fischer, S.A., Graham, M.B., Kuehnert, M.J., Kotton, C.N., Srinivasan, A., Marty, F.M., Comer, J.A., Guarner, J., Paddock, C.D., DeMeo, D.L., Shieh, W.J., Erickson, B.R., Bandy, U., DeMaria, A., Jr., Davis, J.P., Delmonico, F.L., Pavlin, B., Likos, A., Vincent, M.J., Sealy, T.K., Goldsmith, C.S., Jernigan, D.B., Rollin, P.E., Packard, M.M., Patel, M., Rowland, C., Helfand, R.F., Nichol, S.T., Fishman, J.A., Ksiazek, T., Zaki, S.R., and Team, L.i.T.R.I. (2006). Transmission of lymphocytic choriomeningitis virus by organ transplantation. N Engl J Med *354*, 2235-2249.

Francis, S.J., and Southern, P.J. (1988a). Deleted viral RNAs and lymphocytic choriomeningitis virus persistence in vitro. The Journal of general virology *69 (Pt 8)*, 1893-1902.

Francis, S.J., and Southern, P.J. (1988b). Molecular analysis of viral RNAs in mice persistently infected with lymphocytic choriomeningitis virus. Journal of virology *62*, 1251-1257.

Francis, S.J., Southern, P.J., Valsamakis, A., and Oldstone, M.B. (1987). State of viral genome and proteins during persistent lymphocytic choriomeningitis virus infection. Current topics in microbiology and immunology *133*, 67-88.

Franze-Fernandez, M.T., Zetina, C., Iapalucci, S., Lucero, M.A., Bouissou, C., Lopez, R., Rey, O., Daheli, M., Cohen, G.N., and Zakin, M.M. (1987). Molecular structure and early events in the replication of Tacaribe arenavirus S RNA. Virus research *7*, 309-324.

Fuller-Pace, F.V., and Southern, P.J. (1988). Temporal analysis of transcription and replication during acute infection with lymphocytic choriomeningitis virus. Virology *162*, 260-263.

Fuller-Pace, F.V., and Southern, P.J. (1989). Detection of virus-specific RNA-dependent RNA polymerase activity in extracts from cells infected with lymphocytic choriomeningitis virus: in vitro synthesis of full-length viral RNA species. Journal of virology *63*, 1938-1944.

Garaigorta, U., and Chisari, F.V. (2009). Hepatitis C virus blocks interferon effector function by inducing protein kinase R phosphorylation. Cell host & microbe *6*, 513-522.

Garcia, M.A., Meurs, E.F., and Esteban, M. (2007). The dsRNA protein kinase PKR: virus and cell control. Biochimie *89*, 799-811.

Garcin, D., and Kolakofsky, D. (1990). A novel mechanism for the initiation of Tacaribe arenavirus genome replication. Journal of virology *64*, 6196-6203.

Garcin, D., and Kolakofsky, D. (1992). Tacaribe arenavirus RNA synthesis in vitro is primer dependent and suggests an unusual model for the initiation of genome replication. Journal of virology *66*, 1370-1376.

Goldberg, I.G., Allan, C., Burel, J.M., Creager, D., Falconi, A., Hochheiser, H., Johnston, J., Mellen, J., Sorger, P.K., and Swedlow, J.R. (2005). The Open Microscopy Environment (OME) Data Model and XML file: open tools for informatics and quantitative analysis in biological imaging. Genome Biol *6*, R47.

Goni, S.E., Iserte, J.A., Ambrosio, A.M., Romanowski, V., Ghiringhelli, P.D., and Lozano, M.E. (2006). Genomic features of attenuated Junin virus vaccine strain candidate. Virus genes *32*, 37-41.

Grant, A., Seregin, A., Huang, C., Kolokoltsova, O., Brasier, A., Peters, C., and Paessler, S. (2012). Junin virus pathogenesis and virus replication. Viruses *4*, 2317-2339.

Groseth, A., Wolff, S., Strecker, T., Hoenen, T., and Becker, S. (2010). Efficient budding of the tacaribe virus matrix protein z requires the nucleoprotein. Journal of virology *84*, 3603-3611.

Groskreutz, D.J., Babor, E.C., Monick, M.M., Varga, S.M., and Hunninghake, G.W. (2010). Respiratory Syncytial Virus Limits alpha Subunit of Eukaryotic Translation Initiation Factor 2 (eIF alpha) Phosphorylation to Maintain Translation and Viral Replication. Journal of Biological Chemistry *285*, 24023-24031.

Haist, K., Ziegler, C., and Botten, J. (2015). Strand-Specific Quantitative Reverse Transcription-Polymerase Chain Reaction Assay for Measurement of Arenavirus Genomic and Antigenomic RNAs. PloS one *10*, e0120043.

Harding, H.P., Zhang, Y., Bertolotti, A., Zeng, H., and Ron, D. (2000). Perk is essential for translational regulation and cell survival during the unfolded protein response. Molecular cell *5*, 897-904.

Harding, H.P., Zhang, Y., and Ron, D. (1999). Protein translation and folding are coupled by an endoplasmic-reticulum-resident kinase. Nature *397*, 271-274.

Harmon, B., Kozina, C., Maar, D., Carpenter, T.S., Branda, C.S., Negrete, O.A., and Carson, B.D. (2013). Identification of critical amino acids within the nucleoprotein of Tacaribe virus important for anti-interferon activity. The Journal of biological chemistry *288*, 8702-8711.

Harnish, D.G., Leung, W.C., and Rawls, W.E. (1981). Characterization of polypeptides immunoprecipitable from Pichinde virus-infected BHK-21 cells. Journal of virology *38*, 840-848.

Hass, M., Westerkofsky, M., Muller, S., Becker-Ziaja, B., Busch, C., and Gunther, S. (2006). Mutational analysis of the lassa virus promoter. Journal of virology *80*, 12414-12419.

Hastie, K.M., Kimberlin, C.R., Zandonatti, M.A., MacRae, I.J., and Saphire, E.O. (2011a). Structure of the Lassa virus nucleoprotein reveals a dsRNA-specific 3' to 5' exonuclease activity essential for immune suppression. Proceedings of the National Academy of Sciences of the United States of America *108*, 2396-2401.

Hastie, K.M., Liu, T., Li, S., King, L.B., Ngo, N., Zandonatti, M.A., Woods, V.L., Jr., de la Torre, J.C., and Saphire, E.O. (2011b). Crystal structure of the Lassa virus nucleoprotein-RNA complex reveals a gating mechanism for RNA binding. Proceedings of the National Academy of Sciences of the United States of America *108*, 19365-19370.

Hatada, E., Saito, S., and Fukuda, R. (1999). Mutant influenza viruses with a defective NS1 protein cannot block the activation of PKR in infected cells. Journal of virology *73*, 2425-2433.

Hotchin, J. (1973). Transient virus infection: spontaneous recovery mechanism of lymphocytic choriomeningitis virrus-infected cells. Nat New Biol *241*, 270-272.

Hotchin, J. (1974a). Cyclical phenomena in persistent virus infection. J Reticuloendothel Soc *15*, 304-311.

Hotchin, J. (1974b). The role of transient infection in arenavirus persistence. Prog Med Virol *18*, 81-93.

Hotchin, J., Kinch, W., Benson, L., and Sikora, E. (1975). Role of substrains in persistent lymphocytic choriomeningitis virus infection. Bull World Health Organ *52*, 457-463.

Howard, C.R., and Buchmeier, M.J. (1983). A protein kinase activity in lymphocytic choriomeningitis virus and identification of the phosphorylated product using monoclonal antibody. Virology *126*, 538-547.

Huang, A.S. (1973). Defective interfering viruses. Annual review of microbiology *27*, 101-117.

Huang, A.S., and Baltimore, D. (1970). Defective viral particles and viral disease processes. Nature *226*, 325-327.

Huang, C., Kolokoltsova, O.A., Mateer, E.J., Koma, T., and Paessler, S. (2017). Highly pathogenic New World arenavirus infection activates the pattern recognition receptor PKR without attenuating virus replication in human cells. Journal of virology.

Huang, C., Kolokoltsova, O.A., Yun, N.E., Seregin, A.V., Poussard, A.L., Walker, A.G., Brasier, A.R., Zhao, Y., Tian, B., de la Torre, J.C., and Paessler, S. (2012). Junin virus infection activates the type I interferon pathway in a RIG-I-dependent manner. PLoS Negl Trop Dis *6*, e1659.

Huang, D.W., Sherman, B.T., and Lempicki, R.A. (2009a). Bioinformatics enrichment tools: paths toward the comprehensive functional analysis of large gene lists. Nucleic Acids Res *37*, 1-13.

Huang, D.W., Sherman, B.T., and Lempicki, R.A. (2009b). Systematic and integrative analysis of large gene lists using DAVID bioinformatics resources. Nat Protoc *4*, 44-57.

Huang, Q., Shao, J., Lan, S., Zhou, Y., Xing, J., Dong, C., Liang, Y., and Ly, H. (2015). In vitro and in vivo characterizations of pichinde viral nucleoprotein exoribonuclease functions. Journal of virology *89*, 6595-6607.

Iapalucci, S., Chernavsky, A., Rossi, C., Burgin, M.J., and Franze-Fernandez, M.T. (1994). Tacaribe virus gene expression in cytopathic and non-cytopathic infections. Virology *200*, 613-622.

Iapalucci, S., Lopez, N., and Franze-Fernandez, M.T. (1991). The 3' end termini of the Tacaribe arenavirus subgenomic RNAs. Virology *182*, 269-278.

ICTV, A.S.G. (2014a). Create a new genus, Reptarenavirus, comprising three new species in the family
Arenaviridae. (Internation Committee on the Taxonomy of Viruses).

ICTV, A.S.G. (2014b). Rename one (1) genus and twenty-five (25) species in the family Arenaviridae. (International Committee on Taxonomy of Viruses
).

Iwasaki, M., Cubitt, B., Sullivan, B.M., and de la Torre, J.C. (2016). The High Degree of Sequence Plasticity of the Arenavirus Noncoding Intergenic Region (IGR) Enables the Use of a Nonviral Universal Synthetic IGR To Attenuate Arenaviruses. Journal of virology *90*, 3187-3197.

Iwasaki, M., Ngo, N., Cubitt, B., and de la Torre, J.C. (2015). Efficient Interaction between Arenavirus Nucleoprotein (NP) and RNA-Dependent RNA Polymerase (L) Is Mediated by the Virus Nucleocapsid (NP-RNA) Template. Journal of virology *89*, 5734-5738.

Jacamo, R., Lopez, N., Wilda, M., and Franze-Fernandez, M.T. (2003). Tacaribe virus Z protein interacts with the L polymerase protein to inhibit viral RNA synthesis. Journal of virology *77*, 10383-10393.

Jiang, X., Huang, Q., Wang, W., Dong, H., Ly, H., Liang, Y., and Dong, C. (2013). Structures of arenaviral nucleoproteins with triphosphate dsRNA reveal a unique mechanism of immune suppression. The Journal of biological chemistry *288*, 16949-16959.

Kamentsky, L., Jones, T.R., Fraser, A., Bray, M.A., Logan, D.J., Madden, K.L., Ljosa, V., Rueden, C., Eliceiri, K.W., and Carpenter, A.E. (2011). Improved structure, function and compatibility for CellProfiler: modular high-throughput image analysis software. Bioinformatics *27*, 1179-1180.

Kawai, T., and Akira, S. (2008). Toll-like receptor and RIG-I-like receptor signaling. Ann N Y Acad Sci *1143*, 1-20.

Kerber, R., Rieger, T., Busch, C., Flatz, L., Pinschewer, D.D., Kummerer, B.M., and Gunther, S. (2011). Cross-species analysis of the replication complex of old world arenaviruses reveals two nucleoprotein sites involved in L protein function. Journal of virology *85*, 12518-12528.

King, B.R., Hershkowitz, D., Eisenhauer, P.L., Weir, M.E., Ziegler, C.M., Russo, J., Bruce, E.A., Ballif, B.A., and Botten, J. (2017). A Map of the Arenavirus Nucleoprotein-Host Protein Interactome Reveals that Junin Virus Selectively Impairs the Antiviral Activity of Double-Stranded RNA-Activated Protein Kinase (PKR). Journal of virology *91*.

Klaus, J.P., Eisenhauer, P., Russo, J., Mason, A.B., Do, D., King, B., Taatjes, D., Cornillez-Ty, C., Boyson, J.E., Thali, M., Zheng, C., Liao, L., Yates, J.R., 3rd, Zhang, B., Ballif, B.A., and Botten, J.W. (2013). The intracellular cargo receptor ERGIC-53 is required for the production of infectious arenavirus, coronavirus, and filovirus particles. Cell host & microbe *14*, 522-534.

Knopp, K.A., Ngo, T., Gershon, P.D., and Buchmeier, M.J. (2015). Single nucleoprotein residue modulates arenavirus replication complex formation. mBio *6*, e00524-00515.

Kolokoltsova, O.A., Grant, A.M., Huang, C., Smith, J.K., Poussard, A.L., Tian, B., Brasier, A.R., Peters, C.J., Tseng, C.T., de la Torre, J.C., and Paessler, S. (2014). RIG-I enhanced interferon independent apoptosis upon Junin virus infection. PloS one *9*, e99610.

Kranzusch, P.J., and Whelan, S.P. (2011). Arenavirus Z protein controls viral RNA synthesis by locking a polymerase-promoter complex. Proceedings of the National Academy of Sciences of the United States of America *108*, 19743-19748.

Labudova, M., Pastorek, J., and Pastorekova, S. (2016). Lymphocytic choriomeningitis virus: ways to establish and maintain non-cytolytic persistent infection. Acta Virol *60*, 15-26.

Labudova, M., Tomaskova, J., Skultety, L., Pastorek, J., and Pastorekova, S. (2009). The nucleoprotein of lymphocytic choriomeningitis virus facilitates spread of persistent infection through stabilization of the keratin network. Journal of virology *83*, 7842-7849.

Lakdawala, S.S., Wu, Y., Wawrzusin, P., Kabat, J., Broadbent, A.J., Lamirande, E.W., Fodor, E., Altan-Bonnet, N., Shroff, H., and Subbarao, K. (2014). Influenza a virus assembly intermediates fuse in the cytoplasm. PLoS pathogens *10*, e1003971.

Lan, S., McLay, L., Aronson, J., Ly, H., and Liang, Y. (2008). Genome comparison of virulent and avirulent strains of the Pichinde arenavirus. Archives of virology *153*, 1241-1250.

Langland, J.O., and Jacobs, B.L. (2002). The role of the PKR-inhibitory genes, E3L and K3L, in determining vaccinia virus host range. Virology *299*, 133-141.

Lee, K.J., Novella, I.S., Teng, M.N., Oldstone, M.B., and de La Torre, J.C. (2000). NP and L proteins of lymphocytic choriomeningitis virus (LCMV) are sufficient for efficient transcription and replication of LCMV genomic RNA analogs. Journal of virology *74*, 3470-3477.

Lehmann-Grube, F. (1967). A carrier state of lymphocytic choriomeningitis virus in L cell cultures. Nature *213*, 770-773.

Lehmann-Grube, F. (1971). Lymphocytic choriomeningitis virus, Vol 10 (Wien: Springer-Verlag).

Lehmann-Grube, F., Martinez Peralta, L.M., Bruns, M., and Lohler, J. (1983). Persistent infection of mice with the lymphocytic choriomeningitis virus. In Virus-host interactions, receptors, persistence, and neurological diseases, H. Fraenkel-Conrat, and R.R. Wagner, eds. (New York: Plenum Press), pp. 43-103.

Lehmann-Grube, F., Popescu, M., Schaefer, H., and Gschwender, H.H. (1975). LCM virus infection of cells in vitro. Bull World Health Organ *52*, 443-456.

Lehmann-Grube, F., Slenczka, W., and Tees, R. (1969). A persistent and inapparent infection of L cells with the virus of lymphocytic choriomeningitis. The Journal of general virology *5*, 63-81.

Lennartz, F., Hoenen, T., Lehmann, M., Groseth, A., and Garten, W. (2013). The role of oligomerization for the biological functions of the arenavirus nucleoprotein. Archives of virology *158*, 1895-1905.

Leung, W.C., Ghosh, H.P., and Rawls, W.E. (1977). Strandedness of Pichinde virus RNA. Journal of virology *22*, 235-237.

Leung, W.C., and Rawls, W.E. (1977). Virion-associated ribosomes are not required for the replication of Pichinde virus. Virology *81*, 174-176.

Levingston Macleod, J.M., D'Antuono, A., Loureiro, M.E., Casabona, J.C., Gomez, G.A., and Lopez, N. (2011). Identification of two functional domains within the arenavirus nucleoprotein. Journal of virology *85*, 2012-2023.

Li, S., Min, J.Y., Krug, R.M., and Sen, G.C. (2006). Binding of the influenza A virus NS1 protein to PKR mediates the inhibition of its activation by either PACT or double-stranded RNA. Virology *349*, 13-21.

Lindquist, M.E., Mainou, B.A., Dermody, T.S., and Crowe, J.E., Jr. (2011). Activation of protein kinase R is required for induction of stress granules by respiratory syncytial virus but dispensable for viral replication. Virology *413*, 103-110.

Linero, F., Welnowska, E., Carrasco, L., and Scolaro, L. (2013). Participation of eIF4F complex in Junin virus infection: blockage of eIF4E does not impair virus replication. Cellular microbiology *15*, 1766-1782.

Linero, F.N., Thomas, M.G., Boccaccio, G.L., and Scolaro, L.A. (2011). Junin virus infection impairs stress-granule formation in Vero cells treated with arsenite via inhibition of eIF2alpha phosphorylation. The Journal of general virology *92*, 2889-2899.

Lipton, S.A., and Bossy-Wetzel, E. (2002). Dueling activities of AIF in cell death versus survival: DNA binding and redox activity. Cell *111*, 147-150.

Lopez, N., and Franze-Fernandez, M.T. (2007). A single stem-loop structure in Tacaribe arenavirus intergenic region is essential for transcription termination but is not required for a correct initiation of transcription and replication. Virus research *124*, 237-244.

Lopez, N., Jacamo, R., and Franze-Fernandez, M.T. (2001). Transcription and RNA replication of tacaribe virus genome and antigenome analogs require N and L proteins: Z protein is an inhibitor of these processes. Journal of virology *75*, 12241-12251.

Lu, Y., Wambach, M., Katze, M.G., and Krug, R.M. (1995). Binding of the influenza virus NS1 protein to double-stranded RNA inhibits the activation of the protein kinase that phosphorylates the elF-2 translation initiation factor. Virology *214*, 222-228.

Macneil, A., Stroher, U., Farnon, E., Campbell, S., Cannon, D., Paddock, C.D., Drew, C.P., Kuehnert, M., Knust, B., Gruenenfelder, R., Zaki, S.R., Rollin, P.E., Nichol, S.T., and Team, L.T.I. (2012). Solid organ transplant-associated lymphocytic choriomeningitis, United States, 2011. Emerg Infect Dis *18*, 1256-1262.

Maeto, C.A., Knott, M.E., Linero, F.N., Ellenberg, P.C., Scolaro, L.A., and Castilla, V. (2011). Differential effect of acute and persistent Junin virus infections on the nucleo-cytoplasmic trafficking and expression of heterogeneous nuclear ribonucleoproteins type A and B. The Journal of general virology *92*, 2181-2190.

Marq, J.B., Kolakofsky, D., and Garcin, D. (2010). Unpaired 5' ppp-nucleotides, as found in arenavirus double-stranded RNA panhandles, are not recognized by RIG-I. The Journal of biological chemistry *285*, 18208-18216.

Martinez-Sobrido, L., Emonet, S., Giannakas, P., Cubitt, B., Garcia-Sastre, A., and de la Torre, J.C. (2009). Identification of amino acid residues critical for the anti-interferon activity of the nucleoprotein of the prototypic arenavirus lymphocytic choriomeningitis virus. Journal of virology *83*, 11330-11340.

Martinez-Sobrido, L., Giannakas, P., Cubitt, B., Garcia-Sastre, A., and de la Torre, J.C. (2007). Differential inhibition of type I interferon induction by arenavirus nucleoproteins. Journal of virology *81*, 12696-12703.

Martinez-Sobrido, L., Zuniga, E.I., Rosario, D., Garcia-Sastre, A., and de la Torre, J.C. (2006). Inhibition of the type I interferon response by the nucleoprotein of the prototypic arenavirus lymphocytic choriomeningitis virus. Journal of virology *80*, 9192-9199.

Martinez, M.G., Forlenza, M.B., and Candurra, N.A. (2009). Involvement of cellular proteins in Junin arenavirus entry. Biotechnology journal *4*, 866-870.

Matrosovich, M., Matrosovich, T., Garten, W., and Klenk, H.D. (2006). New low-viscosity overlay medium for viral plaque assays. Virol J *3*, 63.

Matthaei, M., Budt, M., and Wolff, T. (2013). Highly pathogenic H5N1 influenza A virus strains provoke heterogeneous IFN-alpha/beta responses that distinctively affect viral propagation in human cells. PloS one *8*, e56659.

McCormick, J.B., King, I.J., Webb, P.A., Scribner, C.L., Craven, R.B., Johnson, K.M., Elliott, L.H., and Belmont-Williams, R. (1986). Lassa fever. Effective therapy with ribavirin. N Engl J Med *314*, 20-26.

McEwen, E., Kedersha, N., Song, B., Scheuner, D., Gilks, N., Han, A., Chen, J.J., Anderson, P., and Kaufman, R.J. (2005). Heme-regulated inhibitor kinase-mediated phosphorylation of eukaryotic translation initiation factor 2 inhibits translation, induces stress granule formation, and mediates survival upon arsenite exposure. The Journal of biological chemistry *280*, 16925-16933.

Meyer, B.J., de la Torre, J.C., and Southern, P.J. (2002). Arenaviruses: genomic RNAs, transcription, and replication. Current topics in microbiology and immunology *262*, 139-157.

Meyer, B.J., and Southern, P.J. (1993). Concurrent sequence analysis of 5' and 3' RNA termini by intramolecular circularization reveals 5' nontemplated bases and 3' terminal heterogeneity for lymphocytic choriomeningitis virus mRNAs. Journal of virology *67*, 2621-2627.

Meyer, B.J., and Southern, P.J. (1994). Sequence heterogeneity in the termini of lymphocytic choriomeningitis virus genomic and antigenomic RNAs. Journal of virology *68*, 7659-7664.

Meyer, B.J., and Southern, P.J. (1997). A novel type of defective viral genome suggests a unique strategy to establish and maintain persistent lymphocytic choriomeningitis virus infections. Journal of virology *71*, 6757-6764.

Momose, F., Sekimoto, T., Ohkura, T., Jo, S., Kawaguchi, A., Nagata, K., and Morikawa, Y. (2011). Apical transport of influenza A virus ribonucleoprotein requires Rab11-positive recycling endosome. PloS one *6*, e21123.

Morin, B., Coutard, B., Lelke, M., Ferron, F., Kerber, R., Jamal, S., Frangeul, A., Baronti, C., Charrel, R., de Lamballerie, X., Vonrhein, C., Lescar, J., Bricogne, G., Gunther, S., and Canard, B. (2010). The N-terminal domain of the arenavirus L protein is an RNA endonuclease essential in mRNA transcription. PLoS pathogens *6*, e1001038.

Mueller, F., Senecal, A., Tantale, K., Marie-Nelly, H., Ly, N., Collin, O., Basyuk, E., Bertrand, E., Darzacq, X., and Zimmer, C. (2013). FISH-quant: automatic counting of transcripts in 3D FISH images. Nature methods *10*, 277-278.

Murphy, F.A. (1975). Arenavirus taxonomy: a review. Bull World Health Organ *52*, 389-391.

Nielsen, E., Severin, F., Backer, J.M., Hyman, A.A., and Zerial, M. (1999). Rab5 regulates motility of early endosomes on microtubules. Nature cell biology *1*, 376-382.

Novoa, R.R., Calderita, G., Arranz, R., Fontana, J., Granzow, H., and Risco, C. (2005a). Virus factories: associations of cell organelles for viral replication and morphogenesis. Biology of the cell / under the auspices of the European Cell Biology Organization *97*, 147-172.

Novoa, R.R., Calderita, G., Cabezas, P., Elliott, R.M., and Risco, C. (2005b). Key Golgi factors for structural and functional maturation of bunyamwera virus. Journal of virology *79*, 10852-10863.

Nturibi, E., Bhagwat, A.R., Coburn, S., Myerburg, M.M., and Lakdawala, S.S. (2017). Intracellular Colocalization of Influenza Viral RNA and Rab11A Is Dependent upon Microtubule Filaments. Journal of virology *91*.

Oldstone, M.B. (1998). Viral persistence: mechanisms and consequences. Curr Opin Microbiol *1*, 436-441.

Oldstone, M.B., and Buchmeier, M.J. (1982). Restricted expression of viral glycoprotein in cells of persistently infected mice. Nature *300*, 360-362.

Ortiz-Riano, E., Cheng, B.Y., de la Torre, J.C., and Martinez-Sobrido, L. (2011). The C-Terminal Region of Lymphocytic Choriomeningitis Virus Nucleoprotein Contains Distinct and Segregable Functional Domains Involved in NP-Z Interaction and Counteraction of the Type I Interferon Response. Journal of virology *85*, 13038-13048.

Ortiz-Riano, E., Cheng, B.Y., de la Torre, J.C., and Martinez-Sobrido, L. (2012). Self-association of Lymphocytic Choriomeningitis Virus Nucleoprotein is mediated by its N-terminal region and is not required for its anti-interferon function. Journal of virology.

Panda, D., Das, A., Dinh, P.X., Subramaniam, S., Nayak, D., Barrows, N.J., Pearson, J.L., Thompson, J., Kelly, D.L., Ladunga, I., and Pattnaik, A.K. (2011). RNAi screening reveals requirement for host cell secretory pathway in infection by diverse families of negative-strand RNA viruses. Proceedings of the National Academy of Sciences of the United States of America *108*, 19036-19041.

Pannetier, D., Faure, C., Georges-Courbot, M.C., Deubel, V., and Baize, S. (2004). Human macrophages, but not dendritic cells, are activated and produce alpha/beta interferons in response to Mopeia virus infection. Journal of virology *78*, 10516-10524.

Pannetier, D., Reynard, S., Russier, M., Carnec, X., and Baize, S. (2014). Production of CXC and CC chemokines by human antigen-presenting cells in response to Lassa virus or closely related immunogenic viruses, and in cynomolgus monkeys with lassa fever. PLoS Negl Trop Dis *8*, e2637.

Parisi, G., Echave, J., Ghiringhelli, D., and Romanowski, V. (1996). Computational characterisation of potential RNA-binding sites in arenavirus nucleocapsid proteins. Virus genes *13*, 247-254.

Patel, C.V., Handy, I., Goldsmith, T., and Patel, R.C. (2000). PACT, a stress-modulated cellular activator of interferon-induced double-stranded RNA-activated protein kinase, PKR. The Journal of biological chemistry *275*, 37993-37998.

Perez, M., and de la Torre, J.C. (2003). Characterization of the genomic promoter of the prototypic arenavirus lymphocytic choriomeningitis virus. Journal of virology *77*, 1184-1194.

Pinschewer, D.D., Perez, M., and de la Torre, J.C. (2003). Role of the virus nucleoprotein in the regulation of lymphocytic choriomeningitis virus transcription and RNA replication. Journal of virology *77*, 3882-3887.

Pinschewer, D.D., Perez, M., and de la Torre, J.C. (2005). Dual role of the lymphocytic choriomeningitis virus intergenic region in transcription termination and virus propagation. Journal of virology *79*, 4519-4526.

Polyak, S.J., Zheng, S., and Harnish, D.G. (1995a). 5' termini of Pichinde arenavirus S RNAs and mRNAs contain nontemplated nucleotides. Journal of virology *69*, 3211-3215.

Polyak, S.J., Zheng, S., and Harnish, D.G. (1995b). Analysis of Pichinde arenavirus transcription and replication in human THP-1 monocytic cells. Virus research *36*, 37-48.

Pythoud, C., Rodrigo, W.W., Pasqual, G., Rothenberger, S., Martinez-Sobrido, L., de la Torre, J.C., and Kunz, S. (2012). Arenavirus nucleoprotein targets interferon regulatory factor-activating kinase IKKepsilon. Journal of virology *86*, 7728-7738.

Pythoud, C., Rothenberger, S., Martinez-Sobrido, L., de la Torre, J.C., and Kunz, S. (2015). Lymphocytic Choriomeningitis Virus Differentially Affects the Virus-Induced Type I Interferon Response and Mitochondrial Apoptosis Mediated by RIG-I/MAVS. Journal of virology *89*, 6240-6250.

Qi, X., Lan, S., Wang, W., Schelde, L.M., Dong, H., Wallat, G.D., Ly, H., Liang, Y., and Dong, C. (2010). Cap binding and immune evasion revealed by Lassa nucleoprotein structure. Nature *468*, 779-783.

Raj, A., van den Bogaard, P., Rifkin, S.A., van Oudenaarden, A., and Tyagi, S. (2008). Imaging individual mRNA molecules using multiple singly labeled probes. Nature methods *5*, 877-879.

Raju, R., Raju, L., Hacker, D., Garcin, D., Compans, R., and Kolakofsky, D. (1990). Nontemplated bases at the 5' ends of Tacaribe virus mRNAs. Virology *174*, 53-59.

Rawls, W.E., Chan, M.A., and Gee, S.R. (1981). Mechanisms of persistence in arenavirus infections: a brief review. Can J Microbiol *27*, 568-574.

Reineke, L.C., and Lloyd, R.E. (2013). Diversion of stress granules and P-bodies during viral infection. Virology *436*, 255-267.

Rivers, T.M., and McNair Scott, T.F. (1935). Meningitis in Man Caused by a Filterable Virus. Science *81*, 439-440.

Rivers, T.M., and Scott, T.F. (1936). Meningitis in Man Caused by a Filterable Virus : Ii. Identification of the Etiological Agent. J Exp Med *63*, 415-432.

Rodrigo, W.W., Ortiz-Riano, E., Pythoud, C., Kunz, S., de la Torre, J.C., and Martinez-Sobrido, L. (2012). Arenavirus nucleoproteins prevent activation of nuclear factor kappa B. Journal of virology *86*, 8185-8197.

Rojek, J.M., and Kunz, S. (2008). Cell entry by human pathogenic arenaviruses. Cellular microbiology *10*, 828-835.

Rojek, J.M., Sanchez, A.B., Nguyen, N.T., de la Torre, J.C., and Kunz, S. (2008). Different mechanisms of cell entry by human-pathogenic Old World and New World arenaviruses. Journal of virology *82*, 7677-7687.

Rowe, W.P., Murphy, F.A., Bergold, G.H., Casals, J., Hotchin, J., Johnson, K.M., Lehmann-Grube, F., Mims, C.A., Traub, E., and Webb, P.A. (1970). Arenoviruses: proposed name for a newly defined virus group. Journal of virology *5*, 651-652.

Russier, M., Pannetier, D., and Baize, S. (2012). Immune responses and Lassa virus infection. Viruses *4*, 2766-2785.

Russier, M., Reynard, S., Carnec, X., and Baize, S. (2014). The exonuclease domain of Lassa virus nucleoprotein is involved in antigen-presenting-cell-mediated NK cell responses. Journal of virology *88*, 13811-13820.

Salvato, M.S., Schweighofer, K.J., Burns, J., and Shimomaye, E.M. (1992). Biochemical and immunological evidence that the 11 kDa zinc-binding protein of lymphocytic choriomeningitis virus is a structural component of the virus. Virus research *22*, 185-198.

Salvato, M.S., and Shimomaye, E.M. (1989). The completed sequence of lymphocytic choriomeningitis virus reveals a unique RNA structure and a gene for a zinc finger protein. Virology *173*, 1-10.

Savidis, G., McDougall, W.M., Meraner, P., Perreira, J.M., Portmann, J.M., Trincucci, G., John, S.P., Aker, A.M., Renzette, N., Robbins, D.R., Guo, Z., Green, S., Kowalik, T.F., and Brass, A.L. (2016). Identification of Zika Virus and Dengue Virus Dependency Factors using Functional Genomics. Cell Rep *16*, 232-246.

Schlie, K., Maisa, A., Freiberg, F., Groseth, A., Strecker, T., and Garten, W. (2010). Viral protein determinants of Lassa virus entry and release from polarized epithelial cells. Journal of virology *84*, 3178-3188.

Schmidt, E.K., Clavarino, G., Ceppi, M., and Pierre, P. (2009). SUnSET, a nonradioactive method to monitor protein synthesis. Nature methods *6*, 275-277.

Scott, T.F., and Rivers, T.M. (1936). Meningitis in Man Caused by a Filterable Virus : I. Two Cases and the Method of Obtaining a Virus from Their Spinal Fluids. J Exp Med *63*, 397-414.

Shivaprakash, M., Harnish, D., and Rawls, W. (1988). Characterization of temperature-sensitive mutants of Pichinde virus. Journal of virology *62*, 4037-4043.

Shtanko, O., Imai, M., Goto, H., Lukashevich, I.S., Neumann, G., Watanabe, T., and Kawaoka, Y. (2010). A role for the C terminus of Mopeia virus nucleoprotein in its incorporation into Z protein-induced virus-like particles. Journal of virology *84*, 5415-5422.

Shtanko, O., Watanabe, S., Jasenosky, L.D., Watanabe, T., and Kawaoka, Y. (2011). ALIX/AIP1 is required for NP incorporation into Mopeia virus Z-induced virus-like particles. Journal of virology *85*, 3631-3641.

Singh, M.K., Fuller-Pace, F.V., Buchmeier, M.J., and Southern, P.J. (1987). Analysis of the genomic L RNA segment from lymphocytic choriomeningitis virus. Virology *161*, 448-456.

Song, T., Zheng, Y., Wang, Y., Katz, Z., Liu, X., Chen, S., Singer, R.H., and Gu, W. (2015). Specific interaction of KIF11 with ZBP1 regulates the transport of beta-actin mRNA and cell motility. Journal of cell science *128*, 1001-1010.

Southern, P.J., Singh, M.K., Riviere, Y., Jacoby, D.R., Buchmeier, M.J., and Oldstone, M.B. (1987). Molecular characterization of the genomic S RNA segment from lymphocytic choriomeningitis virus. Virology *157*, 145-155.

Staneck, L.D., Trowbridge, R.S., Welsh, R.M., Wright, E.A., and Pfau, C.J. (1972). Arenaviruses: cellular response to long-term in vitro infection with parana and lymphocytic choriomeningitis viruses. Infect Immun *6*, 444-450.

Stenglein, M.D., Sanders, C., Kistler, A.L., Ruby, J.G., Franco, J.Y., Reavill, D.R., Dunker, F., and Derisi, J.L. (2012). Identification, characterization, and in vitro culture of highly divergent arenaviruses from boa constrictors and annulated tree boas: candidate etiological agents for snake inclusion body disease. mBio *3*, e00180-00112.

Stenmark, H. (2009). Rab GTPases as coordinators of vesicle traffic. Nat Rev Mol Cell Biol *10*, 513-525.

Stephensen, C.B., Blount, S.R., Lanford, R.E., Holmes, K.V., Montali, R.J., Fleenor, M.E., and Shaw, J.F. (1992). Prevalence of serum antibodies against lymphocytic choriomeningitis virus in selected populations from two U.S. cities. J Med Virol *38*, 27-31.

Thomas, M.G., Loschi, M., Desbats, M.A., and Boccaccio, G.L. (2011). RNA granules: the good, the bad and the ugly. Cellular signalling *23*, 324-334.

Tortorici, M.A., Albarino, C.G., Posik, D.M., Ghiringhelli, P.D., Lozano, M.E., Rivera Pomar, R., and Romanowski, V. (2001a). Arenavirus nucleocapsid protein displays a transcriptional antitermination activity in vivo. Virus research *73*, 41-55.

Tortorici, M.A., Ghiringhelli, P.D., Lozano, M.E., Albarino, C.G., and Romanowski, V. (2001b). Zinc-binding properties of Junin virus nucleocapsid protein. The Journal of general virology *82*, 121-128.

Toth, A.M., Devaux, P., Cattaneo, R., and Samuel, C.E. (2009). Protein Kinase PKR Mediates the Apoptosis Induction and Growth Restriction Phenotypes of C Protein-Deficient Measles Virus. Journal of virology *83*, 961-968.

Tourriere, H., Chebli, K., Zekri, L., Courselaud, B., Blanchard, J.M., Bertrand, E., and Tazi, J. (2003). The RasGAP-associated endoribonuclease G3BP assembles stress granules. The Journal of cell biology *160*, 823-831.

Traub, E. (1935). A Filterable Virus Recovered from White Mice. Science *81*, 298-299.

Tsanov, N., Samacoits, A., Chouaib, R., Traboulsi, A.M., Gostan, T., Weber, C., Zimmer, C., Zibara, K., Walter, T., Peter, M., Bertrand, E., and Mueller, F. (2016). smiFISH and FISH-quant - a flexible single RNA detection approach with super-resolution capability. Nucleic Acids Res *44*, e165.

Urata, S., and Yasuda, J. (2012). Molecular mechanism of arenavirus assembly and budding. Viruses *4*, 2049-2079.

Valiente-Echeverria, F., Melnychuk, L., and Mouland, A.J. (2012). Viral modulation of stress granules. Virus research *169*, 430-437.

Vela, E. (2012). Animal models, prophylaxis, and therapeutics for arenavirus infections. Viruses *4*, 1802-1829.

Viets, H.R., and Watts, J.W. (1929a). Aseptic (Lymphocytic) Meningitis. JAMA *93*, 1553-1555.

Viets, H.R., and Watts, J.W. (1929b). Three Cases of Aseptic (Lymphocytic) Meningitis. N Engl J Med *200*, 633-634.

Weber, E.L., and Buchmeier, M.J. (1988). Fine mapping of a peptide sequence containing an antigenic site conserved among arenaviruses. Virology *164*, 30-38.

Welsh, R.M., O'Connell, C.M., and Pfau, C.J. (1972). Properties of defective lymphocytic choriomeningitis virus. The Journal of general virology *17*, 355-359.

West, B.R., Hastie, K.M., and Saphire, E.O. (2014). Structure of the LCMV nucleoprotein provides a template for understanding arenavirus replication and immunosuppression. Acta Crystallogr D Biol Crystallogr *70*, 1764-1769.

White, J.P., and Lloyd, R.E. (2012). Regulation of stress granules in virus systems. Trends in microbiology *20*, 175-183.

Wichgers Schreur, P.J., and Kortekaas, J. (2016). Single-Molecule FISH Reveals Non-selective Packaging of Rift Valley Fever Virus Genome Segments. PLoS pathogens *12*, e1005800.

Wildy, P. (1971). Classification and Nomenclature of Viruses. In Monographs in Virology, J.L. Melnick, ed. (Basel/New York: S. Karger).

Wolff, S., Becker, S., and Groseth, A. (2013a). Cleavage of the Junin virus nucleoprotein serves a decoy function to inhibit the induction of apoptosis during infection. Journal of virology *87*, 224-233.

Wolff, S., Ebihara, H., and Groseth, A. (2013b). Arenavirus budding: a common pathway with mechanistic differences. Viruses *5*, 528-549.

Young, P.R., Chanas, A.C., Lee, S.R., Gould, E.A., and Howard, C.R. (1987). Localization of an arenavirus protein in the nuclei of infected cells. The Journal of general virology *68 (Pt 9)*, 2465-2470.

Young, P.R., and Howard, C.R. (1983). Fine structure analysis of Pichinde virus nucleocapsids. The Journal of general virology *64 (Pt 4)*, 833-842.

Yun, N.E., and Walker, D.H. (2012). Pathogenesis of Lassa fever. Viruses *4*, 2031-2048.

Zamanian-Daryoush, M., Mogensen, T.H., DiDonato, J.A., and Williams, B.R. (2000). NF-kappaB activation by double-stranded-RNA-activated protein kinase (PKR) is mediated through NF-kappaB-inducing kinase and IkappaB kinase. Molecular and cellular biology *20*, 1278-1290.

Zenklusen, D., Larson, D.R., and Singer, R.H. (2008). Single-RNA counting reveals alternative modes of gene expression in yeast. Nat Struct Mol Biol *15*, 1263-1271.

Zenklusen, D., and Singer, R.H. (2010). Analyzing mRNA expression using single mRNA resolution fluorescent in situ hybridization. Methods Enzymol *470*, 641-659.

Zhang, F., Romano, P.R., Nagamura-Inoue, T., Tian, B., Devert, T.E., Mathews, M.B., Ozato, K., and Hinnebusch, A.G. (2001). Binding of double-stranded RNA to protein kinase PKR is required for dimerization and promotes critical autophosphorylation events in the activation loop. Journal of Biological Chemistry *276*, 24946-24958.

Zhang, Y., Li, L., Liu, X., Dong, S., Wang, W., Huo, T., Guo, Y., Rao, Z., and Yang, C. (2013). Crystal structure of Junin virus nucleoprotein. The Journal of general virology *94*, 2175-2183.

Zhou, S., Cerny, A.M., Zacharia, A., Fitzgerald, K.A., Kurt-Jones, E.A., and Finberg, R.W. (2010). Induction and inhibition of type I interferon responses by distinct components of lymphocytic choriomeningitis virus. Journal of virology *84*, 9452-9462.

Ziegler, C.M., Eisenhauer, P., Bruce, E.A., Beganovic, V., King, B.R., Weir, M.E., Ballif, B.A., and Botten, J. (2016a). A novel phosphoserine motif in the LCMV matrix protein Z regulates the release of infectious virus and defective interfering particles. The Journal of general virology *97*, 2084-2089.

Ziegler, C.M., Eisenhauer, P., Bruce, E.A., Weir, M.E., King, B.R., Klaus, J.P., Krementsov, D.N., Shirley, D.J., Ballif, B.A., and Botten, J. (2016b). The Lymphocytic Choriomeningitis Virus Matrix Protein PPXY Late Domain Drives the Production of Defective Interfering Particles. PLoS pathogens *12*, e1005501.